Charles University, Faculty of Science
Institute for Environmental Studies

Doctoral study program: Environmental Science

Doctoral thesis

ATMOSPHERIC AEROSOL: PHYSICAL CHEMICAL CHARACTERISATION AND SOURCE APPORTIONMENT

Atmosférické částice: fyzikální a chemická charakterizace a identifikace jejich zdrojů

M.Sc. Cecilia Leoni

Supervisor: RNDr. Jan Hovorka, Ph.D.

Prague, 2017

Table of content

Acknowledgements 5

List of Acronyms 6

Abstract 7

Abstrakt 9

Graphical overview 12

List of publications included in the doctoral thesis 13

1.General introduction and motivation 14

1.1. Atmospheric particle size distribution 16

1.1.1 Ultrafine particles 18

1.2 Atmospheric particles number concentration 20

1.3 Remarks on particle chemical composition with focus on UFPs 21

References 22

2.Atmospheric particles measurements 28

2.1 Online measurements 28

2.2 Offline techniques 31

2.3 Ground based measurements 32

2.4 Airborne measurements in the Planetary Boundary Layer 34

References 35

3.Source apportionment 38

3.1 Aerosol particles sources by number size distribution 38

3.2 Receptor modelling with PMF 40

3.3 NSD PMF rules of thumb 41

References 45

4. Research activity 48

4.1 Aims of the Ph.D. study 48

4.2 Major findings critical review 49

4.3 Conclusion 54

References 56

Manuscript 1 58

Manuscript 2 77

Manuscript 3 84

Manuscript 4 117

List of figures

Figure 1 – A: typical example of urban environment SD with size dependent deposition in alveolar and trachea-bronchial regions (Kumar et al., 2010) 17
Figure 2 – Deposition fraction in healthy lung under moderate exertion (Venkataraman, 1999) 19
Figure 3 – DMA schematic representation (*www.tsi.com*) 28
Figure 4 – Schematic representation of a CPC (*www.cas.manchester.ac.uk*). 30
Figure 5 – Schematic representation of APS optic chamber (*www.cas.manchester.ac.uk)* 30
Figure 6 – Schematic representation of multistage cascade impactor (www.pharmacopeia.cn) 31

Prohlášení:

Prohlašuji, že jsem závěrečnou práci zpracovala samostatně a že jsem uvedla všechny použité informační zdroje a literaturu. Tato práce ani její podstatná část nebyla předložena k získání jiného nebo stejného akademického titulu.

V Praze, 28.11.2017 Cecilia Leoni, M.Sc.

Acknowledgements

I would like to take this opportunity to thank the people who have contributed to this thesis and to the research documented herein. Thank you to my supervisor Jan Hovorka for his guidance and to my colleagues and friends Petra Pokorná, Jana Kozáková, Miroslav Klán, and Jan Bendl, for the collaboration to the research papers and for all the practical help. I would like to thank Prof. Tomas Cajthaml, for his collaboration in the manuscript 1 and Prof. Jan Frouz for his advices. To all staff of the ICPF Prague a big thank, for the scientific collaboration in my research activity, but also for the encouragement and the assistance. A thank also to the staff of the Institute for Environmental Studies for their support, and in particular Dr. Zíková for her collaboration in the manuscript 1. Additionally, I would like to acknowledge Dr. Marvanová of the Institute of Veterinary research for their collaboration in the manuscript 1; Dr. Cliff, Dr. Křůmal, Prof. Hopke, Dr. Masiol, Dr. Mikuška, Dr. Topinka, and Dr. Zhao for their collaboration in the manuscript 3.

The research activity herein was financially supported by the grant P503/12/G147 of the Grant Agency of the Czech Republic, and the grant 1354314 of the Grant Agency of the Charles University in Prague. Additional support was provided by the program of Czech Ministry of Education, Spot and Youth, in cooperation with the Czech Ministry of Foreign Affairs, the Czech Embassy in Rome and the Italian Ministry of Foreign Affairs and International Cooperation.

List of Acronyms

APS	Aerodynamic Particle Sizer
BB	Biomass Burning
BS	Bootstrap
CAFE	Clean Air For Europe
CC	Coal Combustion
CPC	Condensation Particle Counter
CPF	Condition Probability Function
DMA	Differential Mobility Analyzer
DRUM	Davis-Rotating Monitoring Unit
EC	Elemental Carbon
EEA	European Environmental Agency
EPA	(US) Environmental Protection Agency
EU	European Union
GC	Gas Chromatography
HPLC	High Performance Liquid Chromatography
IC	Ion Chromatography
IMF	Inter-Modal Fraction
NBL	Nocturnal Boundary Layer
NC	Number Concentration
OC	Organic Carbon
PAH	Polycyclic Aromatic Hydrocarbons
PBL	Planetary Boundary Layer
PCIS	Personal Cascade Impactor Sampler
PM	Particulate Matter
PMF	Positive Matrix Factorization
PNC	Particle Number Concentration
PSCF	Potential Source Contribution Function
SD	Size Distribution
SEM	Scanning Electron Microscopy
SIA	Secondary Inorganic Aerosol
SMPS	Scanning Mobility Particle Sizer
SOA	Secondary Organic Aerosol
TEM	Transmission Electron Microscopy
UFPs	Ultrafine Particles
VOC	Volatile Organic Compounds

Abstract

Atmospheric aerosol is a ubiquitous component of the Earth atmosphere. By mass, aerosol natural sources override anthropogenic ones, the latter constituting less than 5% to the total aerosol loading (Jaenicke, 2008). Nevertheless, in urban environment the contribution can increase to 80-90%. Since anthropogenic sources are mostly associated with high temperature processes, urban aerosol number size distribution is usually dominated by ultrafine particles - UFPs (d<100 nm). The UFPs have the highest surface/mass ratios among aerosol particles and bond the highest pollutant loading as per particle mass. Additionally, the UFPs exhibit the highest deposition efficiency in deep region of the human respiratory tract. Therefore, this study focuses to urban aerosol particle spatial-temporal, physical and chemical characterization and source apportionment with special emphasis to the UFPs.

The first study in residential district of Ostrava-Radvanice and Bartovice, an air pollution *hot spot* in Europe, identified industry being dominant sources of UFPs. High particle number concentrations (NC) were measured at the *hot spot*, with peaks up to $1.4x10^5$ particles cm^{-3} during plume events, i.e. downwind an industrial facility. The plume-originating UFPs were mostly composed of 19−44 nm nanoparticles heavily enriched up to 4.5% of mass with carcinogenic polycyclic aromatic hydrocarbons (PAHs). The industry nanoparticles have short residence time and quickly attach to accumulation mode particles, which explains their enrichment with PAH's, the most serious threat at the at the hot-spot. Also, such finding helps to assess better industrial UFPs impact to human health, since particles of 20−40 nm in diameter exhibit twice the deposition efficiency in pulmonary alveoli than other UFPs (Venkatamaran et al., 1999). The methodology of source impact measurements focusing on particle NC and size distribution (SD) presented in this manuscript combines highly time-and-space airborne and ground-level measurements. This integrated measurement strategy can be applied to identify specific industrial sources in other hot-spots worldwide.

The aerosol NC and the SD can vary at different heights of the planetary boundary layer (PBL). In-situ vertical profile measurements in the PBL, especially up to 300 m height above ground level, are rare. Airship measurements are capable of providing high time-and-space resolution of aerosol vertical distribution directly in the lower troposphere. Airborne measurements in manuscript 2 revealed two temperature inversion layers, at heights 70m and 120m. In the early morning, coarse particles were accumulated below the lower inversion layer with mass

concentrations up to 50 μgm^{-3}, reflecting coarse aerosol sources on the ground, while the UFPs were found enriched, up to $2.5x10^4$ particles cm^{-3}, in the PBL at heights between 90-120m. This indicate a fanning plume from distant source with high emission height and UFPs increase was not registered at the ground. At noon, a sharp increase in number concentrations of UFPs up to $3.7x10^4$ particles cm^{-3} was registered at heights of 380-400m. Since the PBL stratification ceased and gradual turbulent mixing evolved, sudden increase of ultrafine particles concentration $1.5\text{-}2x10^4$ particles cm^{-3} was also registered at the ground. By this way we were able to discriminate sources of UFPs at the hot-spot.

In the same European air pollution *hot spot* presented in the manuscript 1, a more comprehensive study on particles sources was performed, spanning the whole size range, from 14 nm – 10 µm (manuscript 3). The methodology employed in this study, applying Positive Matrix Factorization (PMF) to the particle SD spectra, allowed the identification of sources contributing principally to particle NC and, in particular, to the UFPs. Two factors were resolved in the ultrafine size range: industrial UFPs (28%, number mode diameter - NMD 45 nm), industrial/fresh road traffic nanoparticles (26%, NMD 26 nm). Three factors were resolved in the accumulation size range: urban background (24%, NMD 93 nm), coal burning (14%, volume mode diameter - VMD 0.5 µm), regional pollution (3%, VMD 0.8 µm) and one factor in the coarse size range: industrial coarse particles/road dust (2%, VMD 5 µm). The organic markers homohopanes correlate with coal combustion and the levoglucosan correlates with urban background. The PMF analysis on mass chemical composition ($PM_{0.09\text{-}1.15}$) revealed four factors: secondary inorganic aerosol/coal combustion/biomass burning (SIA/CC/BB, 52%), road dust (18%), sinter/steel production (16%), and iron production (16%). The factors in the ultrafine size range have a positive correlation with sinter/steel production and iron production factors. PAHs measured in 24-hour PM_1 were associated with coal combustion factor, with (r^2 = 0.68), with R-homopane (r^2=0.88) and levoglucosan (r^2 = 0.67). Nevertheless, 24 hours PAHs measurement is not adequate for the source apportionment and higher time resolution is needed to apportion the sources without ambiguity.

The physical and chemical properties of the aerosol SD are variable in space and time according to the meteorological conditions and the sources. The manuscript 4 investigates the size distribution properties with focus on the intermodal fraction. Fine, coarse and intermodal (1-2.5 µm) fractions mass concentration and chemical composition were measured in four Czech locations (industrial-residential hot spot; suburban-residential; Prague urban and

suburban). It was found that the highest mass concentration of all fractions with Fe as the predominant element was measured at the hot spot. Additionally, in case of dry atmospheric condition, the $PM_{1-2.5}$ correspond to the PM coarse fraction; on the other hand, with higher relative humidity, the fine fraction grows into the intermodal fraction, and the $PM_{2.5}$ can be a more representative indicator for the fine fraction.

Abstrakt

Atmosférický aerosol je všudypřítomnou součástí zemské atmosféry. Vztaženo na hmotu, přírodní zdroje aerosolů předčí antropogenní zdroje, které tvoří pouze 5 % celkového zatížení aerosoly (Jaenicke, 2008). Nicméně v průmyslových oblastech může tento podíl narůst až na 80–90%. Antropogenní zdroje jsou většinou spojeny s vysokoteplotními procesy, a proto v městském prostředí co do velikostního rozdělení aerosolů převažují tzv. ultrajemné částice - UFP (d<100 nm). UFP mají nejvyšší poměr povrchu ku hmotnosti mezi ostatními aerosoly, a tudíž, vztaženo k hmotě částic, na sebe váží nejvíce znečišťujících látek. V neposlední řadě mají UFP vysokou účinnost depozice v dolních cestách dýchacích lidského organismu. Z výše uvedených důvodů byla tato práce zacílena na studium městského aerosolu s přihlédnutím k jeho časové a prostorové distribuci, dále k fyzikálním a chemickým vlastnostem a rovněž k identifikaci zdrojů, vše se zvláštním zaměřením na UFP.

V prvním článku předkládané disertační práce, který se zabývá znečištěním ovzduší v residenční části Ostrava-Radvanice a Bartovice, jež je v tomto směru evropským *hot spotem*, byl jako dominantní zdroj UFP identifikován průmysl. Vysoké početní koncentrace částic (NC) byly naměřeny v kouřové vlečce blízkého průmyslového závodu (1.4×10^5 částic cm^{-3}). UFP pocházející z kouřové vlečky se skládaly hlavně z nanočástic o velikosti 19−44 nm s obsahem až 4,5 % karcinogenních polycyklických aromatických uhlovodíků (PAH). Nanočástice z průmyslových zdrojů mají velmi krátkou životnost a rychle se akumulují, což vysvětluje jejich nabohacení PAH, jež představují na takto exponovaných lokalitách největší hrozbu. Tento nález umožní lépe odhadnout vliv průmyslových UFP na lidské zdraví, protože částice o průměru 20−40 nm mají dvakrát vyšší účinnost depozice v plicních alveolách než jiné UFP (Venkatamaran et al., 1999). Metodika měření vlivu zdrojů aerosolů se zaměřením na NC a velikostní rozlišení částic (SD), která je zde prezentována, kombinuje letecká i pozemní měření s vysokým časovým a prostorovým rozlišením. Takto ucelená strategie měření může být

aplikována k identifikaci průmyslových zdrojů znečištění na exponovaných lokalitách po celém světě.

NC a SD se liší dle různých výšek mezní vrstvy zemské atmosféry (PBL). In situ měření vertikálního profilu v PBL, obzvláště ve výškách do 300 m nad zemí, nejsou častá. Jsou-li takováto měření prováděna pomocí vzducholodi, umožňují vyšetření vertikální distribuce částic ve spodní části troposféry s vysokým rozlišením v prostoru i v čase. Letecké měření zmíněné v druhém článku odkrylo 2 teplotní inverzní vrstvy, a to ve výšce 70 a 120 m. Během časného rána byly hrubého částice o hmotnostních koncentracích do 50 µg m^{-3} akumulovány pod první vrstvou teplotní inverze, což odráželo vliv emisí zdrojů hrubých částic. Oproti tomu se UFP o koncentraci 2,5 x 10^4 částic cm^{-3} nacházely ve výškách mezi 90–120 m. Takovéto výsledky ukazují na původ částic v kouřové vlečce ze vzdáleného zdroje o vysoké emisní výšce, protože nárůst UFP při zemi nebyl zaznamenán. V poledne byl ve výškách 380–400 m zaznamenán strmý nárůst v koncentraci UFP až na 3,7 x 10^4 částic cm^{-3}. Protože zvrstvení PBL se v průběhu odpoledne pomalu vytrácelo a pozvolna se vyvíjelo turbulentní směšování, byla následně zaznamenána zvýšená koncentrace UFP při zemi a to o hodnotě 1,5–2 x 10^4 částic cm^{-3}. Tímto způsobem bylo možné na sledované lokalitě rozlišit různé zdroje UFP.

Na stejné lokalitě jako v prvním článku byla provedena i zevrubnější studie zaměřená na zdroje aerosolů v rozsahu velikostí částic 14 nm–10 µm (3. článek). Metodika uplatněná v této studii - aplikace Positive Matrix Factorization (PMF) na velikostní spektrum částic - umožnila identifikaci hlavních zdrojů přispívajících k NC a obzvláště k NC UFP. V ultrajemném rozsahu velikostí byly rozlišeny 2 faktory : průmyslové UFP (28 %, mód velikostního průměru počtu částic – (NMD) 45 nm) a průmyslové/čerstvé nanočástice z dopravy (26 %, NMD 26 nm). Tři faktory byly zjištěny v akumulačním rozsahu velikostí: průmyslové pozadí (24 %, NMD 93 nm), spalování uhlí (14 %, mód velikostního průměru objemu částic - VMD 0,5 µm) a regionální znečištění (3 %, VMD 0,8 µm), a dále jeden faktor hrubých částic: průmyslové hrubé částice/prach z dopravy (2 %, VMD 5 µm). Organické markery - homohopany korelovaly s faktorem spalováním uhlí a levoglukosan s faktorem městské pozadím. PMF analýza chemického složení hmoty ($PM_{0,09–1,15}$) ukázala 4 faktory: sekundární anorganický aerosol/spalování uhlí/spalování biomasy (52 %), prach z dopravy (18 %), sintrování/výroba oceli (16 %), a výroba železa (16 %). Faktory v rozsahu ultrajemných částic mají pozitivní korelaci se sintrováním, výrobou oceli a železa. PAH naměřené během 24 hodin v PM_1 byly spojeny s faktorem spalování uhlí (r^2 = 0,68), s homohopany (r^2=0,88) a levoglukosanem (r^2 =

0,67). Nicméně 24 hodinové měření PAH není dostatečné pro identifikaci zdrojů a vyšší časové rozlišení je nutné k jednoznačnému určení zdrojů.

Fyzikální a chemické vlastnosti SD aerosolů jsou různé v čase a prostoru v návaznosti na aktuální meteorologické podmínky a zdroje. Čtvrtý rukopis článku se zabývá vlastnostmi SD se zaměřením na intermodální frakci. Na 4 lokalitách v České republice (průmyslově-obytná, předměstská-obytná a městská a předměstská) byly měřeny hmotnostní koncentrace a chemické složení jemné, hrubé a intermodální frakce (1–2.5 μm) částic. Bylo zjištěno, že nejvyšší hmotnostní koncentrace s Fe jako převládajícím prvkem ve všech frakcích se nacházejí na nejexponovanější lokalitě (průmyslově-obytná). Navíc v případě nízké relativní vlhkosti $PM_{1–2.5}$ lépe odpovídá hrubé frakci PM. Na druhou stranu s vyšší relativní vlhkostí jemná frakce PM roste do intermodální frakce, a tudíž $PM_{2,5}$ představuje vhodnější indikátor.

Graphical overview

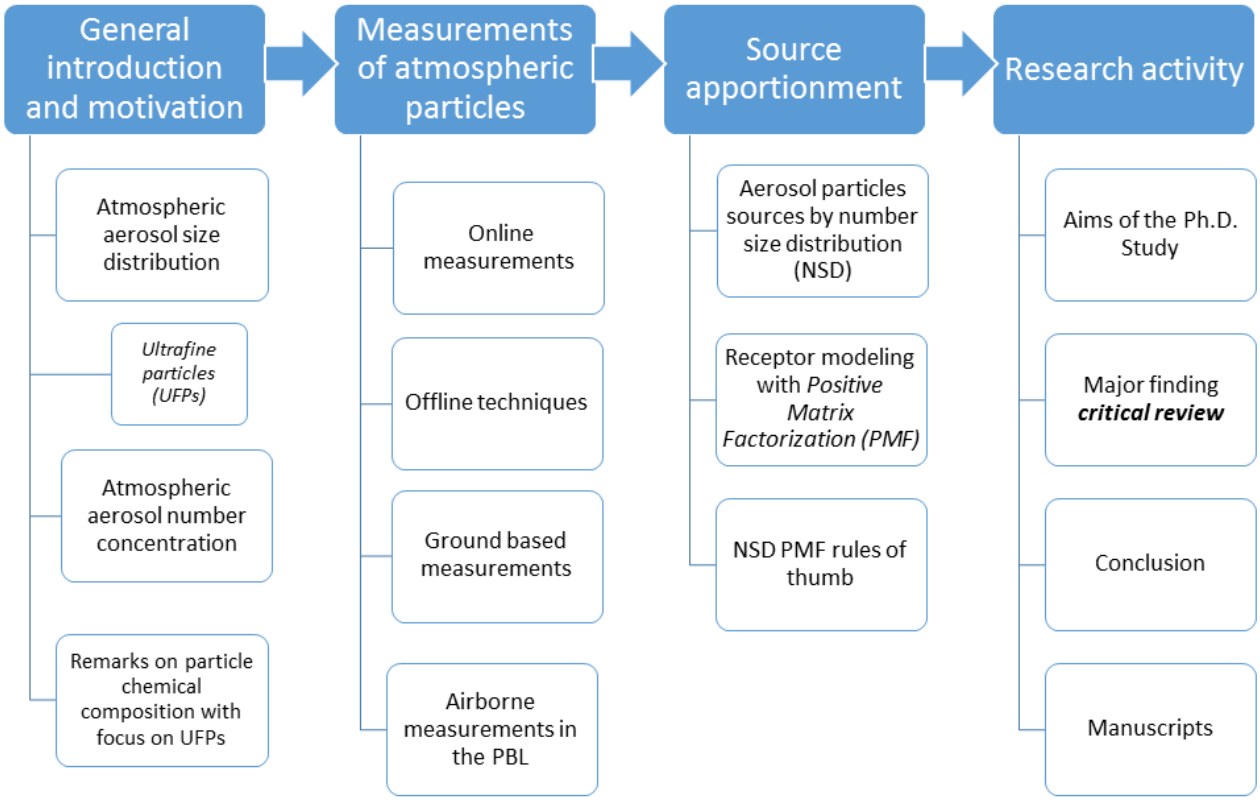

List of publications included in the doctoral thesis

Manuscript 1: Leoni C., Hovorka J., Dočekalová V., Cajthaml T., Marvanová S. 2016. Source impact determination using airborne and ground measurements of industrial plumes. *Environmental Science and Technology*, 50(18), pp. 9881-8, DOI: 10.1021/acs.est.6b02304

Manuscript 2: Hovorka J., Leoni C., Dočekalová V., Ondráček J., Zíková N., 2016. Aerosol distribution in the planetary boundary layer aloft a residential area. *IOP Conference Series: Earth and Environmental Science,* 44 052017, DOI: 10.1088/1755-1315/44/5/052017

Manuscript 3: Leoni C., Pokorná P., Hovorka J., Masiol M., Topinka J., Zhao Y., Křůmal K., Cliff S., Mikuška P., Hopke P. K., 2018. Source apportionment of aerosol particles at a European air pollution hot spot using particle number size distributions and chemical composition. *Environmental Pollution*, 234, 145-154. DOI:10.1016/j.envpol.2017.10.097

Manuscript 4: Kozáková J., Leoni C., Klán M., Hovorka J., Racek M., Ondráček J., Moravec P., Schwarz J. Chemical characterization of $PM_{1\text{-}2.5}$ and its associations with the PM_1, $PM_{2.5\text{-}10}$ and meteorology in urban and suburban environments (submitted to Aerosol and Air Quality Research).

1. General introduction and motivation

Ambient aerosols are suspensions of solid and liquid particles in the air. Aerosol particles affect the atmosphere's radiative properties and the thermal structure by light scattering and absorption; they are involved in the **cloud formation** and precipitation as cloud condensation and ice nuclei. If the atmosphere were totally devoid of particles, clouds could not form, and the water cycle could not occur. Aerosol particles are emitted from natural sources: sea spray, biomass fires, vegetation, soil dust and volcanic eruptions. With the industrial revolution and the fossil fuel burning, human activity has contributed to the total aerosol loading through the modification of natural surface cover and the release in the atmosphere of massive quantities of pollutants. Atmospheric particles became a pollutant, with a direct and indirect harmful effect to the population and to the biosphere. **Air pollution** is a complex environmental and social problem, posing multiple challenges in terms of management and mitigation. In Europe, EU and national policies have established concentration thresholds and quality objectives; have incentivized cleaner fuel types for vehicles, for home heating and cleaner technologies for industry. Nevertheless, exceedances of particulate matter (PM) limits are still registered in different EU regions, especially in the winter (EEA Air quality in Europe report, 2016). Effective actions to reduce the impact of air pollution require a good understanding of the atmospheric aerosol, how pollutants are transported and transformed in the atmosphere, and how they impact humans, ecosystems and climate. Effective air−quality policies call for action and cooperation at global, European, national and local levels, extending across most economic sectors. Holistic solutions involving technological development, structural changes and behavioral changes must be found.

It is well established that the exposure to particulate air pollution is linked to acute and chronic **health effects**. The effects of inhalation are found to be dependent on the size, concentration, shape and chemical composition of the particles and on the exposure length (Oberdörster, 2001). Short-term exposure to fine particles has been associated with adverse respiratory and cardiovascular health effects and premature mortality (Pope et al., 2014). In the recent CAFE (Clean Air for Europe) study by the European Commission **life expectancy** due to air pollution effects was estimated to be reduced by 12-36 months. Pollutants cross borders, and countries with heavy industry may find that their emissions greatly effect a neighboring country or county's population (EEA Air quality in Europe report, 2016).

A standard metric for measuring air quality is the PM mass concentration. However, the PM mass is dominated by larger particles which do not penetrate as deeply into the respiratory system as the smallest fractions. For this reason, in the aspect of human exposure, **particle size distribution (SD)** is an essential parameter. Recently, much attention has focused on the smaller size fractions because in urban area, most particles by number are typically found in the ultrafine mode: according to Seinfeld and Pandis (2006) the 75-90% of urban particles is normally found with diameters smaller than 0.1 μm. According to Kumar et al., (2014) atmospheric particles in the **nano-size range** (particles with diameter < 300 nm) contribute to the 99% of the total **particle number concentration** (PNC) in urban environment. In the recent past, there has been a significant increase in number of studies related to the characterization, monitoring, modelling and human exposure assessment of nanoparticles. Nevertheless, this progress has not been sufficient to establish ambient air quality standards. There still remain a number of inconclusive results on various aspects, for example a clear physical-chemical characterization of various sources, or a standardized sampling method. Moreover, the nanoparticles monitoring requires expensive equipment and specialized personnel. UFPs in the atmosphere derive from a considerable number of sources, even though road traffic emissions are dominant in urban environment, other sources have been observed: industry, power plants, domestic biomass burning, coal combustion, road-tyre interaction, construction and demolition, ship emissions, aircraft and airports emissions, forest fires and agriculture residues, cooking, smoking (Kumar et al., 2013). To date, there has been relatively little work devoted to disaggregation of size distribution into source-related components. This can be achieved with the application of multivariate statistical techniques to large datasets of particle NSD.

The following sessions provide a review of the following subjects: (i) the particle SD and NC with focus on the smallest size fraction, (ii) the measurements techniques (iii) and then the receptor modelling of particle NC and SD for the source apportionment. The last section includes the objectives of the thesis and the major findings critical review, further to the review provided in the manuscripts. Full text and supplementary material of the four manuscripts presented in this Ph.D. research are finally included.

1.1. Atmospheric particle size distribution

The **size** is the most important physical characteristic of the particles that strongly influences the other properties. The size of a particle is described by the **equivalent diameter**. The equivalent diameter is reported as the diameter of a sphere having the same value of a specific physical property as the irregularly shaped particle being measured. For instance, aerodynamic diameter is the diameter of a standard-density (1 g/cm^3) sphere having the same gravitational settling velocity as the particle being measured; the mobility equivalent diameter is the diameter of a sphere with the same mobility as the particle in question (for example, electrical mobility).

Different sources can emit particles with distinct SD that can be modified by evaporation, coagulation, growth, and removal processes. Ambient particles range from few nanometers up to 100 µm, with the lower limit related to molecules and molecular clusters and the upper limit, is defined by fast sedimentation. The size distribution is ideally characterized by a multi-lognormal structure, based on **three main modes**: the ultrafine mode, approximately < 100-150 nm; the accumulation mode between 0.1 and 1 µm; the coarse mode with particles with diameter > 1 µm. The ultrafine and the accumulation mode together constitute the fine particulate matter (PM). The **ultrafine particle SD** can present two distinct modes: the **Aitken mode**, with particles of diameter 20-100 nm, and the **nucleation mode**, with diameter <20 nm. The UFPs dominate the PNC and the surface area, but make small contribution to the PM mass/volume. The **accumulation mode** usually accounts for most of the aerosol surface area and a substantial part of the aerosol mass. The particles in the accumulation mode can be the result of the coagulation of particles in the nuclei mode, or the condensation of vapors onto UFPs, causing them to grow. Under conditions of high humidity, such as in a cloud or fog, the accumulation mode may also have two sub-modes: a condensation mode at 0.2-0.3 µm and a droplet mode at 0.5-0.8 µm, formed by the growth of hygroscopic condensation-mode particles (Hinds, 1999).

The **coarse mode** is composed by particles in the super-micrometer size range, general formed by mechanical processes and usually consists of human-made, natural dust particles, or biogenic particles.

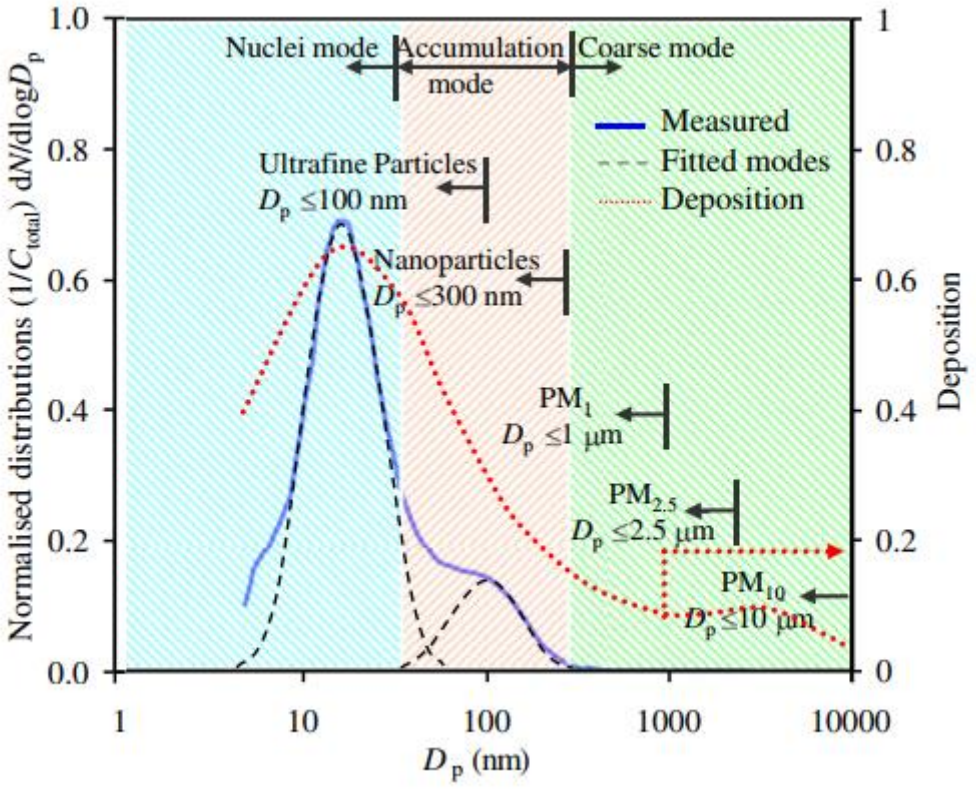

Figure 1 – A: typical example of urban environment SD with size dependent deposition in alveolar and trachea-bronchial regions (Kumar et al., 2010)

The atmospheric **residence time** is a key factor controlled by the particle SD. The UFPs, due to their small size and high mobility, diffuse rapidly and combine with each other, with larger particles and with deposition surfaces, and their atmospheric lifetime is typically tens of minutes or hours. The accumulation mode particles, as the name suggests, accumulate in this size range because the removal mechanisms are weak. Accumulation mode particles are removed by rainout or washout, but they coagulate too slowly to reach the coarse-particle mode (Hinds, 1999). They have lifetime of days in the atmosphere and they can be transported over long distances. The coarse PM, because of its larger size, has higher gravitational settling and it is removed from the atmosphere within hours. Environmental factors, for example meteorology, relative humidity, temperature and pressure, can significantly affect the residence time of the particles.

The separation between ultrafine, accumulation and coarse particles depends on the physical and chemical properties of the particles, on the sources and also on the atmospheric conditions. A major fraction of the accumulation mode PM originates form the UFPs (Sioutas et al., 2005). For this reason, the separation diameter between the ultrafine and the

accumulation modes has varied from 0.1 to 0.2 µm, depending on the location and on the season. Also, a sharp division between fine and coarse fractions cannot be clearly defined, because these two fractions overlap in the size range 1<d<2.5 (up to 3) µm. This size range is called the **intermodal fraction**, or intermediate range, ($PM_{1-2.5}$). During periods of high relative humidity, fine particles from the accumulation mode can grow into the intermodal fraction. On the other hand, coarse particles can shrink into fine particles in arid or semi-arid areas (Kozáková et al. 2017).

1.1.1 Ultrafine particles

What makes UFPs distinct from other pollutants is their dynamic nature and it their on-going transformation of physical and chemical properties, which contribute to substantial temporal and spatial variability. Because of the negligible influence of UFP on PM mass concentration, the number concentration is a better descriptor for UFPs.

The health impact of UFPs has motivated new ambient aerosol studies in recent years. UFPs can be inhaled deep into the respiratory tract and have high deposition efficiency (Venkatamaran et al., 1999). The UPF's surface can carry large amount of adsorbed or condensed toxic air pollutants (oxidant gases, organic pollutants, transition metals, Oberdoster, 2001). Several studies suggested that UFP induce oxidative stress in cells and are more toxic compared to larger particles of similar composition (Li et al., 2003; Nel et al., 2005). Epidemiological studies (Atkinson et al., 2010; Stolzel et al., 2007) have shown a clear association of urban nanoparticle exposure with adverse cardiovascular health outcomes.

UFPs originate in the atmosphere mainly by condensation of supersaturated vapours in fresh combustion emissions; they can form naturally when gases oxidize to compounds with lower vapour pressure and spontaneously nucleate (Kulmala et al., 2004). UFPs contain predominantly carbon and organic compounds including polyaromatic hydrocarbons (PAHs), transition metals, sulfuric acid (H_2SO_4) and free radicals (Chow and Watson, 2007). They often consist of volatile components and the high curvature of the smallest particles (<10 nm) favors evaporation over larger particles with the same composition (*Kelvin effect*). Gases evaporated from small particles can re-condense on larger ones, thereby shifting the distribution towards larger particle diameter (Zhang and Wexler, 2002). Owing their small size and high mobility, UFPs diffuse rapidly and may combine with each other, with bigger particles or with surfaces (dry deposition), within minutes or hours. The outcome of UFPs depends widely on the

pollutants concentration in the air: when the urban atmosphere is highly polluted, the semi-volatile species condense onto pre-existing particles; however, when low PM pollution occurs, semi volatile compounds may result in a large number of nucleation-derived particles.

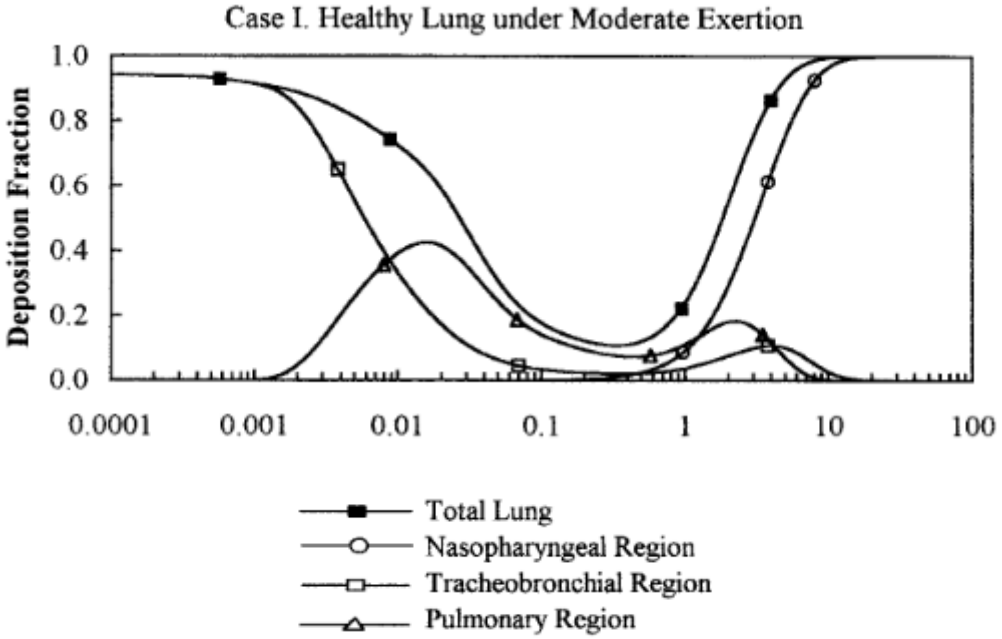

Figure 2 – Deposition fraction in healthy lung under moderate exertion (Venkataraman, 1999)

Most published work on UFPs relates to road transportation activities. Motor vehicles are the primary direct emission sources of UFPs in urban areas; particles form diesel engines are in the size range 20-130 nm, and from petrol engines in the range 20-60 nm (Harrison et al., 1999; Morawska et al. 2008; Dall'Osto et al., 2011).

On the emissions from specific industrial sources there is limited information, and thus considerable uncertainties with regard to the profiles fractionation and the size distribution variation between industrial sectors and activities. Some studies found that also industrial sources can emit high number of UFPs, for example combustion processes in power plants, chemistry, petro-chemistry industrial facilities, steel manufacturing, cement production, waste incinerators (Riffault et al., 2016). Studies on industrial aerosol particles plumes found fine and ultrafine particles in the plumes impacting the surrounding areas (Weitkamp et al., 2015; Marris, et al., 2012). SO_2 containing plumes (especially from coal fired power plants) can result in new particle formation in the 10-100 size range (Stevens et al., 2012). Overall, in EU27 the total emissions of UFPs by industry are estimated to be the 21% of the total UFPs

concentration, followed by residential and commercial sources (15%), agriculture (8%) an dominated by vehicular traffic (56%) (EC report on Industrial emissions of nanomaterials and ultrafine particles, 2011). However, this general estimation is subject to considerable uncertainty.

1.2 Atmospheric particles number concentration

Urban PNCs show quite consistent values in different studies performed in EU cities. Kumar et al., (2012) considered 45 sampling locations in 30 different cities within 15 different EU countries, at roadside and at urban background sites. The average PNC concentration of urban background was $1.63 \pm 0.8 \times 10^4$ particles cm^{-3}; at the roadside was $3.82 \pm 3.25 \times 10^4$ particles cm^{-3}, giving a roadside to background ratio of 2.4. Despite having several uncertainties derived by the measured size range, sampling locations, meteorological and traffic conditions and different years, the PNCs show quite consistent values, and the difference between the minimum (Prague, Ondraček et al., 2011) and the maximum (Zurich, Bukowiecki et al., 2003) at different locations was found to be within a factor 5, which is plausible considering he dynamic nature of the nanoparticles.

In a long-term aerosol particle total number concentration measurements in five metropolitan areas across Europe (Augsburg, Barcelona, Helsinki, Rome, and Stockholm; Aalto et al., 2005), showed a winter monthly average concentrations between 10^4 and 2×10^4 particles cm^{-3}, whereas the summer minimum is $0.5\text{-}0.6 \times 10^4$ particles cm^{-3}. During the weekdays, the maximum of the hourly average concentrations is detected in the morning hours between 7 and 10 a.m. (Aalto et al., 2005; Ruskaanen et al., 2001). The periods with high concentrations are related to particle emissions from traffic during the rush-hours when people are driving to and from work: in Helsinki during winter, the hourly maximum concentration levels reached 1.8×10^5 particles cm^{-3} (Ruuskaneen et al., 2001).

Another contributor to atmospheric PNC is industry. In terms of mass concentration, in developed countries, where stringent regulations on emissions are in place, industrial activities do not represent the major contributor to the global burden of atmospheric particulate matter. In Europe, for instance, estimations based on 25 countries for the year 2000 showed that industrial PM contributed to about 40% of the emissions (Riffault et al., 2015). However, in rapidly developing countries like China, the use of less clean energies

combined with a lack of enforcement of the emerging regulations can lead to higher emissions, industry becomes the major contributor with ~70% of the total.

In terms of NC there are few studies on nanoparticles in the vicinity of the industrial activities, certainly less than the studies dedicated on nanoparticles in urban environment. The interest in the industrial emissions lies in their specificity and the fact that point sources can lead to great human exposure. Recent studies found high PNC near industrial facilities: the PNC within 1 km of a metallurgical coke production factory varied from 1 to $100x10^5$ particles cm^{-3} in Pittsburgh, US (Weitkamp et al., 2005); $3\text{-}5x10^5$ particles cm^{-3} was found at a distance of 2 km of a ferromanganese alloy plant in Dunkirk, France, by Marris et al. (2012); 10 to $60x10^5$ particles cm^{-3} were measured in a grey iron foundry by Evans et al. (2008), and within 10 km of a copper smelter the PNC was $7x10^4$ particles cm^{-3} (Banic et al., 2006). The NC rises at the stack or at the workplace (Riffault et al., 2015, and references therein).

1.3 Remarks on particle chemical composition with focus on UFPs

Many of the effects of atmospheric particles (e.g. radiative effect, health effects) depend on their chemical composition, which rarely consists exclusively of a single component. Atmospheric aerosols are generally composed of variable amounts of sulfate, nitrate, ammonium, carbonaceous compounds (elemental carbon EC, organic carbon OC), sea salt, crustal elements, and trace metals. **OC** can be of both primary and secondary origin, while **EC** is exclusively a primary species (Schwartz et al., 2008). EC arises as the result of incomplete combustion of various kinds of organic material, including coal, oil, petrol, wood and other biomass; OC has similar sources, but it results also from resuspension of traffic related dust and primary biogenic particles like viruses, bacteria, pollens, fungal spores, vegetation debris (Hidelmann et al., 2004). The OC/EC ratio has lower values in the urban sites influenced by traffic emissions, while in the rural sites have the highest OC/EC because the contribution of secondary inorganic aerosol is higher; the industrial sites are usually in between. Chemical analysis of $PM_{2.5}$ in background site in Central Europe showed that carbonaceous aerosol form about half of the $PM_{2.5}$ mass, and the remaining half is mostly composed by secondary inorganic aerosol (Schwartz et al., 2016). The carbonaceous faction of the PM has therefore major importance and it has been determined by many studies; these analyses mainly focus on the measurement of OC and the particle-bound PAHs. PAHs consist of a fuse benzene ring structure and they are ubiquitously present in urban environment. PAHs with more than 3

benzene rings are found almost totally adsorbed on to particles and as the molecular weight increases, the carcinogenicity of PAHs increases too (Ravindra et al., 2008).

Considering the UFPs, there is still a gap in the knowledge of the chemical composition and therefore on the health impact. Studies based in the Los Angeles basin found that a large proportion of UFPs is made up of OC. In a long-term study conducted by Daher et al. (2013) in ten different locations, the chemical mass reconstruction revealed that quasi-UFP (<250 nm) consisted of 49-64% organic matter, 3-6.4% elemental carbon, 9-15% secondary ions, 0.7-1.3% trace ions, and 5.7-17% trace elements.

Not many studies investigated the PAHs content in the UFPs. According to Keyte et al., (2013) modes in the mass size distribution for PAHs are within the ultrafine and accumulation mode (0.1-1 µm). Eiguren-Fernandez et al. (2003) conducted a study in a locality impacted primarily vehicular sources and, to a lesser extent, industrial activities, and found that PAHs were mostly associated with particles <180 nm. Li et al. 2003 found that UFPs (<150 nm) enriched with PAHs are more potent than fine and coarse PM toward inducing cell oxidative stress. In a study conducted in Taiwan (Lin et al., 2008) in a site impacted by urban traffic the distribution of particulate total-PAHs showed a major peak in the Aitken mode (0.032-0.056 µm). In study by Topinka et al. (2015), 7 carcinogenic PAHs were measured in size-segregated aerosol on a daily basis at the EU *hot spot* (Ostrava Radvanice, Czech Republic). PAHs were found in all the PM size fractions, mostly in the upper accumulation mode (0.5-1 µm), but according to scanning electron microscopy, the accumulation mode fraction was composed of agglomerates of UFPs. PAHs might be primarily emitted in the ultrafine size range, and then enrich the fine fraction via coagulation. Corsini et al., (2017) found PAHs in the UFPs collected in Alpine valley impacted by wood burning.

References

- Aalto P., Hämeri K., Paatero P., Kulmala M., Bellander T., Berglind N., Bouso L., Castaño-Vinyals G., Sunyer J., Cattani G., Marconi A., Cyrys J., Von Klot S., Peters A., Zetzsche K., Lanki T., Pekkanen J., Nyberg F., Sjövall B. Forastiere F. 2005. Aerosol Particle Number Concentration Measurements in Five European Cities Using TSI-3022 Condensation Particle Counter over a Three-Year Period during

Health Effects of Air Pollution on Susceptible Subpopulations. *J. Air Waste Manag. Assoc.*, 55:8, 1064-1076.

- Air quality in Europe, European Environmental Agency Report 2016. www.eea.europa.eu/publications/air-quality-in-europe-2016
- Atkinson R.W., Fuller G., Anderson H. R., Harrison R. M., Armstrong B., 2010. Urban Ambient Particle Metrics and Health: A Time-series Analysis. *Epidemiology* 21(4), 501-511.
- Banic C., Leaitch W. R., Strawbridge K., Tanabe R., Wong H., Gariepy C., Simonetti A., Nejedly Z., Campbell J. L., Lu J., Skeaff J., Paktunc D., MacPherson J. I., Daggupaty S., Geonach H., Chatt A., Lamoureux M., 2006. The physical and chemical evolution of aerosols in smelter and power plant plumes: an airborne study. *Geochem. Explor. Environ. Anal.,* 6, 111–120.
- Bukowiecki N., Dommen J., Prevot A. S. H., Weingartner E., and Baltensperger U. 2003. Fine and ultrafine particles in the Zurich (Switzerland) area measured with a mobile laboratory: an assessment of the seasonal and regional variation throughout a year. Atmos. Chem. Phys., 3, 1477–1494.
- Chow J.C., Watson J.G., 2007. Review of measurement methods and compositions for ultrafine particles. *Aerosol Air Qual. Res.,* 7 (2), pp. 121-173.
- Corsini E., Vecchi R., Marabini L., Fermo P., Becagli S., Bernardoni V., Caruso D., Corbella L., Dell'Acqua M., Galli C.L., Lonati G., Ozgen S., Papale A., Signorini S., Tardivo R., Valli G., Marinovich M. 2017. The chemical composition of ultrafine particles and associated biological effects at an alpine town impacted by wood burning. *Sci. Total Environ.* 587-588:223-231.
- Daher N., Hasheminassaba S., Shafer M.M., Schauer J.J., Sioutas C., 2013. Seasonal and spatial variability in chemical composition and mass closure of ambient ultrafine particles in the megacity of Los Angeles. *Environ. Sci. Process Impacts.* 15(1):283-95.
- Dall'Osto M., Thorpe A., Beddows D. C. S., Harrison R. M., Barlow J. F., Dunbar T., Williams P. I., Coe H., 2011. Remarkable dynamics of nanoparticles in the urban atmosphere, *Atmos. Chem. Phys.,* 11, 6623-6637.

- Eiguren-Fernandez A., Miguel A.H., Jaques P., Sioutas C. 2003. Evaluation of a denuder-MOUDI-PUF sampling system to determine the size distribution of semivolatile polycyclic aromatic hydrocarbons in the Atmosphere. *Aerosol Sci. Technol.* 37:201–209.
- European Union official website, Clean air for Europe (CAFE) session http://ec.europa.eu/environment/archives/cafe/general/keydocs.htm
- Evans, D.E., Heitbrink, W.A., Slavin, T.J., and Peters, T.M., 2008. Ultrafine and respirable particles in an automative grey iron foundry. *Ann. Occup. Hyg.* 52(1), 9–21.
- Harrison R. M., Jones M., Collins G., 1999. Measurements of the physical properties of particles in the urban atmosphere. *Atmos. Environ.* 33, 309-321.
- Hildemann, L.M., Klinedinst, D.B., Klouda G.A., Currie L.A., Cass G.R., 1994. Sources of urban contemporary carbon aerosol. *Environ. Sci. Technol.* 28, 1565–1576.
- Hinds W. C. 1999. Aerosol technology, Properties, Behavior, and Measurement of Airborne Particles, Wiley (second edition), USA.
- Jaenicke R., 2008. Is atmospheric aerosol an aerosol?—A look at sources and variability. *Faraday discussion*, vol. 137, 235-43.
- Keyte J., Harrison R. M., Lammel G., 2013. Chemical reactivity and long-range transport potential of polycyclic aromatic hydrocarbons – a review. *Chem. Soc. Rev.* 42, 9333.
- Kozáková J., Pokorna P., Cernikova A., Hovorka J., Branis M., Moravec P., Schwartz J. 2017. The association between intermodal ($PM_{1\text{-}2.5}$) and PM_1, $PM_{2.5}$, coarse fraction and meteorological parameters in various environments in Central Europe. *AAQR*, 17(5) 1234-1243.
- Kulmala M., Vehkamäki H., Petäjä T., Dal Maso M., Lauri A., Kerminen V. M., Birmili W., McMurry P. H., 2004. Formation and growth rates of ultrafine atmospheric particles: a review of observations. *J. Aerosol Sci.* 35, 143–176.
- Kumar P, Morawska L., Birmili W, Paasonen P., Hu M., Kulmala M, Harrison R.M., Norford L., Britter L., 2014. Ultrafine particles in cities, *Environment International*, 66, 1-10.

- Kumar P, Pirjola L., Ketzel M., Harrison R.M., 2013. Nanoparticle emissions from 11 non-vehicle exhaust sources - a review. *Atmos. Environ*., 67, 252-277.
- Kumar P., Morawska L., Harrison R.M., 2012. Nanoparticles in European Cities and Associated Health Impacts. In: Viana M. (eds) Urban Air Quality in Europe. *The Handbook of Environmental Chemistry*, vol 26. Springer, Berlin, Heidelberg.
- Kumar P., Robins A., Vardoulaki S., Britter R. 2010. A review of the characteristics of nanoparticles in the urban atmosphere and the prospects for developing regulatory controls. *Atmos. Environ.* 44(39), 5035-5052.
- Li N., Sioutas C., Froines J.R., Cho A., Misra C., Nel A. 2003. Ultrafine particulate pollutants induce oxidative stress and mitochondrial damage. *Environ. Health Perspect.* 111:455–460.
- Lin C., Chen S. Huang K., Lee K., Wen-Jhy, Lin W., Wen-Yinn, Tsai J., Chaung H., 2008. PAH-Induced Carcinogenic Potency, and Particle-Extract Induced Cytotoxicity of Traffic-Related Nano/Ultrafine Particles. *Environ. Sci. Technol.* 42, 4229–4235.
- Marris, H.; Deboudt, K.; Augustin, P.; Flament, P.; Blond, F.; Fiani, E.; Fourmentin, M.; Delbarre, H. Fast changes in chemical composition and size distribution of fine particles during the near-field transpot of industrial plumes, 2012. *Sci. Total Environ*. 427-428, 126-138.
- Morawska L., Ristovski Z., Jayaratne E.R., Keogh D.U., Ling X., 2008. Ambient nano and ultrafine particles from motor vehicle emissions: characteristics, ambient processing and implications on human exposure. *Atmos. Environ.* 42, 8113-8138.
- Nel A., Air Pollution-Related Illness: Effects of Particles. May 2005, *Science,* 804-806.
- Oberdoster G., 2001. Pulmonary effects of inhaled ultrafine particles. *Int. Arch. Occup. Environ. Health,* 74:1-8.
- Ondráček J., Schwarz J., Ždímal V., Andělová L., Vodička P., Bízek B., Tsai C.-J., Chen S. C., Smolík J., 2011. Prague contribution of the road traffic to air pollution in the Prague city (busy speedway and suburban crossroads). *Atmos. Environ.,* 45(29), 5090-5100.

- Pope C. A., Turner M. C., Burnet, R., Jerrett M., Gapstur S. M., Diver W. R., Brook R. D., 2014. Relationships between Fine Particulate Air Pollution, Cardiometabolic Disorders and Cardiovascular Mortality. *Circ. Res.* 116(1):108-15.
- Ravindra, K.; Sokhi, R.; Van Grieken, R. Atmospheric polycyclic aromatic hydrocarbons: source attribution, emission factors and regulation*. Atmos. Environ.* 2008, 42 (13), 2895-2921.
- Riffault V., Arnds J., Marris H., Mbengue S., Setyan A., Alleman L. Y., Deboudt K., Flament P., Augustin P., Delbarre H., Wenger J., 2015. Fine and ultrafine particles in the vicinity of industrial activities: a review. *Environ. Sci. Technol*., 45 (21), 2305-2356.
- Ruuskanen J., Tuch Th., Ten Brink H., Peters A., Khlystov A., Mirme A., Kos G.P.A., Brunekreef B., Wichmann H.E., Buzorius G., Vallius M., Kreyling W.G., Pekkanen J. 2001. Concentrations of Ultrafine, Fine and $PM_{2.5}$ Particles in Three European Cities; *Atmos. Environ.* 35, 3729-3738. 10.
- Schwarz J., Cusack M., Karban J., Chalupnickova E., Havranek V., Smolik J., Zdimal V., 2016. $PM_{2.5}$ Chemical Composition at a Rural Background Site in Central Europe, Including Correlation and Air Mass Back Trajectory Analysis. *Atmos. Res.* 176-177, 108-120.
- Schwarz J., Kuguang C., Maenhaut W., Civic M., Hovorka J., Smolik J., 2008. Elemental and organic carbon in atmospheric aerosols at downtown and suburban sites in Prague. *Atmos. Res.,* 90(24), 287-302.
- Seinfeld, J. H., & Pandis, S. N. 2006. Atmospheric chemistry and physics: From air pollution to climate change. Hoboken, N.J: J. Wiley.
- Sioutas, C.; Delfino, R. J.; Singh, M. Exposure assessment for atmospheric ultrafine particles (UFPs) and implications in epidemiological research, 2005. *Environ. Health Persp.* 113 (8), 947-955.
- Stevens, R. G., Pierce, J. R., Brock, C., Reed, M. K., Crawford, J. H., Holloway, J., Ryerson, T., Huey, L. G., and Nowak, J. B. (2012). Nucleation and growth of sulfate aerosol in coal-fired power plant plumes: sensitivity to background aerosol and meteorology. *Atmos. Chem. Phys.* 12, 189–206.

- Stölzel M., Breitner S., Cyrys J., Pitz M., Wölke G., Kreyling W., Heinrich J., Wichmann H.E., Peters A. 2007. Daily mortality and particulate matter in different size classes in Erfurt, Germany. *J Expo. Sci. Environ. Epidemiol.* 17:458–467.
- Topinka, J., Rossner, P., Milcová, A., Schmuczerová, J., Penčíková, K., Rossnerova, A., Ambrož, A., Štolcpartová, J., Bendl., J., Hovorka, J, Machala, M., 2015. Day-to-day variability of toxic events induced by organic compounds bound to size segregated atmospheric aerosol. *Environ. Poll*., 202, 135-145.
- Venkatamaraan C., 1999. Comparison of particle lung doses from the fine and coarse fractions of urban PM_{10} aerosols. *Inhal. Toxicol.,* 11:2, 151-169.
- Weitkamp, E. A.; Lipsky, E. M.; Pancras, P. J.; Ondov, J. M.; Polidori, A.; Turpin, B. J.; Robinson, A. L. 2005. Fine particle emission profile for a large coke production facility based on highly time-resolved fence line measurements. *Atmos. Environ.,* 39 (36).
- Zhang, K. M., and A. S. Wexler, 2002. A hypothesis for growth of fresh atmospheric nuclei*, J. Geophys. Res.,* 107(D21), 4577.

2. Atmospheric particles measurements

Particle number, mass concentration, size distribution and chemical composition can be measured using different techniques, sampling strategies, spatial and temporal resolutions. The following sections provide a brief overview of the sampling techniques with focus on the instruments used in the manuscripts.

2.1 Online measurements

In-situ monitoring methods for the analysis of aerosol properties with increase sample frequency and decrease operating costs is the online method. Well established instruments to measure particle number and mass size distributions are the aerosol size spectrometers.

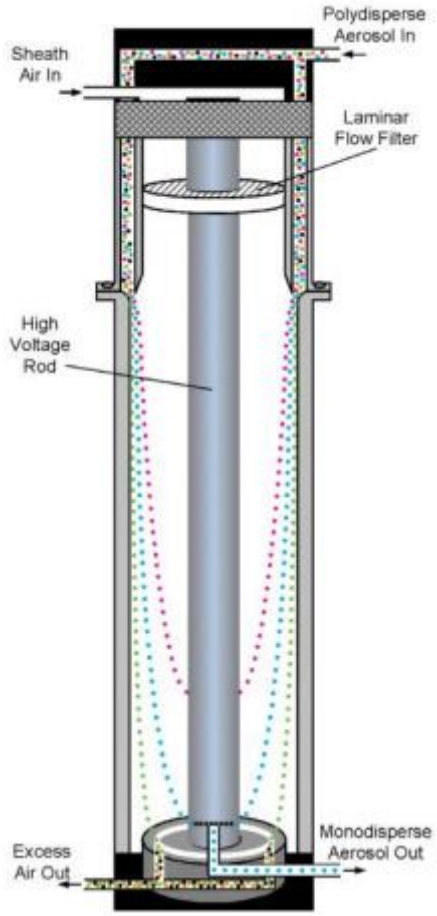

Figure 3 – DMA schematic representation (*www.tsi.com*)

The **Scanning Mobility Particle Sizer (SMPS)** consists of an electrostatic classifier and a condensation particle counter (CPC). The electrostatic classifier contains an impactor, a bipolar charger and a Differential Mobility Analyser (DMA). The aerosol enters the system through the sampling inlet at a determined sample rate and is passed to a bipolar charger which neutralizes the particles according to Boltzmann charge distribution: positive and negative charges are distributed amongst the particles in a predictable manner, providing the aerosol reaches equilibrium in the neutraliser (Wiedensholer, 1988). The particles then enter the DMA where they are classified according to their electrical mobility. The DMA consists of a cylinder with a charged rod in the centre. The main flow of air through the DMA is particle free sheath air, with a laminar flow. The sampled poly-dispersed aerosol enters the DMA and particles with a positive charge move across the sheath flow towards the negatively charged central rod, at a rate determined by the particle's electrical mobility. The electrical mobility is proportional to the diameter: smallest particles have the largest electrical mobility. At a certain voltage, only particles of a certain electrical

mobility pass through the exit slit of the DMA, and reach the CPC to be counted. This determines the particle concentration in that size range. The probability that particles with certain mobility that enter the classification region of the DMA will be included in the classified aerosol flow when the flow rates and applied voltage are for a characteristic mobility is given by the classifier *transfer function* (Collins et al., 2004). Any particle of a certain size with multiple charges will appear in bins with smaller, more mobile particles. Using the known charge distribution, the number counts in the respective bins are reduced accordingly. By sequentially making these corrections to the succession of channels from the lowest to highest mobility, detected particles are attributed to the counting bins for mobilities corresponding to single charging. The SMPS spans a size range from few nm until approximately 700 nm. The upper limit is determined by the biggest particles carrying multiple charges that may be over counted in the highest classification voltage. To avoid this problem, the DMA is used with a precut impactor.

The **Condensation Particle Counter (CPC)** detects and counts particles down to 3 nm (McMurry et al., 2000) by laser scattering, in a very similar way to standard optical particle counters, but in the CPC particles are first grown by condensation to an easy detectable size (10 μm). The original particle constitutes only a minuscule fraction (~10^{-3} 10^{-9}) of the detected droplet. In a supersaturated vapour suspended particles act as nuclei for vapour condensation and may grow to form droplets (heterogeneous nucleation). Supersaturation occurs when the saturation ratio is bigger than 1, and is generally expressed as a percentage. Droplets can form heterogeneously at supersaturations of less than 1%, same as the process of clouds formation in the atmosphere. The size of aerosol particles which will act as condensation nuclei is a function of the supersaturation. In a CPC, supersaturation is carefully controlled to a high value, (for a water CPC it is typically up to 6%) (Franklin et al., 2010), but below the critical supersaturation so that droplets do not cluster homogeneously. There are a number of techniques by which such supersaturations may be achieved; in the most of commercially available CPC's, supersaturation is achieved by heat transfer from the warm aerosol to the walls of the condenser, which are typically maintained at 10°C.

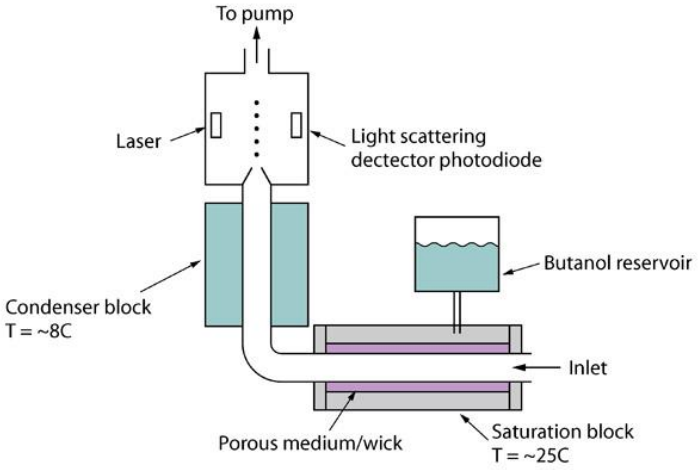

Figure 4 – Schematic representation of a CPC (*www.cas.manchester.ac.uk*).

The **Aerodynamic Particle Sizer (APS)** measures size range 0.5-20 µm using the principle of inertia. In this instrument the particle and sheath flow are constricted through a nozzle, accelerating the airflow. The APS measures particle velocity by passing the particles through two laser beams distant 200 microns. A particle passing through both beams produces two pulses of scattered light. The time between the pulses is related to the particle velocity and hence to the particle aerodynamic diameter. Because the APS does not measure aerodynamic diameter in still air problems can arise when measuring aerosols with different densities. The flow velocity of 150 m/s results in high Reynolds numbers which are outside the Stokes regime (Wang and John, 1987). In the non-Stokesian regime, the particle acceleration depends not only on the aerodynamic diameter but also on physical diameter, hence on particle density.

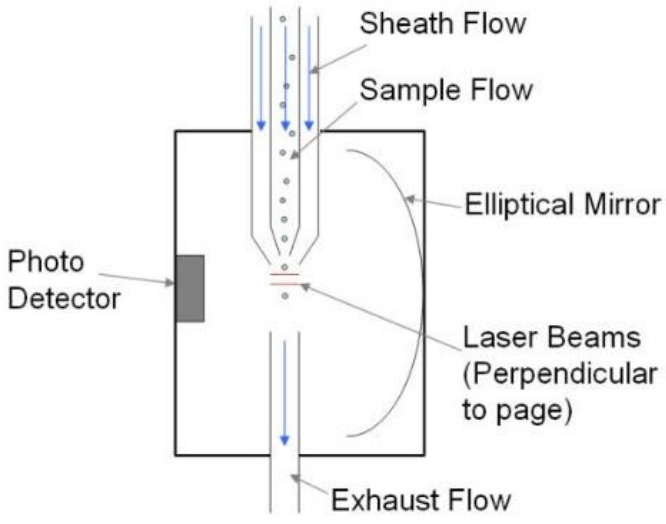

Figure 5 – Schematic representation of APS optic chamber (*www.cas.manchester.ac.uk)*

The non-Stokes error can be corrected if the density is known; however, when measuring the outdoor atmospheric aerosol the density can be difficult to estimate. Density of 1.5 μgm^{-3} is used as standard for urban atmospheric aerosol (Hinds, 1999).

OC and EC are usually measured by in-situ **thermal optical methods**. These measurements are typically performed on filter samples, but

online analysis is also possible with commercial instruments. The analysis is performed in two steps: (i) the measurement of OC in an oxygen-free environment subjected to a temperature gradient to vaporize organic materials which will be quantitatively converted to CO_2, and finally reduced to methane; (ii) the measurement of EC under oxidizing conditions leading again to methane. The methane is detected by a flame ionization detector, which enables the quantification of OC and EC sequentially.

2.2 Offline techniques

In offline analysis, aerosol particles are collected on a filter or grid and then analysed with various techniques. The main benefits of the offline methods are determination of (i) structural information, such as crystallographic structure, coatings, embedding, or aggregation and (ii) heavy metal content, both of which are not well characterized by the currently available online techniques. The main disadvantages are (i) longer time integration and delay in sample analysis (samples must be taken to a remote laboratory) and (ii) challenges in source apportionment (longer sampling and analysis times are required, leading to smaller datasets than typically obtained with online techniques). The aerosol collection on a filter is typically based on impaction principles (Hinds, 1999). The impactors are used to separate the particles according to their aerodynamic diameter. **Multistage impactors** (Figure 6) measure the mass of the particles collected at each stage, which allows for gravimetric analysis under temperature and relative humidity-controlled conditions. Sampling artifacts can occur when reactive or semi-volatile species are sampled and during the gravimetric analysis. A largely employed cascade impactor is the personal cascade

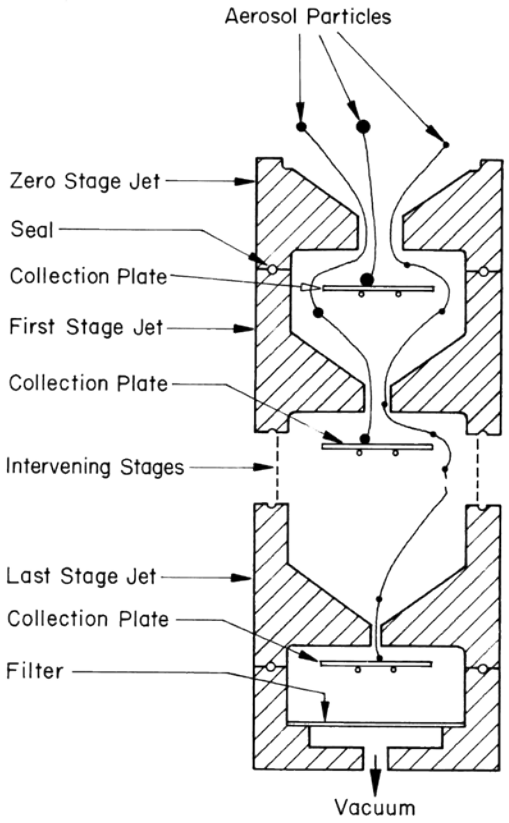

Figure 6 – Schematic representation of multistage cascade impactor (www.pharmacopeia.cn)

impactor sampler (PCIS) (Misra et al., 2002). Particles can be separated in the following aerodynamic particle diameter ranges: <0.25; 0.25 to 0.5; 0.5 to 1.0; 1.0 to 2.5; and 2.5 to 10 µm. The 8DRUM impactor (Cahill and Barnes, 2009) collects particulate matter on rectangular strips of Mylar film fixed to 8 rotating drums downstream 8 jets, with theoretical 50% cut-off collection aerodynamic diameters of 0.09 to 0.26, 0.26 to 0.34, 0.34 to 0.56, 0.56 to 0.75, 0.75 to 1.15, 1.15 to 2.5, 2.5 to 5 µm, and programmable between 0.4 and 48 h. The impactor operates continuously with a flow rate of 8 L/min drawn by an external pump. To obtain the elemental concentration, the Mylar foils are analyzed using X-ray fluorescence.

The size and shape of atmospheric particles are commonly investigated using scanning electron microscopy (SEM) or transmission electron microscopy (TEM) for the finest fraction. Energy dispersive X-ray spectrometry, used in combination with SEM (SEM/EDX) can also be useful for identification of elements contained in single particles.

Among offline methods, **chromatography** is widely used to quantify chemical components in atmospheric aerosol, for example water soluble ions and organic carbon species and can help reach chemical mass closure. The most widely employed techniques are high performance liquid chromatography (HPLC), gas chromatography (GC), ion chromatography (IC). These techniques are destructive because they typically require filter treatments, for example digestion of the particles using acids or bases. The analysis of organic compounds, such as PAHs, are usually carried out by gas chromatographic methods coupled to various detectors depending on the targeted compounds (mass spectrometers, flame ionization detectors, UV detectors).

2.3 Ground based measurements

In aerosol science, a sound study on atmospheric particles and air pollution requires careful preparation. One of the most important steps in a study is the collection of all the relevant existing information about atmospheric pollution in the area under examination (Belis et al., 2012). For **source apportionment**, sites representative of the mixture of sources in a given area are preferable to sites influenced by specific sources. To establish the number and location of sources, it is necessary to study the emission source distribution, wind roses and typical dispersion patterns (upwind, downwind of major sources) (Kim Oanh et al., 2009). The **Conditional Probability Function** (CPF; Ashbaugh et al., 1985) is a common tool used to analyze point source impacts from varying wind directions using the source contribution

estimates from receptor models coupled with the wind direction values measured on site (Kim et al., 2003). Another method combining the aerosol data with the air parcel backward trajectories is the **Potential Source Contribution Function** (PSCF) calculation. PSCF produces a probability field for source emission potential and it implies the choice of a threshold above which the air mass is considered polluted.

In addition to having a good conceptual understanding of the sources in the study area, it is important to understand the physical nature of the system. The **topography**, natural or artificial, has a significant influence on the local source receptor relationships (e.g. Chow et al., 2007), and a lack of understanding of the physical system can lead to problems in interpreting and understanding the source apportionment results. A number of elements of the physical system should be identified and incorporated into the planning and execution of a project as well as in the analysis of the subsequently generated data, in particular: mountains/valley terrain, tall buildings, local source complexes, transportation information, and distant sources.

Prevailing wind directions determine the probability of emitted materials being transported to the measurement site. Although primary emissions are diluted over time and distance, secondary pollutants, e.g. produced by gas-to-particle conversion processes, can increase the concentrations over relatively long distances, particularly for species such as secondary sulfate and secondary organic aerosols that take time to form in the atmosphere.

The minimum number of samples required to achieve representative study of the totality of the sources cannot be established a priori as it depends on the amount of information contained in the dataset. The criteria is: there should be enough samples to catch the variability of the sources, including samples where some sources are absent or negligible. In filter-based systems, the most common configuration is the collection of 24-hour samples. 24-hour **integration time** is considered to be representative of all the sources occurring in one day-to-night cycle and hence an appropriate unit for data elaboration (Belis et al., 2012). A practical reason for selecting 24-hour sampling also derives from the need to collect enough mass for chemical analysis. This limitation is especially true for low-volume samplers when PM levels are low; in urban environment, four- to six-hour sampling times can be enough material for major component analyses (e.g. Vecchi et al., 2009; Bernardoni et al., 2011). With high-volume samplers, two- to four-hour samples can be sufficient. If the measured properties has fast dynamics, **high time resolution** measurements are necessary. Higher time resolutions can

be achieved using aerosol size spectrometers that can measure particle number/mass concentration every 5 minutes, or semi-continuous systems for analysis of physical or chemical properties, for example semicontinuous EC/OC, with resolutions ranging from a few minutes to one hour. Physical parameters associated with particle size or optical properties (scattering, absorption) can be obtained with time resolutions close to a minute or less.

2.4 Airborne measurements in the Planetary Boundary Layer

Measurement in aerosol science are generally performed at a ground receptor site. Few studies employ **mobile monitoring platforms**, for example airships, airplanes, drones (Frick et al., 2000, Kantor et al., 2001, Brock et al., 2002, Banic et al., 2006, Brady et al., 2016,). Measurements of particle concentration and size distributions over a broad vertical range of the **planetary boundary layer** (PBL), especially its lowest part (300 m above ground level) are rare. The PBL constitutes the lower region of the troposphere, strongly influenced by interaction with the surface. Surface heating during the day results in a turbulent, well-mixed PBL, in which surface heating can sustain high boundary layer heights (ca. 1-3 km). The surface cooling after sunset creates a much shallower stable nocturnal boundary layer (ca. 100-200 m) in which the remainder of the daytime PBL is disconnected from the surface layer. A temperature inversion separates the nocturnal boundary layer (NBL) from the residual layer above almost until noon (Li et al., 2014). This **inversion** restricts vertical mixing of air constituents, and isolates the residual layer from influences of Earth's surface, as long as the temperature inversion is maintained, resulting in enhanced particles concentration. Within the PBL, the **vertical concentration profiles** of aerosols and trace gases are normally nonlinear due to the natural air turbulence caused by wind shear and temperature gradients.

Airships have been used for PBL profiling (Hoppel et al., 1994, Hovorka et al., 2016): the slow speed of an airship makes it an ideal platform to do **high spatial resolution vertical profile**. In case of elevated emission sources, for example stack plumes, with unpredictable dispersion conditions, airships allow the high spatial resolution horizontal profiling and the plume tracking. The aerosol **plumes** can be transported by complex wind patterns leading to inhomogeneous plume dispersion. Additionally, plumes are mostly emitted by high-temperature processes and can evolve very quickly inside the plume: physical processes like condensation, coagulation and heterogeneous reactions can occur rapidly to form complex heterogeneous particles mixtures.

Accurate assessment of the degree to which surface measurements represent the entire PBL are required for validation of remote sensing techniques. Current research activities employing satellites demonstrate the necessity to constrain aerosol and trace gas profiles within the troposphere for improved interpretation of satellite observations (NASA's study DISCOVER-AQ).

References

- Ashbaugh L.L., Malm W.C., Sadeh W.Z., 1985. A residence time probability analysis of sulfur concentrations at Grand Canyon National Park. *Atmos. Environ*., 19(8):330 1263-1270
- Banic C., Leaitch W. R., Strawbridge K., Tanabe R., Wong H., Gariepy C., Simonetti A., Nejedly, Z., Campbell J. L., Lu J., Skeaff J., Paktunc D., MacPherson J. I., Daggupaty S., Geonach H., Chatt A., Lamoureux M., 2006. The physical and chemical evolution of aerosols in smelter and power plant plumes: an airborne study. *Geochem. Explor. Environ. Anal*. 6, 111–120.
- Belis C. A., Larsen B.R., Amato F., El Haddad I., Favez O., Harrison R. M., Hopke P. K., Nava S., Paatero P., Prévôt A., Quass U., Vecchi R, Viana M., 2014. European Guide on with Receptor Models Air Pollution Source Apportionment. Joint Research Centre Reference Report, http://www.jrc.ec.europa.eu.
- Bernardoni, V., Vecchi, R., Valli, G., Piazzalunga, A., Fermo, P., 2011. PM_{10} source apportionment in Milan (Italy) using time-resolved data. *Sci. Total Environ.* 409, 4788-4795.
- Brady J.M., Stokes M.J., Bonnardel J., Bertram T.H., 2016. Characterization of a Quadrotor Unmanned Aircraft System for Aerosol-Particle Concentration Measurements. *Environ. Sci. Technol.* 50, 1376-1383.
- Brock C., Washenfelder R., Trainer M., Ryerson T., Wilson J., Reeves J., Huey G., Holloway J., Parrish D., Hubler G., and Fehsenfeld F., 2002. Particle growth in the plumes of coal-fired power plants. *J. Geophys. Res.* 107(D12).
- Cahill T. A. and Barnes D. E., 2009. Comparison of fine mass, UC Davis DRUM versus FRM, at the ARB 13_{th} and T. Street Site, UC Davis DELTA Group, and the Breathe California of Sacramento-Emigrant Trails Health Effects Task Force.

http://delta.ucdavis.edu/Reports/ARB%2013th%20and%20T%20FINAL%20Report.pdf

- Collins D.R., Cocker D.R., Flagan R.C., Seinfeld J.H., 2004. The Scanning DMA Transfer Function. *Aerosol Sci. Technol.,* 38:833-850.
- DISCOVER AQ - https://www.nasa.gov/mission_pages/discover-aq/index.html
- Franklin L. M., Bika A. S., Watts W. F., Kittelson D. B. 2010. Comparison of Water and Butanol Based CPCs for Examining Diesel Combustion Aerosols, *Aerosol Sci. Technol.*, 44:8, 629-638
- Frick G.M., Hoppel W.A., 2000. Airship measurements of ships exhausts plumes and their effect on marine boundary layer clouds. *J. Atmos. Sci.*, 57, 2625–2648.
- Hinds W. C. 1999. Aerosol technology, Properties, Behavior, and Measurement of Airborne Particles, Wiley (second edition), U.S.A.
- Hoppel W. A., Frick G. M., Fitzgerald J. W., Larson R. E., 1994. Marine boundary layer measurements of new particle formation and the effects non precipitating clouds have on aerosol size distribution. *J. Geoph. Res.* 99(D7), 14443–14459.
- Hovorka J., Leoni C., Dočekalová V., Ondráček J. and Naděžda Zíková, 2016. Aerosol Distribution in the Planetary Boundary Layer aloft a Residential Area. *6 IOP Conf. Ser.: Earth Environ. Sci.* 44 052017.
- Kantor G., Wettergreen D., Ostrowski J.P., Singh S., 2001. Collection of environmental data from an airship platform. *In: proceedings of SPIE Conference on Sensor Fusion and Decentralized Control IV,* October 28-29, 2001, vol. 4571, pages: 76-83.
- Kim E., Hopke P.K., Edgerton E.S. 2003. Source identification of Atlanta aerosol by positive matrix factorization. *J. Air Waste Manag. Assoc*, 53, pp. 731-739.
- Kim Oanh N.T., Pongkiatkul P., Upadhyay N., Hopke P.K., 2009. Designing ambient particulate matter monitoring program for source apportionment study by receptor modeling. *Atmos. Environ.* 43(21), 3334-44.
- Li X., Rohrer F., Hofzumahaus A., Brauers T., Häseler R., Bohn B., Broch S., Fuchs H., Gomm S., Holland F., Jäger J., Kaiser J., Keutsch F. N., Lohse I., Lu K., Tillmann R., Wegener R., Wolfe G. M., Mentel T. F., Kiendler-Scharr A., Wahner A., 2014.

Missing Gas-Phase Source of HONO Inferred from Zeppelin Measurements in the Troposphere. 2014, *Science*, 18 April, 292-296.

- McMurry P., 2000. A review of atmospheric aerosol measurements, *Atmosp. Environ.* 34, 1959-1999.
- Misra, C., Singh, M., Shen, S., Sioutas, C., & Hall, P., 2002. Development and evaluation of a personal cascade impactor sampler (PCIS). *J. Aerosol Sci*. 33(7), 1027-1047.
- Vecchi R, Bernardoni V, Fermo P, Lucarelli F, Mazzei F, Nava S, Prati P, Piazzalunga A, Valli G., 2009. 4-hours resolution data to study PM_{10} in a hot spot area in Europe. *Environ. Monit. Assess.* 154(1-4), 283-300.
- Wang H. and John W. 1987. Particle Density Correction for the Aerodynamic Particle Sizer, *Aerosol Sci. Technol.,* 6(2), 191-198.
- Wiedensohler A., 1988. An Approximation of the Bipolar Charge Distribution for Particles in the Submicron Size Range. *J. Aerosol Sci.* 19. 387-389.

3. Source apportionment

3.1 Aerosol particles sources by number size distribution

Atmospheric aerosol particles can be emitted by **natural or anthropogenic sources**. Naturally occurring particles are typically produced by the oceans (sea spray), biomass fires, and dust from arid soils, volcanic eruptions, as well as biological sources, including pollen, plant debris, animal fragments, algae, fungi, bacteria, spores, and viruses, and also secondary organic aerosol (SOA) particles formed in the atmosphere from biogenic volatile organic compounds (VOCs). Anthropogenic emissions arise from many sources: fossil fuel burning in vehicles, biomass burning for domestic heating, power plants and industrial processes, waste incineration, crushing and demolition processes, surface mining, metal smelting.

Particles emitted from different sources show different **particle NSD**, and the shape of a measured NSD in the atmosphere depends on the source nature and atmospheric processing between source and receptor. The particle NSD changes with increasing distance from local emissions. For example, Zhu et al., 2002, reported the ultrafine particle size distribution changes significantly with increasing distance form a freeway. Particle NDS altered due to nucleation, coagulation, condensation, dilution. The specific characteristics of the **modal structure** of distributions, as well as the particles **temporal pattern**, imply that particle size distribution and concentrations profiles may be utilized to help the source identification, where knowledge gaps are present.

Vehicles emissions are considered a major source in urban atmosphere; part of the emissions is generated directly from the engine or they form in the air by condensation and nucleation of hot gaseous emissions. The combustion generated particles consist mostly of solid graphitic carbon with a smaller amount of metallic ash, hydrocarbons and sulfur compounds (Vu et al., 2015). These particles are found mainly in the Aitken and accumulation mode, with a size ranging from 30 nm to 0.5 μm. The smaller sized mode is believed to be formed by binary nucleation of H_2SO_4-H_2O or ternary nucleation H_2SO_4-NH_3-H_2O, which comprise small hydrated sulfuric acid core coated with condensed hydrocarbons. (Harrison, 1999). Non-exhaust particles which typically arise from road-tyre interaction, break wear, and re-suspension also contribute significantly to urban concentrations, generating particles with a wide range of diameters, from few hundred nanometers to tens of micrometers.

Industry is another major contributor to air pollution in urban areas. The emissions from industrial combustion processes contribute mainly to the fine and ultrafine fraction (Riffault et al., 2015). Weitkamp et al, (2005) registered industrial plumes with UFPs peaking around 40 nm; Marris et al., 2012, observed particles of 10 – 30 nm downwind from a large steel complex. Industrial sources can emit also coarse particles, dall'Osto et al. (2008) in a study on Port Talbot, found Fe-rich particles with a mass size distribution peaking at 6 μm.

Combustion of coal and biomass generates particles ranging from few nanometers to millimeters, and the small particles initially formed by nucleation and chemical reactions and growth due to coagulation contain predominantly condensed and semi-volatile materials while the larger consist of carbonaceous materials, inorganic fly ash and trace elements. The median diameter of the number size distribution varies between 30-80 nm, depending on a range of factors: coal type, combustion temperature, dilution, residence time (Vu et al., 2015). Also freshly generated particles from biomass burning consist mostly of carbon with 10-20% of black carbon and inorganic species found predominantly in the accumulation mode. Most studies have shown a consistent size distribution with count median diameter of 100-160 nm for fresh smoke (Janhall et al., 2010); during the aging process, the count median diameter increase to > 200 nm by coagulation/condensation.

Long range transported aerosol comprises mostly accumulation mode particles with the major number peak mode around 100-200 nm. During long range transport SO_2 can oxidize leading to nucleation and then growth, hence sometime long range transported air masses contain UFPs (Wang et al., 2011). The long range transported particle size distribution at remote sites has been observed, for example desert dust and anthropogenic aged sulfates in the size range 100-200 nm were measured by Raes et al., 1997, in Tenerife.

New particles formation by nucleation account for a significant fraction of the total number of particles in the atmosphere; nucleation events are found in both polluted and clean environments (Kulmala et al., 2004). Among natural sources, the marine particle number spectra show two modes: at Aitken mode with a mean diameter around 40-52 nm and accumulation mode with a mean diameter of around 150-175 nm (Vu et al., 2015). A sea salt mode with mean diameter above 400 nm is frequently found in the marine boundary layer (Heintzenberg ae al., 2000). In indoor environments, cooking emissions are a major source of submicron particles. Wallace (2006) found that aerosol concentrations generated during cooking are predominantly in the ultrafine size range. The particles size distribution from

cooking activities has been reported as unimodal with a peak between 20 – 70 nm or 100-160 nm depending on the food type and the cooking temperature (Hussein et al., 2006). Cooking aerosol can contribute significantly to ambient concentration: Harrison et al., 2011, found that the cooking contribution at a major kerbside in London is 7%.

3.2 Receptor modelling with PMF

In aerosol science, **receptor models** are mathematical approaches used for identifying and quantifying different atmospheric particles sources. Specifically, PMF model identifies and quantifies the contribution to each source to the samples. The identification is based on key species (tracers), combination of species, or size distribution characteristics (Hopke, 2016).
The fundamental principle of PMF is the **mass conservation** and the goal of PMF is to solve the chemical mass balance equation. The main physical **constraint** is that the source composition must be positive. In fact, a source does not emit a negative quantity of pollution, or it becomes a sink. Also, the sum of the predicted contributions for each source must be less than or equal to the total measured mass for each variable. The model performs a **matrix factorization**, which consists of decomposing a matrix of sample data X into **two sub-matrices**. The two sub-matrices contain the species profile for each factor (G), and the amount of mass/number contributing by each factor to each individual sample (F), plus the unexplained part E (difference between measured and calculated species concentration) (Brown et al., 2015).

$$X = GF + E$$

PMF solutions are interpreted based on: modal characteristics of number and volume size distribution, diurnal patterns of contributions, source contribution to total number or volume concentration, correlation of the G matrix with the measured gaseous or composition species, the source directionality by the local wind trajectories and conditional probability functions (Ogulei et al., 2006). In addition, many studies combine PMF results with auxiliary information for example to link factor profiles to source type. The correlation between the G matrix (source contribution) and auxiliary information such as chemical composition data contributes towards the identification of the nature of the sources.

The majority of the studies on source apportionment apply the PMF on the mass chemical composition of atmospheric particles. Recently, source apportionment studies focus not only on particle mass, but also NSD (Harrison et al., 2011, Beddows et al., 2015, Masiol et al., 2016, 2017, Sowlat et al., 2016). The analysis of the mass chemical composition data distinguishes sources contributing mainly to particle mass, while the analysis of the particle NSD identifies sources contributing principally to particle number, enabling the source apportionment down to nanoparticles. In fact, as UFP dominate the particle number concentration, this approach based on particle size spectra data provides insight into the sources of UFP which may be not possible to achieve with source apportionment based on chemical composition, due to the low contribution of UFPs on the PM mass. Source profiles based on size spectra provide the source information from the physical aspect, which differs from the chemical aspect.

There is an urgent need to know the consistency or discrepancy of sources obtained from the two methods. However, currently there are only few studies published on the relationship of the source apportionment results from the two kinds of data set. Individual PMF analysis of size spectra and mass chemical composition was conducted by Beddows et al., (2015). The factors resolved with the two methods overlap and allowed a combined view of the results. Gu et al. (2011) showed moderate to strong correlations between factors obtained with particle NSD and with chemical composition.

3.3 NSD PMF rules of thumb

This section has the purpose to provide rules of thumb for the preparation of the input for NSD PMF, the interpretation of the diagnostics and of the results. These rules of thumb were accumulated during a detailed study of the model, literature study, and discussions during conferences. These rules are meant to give the elements to understand the quality of the output. The interpretation of the PMF results and the choice of the best solution is the most crucial step that must be done by the operator. All the diagnostics must be evaluated and the best solution is a trade-off between its physical meaning, the diagnostics of the model and the goodness of the fit. The knowledge of the EPA PMF 5.0 User Guide is recommended prior to this section.

- **Prepare the concentration and uncertainty matrices.** To smooth the size distribution data and reduce the uncertainty in the number concentration, it is useful to reduce the

original number of bins. Different methods exist in the literature how to calculate the uncertainties for the PMF.

- **Decide if a variable is strong/weak/bad**. First, to understand if a variable is strong/weak/bad, a detailed knowledge of the dataset, of the sampling and the analytical techniques is needed. Than the signal to noise ratio (S/R) must be observed. A variable is weak if it has signal and noise in comparable amounts (S/R=1). Similarly, variables having more noise than signal are termed bad variables (Reff et al., 2007). Downweighing the weak variables by a factor 3 is recommended, to protect in the case that the error level of some variables has been underestimated. Regarding bad variables, where hardly a signal is visible from the noise, the recommendation is to omit these variables, or to strongly downweight by a factor 5 or 10 (Paatero and Hopke, 2003). It is important to know whether a variable can be retained in the analysis. For the particle number size distribution, the weak variables that might be considered for exclusion are typically the first and last SMPS size bins, and the last APS bins, due to the high variability and the presence of zeroes. Also, the overlap variable between SMPS and APS has to be observed.
- **Observe the time series.** It is necessary to determine whether temporal patterns are present and if there are unusual events or outliers. Extreme events can be excluded from the modeling if they perturb the solution, they cause high scale residuals number, they generate spurious factors.
- **Choose the numbers of factors.** The model must be run with different number of factors and for each run diagnostics must be evaluated. The choice of the factors number is crucial. Too few factors lead to the combination of sources, while too many factors split one source into two non-existing sources. To understand the correct number of factors is necessary to observe the Q value. The $Q_{theoretical}$ gives information about the quality of the fit since the optimal solution should have a Q_{true} not too different from the $Q_{theoretical}$. The ratio $Q_{true}/Q_{theoretical}$ must be around 1. In some cases, the optimal solution does not fully satisfy this requirement, for example when a dataset contains a lot of weak variables. The $Q_{theoretical}$ can be calculated according to the EPA PMF 5.0 User Guide.
- **Run the model.** To find the optimal solution, several runs with different conditions must be made, and the output must be compared. Different solutions can be found

due to the mathematical nature of the matrix factorization and the constrained applied.

- **Analyze the scaled residuals**. If the input data are solid, the plot of scaled residuals values against their frequency should be normally distributed, with the majority between -3 and +3. If some residuals are outside this region, it is possible that there are extreme events or outliers in the data, or the number of factors is not optimal, it might be too low and a factor can be overlooked. Distribution with large spread indicates that the uncertainty is too low, while a distribution centered near zero indicates that uncertainty is too high.
- **Observe the goodness of fit**, to compare predicted species with the original concentrations, using linear regression and time series. The observed/predicted regression coefficients must be as close as possible to 1 and the time series of modeled variables should fit as best as possible the time series of the original variable.
- **Observe the G-plots**. The G-plots show scatter plots of one factor versus another factor are they are important to verify the relationship between the factors. The G plots are generated with the assumption that the determined factors are uncorrelated between each other. The more stable solution will have many samples with zero contribution on both axes. Imagining straight lines passing through the origin of axes including all the points between them, the lines should be as much close to the Cartesian axes. If the points are not aligned with the Cartesian axes, an edge can be observed in the plot, which means there might be an overlooked factor or there is rotational ambiguity in the solution.
- **Evaluate the error with bootstrap (BS)**. A number of phenomena can contribute to the uncertainty of the solution modeled by PMF: temporal variation of PM sources, measurements errors, sampling variability, errors in the model, for example wrong factor number (Reff et al., 2007). The technique of bootstrapping is used to check the validity of the solution. Bootstrapping consist of randomly selecting n samples to create new datasets and executing the PMF on each new dataset. Multiple PMF solutions are generated using the series of data that are resampled version of the original dataset. Several hundreds of bootstrapped samples can be used, and the summary statistics are calculated by the model. In this study for example, 100 BS runs were performed for both NSD and chemical composition solutions. If the same sources

are identified in most of the bootstrapped samples, the solution of the original dataset can be considered stable. Mapping over 80% of the factor indicates that the number of factor can be appropriate.

- **Evaluate the error with displacement (DISP)** explores the rotational ambiguity in a PMF solution by assessing the largest range of source profile values without appreciable increase in the Q value. Each fitted element in the factor profile matrix in the base PMF solution is displaced from its fitted value far enough so that the Q increases by a predetermined amount called Q_{max}. The variables are perturbed within a certain interval, which has a certain extension (the boxplot in the results diagnostics). If the variable is perturbed so much that the factor changes its identity, a swap occurs. If a swap occurs, it means that the solution is not robust enough and another solution might be a better choice.
- **Evaluate the error with BS-DISP**. BS-DISP is a combination of the two methods, where each BS resample undergoes a DISP analysis. BS-DISP may take many hours to run due to the number of combinations that are evaluated, so first it can be useful to evaluate the BS-DISP with 50 runs, than with 100 for the final BS-DISP result.
- **Rotate the solution.** The PMF produces a large number of plausible solutions, because an infinite number of G and F matrices can produce the same minimum value of Q. The constraint of non-negativity is generally insufficient to wholly eliminate the rotational problem. The existence of this range of possible solution is called rotational freedom and contributes to the uncertainty of the PMF solution (Reff et al., 2007). To begin, to help determine whether an optimal solution has been found, the G plots for selected pairs of factors must be observed. Then, when the Fpeak profiles/contributions have to be observed, in order to fond deviations: if the Fpeak value increases or decreases in a particular species in a factor compared to the base model results. If deviations occur, there can be a different possible rotated solution that better represents the problem under analysis.

References

- Beddows, D.C.S., Harrison, RM., Green, DC, Fuller, GW., 2015. Receptor modeling of both particle composition and size distribution. *Atmos. Chem. Phys.* 15, 10107-10125.
- Brown S.G., Eberly S., Paatero P., Norris G., A., 2015. Methods for estimating uncertainties in PMF solutions: examples with ambient air and water quality data and guidance reporting PMF results. *Sci. Total Environ.*, 518-519 626-635.
- Dall'Osto M., Booth M.J., Smith W., Fisherb R., Harrison R.M., 2008. A study of the size distributions and the chemical characterization of airborne particles in the vicinity of a large integrated steelworks. *Aerosol Sci. Technol.,* 42, 981–991.
- Gu J., Pitz M., Schnelle-Kreis J., Diemer J., Reller A., Zimmermann R., Soentgen, J. Stoelzel, M., Wichmann H.E., Peters A., Cyrys, J., 2011. Source apportionment of ambient particles: comparison of positive matrix factorization analysis applied to particle size distribution and chemical composition data. *Atmos. Environ.* 45, 1849-1857.
- Harrison R. M., Jones M., Collins G. 1999. Measurements of the physical properties of particles in the urban atmosphere. *Atmos. Environ*. 33, 309-321.
- Harrison, R.M., Beddows, D.C.S., Dall'Osto, M., 2011. PMF analysis of wide-range particle size spectra collected on a major highway. *Environ. Sci. Technol.* 45, 5522-5528.
- Heintzenberg, J., Covert, D., Van Dingenen, R., 2000. Size distribution and chemical composition of marine aerosols: a compilation and review. *Tellus* B 52, 1104-1122.
- Hopke P. K., 2016. Review of receptor modelling methods for source apportionment. *J. Air Waste Manag. Assoc.,* 66(3), 237–259.
- Hussein T., Glytsos T., Ondracek J., Dohanyosov P., Zdímal V., Hameri K., Lazaridis M., Smolík J., Kulmala M., 2006. Particle size characterization and emission rates during indoor activities in a house. *Atmos. Environ.* 40, 4285-4307.
- Janhall S., Andreae M. O., and Poschl U., 2010. Biomass burning aerosol emissions from vegetation fires: particle number and mass emission factors and size distributions. *Atmos. Chem. Phys.*, 10, 1427–1439.

- Kulmala M., Vehkamaki H., Petaja T., Dal Maso M., Lauri A., Kerminen V.-M., Birmili W., McMurry P.H., 2004. Formation and growth rates of ultrafine atmospheric particles: a review of observations. *J. Aerosol Sci.* 35, 143-176
- Marris, H.; Deboudt, K.; Augustin, P.; Flament, P.; Blond, F.; Fiani, E.; Fourmentin, M.; Delbarre, H. Fast changes in chemical composition and size distribution of fine particles during the near-field transport of industrial plumes, *Sci. Total Environ.* 2012, 427-428, 126-138.
- Masiol M., Vu T. V., Beddows D. C. S., Harrison R. M., 2016. Source apportionment of wide range particle size spectra and black carbon collected at the airport of Venice (Italy), *Atmos. Environ.* 139, 56-74.
- Masiol, M., Hopke, P.K., Felton, H.D., Frank, B.P., Rattigan, O.V., Wurth, M.J. and LaDuke, G.H., 2017. Source apportionment of $PM_{2.5}$ chemically speciated mass and particle number concentrations in New York City. *Atmos. Environ.* 148, 215-229.
- Ogulei D., Hopke, P., Wallace, L., 2006. Analysis of indoor particle size distributions in an occupied townhouse using positive matrix factorization. *Indoor Air* 16, 204-215.
- Paatero P, Hopke PK., 2003. Discarding or down weighting high-noise variables in factor analytic models. *Anal. Chim. Acta* 490, 277–89.
- Raes F., Van Dingenen R., Cuevas E., Van Velthoven P.F., Prospero J.M., 1997. Observations of aerosols in the free troposphere and marine boundary layer of the subtropical Northeast Atlantic: discussion of processes determining their size distribution. *J. Geophys. Res. Atmos.* 102, 21315-21328.
- Reff A., Eberly S. I., Bhave, P. V., 2007. Receptor modeling of ambient particulate matter data using Positive Matrix Factorization: Review of existing methods, *J. Air Waste Manag. Assoc.* 57:146-154
- Riffault V., Arnds J., Marris H., Mbengue S., Setyan A., Alleman L. Y., Deboudt K., Flament P., Augustin P., Delbarre H., Wenger J. 2015. Fine and ultrafine particles in the vicinity of industrial activities: a review. *Environ. Sci. Technol.,* 45 (21), 2305-2356.
- Sowlat M. H., Hasheminassab S., Sioutas C., 2016. Source apportionment of ambient particle number concentrations in central Los Angeles using positive matrix factorization (PMF). *Atmos. Chem. Phys*. 16, 4849-4866.

- Vu T., Delgado Saborit J. M., Harrison R. M., 2015. Review: particle number size distribution form seven major sources and implications for source apportionment studies. *Atmos. Environ.* 122, 144-132.
- Wallace L., 2006. Indoor sources of ultrafine and accumulation mode particles: size distributions, size-resolved concentrations, and source strengths. *Aerosol Sci. Technol.* 40, 348-360.
- Wang, Y., Hopke, P.K., Chalupa, D.C., Utell, M.J., 2011. Long-term study of urban ultrafine particles and other pollutants. *Atmos. Environ*. 45, 7672-7680.
- Weitkamp E. A., Lipsky E. M., Pancras P. J., Ondov J. M., Polidori A., Turpin B. J., Robinson A. L., 2005. Fine particle emission profile for a large coke production facility based on highly time-resolved fence line measurements. *Atmos. Environ.,* 39 (36), 6719–6733.
- Zhu Y., Hinds W.C., Kim S., Sioutas C., 2002. Concentration and size distribution of ultrafine particles near a major highway. *J.* Air Waste *Manag. Assoc*. 52, 1032-1042.

4. Research activity

4.1 Aims of the Ph.D. study

1. Study of the size distribution properties and dynamics, with various sources and meteorological conditions, with focus on the ultrafine fraction, in a European air pollution *hot spot*. Test and develop a methodology that combines highly time-and-space airborne and ground-level measurements.

2. To investigate vertical atmospheric aerosol profiles of size-segregated particles and the PBL stratification.

3. Perform the source apportionment of atmospheric aerosol with PMF receptor modelling in the EU air pollution *hot spot*; with number size distribution spectra as input and focus on the smallest fractions. Test the methodology of combining PMF application on particle number size distribution and particle mass chemical composition.

4. To elucidate the particles size distribution dynamics focusing on the intermodal fraction; investigate the associations between $PM_{1\text{-}2.5}$ and fine (PM_1) and coarse ($PM_{2.5\text{-}10}$) fractions on the basis of statistical analysis, chemical composition analysis, and meteorological analysis, in various locations, during both winter and summer.

4.2 Major findings critical review

Manuscript 1: Leoni C., Hovorka J., Dočekalová V., Cajthaml T., Marvanová S. 2016. Source impact determination using airborne and ground measurements of industrial plumes. *Environmental Science and Technology*, 50(18), pp. 9881-8.

The first study performed in Ostrava, an air pollution *hot spot* in Europe, clearly identifies industrial sources of UFPs. High particle number concentrations were measured at the sampling site, with total campaign average of $1.6\pm1x10^4$ cm^{-3}, but with peaks up to $1.4x10^5$ particles cm^{-3} during plume events, i.e. downwind the industrial facility. These concentrations fit well with the average PNC of $3\text{-}5x10^4$ particles cm^{-3} reported by Marris et al. (2012) within 2 km of a metallurgical facility. The study reveals that industrial particles of 19−44 nm enriched up to 4.5% of mass with carcinogenic PAHs, contributes to the elevated carcinogenic PAHs concentrations at the hot-spot. This also help to assess better industrial UFPs possible impact to human health, since particles of 20−40 nm in diameter exhibit twice the deposition efficiency in pulmonary alveoli than other UFPs. This confirms previous findings of 40 nm UFPs within 1 km of a coke production plant in Pittsburgh, US (Weitkamp et al., 2005), or at the workplace, Cheng et al. (2008) found the same modal dimeter in a steelwork facility, as well as Thomassen et al., (2006), in a primary aluminum smelter in Sweden. PAHs in the UFPs studies are rare and the knowledge on the chemicals that constitute or are adsorbed on UFPs is very limited, due to technical constraints, reactive nature of PAHs and the fast changes of naoparticles. Dall'Osto et al. (2012) found PAHs in the organic content of particle with size 100 nm - 3 µm near large steelworks in Port Talbot. No other studies on the were found in literature: most published work on UFPs relates to road transport activities, while there is limited information on the UFPs emissions from specific industrial sources and the relative PAHs enrichment.

The physical and chemical properties of atmospheric particles, observed in the vicinity of industrial activities, demonstrates the need of new methodologies development. These methodologies have to focus on the particle size, one of the main factors, and on the plume deposition. Integrated measurement strategy combining high-time-resolution instruments with filter collections can facilitate the direct observation of the industrial plumes. The methodology of source impact measurements presented in this manuscript, combining highly

time-and-space airborne and ground-level measurements, is good example of such integrated measurements and can be applied to identify specific industrial PAH sources in other hot-spots worldwide.

Manuscript 2: Hovorka J., Leoni C., Dočekalová V., Ondráček J., Zíková N., 2016. Aerosol distribution in the planetary boundary layer aloft a residential area. *IOP Conference Series: Earth and Environmental Science* 44 052017.

The aerosol number concentration and the size distribution can vary at different heights of the PBL. The structure of the PBL is a key factor in determining the vertical profile of the number concentration. However, the measurements of temperature stratification and particle concentration and size distributions over a broad vertical range of the PBL, especially its lowest part (300 m above ground level) are rare. Long-term observations are needed to characterize the height-resolved aerosol properties and provide essential validation to the models and the satellite remote sensing. Airship measurements are capable of providing such resolution in situ data of aerosol vertical distribution directly observed in the low troposphere. In this study, airborne measurements reveal early morning temperature stratification of the PBL and coarse particles to be accumulated below the inversion layer. Two temperature inversion layers were observed: the first was formed up to 70 m a.g.l. while the second reached heights 180-230 m a.g.l. Coarse aerosol mass concentrations 20-50 μgm^{-3} below the first inversion layer reflected coarse aerosol sources on the ground. Enhanced concentration of particles below the inversion layer occurs due to the reduced turbulence and mixing. The effect of reduced mixing of an aerosol is a decreased dilution and deposition velocity, while coagulation and condensation of trace gases on pre-existing particles become more important. Additionally, the measurement site exhibit low temperatures (around -1 °C), that can have an impact on aerosol processes, e.g. by enhancing condensation of low volatile compounds (Janhall et al., 2006).

On the other hand, UFPs emitted from distant source with high emission height, can be trapped at higher altitude in the PBL. In this study, the UFPs number concentration measured with the airship at higher altitudes of the PBL (90-120 m a.g.l) were very high, up to $2.5x10^4$ cm^{-3}, which may indicate a fanning plume from a distant emission source with a high emission height. Based on existing atmospheric modeling and monitoring it is possible that emissions

from elevated stacks from industrial sources affect ground level concentration over a wide area. Recent research indicates that the aerosol pollutants released at different height in the PBL can be transported by local circulations (De Foy et al., 2011), forming also elevated pollution layer at higher altitudes (Zhang et al., 2006; Han et al., 2008).

During the course of day, the PBL stratification ceases and gradually evolved turbulent mixing led to a downward transport of ultrafine particles that were before at higher elevations. A sharp increase in number concentrations of ultrafine particles up to $3.7x10^4$ cm^{-3} recorded at heights of 380-400 meters a.g.l. at noon is followed by a sudden increase of ultrafine particles concentration $1.5\text{-}2x10^4$ cm^{-3} at the ground, after 20 minutes. This finding confirms the observation of a recent study (Platis et al., 2016) where new particle formation was measured at 400-500 m a.g.l. and after the break of the stratification the nanoparticles were measured at the ground level, showing the downward mixing of the inversion.

Manuscript 3: Leoni C., Pokorná P., Hovorka J., Masiol M., Topinka J., Zhao Y., Křůmal K., Cliff S., Mikuška P., Hopke P. K. Source apportionment of aerosol particles at a European air pollution hot spot using particle number size distributions and chemical composition. *Environmental Pollution, in press.*

In the same European air pollution *hot spot* presented in the manuscript 1, a more comprehensive study on sources identification of particles, spanning the whole size range (14 nm – 10 µm) allowed to clarify the major sources, down to nanoparticles. The methodology employed in this study is relatively new, and it consist of applying PMF to the particle number size distribution (NSD). It has been shown that very different size distributions are found in different locations and times, and this can be interpreted in terms of the known sources and the meteorological processes affecting the particles. This give confidence that an analysis of particle size spectra should be able to determine sources of the constituent particles. PMF has been applied generally to particle mass concentration, but recently few studies started to apply PMF modeling on particle size spectra (Harrison et al., 2011, Beddows et al., 2015, Masiol et al., 2017, Sowlat et al., 2016). The main element of novelty of the size spectra analysis with PMF is the identification of sources contributing principally to particle number and in particular the UFPs. In addition, this study not only resolves the sources that contribute to the PNC, but also compares the NSD PMF factors with factors resolved with mass chemical

composition. This comparison elucidated many components in common, as well as other factors which unique to each method.

The major finding of the manuscript 3 is that the industrial source is the major source of PNC at the receptor, confirming the conclusion of the manuscript 1. Two factors were resolved in the ultrafine size range: industrial UFPs (28%, number mode diameter - NMD 45 nm), industrial/fresh road traffic nanoparticles (26%, NMD 26 nm). Nevertheless, the study was not able to make a clear separation of factor 1 nanoparticles originated from industry or road traffic. Three factors were resolved in the accumulation size range: urban background (24%, NMD 93 nm), coal burning (14%, volume mode diameter - VMD 0.5 µm), regional pollution (3%, VMD 0.8 µm) and one factor in the coarse size range: industrial coarse particles/road dust (2%, VMD 5 µm). The PMF analysis of $PM_{0.09-1.15}$ revealed four factors: SIA/CC/BB (52%), road dust (18%), sinter/steel (16%), and iron production (16%). Comparing the output of PMF applied on NSD and chemical composition, it was found that the factors in the ultrafine size range have a positive correlation with sinter/steel production and iron production factors. Coal combustion factor resolved with NSD has moderate correlation with SIA/CC/BB factor. The organic markers homohopanes correlate with coal combustion and the levoglucosan correlates with urban background.

The manuscript 3 objective was to give further insight on the PAHs in PM_1 associations with factors, chemical markers, and other auxiliary variables. PAHs were found to be associated with coal combustion factor, with (r^2 = 0.68); PAHs showed positive correlation with R-homopane (r^2=0.88) and levoglucosan (r^2 = 0.67). Nevertheless, PAHs time resolution (24 hours) is not adequate for the source apportionment. Higher time resolution is needed to apportion the sources without ambiguity. In general, considering the previous and present studies, various sources contribute to particulate pollution at the hotspot and to PAHs concentration: industrial emissions of UFPs with southwesterly wind, combustion emissions (biomass and coal) of fine particles with north-northeasterly wind. Highly resolved PAH analysis and comparison with the WS and direction provide information on the variable impact of industrial/combustion emissions, and consequently can elucidate the major PAHs source.

Manuscript 4: Kozáková J., Leoni C., Klán M., Hovorka J., Racek M., Ondráček J., Moravec P., Schwarz J. Chemical characterization of $PM_{1-2.5}$ and its associations with the PM_1, $PM_{2.5-10}$ and

meteorology in urban and suburban environments (*submitted to Aerosol and Air Quality Research)*

The physical and chemical properties of the aerosol are highly variable in space and in time. The size distribution varies according to the meteorological conditions and the sources at the location. During periods of high relative humidity, fine particles, specifically from the accumulation mode, can grow into the intermodal fraction. Conversely, coarse particles can occur in the particle size range of less than 2.5 µm in arid, semi-arid areas, or dry conditions (Kozáková et al., 2017). It is evident that the particle size range between 1–2.5 µm can include both particles of fine (specifically accumulation, the tail of the fine mode) mode origins and coarse particles formed by mechanical processes (the tail of the coarse mode, formed by resuspended dust, sea salt, primary biological particles). A sharp division between fine and coarse particles is not clearly defined because these two fractions overlap in the range $PM_{1-2.5}$. No previous study that has examined the intermodal fraction (IMF, $PM_{1-2.5}$) particulate fraction in middle latitude areas, such as Central Europe.

In all the Czech sampling locations in this study (Ostrava industrial-residential; Plesná suburban-residential; Benatska-urban; Suchdol-suburban) the IMF accounts for 3-8% of PM_{10} mass. The highest mass concentration of IMF, PM_1, and $PM_{2.5-10}$ with Fe as the predominant element in all fractions was measured at the Ostrava industrial-residential site. Crustal elements were similarly distributed in the IMF and in the coarse fraction at every site. No seasonal differences were found in Ca^{2+} concentrations. PM_1 showed the highest SO_4^{2-} concentrations, especially at the suburban and urban sites in the winter.

Both $PM_{2.5-10}$ and PM_1 contribute to the IMF. The relative humidity (RH) is the most important parameter that influences the IMF and the size distribution in general. Hygroscopic ions, which account for a significant fraction of fine PM, enhance the particles growth to sizes larger than 1 µm. On the other hand, with dryer atmospheric condition, the IMF is associated to coarse PM, composed mainly by crustal dust or resuspended road dust. This investigation on IMF at four different locations in the Czech Republic suggests that in case of dry atmospheric condition, the PM_1 can be monitor as better representation of the PM fine fraction. On the other hand, with higher relative humidity, the fine fraction contributes to the IMF, and the $PM_{2.5}$ can be a more representative indicator.

4.3 Conclusion

The common denominator of this Ph.D. thesis and the manuscripts herein is: the study or the atmospheric aerosol particle number concentration and size distribution, with attention to the ultrafine fraction. The source apportionment is another leading thread of this work. The source apportionment focuses on the smallest size fraction. These particles contribute more to the NC than to the mass concentration. The manuscripts 1 and 3 identify industrial sources as the major UFPs emitter at the *hot spot*. The manuscript 2 identifies UFPs at higher altitudes in the PBL that can be related to high emission sources. The manuscript 4 identifies industrial and combustion sources as important contributors to PM in all size fractions at the *hot spot*, compared to other locations not impacted by industry.

In terms of methodology for aerosol sampling and modelling, this research work brings the following novelties. The source impact measurement methodology presented in the manuscript 1, combining highly time-and-space airborne and ground-level measurements, was not applied elsewhere, and it represents a good example of an integrated measurements that can be applied to estimate point sources of particles and the relative impact on the surroundings. The manuscript 2 is one of the rare examples of vertical profile aerosol particle NC and SD measurements, performed with high time and space resolution, in the lower portion of the PBL. The methodology employed in the manuscript 3, applying PMF to the particle NSD spectra, is relatively new: PMF has been applied typically to particle mass concentration. The main element of novelty of the size spectra analysis with PMF is the identification of sources contributing principally to particle number and in particular the UFPs. In addition, manuscript 3 not only resolves the sources that contribute to the PNC, but also compares the NSD PMF factors with factors resolved with mass chemical composition, revealing components in common as well as unique to each method. The manuscript 4 provides a multi-location study and the same *hot spot* and manuscript 1 and 3 is included. The manuscript 4 is the only study on the intermodal fraction size distribution focused on intermodal fraction performed with Central Europe meteorological conditions.

The results presented in this research work do not enable to quantify the sources of PAHs at the *hot spot*. In a previous study performed by Topinka et al. (2015) in the same *hot spot*, PAHs were measured in the size segregated PM with 24 hour time resolution, and they were found in all the PM size fractions, mostly in the upper accumulation mode (0.5–1 μm). Nevertheless,

the observation with the SEM suggested that the accumulation mode fraction was mostly composed of UFPs aggregates. This finding was confirmed by the manuscript 1: high concentrations of UFPs highly enriched with PAHs were measured when downwind of the large steelworks. Nevertheless, in manuscript 3, PAH concentrations measured with 24 hour time resolution in PM_1, showed association with organic markers relative to CC and BB (homohopanes and levoglucosan), with low wind speed or N-NE wind direction, upwind the metallurgy complex.

It is evident that different sources are contributing to PAH pollution at the *hot spot*, and it is plausible that industrial emissions of UFPs are dominant with southwesterly wind, while combustion emissions of BB and CC are dominant with north-northeasterly wind. The contribution of industrially emitted UFP to the accumulation fraction especially with calm wind conditions it is difficult to quantify. High time resolution size distribution PAHs analysis, for example hourly resolved measurement, can give further insight on their sources. Highly resolved PAH analysis, compared with the WS and direction, provide information on the variable impact of industrial/combustion emissions, and consequently can quantify their sources with precision.

The concentrations of benzo[a]pyrene in all the air quality sampling stations in Ostrava remain the highest in all of the Czech Republic and the limit of 1 ng/m^3/year in PM_{10} is exceeded every year (CHMI, 2017). These pollution levels give rise to severe concerns regarding health risks. Effective air quality policies call for action and cooperation at European, national and local levels, extending across most economic sectors. International and national policies to incentivize cleaner technologies for industry and cleaner fuel types for domestic heating are needed and the source apportionment can facilitate the targeting of the policies.

References

- Beddows, D.C.S., Harrison, RM., Green, DC, Fuller, GW., 2015. Receptor modeling of both particle composition and size distribution. *Atmos. Chem. Phys.* 15, 10107-10125.
- Cheng, Y.H.; Chao, Y.C.; Wu, C.H.; Tsai, C.J.; Uang, S.N.; Shih, T.S. Measurement of ultrafine particles concentrations and size distribution in an iron foundry. *J. Hazard. Mater.* 2008, 158, 124-130.
- Czech Hydrometeorological Institute (CHMI) http://portal.chmi.cz/files/portal/docs/uoco/isko/tab_roc/tab_roc_EN.html
- Dall'Osto M., Drewnick F., Fisher R., Harrison R.M., 2012. Real-Time Measurements of Nonmetallic Fine Particulate Matter Adjacent to a Major Integrated Steelworks, *Aerosol Sci. Technol.* 46(6), 639-653.
- De Foy B., Burton S. P., Ferrare R. A., Hostetler C. A., Hair J. W., Wiedinmyer C., Molina L. T., 2011. Aerosol plume transport and transformation in high spectral resolution Lidar measurements and WRF-Flexpart simulations during the MILAGRO Field Campaign *Atmos. Chem. Phys.,* 11, 3543–3563.
- Han Y., Fang, X., Zhao, T. and Kang, S. 2008. Long range trans-Pacific transport and deposition of Asian dust aerosols. *J. Environ. Sci.* 20, 424–428.
- Harrison, R.M., Beddows, D.C.S., Dall'Osto, M., 2011. PMF analysis of wide-range particle size spectra collected on a major highway. *Environ. Sci. Technol.* 45, 5522-5528.
- Janhall S., Olofson K., Frans G., Andersson P.U., Pettersson J.B.C., Hallquist M., 2006. Evolution of the urban aerosol during winter temperature inversion episodes. *Atmos. Environ.,* 40(28), 5355-536.
- Kozáková J., Pokorna P., Cernikova A., Hovorka J., Branis M., Moravec P., Schwartz J. 2017. The association between intermodal ($PM_{1\text{-}2.5}$) and PM_1, $PM_{2.5}$, coarse fraction and meteorological parameters in various environments in Central Europe. *AAQR*, 17(5) 1234-1243.
- Marris H., Deboudt K., Augustin P., Flament P., Blond F., Fiani E., Fourmentin M., Delbarre H. 2012. Fast changes in chemical composition and size distribution of fine particles during the near-field transport of industrial plumes, *Sci. Total Environ*. 427-428, 126-138.

- Masiol M., Vu T. V., Beddows D. C. S., Harrison R. M., 2016. Source apportionment of wide range particle size spectra and black carbon collected at the airport of Venice (Italy), *Atmos. Environ.* 139, 56-74.
- Platis A., Altstädter B., Wehner B., Wildmann N., Lampert A., Hermann M., Birmili W., Bange J. 2016. An observational case study on the influence of atmospheric boundary-layer dynamics on new particle formation*, Boundary-Layer Meteorol*., 158, 67–92.
- Sowlat M.H., Hasheminassab S., Sioutas C., 2016. Source apportionment of ambient particle number concentrations in central Los Angeles using positive matrix factorization (PMF). *Atmos. Chem. Phys.* 16, 4849-4866.
- Thomassen Y., Koch W., Dunkhorst W., Ellingsen D.G., Skaugset N.P., Jordbekken L., Arne Drabløs P., Weinbruch S. 2005. Ultrafine particles at workplaces of a primary aluminium smelter. *J. Environ. Monit.* 8(1):127-33
- Topinka, J., Rossner, P., Milcová, A., Schmuczerová, J., Penčíková, K., Rossnerova, A., Ambrož, A., Štolcpartová, J., Bendl., J., Hovorka, J, Machala, M., 2015. Day-to-day variability of toxic events induced by organic compounds bound to size segregated atmospheric aerosol. *Environ. Poll*., 202, 135-145.
- Weitkamp, E. A.; Lipsky, E. M.; Pancras, P. J.; Ondov, J. M.; Polidori, A.; Turpin, B. J.; Robinson, A. L. 2005. Fine particle emission profile for a large coke production facility based on highly time-resolved fence line measurements. *Atmos. Environ.*, 39 (36).
- Zhang Q., Zhao C., Tie X., Wei Q., Huang M., Li G., Ying Z., Li C., 2006. Characterizations of aerosols over the Beijing region: A case study of aircraft measurements. *Atmos. Environ.,* 40(24), 4513-4527

Manuscript 1:

Leoni C., Hovorka J., Dočekalová V., Cajthaml T., Marvanová S.

Source impact determination using airborne and ground measurements of industrial plumes

Environmental Science & Technology

Article

pubs.acs.org/est

Source Impact Determination using Airborne and Ground Measurements of Industrial Plumes

Cecilia Leoni,[†] Jan Hovorka,[*,†] Veronika Dočekalová,[†] Tomáš Cajthaml,[†] and Soňa Marvanová[‡]

[†]Institute for Environmental Studies, Faculty of Science, Charles University in Prague, Benátská 2, 128 01 Prague 2, Czech Republic
[‡]Department of Chemistry and Toxicology, Veterinary Research Institute, Hudcova 296/70, 621 00 Brno, Czech Republic

Supporting Information

ABSTRACT: Industrial particulate matter (PM) air pollution exposing nearby residential areas forms several European air pollution hot-spots. One of these hot-spot is the residential district of Ostrava Radvanice-Bartovice with frequent exceedances for PM and benzo-[*a*]pyrene B[a]P, a carcinogenic polycyclic aromatic hydrocarbon (PAH) of MW > 228 amu. Such PAHs are highly bonded to the ultrafine particles (UFPs), the smallest PM size fraction, which deposits most efficiently in the alveolar region of human lungs. Airborne measurements identified UFP point sources in the adjacent metallurgical complex and mapped limited horizontal and vertical dispersion of industrial plumes enriched with UFPs ($3.2 \times 10^5 cm^{-3}$). The plumes, episodes of simultaneous peaks of UFPs ($1.4 \times 10^5 cm^{-3}$), SO_2 (88.2 ppb), and CO (11.3 ppm), were recorded on the ground downwind in the residential district when wind speeds >1 ms^{-1}. In the plumes, UFPs were mostly 19−44 nm in diameter, enriched with PAHs/B[a]P up to 43.8/3.5 $mg \cdot g^{-1}$. Electron microscopy showed that these plume UFPs were mostly agglomerates of spherules of 30−50 nm in diameter. These source impact measurements, that combine airborne and ground-level measurements, are applicable to clearly identify specific industrial air pollution sources and provide information to assess their possible impact to human health in similar hot-spots worldwide.

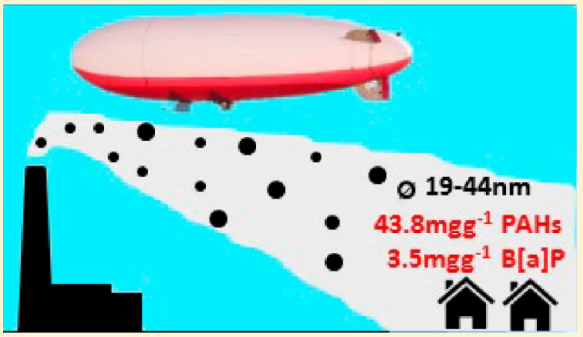

INTRODUCTION

In recent years, studies of the atmospheric aerosol have acquired major importance due to the relevance to climate and to human health. The adverse health effects of aerosol particles have been demonstrated by toxicological and epidemiological studies.[1,2] Atmospheric particles include also ultrafine particles (UFPs). The UFPs are the smallest aerosol particles in the atmosphere, with an aerodynamic diameter (d_{ae}) of approximately <0.150 nm. The high particle number concentration in the air and the high lung deposition efficiency make UFPs particularly hazardous to human health.[3]

The UFPs can be either directly emitted from the combustion processes (primary particles) or formed by nucleation from precursor vapors (secondary particles). Emissions of stationary combustion sources such as industrial stack plumes can contain a high UFPs number. Depending on the plume characteristics and the meteorological conditions, the particles can be spread from the stack to the nearby areas. Studies performed at a receptor site in the vicinity of industrial plants have observed the presence of UFPs when downwind from the emission source.[4−6] The UFPs concentration and the size distribution evolve very quickly once emitted into the atmosphere, influenced by numerous parameters: meteorology (wind speed/direction, boundary layer height) concentration of precursor gases (SO_2 and NO_x) and concentration of pre-existing particles.[7] The fast changes and the transient nature of the plumes require high time-resolved measurements, which can reveal short pollution events in the atmosphere.

Evidence now shows that UFPs carry considerable amount of toxics, and also polycyclic aromatic hydrocarbons (PAHs).[3,8−10] PAHs are persistent organic pollutants originated from the incomplete combustion of fossil fuels and wood, and they have been associated with respiratory diseases and cancer.[11,12] PAHs are present in various size fractions in the particulate matter. Close to the emission source the PAHs' mass size distribution peaks in the ultrafine (<150 nm d_{ae}) and accumulation (0.1−1 μm d_{ae}) size ranges.[13]

The Ostrava region (Czech Republic) is known as a European air pollution hot-spot.[14−18] Coal combustion and metallurgic activities are the main sources of PM in Ostrava.[17,18] In the recent CAFE (Clean Air For Europe) study by the European Commission, life expectancy in the Ostrava region was estimated to be reduced by 12−36 months due to the air pollution.[19] In the residential district of Ostrava-Radvanice and Bartovice the PM_{10} annual limits have been exceeded every year since 2000 and the benzo[*a*]pyrene concentration in the PM_{10} is ten times higher than the EU

Received: May 10, 2016
Revised: July 23, 2016
Accepted: August 22, 2016

DOI: 10.1021/acs.est.6b02304
Environ. Sci. Technol. XXXX, XXX, XXX−XXX

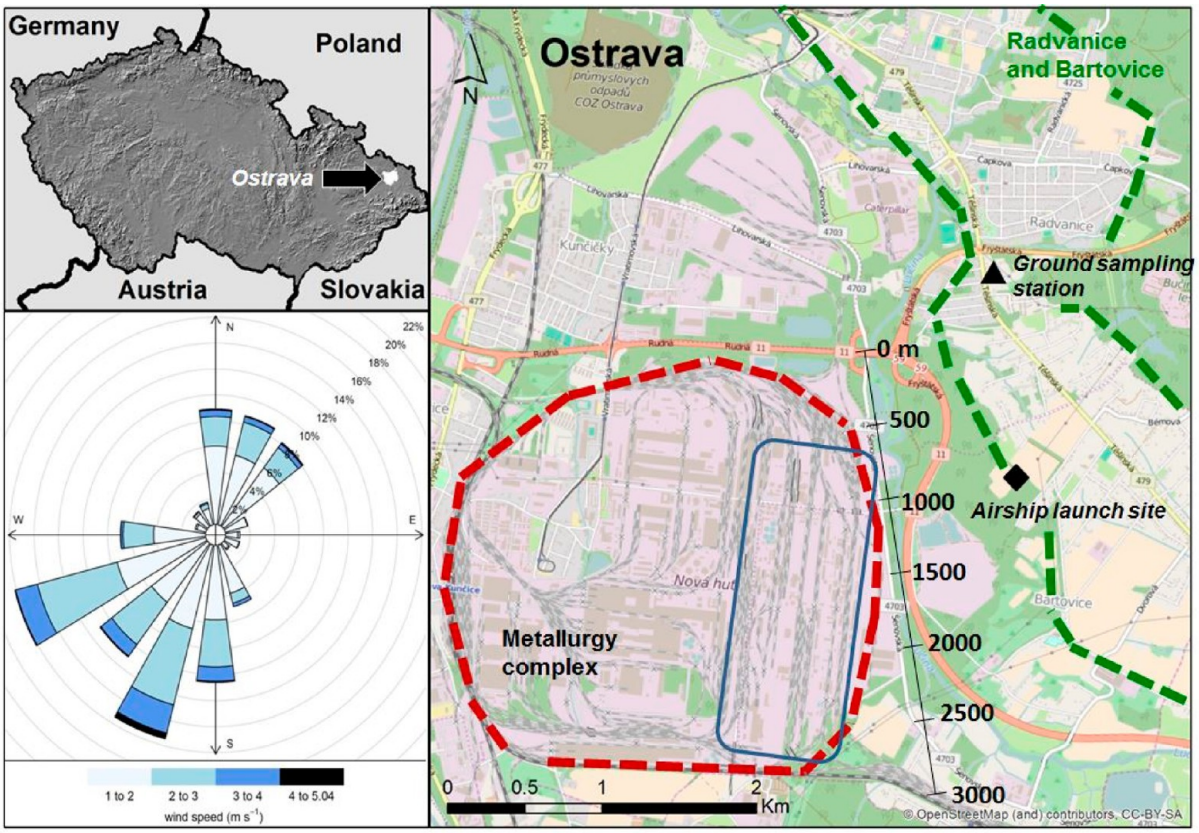

Figure 1. Upper left: Czech Republic with Ostrava city position. Bottom left: Campaign average windrose, calm wind data (WS < 1 m·s^{-1}) are not included. Right: Ostrava-Radvanice and Bartovice district (green line) with the ground sampling station and the airship launch site, the metallurgy complex to the southwest (red dashed line). The blue line rectangle and the mark scale correspond to the flying corridors above the metallurgy complex and the nearby freeway.

limits.[20] In a previous study carried out in the same locality in 2012 by Topinka et al., 7 carcinogenic PAHs were measured in size-segregated aerosol on a daily basis. PAHs were found in all the PM size fractions, mostly in the upper accumulation mode (0.5−1 μm d_{ae}).[10] According to scanning electron microscopy, the accumulation mode fraction was also composed of agglomerates of UFPs. PAHs might be primarily emitted in the ultrafine size range, and then enrich the fine fraction via coagulation. Information is missing on the PAHs size distribution and evolution in the atmosphere, and the process that governs the PAHs distribution in the different PM size fractions is still unclear.

This paper analyzes the temporal variability of UFPs concentration/size distribution and the enrichment with high molecular mass PAHs during a monthly winter sampling campaign in Ostrava-Radvanice and Bartovice. The aim of this paper is to disclose the main sources of UFPs and to identify particle sizes the most enriched with PAHs within the UFPs range. Also, this study complements our previous source apportionment studies of size segregated aerosol particles in the same location.[17,18]

EXPERIMENTAL SECTION

Site Description. The measurements were performed from the 5th of February to the 7th of March 2014 in the residential district of Ostrava-Radvanice and Bartovice (Figure 1). The district has 6800 inhabitants and is situated in the southwest part of the city of Ostrava. Ground measurements were conducted using a mobile sampling station, located in a private garden (49.811044° N, 18.337858° E). The nearest crossroad, about 100 m from the receptor site, had moderate vehicular traffic (<10 thousand vehicles/day), while a freeway (15−25 thousand vehicles/day) is located 1 km to the southwest.[21] A large iron and steel factory is located 1.5 km southwest of the station. The factory consists of an integrating plant with a liquid phase (coke oven, sintering plant and blast furnace) and a steel plant. It has an annual production of 3 million tons of steel. The airship launch site is situated 1.3 km south of the sampling station (Figure 1).

Airborne Measurements. An unmanned, remotely controlled airship with GPS 1 Hz position tracking, electrically powered with propulsion vectoring which allows an average cruising airspeed of 5 m.s^{-1} was used. The precision of the airship position tracking was 5−10 m vertically and about 5−8 m horizontally. The airship was equipped with a specially designed gondola carrying a lightweight sampler for size-segregated aerosols,[17] a temperature sensor (111DL, Voltcraft), a laser nephelometer (DustTrak DRX-8533, TSI Inc.), and two condensation nuclei counters (P-trak 8525, TSI Inc.). The nephelometer was used to measure the mass concentration of coarse aerosol particles (PM_{10}−PM_1). Each of the counters was equipped with Particle Size Selector - PSS (model 376060. TSI Inc.) at the aerosol inlet. The PSS segregates aerosol particles by diffusional trapping on fine-mesh screen. Since smaller particles diffuse faster than larger ones, penetration of smaller particles through the screen is lower than for large particles and higher number of the screens determines larger diameter of effectively penetrating particle. The first PSS housing holds

DOI: 10.1021/acs.est.6b02304
Environ. Sci. Technol. XXXX, XXX, XXX−XXX

seven screens which raises the smallest detectable particle diameter to about 100 nm while there were no screens at the second PSS housing. Therefore, the first counter detects particles within the diameter range of 100−1000 nm while the second detects particles within the diameter range of 20−1000 nm. The particle number concentrations (PNC) within the diameter range of 20−100 nm are obtained by the difference. The temperature sensor and the entire aerosol monitors acquired 1 Hz data. The monitors were connected to 50 cm long preheated (50 °C) inlet, which assures sampling above a dew point and prevents inlet clogging by cloudwater. Effective temperature of sampled air was about 40 °C, which dries aerosol to 5−11% RH depending on ambient air RH and T. The airship flew above the industrial area and residential district in the nights and early mornings on February 26th, 27th, and 28th.

Ground Measurements. The following parameters were recorded with 5 min integration time at the station: particle number size distributions within the size ranges 14−730 nm and 0.523−10 μm by a Scanning Mobility Particle Sizer (SMPS-3936L25, TSI Inc.) and an Aerodynamic Particle Sizer (APS-3321, TSI Inc.) respectively; wind speed − WS and wind direction − WD (WindSonic, Gill Instruments Ltd.); temperature − T (Comet 200−80/E); precipitation by disdrometer (Laser Precipitation Monitor, Thies); CO, NO_2, NO, O_3, SO_2, CH_4 and nonmethane hydrocarbons − NMHC were measured by automatic monitors (Horiba-360 series). Also, 24h samples of UFPs were collected on the backup filter (PTFE, 37 mm, R2PJ037, Pall) of an 8 stage Davis Rotating-drum Uniform-size-cut Monitor −8DRUM (DELTA Group, UC-Davis). Instruments for online and off-line aerosol analysis were sheltered in the station and equilibrated to 25 °C, which dried aerosol to 13−19% RH depending on ambient air RH and T. The mass concentrations of the UFPs were determined with microanalytical balance (Mettler Toledo M5) at 50% RH. There were 28 samples of UFPs collected during the campaign.

UFPs Analysis for PAHs and Microscopy. The UFPs collected at the backup filter of the 8DRUM were analyzed for eight carcinogenic PAHs, listed in the 16 PAHs of the US-EPA method 610. They were chrysene - CHRY, benzo[*b*]-fluoranthene - B[b]F, benzo[*k*]fluoranthene - B[k]F, benzo-[*a*]pyrene - B[a]P, benz[*a*]anthracene - B[a]A, dibenz[*a,h*]-anthracene - DB[ah]A, benzo[*g,h,i*]perylene - B[ghi]P and indeno[1,2,3-*cd*]pyrene - I[cd]P. The whole filters were extracted using an ASE 200 System (Dionex, Voisins-le-Bretonneux) with a mixture of hexane and acetone (3:1).[22] Three extraction cycles were performed at 150 °C and 10.3 MPa, the sample extracts were then concentrated in nitrogen and directly injected into a gas chromatograph coupled with mass spectrometry detector (GC-MS; 456-GC, SCION SQ mass detector, Bruker). The analysis was calibrated using the certified analytical standard mixture PAH MIX−9 (Dr. Ehrenstorfer GmbH) with octafluoronaphthalene (Sigma-Aldrich) as an internal standard.

To visualize aerosol particles at the backup filters, the PTFE membrane was cut from the holding ring with stainless steel tools and coated with Pt/Pd layer sputter coater (Cressington, 208HR). The particles were viewed with a scanning electron microscope, SEM (Hitachi SU8010) at magnifications up to 10^5 times.

RESULTS AND DISCUSSION

Meteorological Conditions. Winter was mild, with an average T of 5 °C and average RH of 76%. High-pressure and low cloudiness dominated, though there were also seven precipitation events. The longest rain occurred for 9 h on the 10th of February and one snow event occurred in the morning of the 12th of February. The precipitation periods accounted for about 5.5% of the campaign (SI Figure S1). Calm winds (WS < 1 m.s^{-1}) accounted for 50% of the campaign. Out of the calm wind periods, winds from the third quadrant of the windrose were the most frequent (32% of the campaign) and they had the highest WS of 5 m.s^{-1} (avg. 2.1 m·s^{-1}) (Figure 1, left bottom). During this period the mobile station was downwind from the metallurgical complex, which is located to the southwest. The northeast wind was the second most frequent (10% of the campaign), with an average WS of 1.6 m·s^{-1} (Figure 1, left-bottom).

Airborne Measurements. The first airship flying sequence was conducted in a north−south direction right above the freeway situated eastwards of the metallurgical complex. The airship started at 90 m above ground level following precisely the scale (Figure 1), kept a constant flight level until the end of the scale, then climbed about 50 m and repeated the same flying sequence at higher flight levels up to 250 m above the ground (Figure 2, SI Figure S2). Vertical temperature profile of

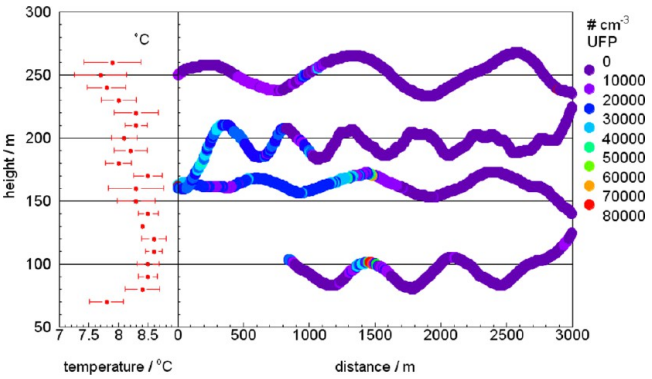

Figure 2. Vertical profile within atmospheric boundary layer of temperature (left) and UFPs number concentrations at the scale distances above the freeway near the metallurgical complex (right). The height indicates the vertical distance above the ground.

atmospheric boundary layer (ABL) was rather neutral and no temperature inversion within the ABL height from 70 m and higher was recorded (Figure 2 left). Nevertheless, the upward vertical dispersion of UFPs (10^5·cm^{-3}) from point source, located at 1500 m of the scale distance (Figure 1), was limited to the height of 170 m (Figure 2 right). Upward vertical dispersion of coarse aerosol (100 μg.m^{-3}) exhibited a similar pattern (SI Figure S2).

The second flying sequence was conducted aloft the metallurgical complex and the nearby areas. Due to technical and safety reasons, it was not possible to perform vertical scans so just horizontal scans at fairly constant flight level of 480 m (240 m above the ground) were conducted. The majority of the measured UFPs number concentrations, white circles of the airship tracks (Figure 3), were below UFPs median value (10^4·cm^{-3}) recorded by ground measurements during the off-plume periods (SI Table S2). This agrees with limited upward pollutant vertical dispersion from ground-based sources at the

DOI: 10.1021/acs.est.6b02304
Environ. Sci. Technol. XXXX, XXX, XXX−XXX

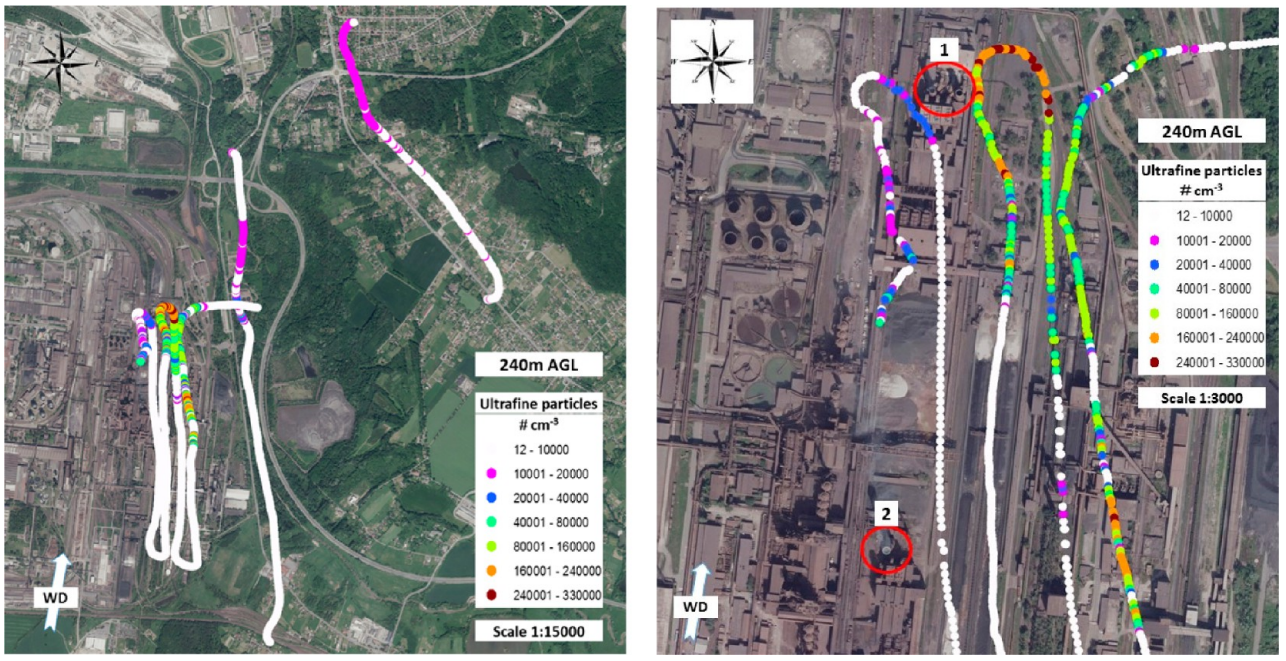

Figure 3. Aerial view of airship flight tracks at flight level 480 m (240 m above the ground) marked with UFPs number concentrations aloft the metallurgical complex and neighborhood areas (left) and detailed view of the tracks aloft the metallurgical complex (right) also indicating potential UFPs sources by red circles (with number 1 and 2).

locality to a rather high flight level as revealed by vertical scans (Figure 2 and SI Figure S2). UFPs values in a range 10^4–$2 \times 10^4 \cdot cm^{-3}$, magenta circles of the airship tracks, were recorded out of the metallurgical complex and may indicate UFPs emissions from nearby crossroads and a freeway directed in a west-east direction at the bottom of shallow valley (Figure 3 left).

Nevertheless, UFPs number concentrations higher than $2.4 \times 10^5 \cdot cm^{-3}$ were recorded in very narrow area above the metallurgical complex, indicating limited horizontal UFPs dispersion from various industrial technologies. Disclosed pollutant sources are marked with red circles (Figure 3 right). Red circle 1, marks twin 80 m tall chimneys of the dedusting unit of the sinter plant, a dominant UFPs source at the metallurgical complex, which matches with our previous source apportionment studies.[17,18] The sinter plant is a production plant for the sintering of coke, iron ore, limestone and other ores used for the preparation of charging material for the blast furnace. Downwind of the twin chimney, the UFPs increase more than ten times up to a value of $3.2 \times 10^5 \cdot cm^{-3}$, whereas several 10ths of a meters upwind of the chimney, the UFPs concentration drops to the campaign median recorded at the receptor site (Figure 3 right). Red circle 2 marks the 120 m tall chimney of the sintering plant, which apparently does not produce UFPs. This contrasts with very high concentrations of coarse aerosol particles ($256\ \mu \cdot gm^{-3}$) recorded close by this chimney and downwind (SI Figure S3) and therefore, unlike in the case of UFPs, this chimney is revealed as a strong source of coarse aerosol particles.

Ground Measurements. During the downwind period and WS > 1 ms^{-1}, coincident peaks of UFPs number, CO and SO_2 concentrations were frequently registered (Figure 4, SI Figure S4). Peak durations varied from 30 min up to several hours (SI Table S1), and occurred for 42% of the downwind period (16% of the campaign). During the peaks, UFPs number concentrations suddenly increased and were always higher than $2 \times 10^4 \cdot cm^{-3}$ (median $2.4 \times 10^4 \cdot cm^{-3}$, max. $1.4 \times 10^5 \cdot cm^{-3}$) and CO and SO_2 concentration medians were 0.9 ppm and 6.2 ppb (SI Table S2). Since the pollutant peaks were always observed when the station was downwind of the metallurgical complex (southwestern WD), and elevated UFPs concentrations at the sites close to industry indicates an industrial plume,[4−6] we define these pollutant episodes as plume period. Conversely, during the off-plume period the pollutants peaks coincidence was scarce (SI Figure S5), the UFPs numbers were $<2 \times 10^4 \cdot cm^{-3}$the median concentrations of UFPs, CO and SO_2 were $1.0 \times 10^4 \cdot cm^{-3}$, 0.4 ppm, and 1.8 ppb respectively (SI Table S2). The off-plume period (72% of the campaign) was characterized mainly by calm winds (55%), or a north−northeast wind direction (17%) (SI Figure S5). Also, there was an intermediate period between plume and off-plume (12% of the campaign), characterized by rather high median concentrations of UFP numbers ($2.2 \times 10^4 \cdot cm^{-3}$) and CO (0.9 ppm), but low SO_2 (2.5 ppb). Calm winds and missing SO_2 peaks differentiate the most the intermediate and plume periods. The intermediate periods may precede (SI Figure S4) or follow (Figure 4) the plume periods, so UFPs during the intermediate period may partially originate from industry but are transported by turbulent diffusion rather than by convection.

Also, coincident peaks of UFPs number, NO (50−100 $\mu g.m^{-3}$), occasionally CO (>1 ppm), but not SO_2 concentrations were registered during the intermediate period. These peaks are exclusively observed early morning on weekdays (Figure 4 and SI Figure S8) and can be apportioned to traffic. This agrees with elevated UFPs number concentrations about $2 \times 10^4 \cdot cm^{-3}$ recorded by airship at height 240 m above the crossroads (Figure 2).

Particle number size distributions remarkably differ between plume and off-plume periods (Figure 5 left). While the off-plume average number size distribution was bimodal with peaks at 25 and 100 nm (Figure 5 left), the plume average distribution is monomodal (Figure 5 left). Subtracting the

DOI: 10.1021/acs.est.6b02304
Environ. Sci. Technol. XXXX, XXX, XXX−XXX

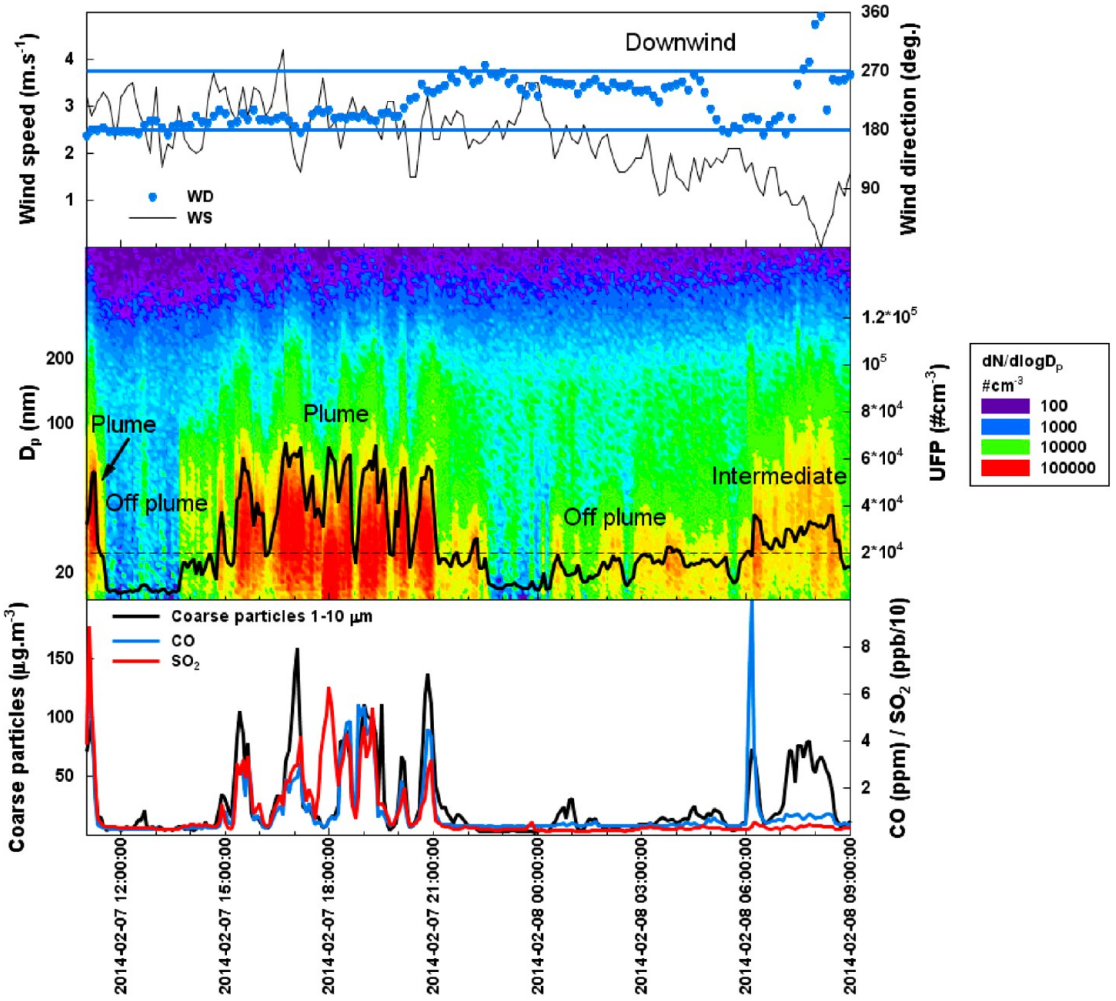

Figure 4. Top: time series of wind speed and direction, frame marks WD sector downwind from the metallurgy complex. In the middle: dynamics of particle number size distribution and the UFPs number concentrations. The bottom: time series of CO, SO_2, and coarse particle mass concentrations.

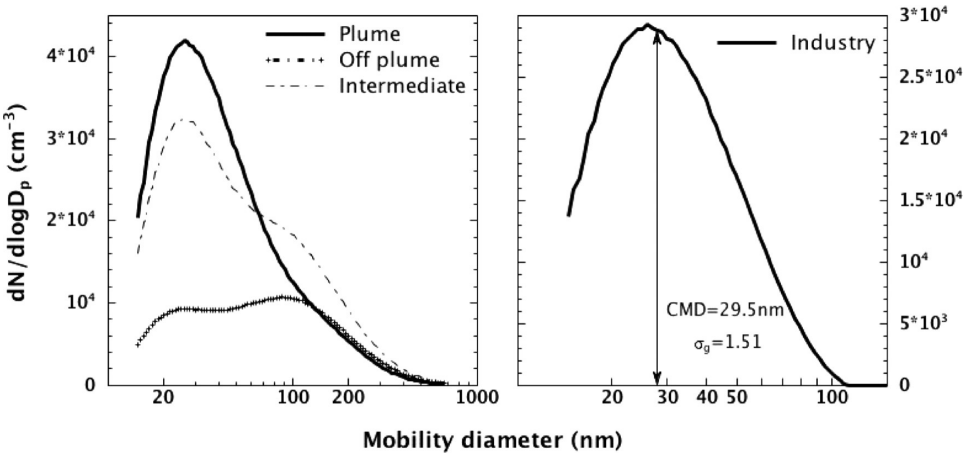

Figure 5. Aerosol particle number size distributions averages for plume (1327 scans), off-plume (6033 scans) and intermediate (971 scans) periods (left) and calculated for industrial UFPs (right).

off-plume from the plume size distribution results in monomodal average distribution attributable solely to industrial UFPs (Figure 5 right). Assuming log-normality of this industrial UFP size distribution,[23] then location and scale of the distribution are count median diameter—CMD = 29.5 nm and geometric standard deviation, σ_g = 1.51 respectively, and about 70% of industrial UFPs have diameter in the size range of 19−44 nm. This matches with particle diameters of 10−30 nm downwind from large steel complex,[4] about 35 nm in industrial plumes,[5] or 32−56 nm emitted by an iron foundry.[24]

DOI: 10.1021/acs.est.6b02304
Environ. Sci. Technol. XXXX, XXX, XXX−XXX

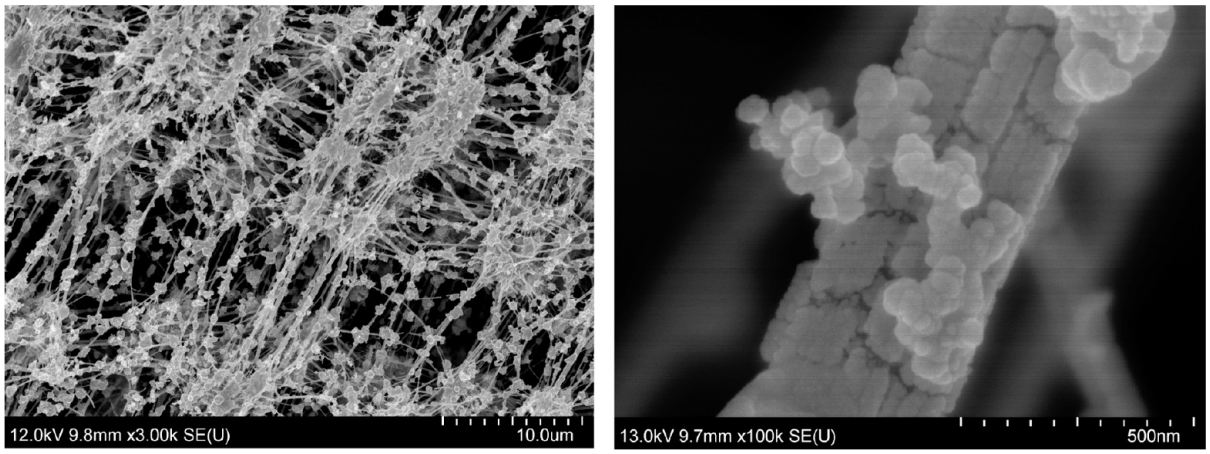

Figure 6. SEM images of aggregates of primary particles collected on fibers of the back-up PTFE filter at magnification 3×10^3 (left) and on a single fiber at magnification 10^5 (right), which shows the aggregates constituted by spherules <50 nm in diameter (sampled on 7.02.2014).

The SEM images of UFPs on backup filter show numerous particles trapped on PTFE filter fibers (Figure 6. left) and reveal these are predominantly agglomerates of the primary spherules 30−50 nm in diameter (Figure 6 right). Also, there are neither chains nor aggregates of particles smaller than 19 nm in diameter, the spherules are easily distinguished and no considerable coating is evident, which confirms the spherules primary origin.[29] Those observations are in accordance with online measurements.

Detailed information on particulate and gaseous air components during the plume provide additional arguments for why industrial plumes originate at the metallurgical complex nearby. First, UFPs have short residence due to coagulation.[23] Within 12 min, when plume travels between source and receptor (1.5 km, WS 2.1 $m.s^{-1}$), initial concentration of industrial UFPs (CMD = 29.5 nm) ($3.2 \times 10^5 \cdot cm^{-3}$) decreased by 18% due to self-coagulation[30] and by 9% due to coagulation with ambient aerosol particles[31] ∼ 100 nm in diameter (Figure 5 left). Second, we did not observe new particle formation events followed by a condensational particle growth at the site. Therefore, the elevated UFPs concentration is due to primary emissions and secondary UFPs are of minor importance. Third, the anticorrelation between O_3 and the NO_x (SI Figure S7) is typical for fresh plumes of local origin, where the primary pollutants in the plume consume O_3.[5]

Besides the UFPs, the plume episodes were often accompanied by about four times higher mass concentrations of coarse particles (1−10 μm d_{ae}) than during the off-plume (SI Table S2). The average mass size distribution of coarse particles has a peak at 7 μm, more prominent in the plume than in the off-plume period (SI Figure S6). This agrees with a mass size distribution peaking at 6 μm of Fe-rich particles in Port Talbot.[25] Similarly to UFPs number size distributions, the coarse particle peaks coincided with CO and SO_2 peaks, with southwestern WD and with WS > 1 $m.s^{-1}$. The plume-driven coarse particles contribute about 35% to the campaign median of coarse particle mass despite the fact that the plume lasts for 12% of the campaign.

Carcinogenic PAHs in Ultrafine Particles. In general, the PAHs are distributed in the atmosphere within the gaseous and particulate phase reflecting vapor pressure of individual PAH, atmospheric temperature, pressure and water vapor. Since the 8 carcinogenic PAHs analyzed have the vapor pressure <2.8×10^{-5} Pa, they are predominantly bonded to the particulate phase.[26,27]

The PAHs concentration in UFPs varied daily over a wide range, from 0.15 to 19.9 $ng.m^{-3}$, with a campaign average of 6.2 ± 5.1 $ng.m^{-3}$ (SI Table S1). The UFPs were highly enriched with PAHs, on average 2.1 $mg \cdot g^{-1}$, which agrees with 0.9 $mg \cdot g^{-1}$ of 7 carcinogenic PAHs in the quasi-ultrafine particles (d_{ae} < 170 nm) sampled at the same location in 2012.[10] The enrichment of UFPs by PAHs was on average 2.9 $mg \cdot g^{-1}$ during the plume, while 0.9 $mg \cdot g^{-1}$ off the plume. Proportionalities of individual PAHs in UFPs decreased as their MWs increased and did not significantly differ between the plumes and off-plumes. On average, both CHRY and B[a]A formed about 30% and B[a]P about 8% of PAHs in UFPs (SI Figure S9) and the ratios B[a]A/CHRY and I[cd]P/B[ghi]P were 1.03 ± 0.24 and 0.81 ± 0.08, indicating coke/coal combustion and metallurgy, respectively.[32] Additionally, during the plume, PAHs enrichment in the UFPs (y in $mg \cdot g^{-1}$) increases significantly ($r^2 = 0.75$, $n = 17$) with relative mass (x %) of the industrial particles 19−44 nm in diameter, identified by online measurements (Figure 7). One data point, the ninth of February, was excluded from the linear regression in Figure 7 because there was a 9 h rain event causing very low UFPs mass (SI Figure S1). On the other hand, by erasing the data point of the 15th February, the slope of the linear regression remains unchanged ($y = 45.6x - 0.98$) while the tightness increases significantly ($r^2 = 0.88$). Unfortunately, we could not well justify erasing the 15th February data point.

Such a tight linear regression enables us to predict the UFPs enrichment by PAHs/B[a]P up to 43.8/3.5 $mg \cdot g^{-1}$ if composed exclusively of industrial particles in diameter 19−44 nm.

This study agrees with results of our 2012 study in this European air quality hotspot,[17,18] and clearly identifies industrial sources of UFPs. Additionally, the study reveals that elevated carcinogenic PAHs concentrations at the hot-spot are caused by industrial particles of 19−44 nm enriched up to 4.5% of mass with carcinogenic PAHs. This also help to assess better industrial UFPs possible impact to human health, since particles of 20−40 nm in diameter exhibit twice the deposition efficiency in pulmonary alveoli than other UFPs.[28]

Recent review article,[7] analyzing the current state-of-the-knowledge on the physical and chemical properties of $PM_{2.5}$, PM_1 and in particular UFPs, observed in the vicinity of industrial activities, clearly demonstrates the need of new

DOI: 10.1021/acs.est.6b02304
Environ. Sci. Technol. XXXX, XXX, XXX−XXX

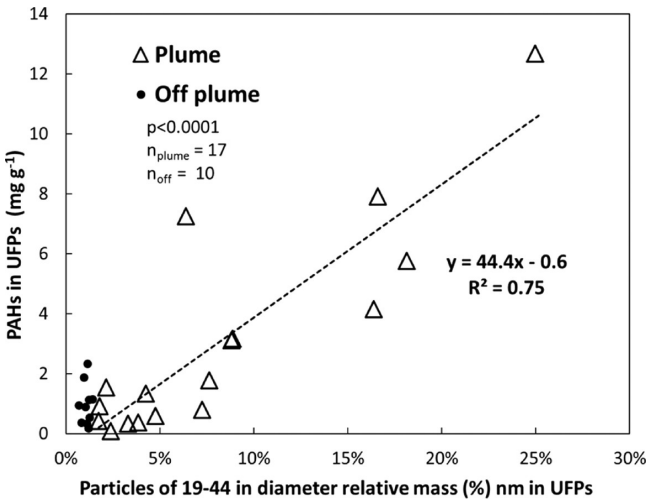

Figure 7. 24 h PAHs concentrations versus relative mass (%) of particles in diameter between 19 and 44 nm in the UFPs during plume (triangles) and off-plume (circles) days. Mass of particles 19−44 nm in diameter was calculated from SMPS particle size distributions with density of 1.5 g·cm^{-3}.

methodologies development. These methodologies have to focus on the particle size, one of the main factors and deposition of plumes, and utilize an integrated measurement strategy combining high-time-resolution instruments with filter collections and are capable to facilitate the direct observation of the industrial plumes. Presented methodology of source impact measurements, that combines highly time-and-space airborne and ground-level measurements, is good example of such integrated measurements and is applicable to clearly identify specific industrial PAH sources in hot-spots, similar to one investigated in this study. According to the recent studies, the hot-spots are harbor cities like Hamilton in Canada,[33] where differences in PAH ratios in urban air down/up wind of the industry were discussed but did not reveal specific industrial sources, Conception city in Chile,[34] where steel industry contribution was also considered, but its quantification was rather vague, Taranto in Italy,[35] where industrial emissions were also found as the main source of PAHs but specific sources contribution was not resolved, and also in Gipuzkoa territory in Spain,[36] group of small towns with high levels of industrial activity, where the main origin of PAH may be industrial processes but specific sources were not resolved yet. Nevertheless, the main areas of our methodology application to better resolve industrial PAH sources in an urban airshed close to industry are in rapidly developing countries in industrial central India,[37] Tangshan[38] and six industrial cities in Northeast Region[39] in China.

■ ASSOCIATED CONTENT

Supporting Information

The Supporting Information is available free of charge on the ACS Publications website at DOI: 10.1021/acs.est.6b02304.

Figure S1 shows campaign time series for temperature, RH and precipitation, Figure S2 and Figure S3 show vertical profile and aerial views of airship tracks for coarse particle mass. Figures S4−5 show temporal variation of: WS, WD, UFP number concentration and size distribution, CO, SO_2, and coarse particle mass concentration for plume, off-plume and intermediate periods. Figure S6 depicts the period averages for coarse particle mass size distribution. Figure S7 is linear regression between O_3 and NO_x for plume period, Figure S8 shows time series of UFP and NO for off-plume period, Figure S9 are pie charts of concentrations of individual PAHs for plume and off-plume periods. Tables summarize for plume, off-plume and intermediate periods: the period durations and ambient air PAHs concentrations (Table S1), basic statistics of UFP number and coarse particle mass, CO and SO_2 concentrations (Table S2) (PDF)

■ AUTHOR INFORMATION

Corresponding Author

*Phone: +420 221951910; fax: +420 224914803; e-mail: jan.hovorka@natur.cuni.cz.

Notes

The authors declare no competing financial interest.

■ ACKNOWLEDGMENTS

This work was supported by grant P503/12/G147 of the Grant Agency of the Czech Republic and 1354314 of the Grant Agency of the Charles University in Prague. We are grateful to P.K.Hopke of Clarkson University for valuable comments to the manuscript, to J. Ondráček of the Institute of Chemical Processes Fundamentals for aerosol spectrometers collocation and (C.L.) acknowledges help in aerosol size spectra evaluation to N. Zíková of the Institute for Environmental Studies.

■ REFERENCES

(1) Schwartz, J.; Dockery, D. W.; Neas, L. M. Is daily mortality associated specifically with fine particles? *J. Air Waste Manage. Assoc.* **1996**, *46*, 927−939.

(2) Pope, C. A., 3rd; Burnett, R. T.; Thun, M. J.; Calle, E. E.; Krewski, D.; Ito, K.; Thurston, G. D. Lung cancer, cardiopulmonary mortality and long term exposure to fine particulate air pollution. *JAMA* **2002**, *287* (9), 1132−1141.

(3) Sioutas, C.; Delfino, R. J.; Singh, M. Exposure assessment for atmospheric ultrafine particles (UFPs) and implications in epidemiological research. *Environ. Health Persp.* **2005**, *113* (8), 947−955.

(4) Marris, H.; Deboudt, K.; Augustin, P.; Flament, P.; Blond, F.; Fiani, E.; Fourmentin, M.; Delbarre, H. Fast changes in chemical composition and size distribution of fine particles during the near-field transport of industrial plumes. *Sci. Total Environ.* **2012**, *427−428*, 126−138.

(5) Young, L. H.; Keeler, G. Summertime ultrafine particles in urban and industrial air: Aitken and nucleation mode particles events. *Aerosol Air Qual. Res.* **2007**, *7* (3), 379−402.

(6) Weitkamp, E. A.; Lipsky, E. M.; Pancras, P. J.; Ondov, J. M.; Polidori, A.; Turpin, B. J.; Robinson, A. L. Fine particle emission profile for a large coke production facility based on highly time-resolved fence line measurements. *Atmos. Environ.* **2005**, *39* (36), 6719−6733.

(7) Riffalut, V.; Arnds, J.; Marris, H.; Mbengue, S.; Setyan, A.; Alleman, L. Y.; Deboudt, K.; Flament, P.; Augustin, P.; Delbarre, H.; et al. Fine and ultrafine particles in the vicinity of industrial activities: A review. *Crit. Rev. Environ. Sci. Technol.* **2015**, *45* (21), 2305−2356.

(8) Miguel, A. H.; Eiguren-Fernandez, A.; Sioutas, C.; Fine, P. M.; Geller, M.; Mayo, P. R. observations of twelve USEPA priority polycyclic aromatic hydrocarbons in the Aitken size range (10−32 nm Dp). *Aerosol Sci. Technol.* **2005**, *39* (5), 415−418.

(9) Topinka, J.; Hovorka, J.; Milcová, A.; Schmuczerová, J.; Kroužek, J.; Rossner, P., Jr.; Šrám, R. J. An acellular assay to assess genotoxicity of size segregated aerosols. Part I: DNA adducts. *Toxicol. Lett.* **2010**, *198* (3), 304−311.

DOI: 10.1021/acs.est.6b02304
Environ. Sci. Technol. XXXX, XXX, XXX−XXX

(10) Topinka, J.; Rossner, P.; Milcová, A.; Schmuczerová, J.; Penciková, K.; Rossnerová, A.; Ambroz, A.; Stolcpartová, J.; Bendl, J.; Hovorka, J.; et al. Day to day variability of toxic events induced by organic compounds bound to size segregated atmospheric aerosol. *Environ. Pollut.* **2015**, *202*, 135−145.
(11) Kameda, Y.; Shirai, J.; Komai, T.; Nakanishi, J.; Masunaga, S. Atmospheric polycyclic aromatic hydrocarbons: size distribution, estimation of their risk and their deposition to the human respiratory tract. *Sci. Total Environ.* **2005**, *340* (1−3), 71−80.
(12) *Health risks of Persistent Organic Pollutants from Long-Range Transboundary Air Pollution*, Joint WHO/Convention task force on health aspect of air pollution; World Health Organization, 2003; http://www.euro.who.int/__data/assets/pdf_file/0009/78660/e78963.pdf.
(13) Keyte, J.; Harrison, R. M.; Lammel, G. Chemical reactivity and long-range transport potential of polycyclic aromatic hydrocarbons − a review. *Chem. Soc. Rev.* **2013**, *42*, 9333.
(14) Houthuijs, D.; Breugelmans, O.; Hoek, G.; Vaskövi, É.; Miháliková, E.; Pastuszka, J. S.; Jirik, 12 V.; Sachelarescu, S.; Lolova, D.; Meliefste, K.; et al. PM_{10} and $PM_{2.5}$ concentrations in Central and Eastern Europe: results from the Cesar study. *Atmos. Environ.* **2001**, *35* (15), 2757−2771.
(15) Šrám, R. J.; Dostál, M.; Libalová, H.; Rossner, P.; Rossnerová, A.; Svecová, V.; Topinka, J.; Bartonová, A. The European hot spot of B[a]P and $PM_{2.5}$ exposure-the Ostrava region, Czech Republic: health research results. *ISRN Public Health*, **2013a**, article ID 416701. *2013*, 1, 10.1155/2013/416701.
(16) Šrám, R. J.; Binková, B.; Dostal, M.; Merkerová-Dostalová, M.; Libalová, H.; Milcov, A.; Rossner, P., Jr.; Rossnerová, A.; Schmuczerová, J.; Svecová, V.; et al. *Int. J. Hyg. Environ. Health* **2013b**, *216* (5), 533−540.
(17) Pokorná, P.; Hovorka, J.; Klán, M.; Hopke, P. K. Source apportionment of size resolved particulate matter at a European air pollution hot spot. *Sci. Total Environ.* **2015**, *502*, 172−183.
(18) Pokorná, P.; Hovorka, J.; Hopke, P. K. Elemental composition and source identification of very fine aerosol particles in a European air pollution hot-spot. *Atmos. Pollut. Res.* **2016**, *7*, 671−679.
(19) European Union official website, Clean air for Europe (CAFE) session. http://ec.europa.eu/environment/archives/cafe/general/keydocs.htm.
(20) Czech Hydro-meteorological Institute (CHMI) website, annual graphic overview. http://portal.chmi.cz/files/portal/docs/uoco/isko/grafroc/14groc/gr14e/Obsah_GB.html.
(21) Road and Motorway Directorate of the Czech Republic website, interactive map. http://scitani2010.rsd.cz/pages/map/default.aspx.
(22) Covino, S.; Čvančarová, M.; Muzikář, M.; Svobodová, K.; D'Annibale, A.; Petruccioli, M.; Federici, F.; Křesinová, Z.; Cajthaml, T. An efficient PAH-degrading Lentinus (Panus) tigrinus strain: effect of inoculum formulation and pollutant bioavailability in solid matrices. *J. Hazard. Mater.* **2010**, *183* (1−3), 669−676.
(23) Hinds, W. C. *Aerosol technology, Properties, Behavior, and Measurement of Airborne Particles*, 2 ed.; Wiley, 1999.
(24) Cheng, Y. H.; Chao, Y. C.; Wu, C. H.; Tsai, C. J.; Uang, S. N.; Shih, T. S. Measurement of ultrafine particles concentrations and size distribution in an iron foundry. *J. Hazard. Mater.* **2008**, *158*, 124−130.
(25) Dall'Osto, M.; Booth, M. J.; Smith, W.; Fisherb, R.; Harrison, R. M. A study of the size distributions and the chemical characterization of airborne particles in the vicinity of a large integrated steelworks. *Aerosol Sci. Technol.* **2008**, *42*, 981−991.
(26) Ravindra, K.; Sokhi, R.; Van Grieken, R. Atmospheric polycyclic aromatic hydrocarbons: source attribution, emission factors and regulation. *Atmos. Environ.* **2008**, *42* (13), 2895−2921.
(27) Finlayson-Pitts, B.; Pitts, J. N. *Chemistry of the Upper and Lower Atmosphere*; Academic Press, 1999.
(28) Center for Aerosol Impacts on Climate and the Environment (CAICE) website, learning with CLEAR: aerosol impact on health session; http://caice.ucsd.edu/index.php/education/clear/learning-with-clear/aerosols-and-health/.
(29) China, S.; Mazzoleni, C.; Gorkowski, K.; Aiken, A. C.; Dubey, M. K. Morphology and mixing state of individual freshly emitted wildfire carbonaceous particles. *Nat. Commun.* **2013**, *2122* (4), 1−7.
(30) Park, S. H.; Lee, K. W.; Otto, E.; Fissan, H. The log-normal size distribution theory of Brownian aerosol coagulation for the entire particle size range: Part I—analytical solution using the harmonic mean coagulation kernel. *J. Aerosol Sci.* **1999**, *30* (1), 3−16.
(31) Fuchs, N. A. *The mechanic of aerosols*, Pergamon Press, Oxford, 1964.
(32) Dickhut, R. M.; Canuel, E. A.; Gustafson, K. E.; Liu, K.; Arzayus, K. M.; Walker, S. E.; Edgecombe, G.; Gaylor, M. O.; MacDonald, E. H. Automotive Sources of Carcinogenic Polycyclic Aromatic Hydrocarbons Associated with Particulate Matter in the Chesapeake Bay Region. *Environ. Sci. Technol.* **2000**, *34* (21), 4635−4640.
(33) Sofowote, U. M.; Allan, L. M.; McCarry, B. E. A comparative study of two factor analytic models applied to PAH data from inhalable air particulate collected in an urban-industrial environment. *J. Environ. Monit.* **2010**, *12*, 425−433.
(34) Scipioni, C.; Villanueva, F.; Pozo, K.; Mabilia, R. Preliminary characterization of polycyclic aromatic hydrocarbons, nitrated polycyclic aromatic hydrocarbons and polychlorinated dibenzo-p-dioxins and furans in atmospheric PM10 of an urban and a remote area of Chile. *Environ. Technol.* **2012**, *33* (7), 809−820.
(35) Amodio, M.; Andriani, E.; de Gennaro, G.; Di Gilio, A.; Ielpo, P.; Placentino, C. M.; Tutino, M. How a steel plant affects air quality of a nearby urban area: A study on metals and PAH concentrations. *Aerosol Air Qual. Res.* **2013**, *13*, 497−508.
(36) Villar-Vidal, M.; Lertxundi, A.; Martinez López de Dicastillo, M. D.; Alvarez, J. I.; Santa Marina, L.; Ayerdi, M.; Basterrechea, M.; Ibarluzea, J. Air Polycyclic Aromatic Hydrocarbons (PAHs) associated with PM2.5 in a North Cantabric coast urban environment. *Chemosphere* **2014**, *99*, 233−238.
(37) Giri, B.; Patel, K. S.; Jaiswal, N. K.; Sharma, S.; Ambade, B.; Wang, W.; Massey Simonich, S. L.; Simoneit, B. R. T. Composition and sources of organic tracers in aerosol particles of industrial central India. *Atmos. Res.* **2013**, *120−121*, 312−324.
(38) Shi, G. L.; Feng, Y. C.; Wu, J. H.; Li, X.; Wang, Y. Q.; Xue, Y. H.; Zhu, T. Source identification of polycyclic aromatic hydrocarbons in urban particulate matter of Tangshan, China. *Aerosol Air Qual. Res.* **2009**, *9*, 309−315.
(39) Li, W.; Peng, Y.; Shi, J.; Qiu, W.; Wang, J.; Bai, Z. Particulate polycyclic aromatic hydrocarbons in the urban Northeast Region of China: Profiles, distributions and sources. *Atmos. Environ.* **2011**, *45*, 7664−7671.

DOI: 10.1021/acs.est.6b02304
Environ. Sci. Technol. XXXX, XXX, XXX−XXX

Supplementary material for:

Source Impact Determination using Airborne and Ground Measurements of Industrial Plumes

Cecilia Leoni, Jan Hovorka, Veronika Dočekalová, Tomáš Cajthaml, Soňa Marvanová

Number of Figures: 9

Number of Tables: 2

Number of pages: 10

Figures

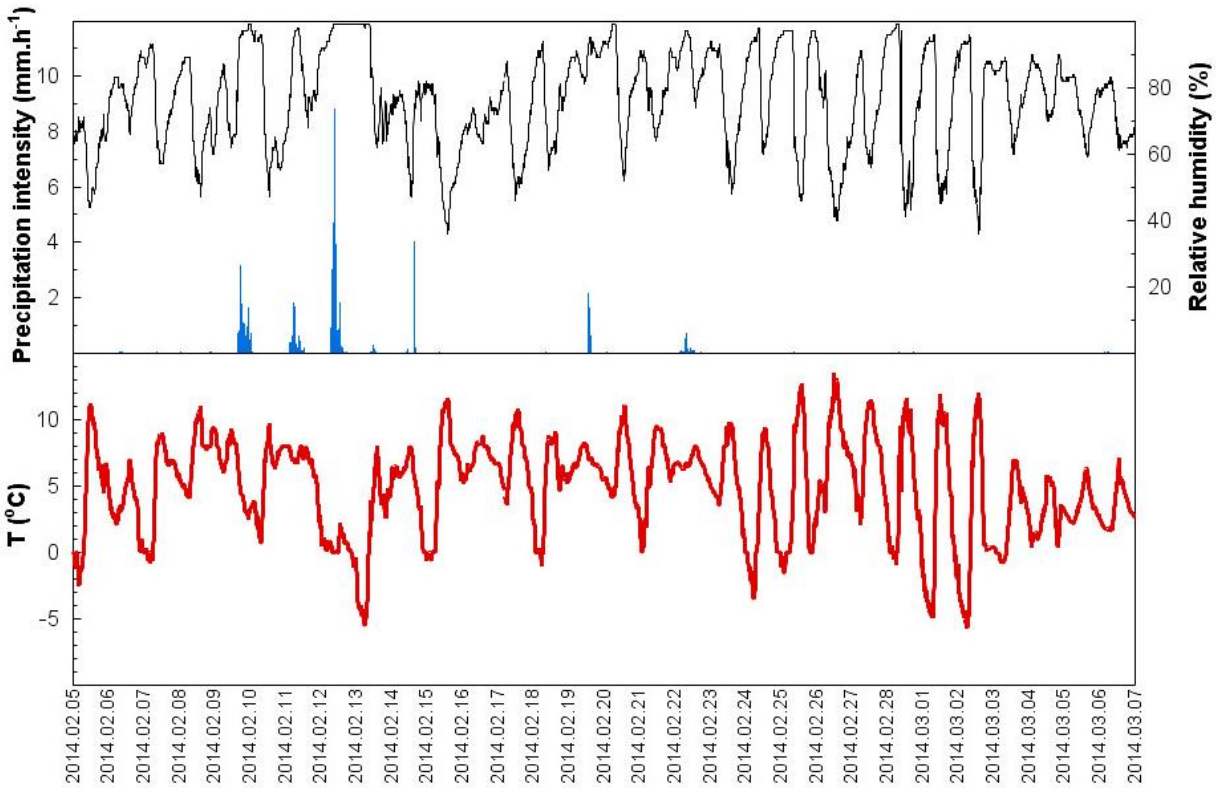

Figure S1. Time series of relative humidity, precipitation intensity and temperature in Ostrava-Radvanice and Bartovice for the period of 5.2-7.3.2014.

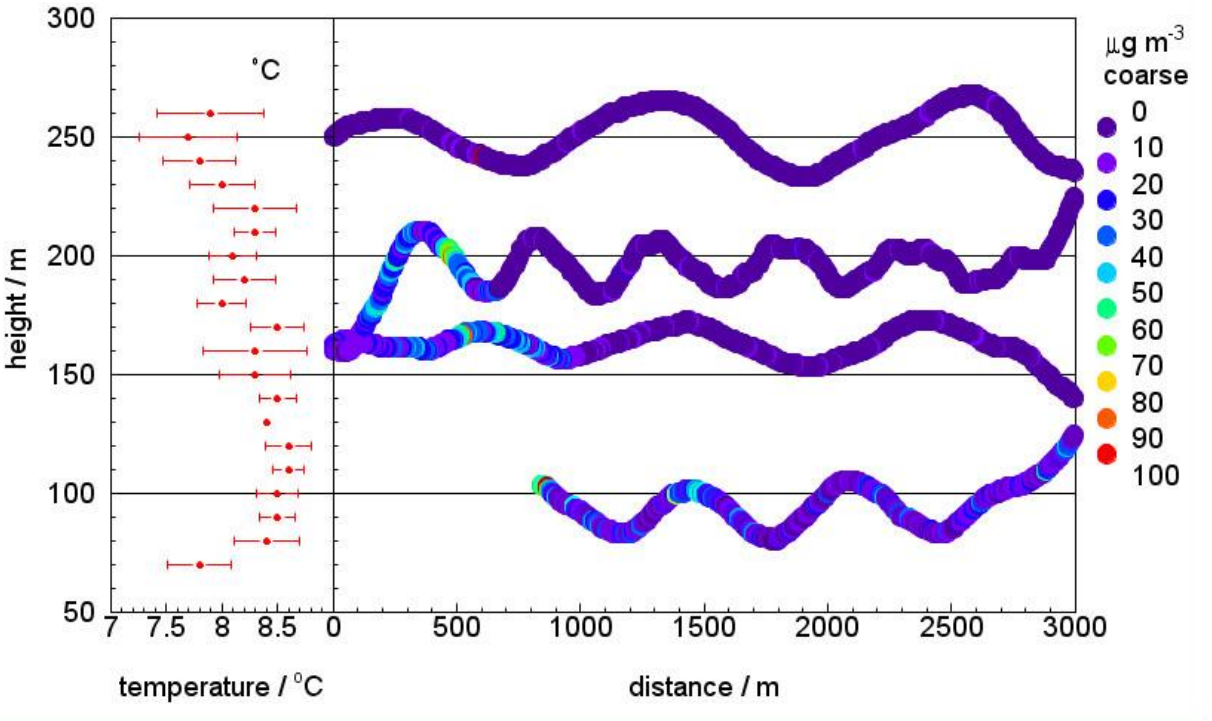

Figure S2. Vertical profile within atmospheric boundary layer of temperature (left); vertical and horizontal profiles of coarse aerosol particle mass concentrations (right) above the freeway near the metallurgy complex.

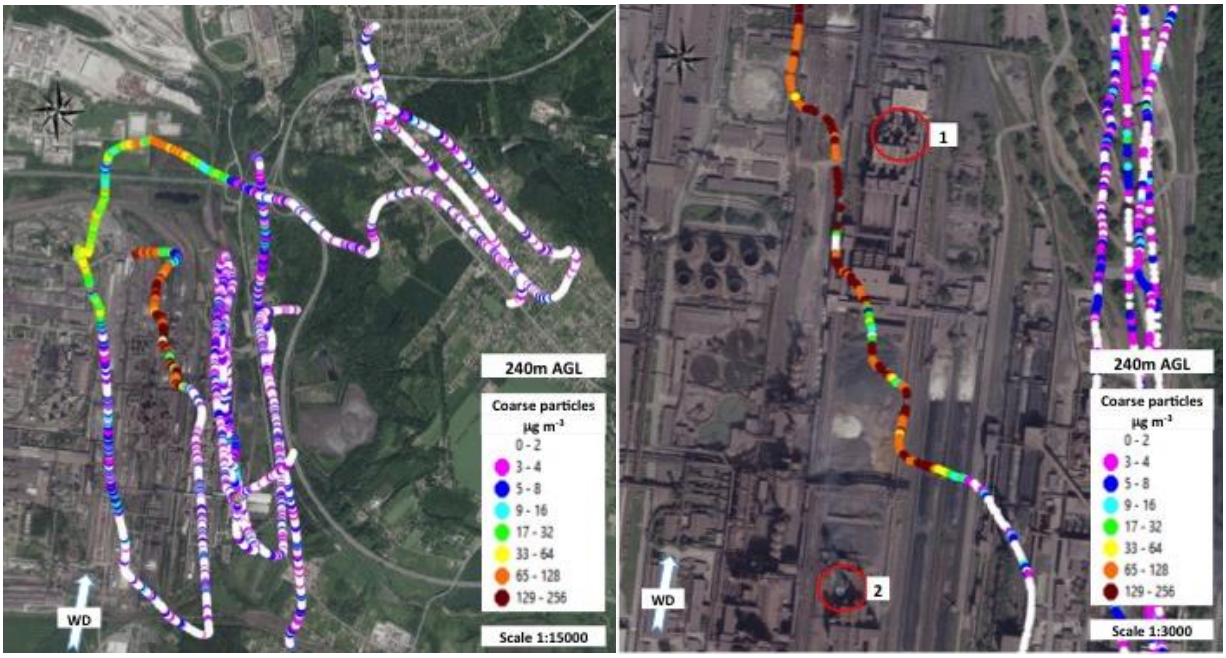

Figure S3. Aerial view of airship flight tracks at flight level 480m (240m above the ground) marked with coarse aerosol mass concentrations aloft the metallurgy complex and neighborhood areas (left); detailed view of the tracks aloft the metallurgy complex indicating potential coarse aerosol particle sources (red circles).

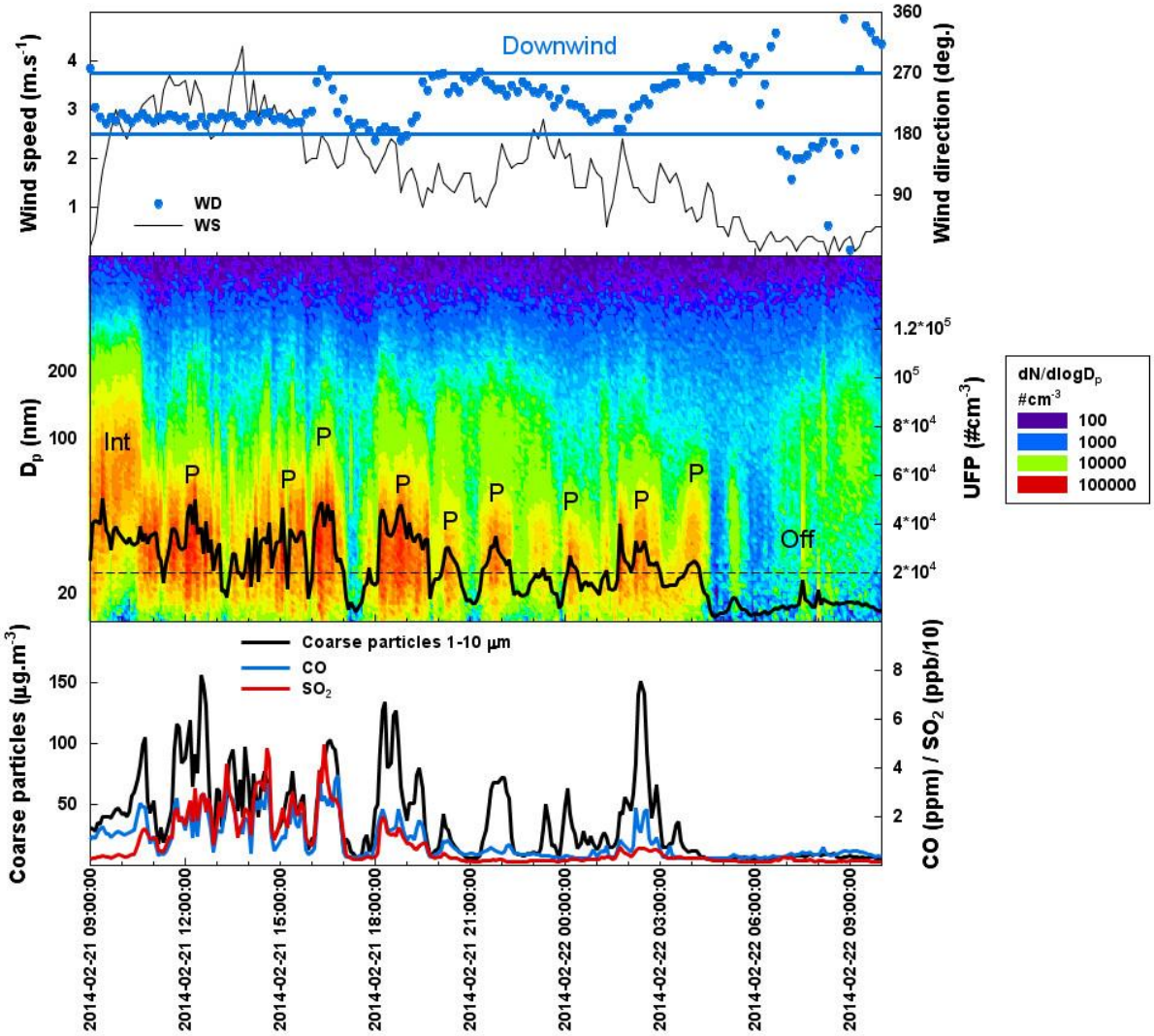

28

29 **Figure S4.** Plume (P) and intermediate (Int) and off-plume (Off) episodes on the 21.02.2014. The
30 top: time series of wind speed and direction, blue lines mark the WD sector downwind from the
31 metallurgy complex. In the middle: dynamics of particle number size distribution and the UFPs
32 number concentrations. The bottom: time series of CO, SO_2 and coarse particle mass
33 concentrations.

34

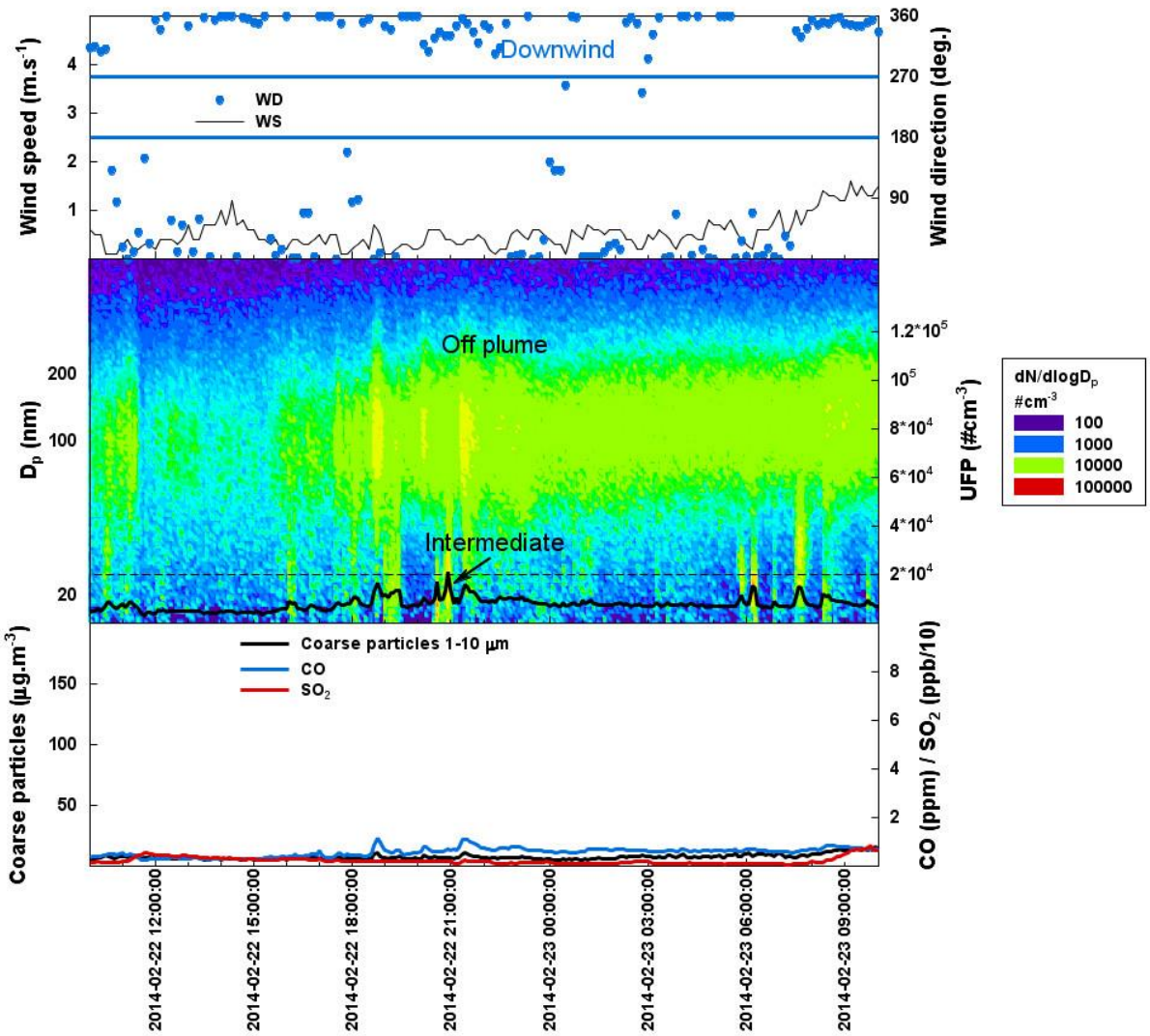

Figure S5. Off plume episodes and one short intermediate episode on the 22.02.2014. The top: time series of wind speed and direction, blue lines mark the WD sector downwind from the metallurgy complex. In the middle: dynamics of particle number size distribution and the UFPs number concentrations. The bottom: time series of CO, SO_2 and coarse particle mass concentrations.

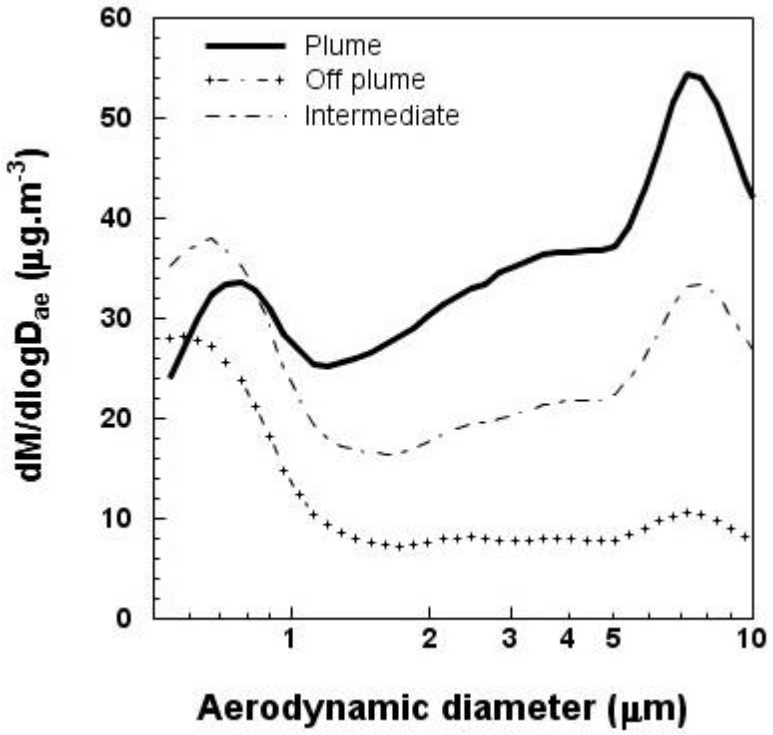

Figure S6. Average coarse particle mass size distributions for plume, off-plume and intermediate periods averaged for 1379, 6033 and 979 scans by an APS respectively.

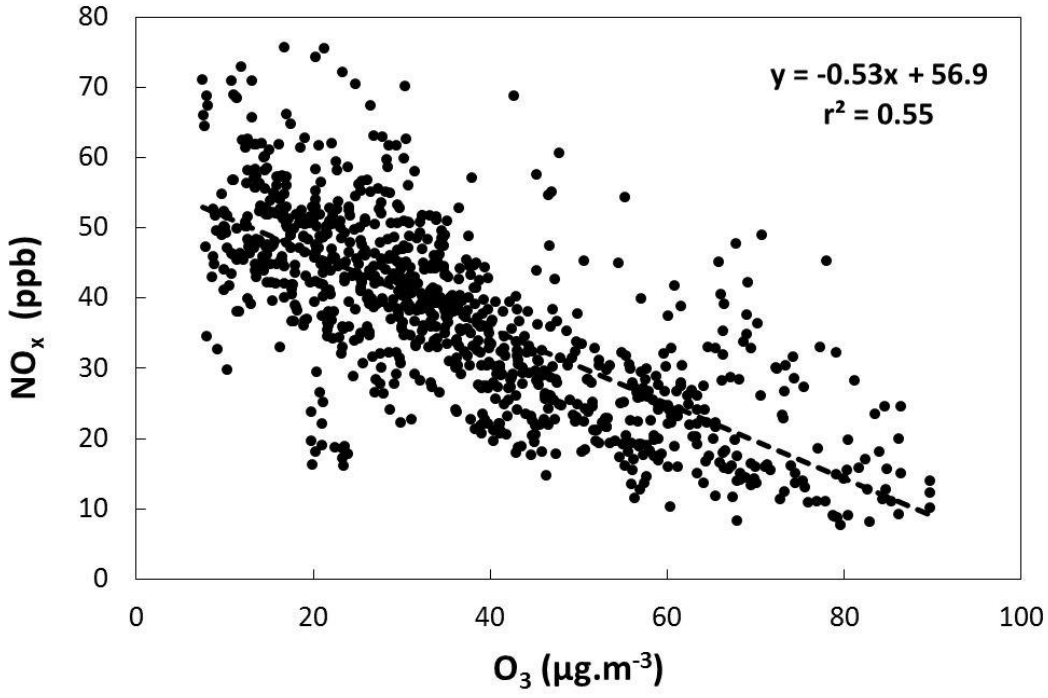

Figure S7. Linear regression between 5 minute data of O_3 and NO_x during plume periods.

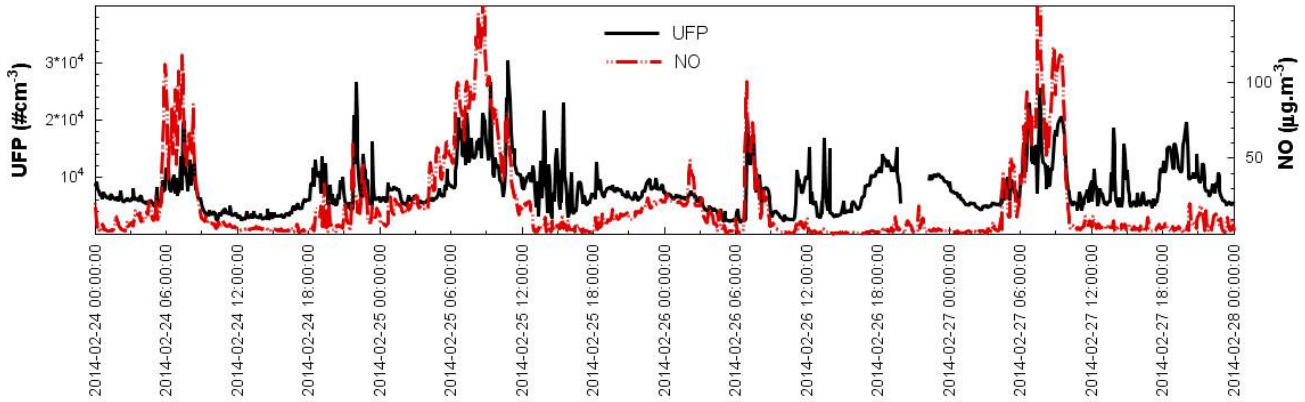

Figure S8. Time series of UFP number and NO concentrations, four consecutive weekdays, mostly off-plume and several intermediate episodes. Traffic related peaks of NO and UFP in the early mornings.

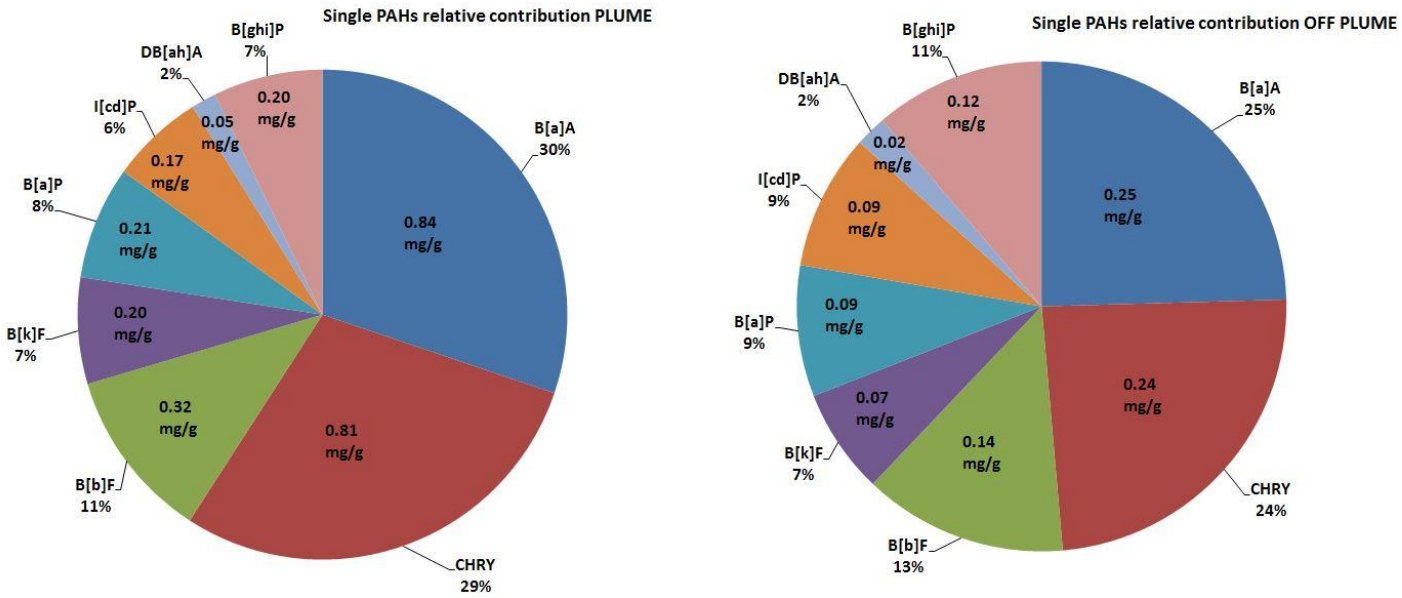

Figure S9. Average concentrations (mg.g^{-1}) and contribution (%) for individual PAHs in mass of UFPs samples, during plume (left) and off-plume (right) periods.

Tables

Table S1. The durations of the plume, off-plume and intermediate periods (hh:mm) within 24 hours (approximately from 10 AM to 10 AM next day) and appropriate PAHs concentrations in UFPs. Sampling period exceptions: * = 5 Feb 0:00 - 6 Feb 10:00, $^{+}$ = 6 Feb 10:00 – 7 Feb 11:00, # = power outage

Date	Plume hh:min	Off plume hh:min	Intermediate hh:min	PAHs mg/g	PAHs ng/m^3
5-Feb*	11:45	16:30	5:40	-	-
6-Feb^{+}	5:20	11:10	8:35	0.1	0.7
7-Feb	9:55	10:45	2:20	7.9	16.1
8-Feb	7:40	16:05	0:10	5.8	4.9
9-Feb	3:50	14:40	1:15	0.2	0.1
10-Feb	5:30	17:30	1:05	12.7	7.5
11-Feb	5:40	16:30	1:15	4.2	4.1
12-Feb	0:45	16:40	6:35	3.1	5.2
13-Feb	3:05	15:45	5:10	1.3	7.1
14-Feb	0:30	20:20	3:10	0.4	2.2
15-Feb	8:05	15:35	0:20	7.3	19.9
16-Feb	9:45	10:30	3:45	0.8	2.6
17-Feb	4:20	14:20	5:20	0.4	1.7
18-Feb	5:35	13:20	5:05	0.6	2.9
19-Feb	4:45	12:05	7:10	1.8	5.5
20-Feb	3:55	16:20	2:50	1.5	8.9
21-Feb	11:45	11:30	1:40	3.2	10.9
22-Feb		23:55	0:05	0.3	1.6
23-Feb		20:15	3:45	0.9	9.0
24-Feb		19:45	4:15	0.9	5.6
25-Feb		20:50	3:10	1.1	6.9
26-Feb$^{\#}$		17:05	4:40	1.1	7.1
27-Feb		19:10	3:55	1.9	13.9
28-Feb	4:25	19:25	0:40	0.3	1.2
1-Mar	4:00	22:15	0:50	0.9	4.9
2-Mar		20:10	0:45	0.4	2.5
3-Mar$^{\#}$		14:35		2.3	16.6
4-Mar$^{\#}$		13:20	0:15	0.5	2.3
5-Mar		23:45		0.2	0.9
6-Mar		20:25		0.1	0.7
Total	04 days 14:35	21 days 00:30	03 days 11:45	Mean 2.1$\pm$2.9	Mean 6.2$\pm$5.1

Table S2. Statistics of UFPs number and coarse particle mass concentrations, CO and SO_2 and concentrations. The plume, off-plume and intermediate periods accounted for 16%, 72%, and 12% of the campaign time respectively.

	Plume				Off-plume				Intermediate			
	UFPs $10^4 \cdot cm^{-3}$	CO ppm	SO_2 ppb	Coarse $\mu g.m^{-3}$	UFPs $10^4 \cdot cm^{-3}$	CO ppm	SO_2 ppb	Coarse $\mu g.m^{-3}$	UFPs $10^4 \cdot cm^{-3}$	CO ppm	SO_2 ppb	Coarse $\mu g.m^{-3}$
Mean ±SD	2.7 ±1.4	1.4 ±1.3	12 ±12.3	37 ±34	1 ±0.4	0.5 ±0.3	2.7 ±2.8	8.7 ±7.6	2.3 ±0.6	0.9± 0.6	3.6 ±3.1	22.1 ±17.5
Max	14.3	11.3	88.2	403.1	2	5.7	35.6	89.6	7.6	8	29.1	153.4
Median	2.4	0.9	6.2	28.2	1	0.4	1.8	6.7	2.2	0.9	2.5	16.3
75^{th}	3.3	2	15.5	47.9	1.3	0.7	3.3	10.3	2.6	1.2	4	29.5
25^{th}	1.8	0.5	3.3	15.1	0.6	0.3	1.2	4.3	1.9	0.5	1.8	11

Manuscript 2:

Hovorka J., Leoni C., Dočekalová V., Ondráček J., Zíková N.

Aerosol distribution in the planetary boundary layer aloft a residential area

Aerosol Distribution in The Planetary Boundary Layer Aloft a Residential Area

Jan Hovorka [1], Cecilia Leoni [1], Veronika Dočekalová [1], Jakub Ondráček [2], Naděžda Zíková [1]

[1] Institute for Environmental Studies, Faculty of Science, Charles University in Prague, Benátská 2, 128 01 Prague 2, Czech Republic
[2] Laboratory of Aerosol Chemistry and Physics, Institute of Chemical Process Fundamentals of the CAS, v. v. i., Rozvojová 2/135, 165 02 Prague 6, Czech Republic

E-mail: leonic@natur.cuni.cz

Abstract. Atmospheric aerosol is an omnipresent component of the Earth atmosphere. Aerosol particle of diameters < 100 nm or > 1 μm defines ultrafine or coarse aerosol particles, respectively. Aerosol particle concentrations within the planetary boundary layer - PBL are measured at the ground level while their vertical profiles in the PBL are usually estimated by modelling. The aim of this study was to construct vertical concentration profiles of ultrafine and coarse aerosol particles from airborne and ground measurements conducted in an urban airshed. Airborne measurements were done by an unmanned airship, remotely controlled with GPS 10 Hz position tracking, and electrically powered with propulsion vectoring, which allows average cruising speed of 6 $m.s^{-1}$. The airship carried three aerosol monitors and a temperature sensor. The monitors acquired 1 Hz data on mass concentration of coarse and number concentration of ultrafine particles. Four flight sequences were conducted on the 2nd of March 2014 above Plesna village, up-wind suburb of Ostrava in the Moravian-Silesian region of the Czech Republic. The region is a European air pollution hot-spot. Repeated flights were carried out in several height levels up to 570 m above ground level - a.g.l. Early morning flight revealed a temperature inversion in the PBL up to 70 m a.g.l. This lead to coarse particle concentrations of 50 μgm^{-3} below the inversion layer and 10 μgm^{-3} above it. Concurrently, air masses at 90-120 m a.g.l. were enriched with ultrafine particles up to $2.5x10^4$ cm^{-3}, which may indicate a fanning plume from a distant emission source with high emission height. During the course of the day, concentrations of ultrafine and coarse particle gradually decreased. Nevertheless, a sudden increase of ultrafine particle concentrations up to $3.7x10^4$ cm^{-3} was registered at 400 m a.g.l. at noon and also after a lag of 20 min at the ground. This may indicate formation of new aerosol particles at higher altitudes, which are then transported downward by evolved convective mixing. Detailed information acquired by the airship measurements allow us to better understand processes resulting in the increase of aerosol particle concentrations at ground level in urban air.

1. Introduction

The planetary boundary layer - PBL, the lowest part of the troposphere, is influenced by the exchange of heat, water vapour, trace gases and aerosol particles with the Earth surface [1]. Surface heating produces a turbulent, well-mixed PBL during the day, while surface cooling after sunset may lead to a temperature inversion which causes the PBL stratification. Key constituent of the PBL is atmospheric

aerosol, a colloid originating from natural and anthropogenic sources. While natural aerosol sources prevail over the anthropogenic ones at remote locations or open troposphere [2], anthropogenic sources dominate in urban environment. Additionally, temperature inversion in the PBL prevents mixing of the anthropogenic aerosol with the free troposphere. Therefore, knowing the atmospheric aerosol distribution within the PBL at urban microscale is important for human exposure assessment. Unmanned aerial systems offer advantages as research platforms because of the possibility to investigate atmospheric parameters at small scale and low altitudes. Airships have the possibility to fly with low cruising speed at constant heights, with minimal logistic requirements and lower costs compared to the aircrafts [3, 4, 5, 6]. Also, compared to drones, airships can carry heavier payload [7]. This work presents and discusses airborne and ground-based measurement of the aerosol particles concentration, performed in March 2014 in a suburb of Ostrava, Czech Republic. This city is known as a European air pollution hot-spot [8, 9, 10]. The aim of this study was to construct vertical concentration profiles of size-segregated aerosol particles from airborne and ground measurements conducted in this urban air pollution hot-spot.

2. Methods

The measurements were performed in Ostrava city suburb Plesna (Figure 1) mainly composed of family houses. The suburb is relatively far from any direct industrial and/or traffic pollution. The airborne measurements were realized with an unmanned airship, remotely controlled with GPS 10 Hz position tracking and electrically powered with propulsion vectoring, which allows average cruising speed of 6 $m.s^{-1}$. The precision of the airship position tracking was 5 – 10 m vertically and 5–8 m horizontally. The scientific payload was composed of a laser nephelometer (DustTrak DRX-8533, TSI Inc.), two condensation nuclei counters (P-track 8525, TSI Inc.), and temperature sensor (111DL, Voltcraft). The nephelometer measured the mass concentration of coarse aerosol particles. Each of the counters was equipped with Particle Size Selector - PSS (model 376060. TSI Inc.) at the aerosol inlet but with different adjustments. The first PSS housing holds 7 screens, which raises the smallest detectable particle size limits to about 100 nm while there were no screens at the second PSS housing.

Figure 1. Aerial view of Plesna village, Ostrava city suburb, indicating the fixed site and the airship launch site; the scale bar shows the distances in meters of the airship-flying track

Therefore, the first counter detects particles within the size range of 100 – 1000 nm while the second within the size range of 20 - 1000 nm. The particle number concentrations - PNC within the ultrafine size range 20 – 100 nm are obtained by the difference of the first and second counter. The temperature sensor and also aerosol monitors acquired 1 Hz data. Concurrent ground measurements were conducted at fixed site (49°51'57.31"N, 18° 7'55.52"E, 290 m altitude), approximately 300 m far from the airship launch site (Figure 1). Five minute integrates of particle number concentrations and size distribution in size range 14 – 10000 nm were measured by a Scanning Mobility Particle Sizer (SMPS model 3936L75, TSI Inc.) and an Aerodynamic Particle Sizer (APS-3321, TSI Inc.). Meteorological parameters (wind speed, wind direction, relative humidity and temperature) were also recorded.

3. Results and discussions

Four flights were conducted: 1st at 06:40-7:50, 2nd at 8:13-9:40, 3rd at 9:55-11:11 and 4th at 11:25-12:19. During the first flight in the early morning, two temperature inversion layers were observed (Figure 2, left). The first was formed up to 70 m a.g.l. while the second reached heights 180-230 m a.g.l. Coarse aerosol mass concentrations 20-50 μgm^{-3} below the first inversion layer reflected coarse aerosol sources on the ground, also indicated by the elevated coarse particle concentration recorded at the fixed site on the ground (Figure 5, top). Above the first inversion layer, the concentration dropped to less than 10 μgm^{-3} (Figure 2, right). In contrast to coarse particles, ultrafine particle number concentrations were very high, up to $2.5x10^4$ cm^{-3}, at heights 90-120 m a.g.l., which may indicate a fanning plume from a distant emission source with a high emission height (Figure 3, right).

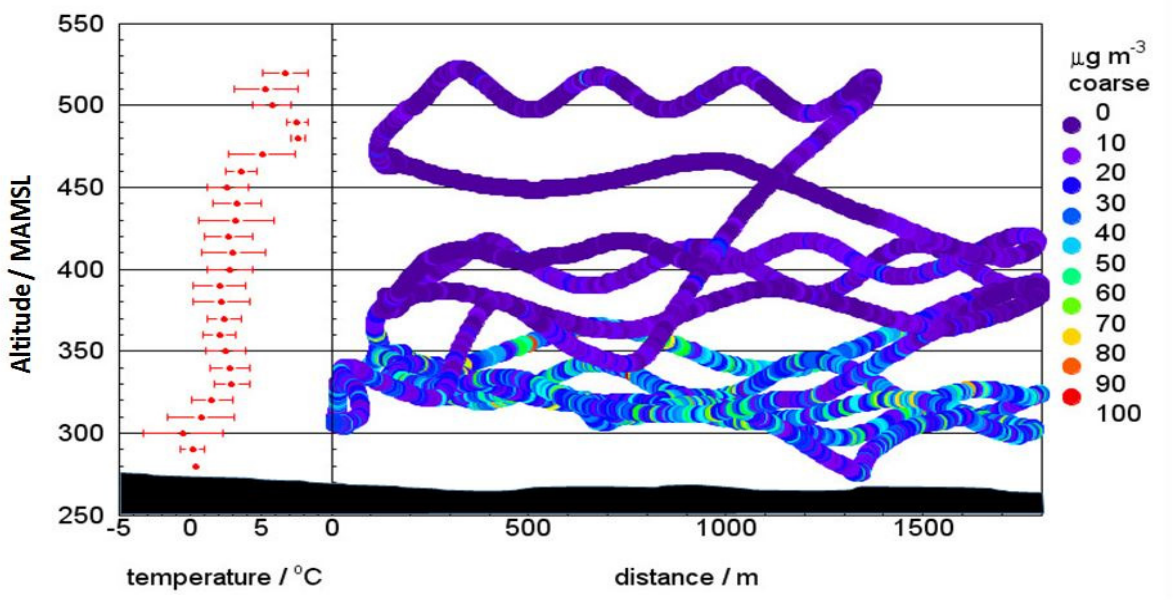

Figure 2. The PBL vertical profile of temperature (left) and coarse particle concentrations at the scale distances above Plesna village (right) during the 1st flight, 06:40-7:50

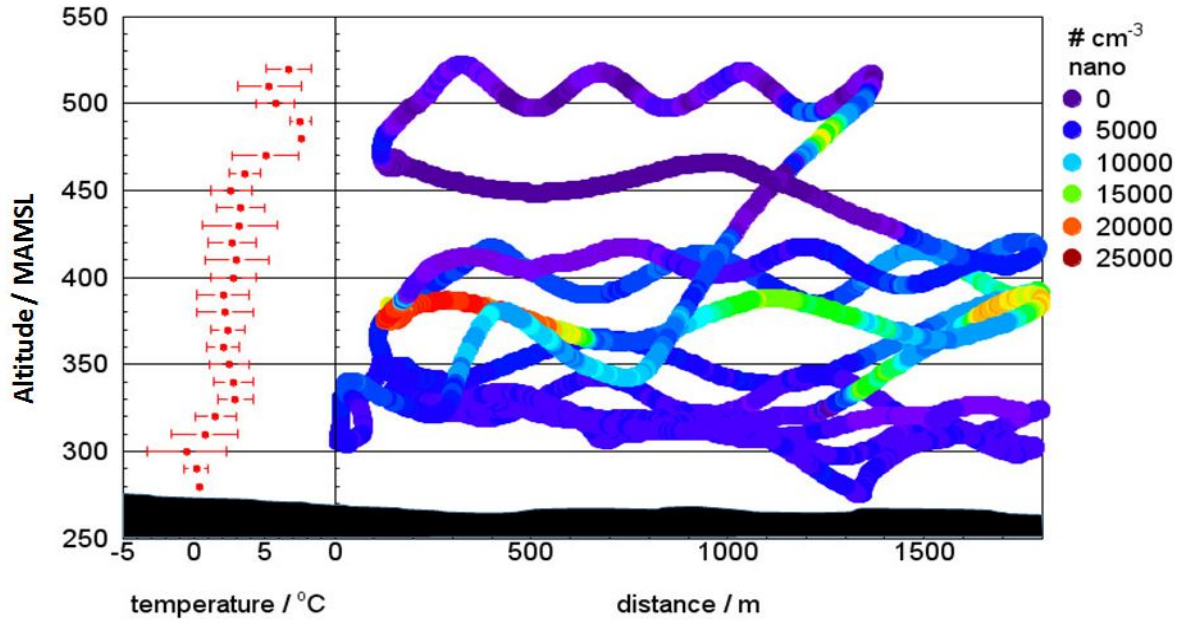

Figure 3. The PBL vertical profile of temperature (left) and ultrafine particle concentrations (right) at the scale distances above Plesna village during the 1st flight, 06:40-7:50

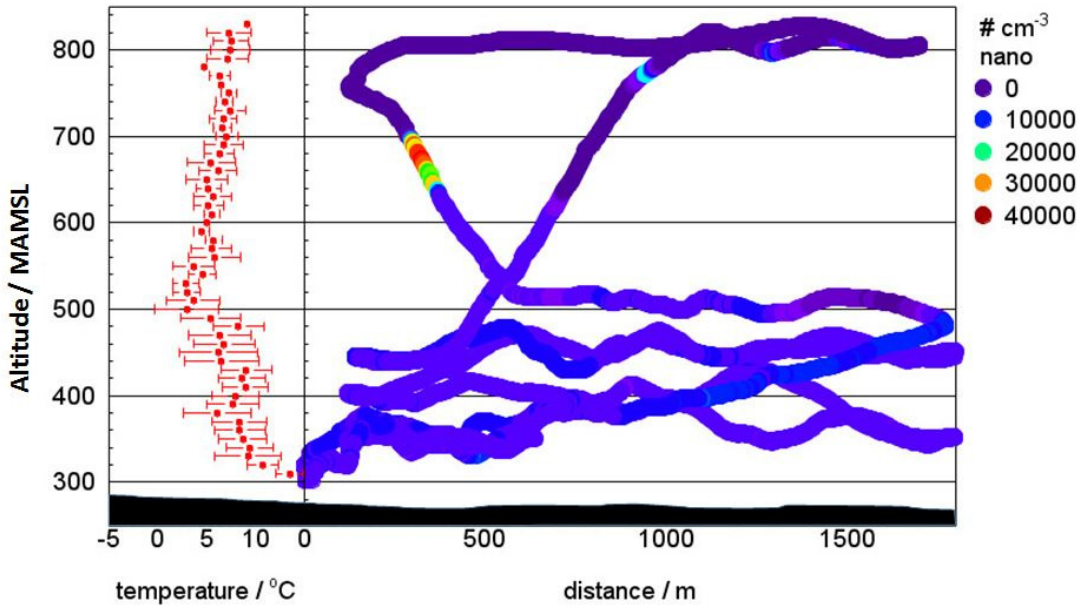

Figure 4. The PBL vertical profile of temperature (left) and ultrafine particle concentrations (right) at the scale distances above Plesna village. 4. Flight, 11:25-12:19

During the second flight, temperature inversion layer was observed only at heights 150-280 m a.g.l. as a consequence of surface heating. There were concentrations of coarse particle mass up to 39 μgm^{-3}

and number of ultrafine particles up to $20x10^4$ cm^{-3} recorded in this layer. During the third and fourth flights, the inversion disappeared due to the heating of the Earth's surface. Air masses can vertically mix and the concentration of both coarse and nanoparticles in the PBL decreased. Nevertheless, sharp increase in number concentrations of ultrafine particles up to $3.7x10^4$ cm^{-3} was recorded at heights of 380-400 meters a.g.l. (Figure 4, right) during the descending flight of the airship at 12:00:23-12:00:47. After a delay of 20 minutes, at 12:20-12:50, there was also a sudden increase of ultrafine particles concentration $1.5\text{-}2x10^4$ cm^{-3} observed at fixed site on the ground (Figure 5, bottom). This may indicate the process of formation of new particles occurring at higher altitude, which are subsequently transported downward by enhanced convective mixing and registered on the ground. Similar spatial/temporal dynamic of the PBL were observed in Melpitz, Germany [11].

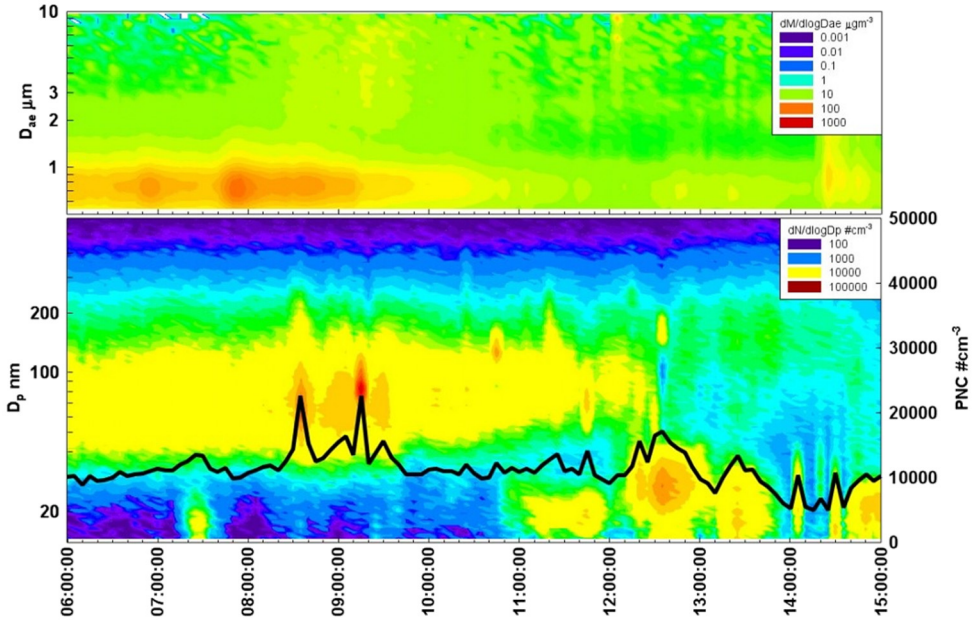

Figure 5. Contour graphs of the temporal variation of aerosol size distribution for mass (top, size range 0.5-10 µm) and for number (bottom, size range 14-732 nm), and ultrafine particle number concentration registered at the fixed site

4. Conclusions

Dynamics of vertical profiles for temperature, coarse and ultrafine aerosol particle concentration in the PBL in microenvironment of urban airshed was revealed by measurements with an unmanned airship. Early morning, temperature stratification of the PBL caused coarse particles to be accumulated below the inversion layer while ultrafine particles, emitted from distant source with high emission height, were trapped at heights 90-120 m a.g.l. During the course of day, the PBL stratification ceased and gradually evolved turbulent mixing led to a downward transport of ultrafine particles newly formed in higher elevations. Detailed information allows us to understand processes and apportion sources of aerosol particles in ground level in the urban micro environment and unmanned airship seems to be an optimal platform for airborne measurements.

Acknowledgment(s)

This project was supported projects No. P503/12/G147 of the Grant Agency of the Czech Republic and 1354314 of the Grant Agency of the Charles University in Prague.

References

[1] Finlayson-Pitts B., and Pitts J. N. 1999. *Chemistry of the Upper and Lower Atmosphere*, Academic Press, U.S.A.

[2] Jaenicke R. Is atmospheric aerosol an aerosol? - A look at sources and variability. *Farad. Discuss.*, 2008, 137, 235-243.

[3] Frick G.M., Hoppel W.A. Airship measurements of aerosol size distributions, cloud droplet spectra, and trace gas concentrations in the marine boundary layer. *B. Am. Meteorol. Soc,* 1993, 74(11), 2195-2202.

[4] Frick G.M., Hoppel W. A. Airship measurements of ships exhausts plumes and their effect on marine boundary layer clouds. *J. Atmos. Sci.,* 2000, 57, 2625–2648.

[5] Kantor G., Wettergreen D., Ostrowski J. P., Singh S., 2001. Collection of environmental data from an airship platform. *In: proceedings of SPIE Conference on Sensor Fusion and Decentralized Control IV*, October 28-29, 2001, vol. 4571, pages: 76-83.

[6] Gozzi F., Della Ventura G., Marcelli A. Mobile monitoring of particulate matter: state of the art and perspectives. *APR*, 2016, 7, 228-234.

[7] Brady J. M., Stokes M. D., Bonnardel J, Bertram T.H. Characterization of a quadrotor unmanned aircraft system for aerosol-particle-concentration measurements. *Environ. Sci. Technol.*, 2016, 50, 1376-1383.

[8] Pokorná P., Hovorka J., Hopke P. K. Elemental composition and source identification of very fine aerosol particles in a European air pollution hot-spot. *APR*, 2016, 7(14), 4671–679.

[9] Pokorná P.; Hovorka J.; Klán M.; Hopke P. K. Source apportionment of size resolved particulate matter at a European air pollution hot spot. *Sci. Total Environ.*, 2015, 502, 172-183.

[10] Šrám R. J., Dostál M., Libalová H., Rossner P., Rossnerová A., Švecová V., Topinka J., Bartonová A. The European hot spot of B[a]P and $PM_{2.5}$ exposure at the Ostrava region, Czech Republic: Health research results. *ISRN Public Health*, 2013, article ID 416701, 12 pages.

[11] Platis A., Altstädter B., Wehner B., Wildmann N., Lampert A., Hermann M., Birmili W., Bange J. An observational case study on the influence of atmospheric boundary-layer dynamics on new particle formation, *Boundary-Layer Meteorol.*, 2016, 158, 67–92.

Manuscript 3:

Leoni C., Pokorná P., Hovorka J., Masiol M., Topinka J., Zhao Y., Křůmal K., Cliff S., Mikuška P., Hopke P. K.

Source apportionment of aerosol particles at a European air pollution hot spot using particle number size distributions and chemical composition

Environmental Pollution 234 (2018) 145–154

Contents lists available at ScienceDirect

Environmental Pollution

journal homepage: www.elsevier.com/locate/envpol

Source apportionment of aerosol particles at a European air pollution hot spot using particle number size distributions and chemical composition☆

Cecilia Leoni [a, *], Petra Pokorná [a, b], Jan Hovorka [a], Mauro Masiol [c, g], Jan Topinka [d], Yongjing Zhao [e], Kamil Křůmal [f], Steven Cliff [e], Pavel Mikuška [f], Philip K. Hopke [c, g]

[a] Institute for Environmental Studies, Faculty of Science, Charles University, Benátská 2, 128 01 Prague 2, Czech Republic
[b] Laboratory of Aerosol Chemistry and Physics, Institute of Chemical Process Fundamentals CAS, Rozvojová 2/135, 165 02 Prague 6, Czech Republic
[c] Center for Air Resources Engineering and Science, Clarkson University, Potsdam, NY 13699-5708, USA
[d] Department of Genetic Toxicology and Nanotoxicology, Institute of Experimental Medicine CAS, Vídeňská 1083, 142 20 Prague 4, Czech Republic
[e] Air Quality Research Center, University of California, Davis, CA 95616, USA
[f] Institute of Analytical Chemistry CAS, Veveří 967/97, 602 00 Brno, Czech Republic
[g] Department of Public Health Sciences, University of Rochester Medical Center, Rochester, NY, USA

ARTICLE INFO

Article history:
Received 28 July 2017
Received in revised form
7 October 2017
Accepted 25 October 2017

Keywords:
Industry
Local heating
Nanoparticles
Positive matrix factorization
Polycyclic aromatic hydrocarbons

ABSTRACT

Ostrava in the Moravian-Silesian region (Czech Republic) is a European air pollution *hot spot* for airborne particulate matter (PM), polycyclic aromatic hydrocarbons (PAHs), and ultrafine particles (UFPs). Air pollution source apportionment is essential for implementation of successful abatement strategies. UFPs or nanoparticles of diameter <100 nm exhibit the highest deposition efficiency in human lungs. To permit apportionment of PM sources at the hot-spot including nanoparticles, Positive Matrix Factorization (PMF) was applied to highly time resolved particle number size distributions (NSD, 14 nm-10 μm) and $PM_{0.09\text{-}1.15}$ chemical composition. Diurnal patterns, meteorological variables, gaseous pollutants, organic markers, and associations between the NSD factors and chemical composition factors were used to identify the pollution sources. The PMF on the NSD reveals two factors in the ultrafine size range: industrial UFPs (28%, number mode diameter - NMD 45 nm), industrial/fresh road traffic nanoparticles (26%, NMD 26 nm); three factors in the accumulation size range: urban background (24%, NMD 93 nm), coal burning (14%, volume mode diameter - VMD 0.5 μm), regional pollution (3%, VMD 0.8 μm) and one factor in the coarse size range: industrial coarse particles/road dust (2%, VMD 5 μm). The PMF analysis of $PM_{0.09\text{-}1.15}$ revealed four factors: SIA/CC/BB (52%), road dust (18%), sinter/steel (16%), iron production (16%). The factors in the ultrafine size range resolved with NSD have a positive correlation with sinter/steel production and iron production factors resolved with chemical composition. Coal combustion factor resolved with NSD has moderate correlation with SIA/CC/BB factor. The organic markers homohopanes correlate with coal combustion and the levoglucosan correlates with urban background. The PMF applications to NSD and chemical composition datasets are complementary. PAHs in PM_1 were found to be associated with coal combustion factor.

1. Introduction

During the last 15 years, the 75% of the air quality monitoring stations in European Union (EU) registered a drop in the concentrations of atmospheric particulate matter (PM, EEA Report 2016). However, the concentrations of PM_{10} and $PM_{2.5}$ still exceed the EU limit values in some regions (EEA, 2016). Recently, ultrafine particles (UFPs, diameter <100 nm) have received great attention because they are particularly hazardous for human health: (i) they can reach the alveolar region of lung; (ii) they have high deposition efficiency (Venkatamaraan, 1999); and (iii) they have orders of magnitude higher surface area to mass ratios compared to larger particles.

☆ This paper has been recommended for acceptance by Eddy Y. Zeng.

* Corresponding author.
E-mail address: leonic@natur.cuni.cz (C. Leoni).

https://doi.org/10.1016/j.envpol.2017.10.097
0269-7491/

The Moravian-Silesian region (Fig. 1), in the north-eastern part of the Czech Republic, is an EU *hot spot* for air pollution. Epidemiological studies have demonstrated that the air pollution in Ostrava, the major city of the region, significantly affects the health of the population, with an increased rate of respiratory illnesses compared to other regions of the Czech Republic (Šrám et al., 2013a; Topinka et al., 2015). High anthropogenic emissions, due to the steel industry, coke plants, domestic heating, vehicular traffic, and the transport of polluted air masses from Poland, contribute to the worsening of air quality especially in the winter (Mikuška et al., 2015; Pokorná et al., 2015, 2016). The 24-h PM_{10} limit (50 μg m^{-3}) is frequently exceeded (CHMI, 2017) along with elevated concentrations of polycyclic aromatic hydrocarbons (PAHs) (Mikuška et al., 2015). High concentrations of UFPs (up to 1.4×10^5 cm^{-3}) highly enriched with PAHs (2.9 mg/g) were observed in the winter 2014 (Leoni et al., 2016). PAHs are formed by the incomplete combustion of fossil fuels and wood, and they have carcinogenic and mutagenic properties (Ravindra et al., 2008).

The planning and the application of abatement strategies to improve air quality are only possible when the pollution sources are identified and apportioned. This is challenging in this location, due to the presence of several sources, some of them situated near urban settlements. The source apportionment is possible through the application of Positive Matrix Factorization (PMF) bilinear model (Polissar et al., 2001; Hopke, 2016), where input data are composed of two matrices of temporal variability of aerosol chemical composition and mass. Highly time resolved aerosol data provide information at temporal resolution capable of identifying not only the main PM sources, but also sources that may have too short duration impact to be observed in 24 h integrated samples (e.g. Elsasser et al., 2012; Ancelet et al., 2012, 2014; Pancras et al., 2013; Moreno et al., 2013; Hovorka et al., 2015). Recently, source apportionment studies focus not only on particle mass, but also NSD (Harrison et al., 2011; Beddows et al., 2015; Masiol et al., 2017; Sowlat et al., 2016). The analysis of the mass chemical composition data distinguish sources contributing mainly to particle mass, while the analysis of the particle NSD identifies sources contributing principally to particle number, enabling the source apportionment down to nanoparticles (Beddows et al., 2015; Masiol et al., 2017).

Recent pollution source apportionment studies in this EU air pollution *hot spot,* based on size segregated aerosol chemical composition (Pokorná et al., 2015, 2016) revealed coal combustion, raw iron production, steel production and traffic being sources of $PM_{0.34\text{-}1.15}$ and road dust source of coarse particles ($PM_{1.15\text{-}10}$). The use of specific molecular markers (Mikuška et al., 2015) revealed combustion of wood and coal, vehicular emissions and industrial production of coke and iron the main $PM_{2.5}$ sources. Despite these studies, detailed pollution source identification down to nanoparticles was not performed yet.

The aim of this study is to give further insights on sources of winter air pollution including nanoparticles at the district Ostrava-Radvanice and Bartovice in, the example of industry impacted residential receptor site. Gaseous pollutants, organic markers and meteorological variables are used to help the source identification. The factors resolved with NSD are compared with mass chemical composition factors and associations are disclosed. Lastly, since PAHs are in high concentration in Ostrava and they are strongly harmful to human health, their association with PMF factors is discussed.

2. Methods

2.1. Experimental

An intensive sampling campaign was performed from 4th February to 7th March 2014 in the residential district of Ostrava – Radvanice and Bartovice, at the same site as in 2012 (Pokorná et al., 2015, 2016; Mikuška et al., 2015). The site was proven being representative at least for the district by $PM_{2.5}$ network measurements (Pokorná et al., 2015). A large metallurgy complex is located 1.5 km southwest of the sampling station (Fig. 1). The instruments were placed in an air-conditioned container. Five-minute integrated particle NSD were measured with a Scanning Mobility Particle Sizer (14–730 nm, SMPS-3936L25, TSI Inc.) and an Aerodynamic Particle Sizer (0.523–10 μm, APS-3321, TSI Inc.). Size segregated PM was collected with a Davis Rotating-drum Uniform-size-cut Monitor – 8DRUM (DELTA Group UC-Davis), from the 10th to 28th of February and is used to provide 2-h resolved PM compositions. Particles were collected on Mylar substrates lightly greased with Apiezon™. The 8DRUM collects particles in 8 size ranges from 0.09 μm to 10 μm. The five smallest size range samples, from 0.09 μm to 1.15 μm, were analyzed for 24 elements (Na, Mg, Al, Si, P, S, Cl, K, Ca, Ti, V, Cr, Mn, Fe, Co, Ni, Cu, Zn, Ga, As, Se, Br, Rb, Pb)

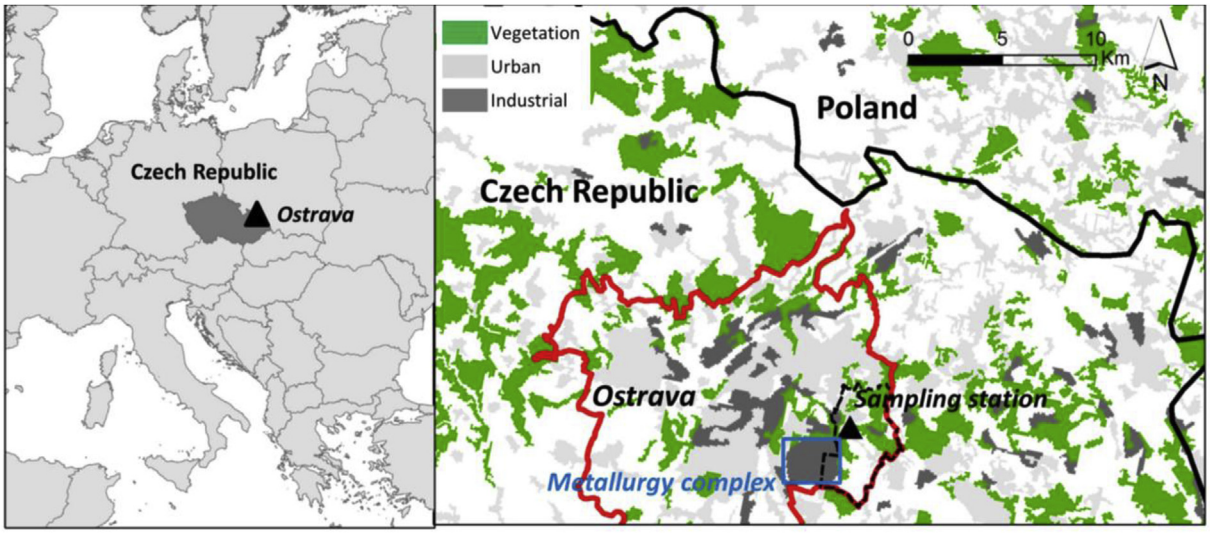

Fig. 1. Left: Czech Republic and Ostrava. Right: Sampling station (triangle), close to the metallurgy complex. Background map: Corine Land Cover 2012 version v.18.5.1.

using synchrotron X-ray fluorescence (S-XRF) by the Air Quality Research Center, University of California. For the modeling, data from the five size ranges were merged in $PM_{0.09\text{-}1.15}$ to overlap the size range of the NSD. The 2-h mass concentrations were measured with beta attenuation monitor (Ortec 590A).

Five-minute PM_{10} mass concentration was measured with a beta attenuation monitor (FH 62 I-R, Thermo ESM Andersen); wind speed – WS and wind direction – WD (WindSonic, Mc Gill); temperature – T (Comet 200-80/E); precipitation by disdrometer (Laser Precipitation Monitor, Thies); CO, NO_2, NO, O_3, SO_2, CH_4 and non-methane hydrocarbons with automatic monitors (Horiba-360 series). Hourly concentrations of organic and elemental carbon – OC/EC $PM_{2.5}$ (Sunset) were measured in semi continuous regime (45 min collection and 15-min analysis) using the NIOSH protocol (Birch and Cary, 1996), but only total carbon (TC) was eventually available for the data analysis due to technical problems with the analyzer. 24-hours levoglucosan, 16 US-EPA PAHs, 22R-17α(H),21β(H)-homohopane and 22S-17α(H),21β(H)-homohopane were determined in PM_1 collected on quartz filters using a high volume sampler (DHA-80, Digitel, 30 m^3 h^{-1}). Details of the sample preparation and the GC-MS analysis are described in the supplementary material.

2.2. PMF modeling

PMF (USEPA version 5.0) was applied to NSD data (14 nm–10 μm) and to $PM_{0.09\text{-}1.15}$ chemical composition separately.

For the NSD PMF we tested time resolution from 5 min to 2-h and determined 15-min resolution was optimal as these data are the best compromise to maintain a high time resolution but avoid unwanted noise. Additionally, the input data were handled by merging three consecutive bins, in order to (i) reduce the noise of the raw data, (ii) to decrease the variables number, (iii) to reduce the number of zeroes found in the coarse SMPS and APS bins (Masiol et al., 2016). Since the size segregation of SMPS is based on particle electrical mobility while the APS and 8DRUM impactor use particle aerodynamic properties, the mobility diameter was converted into aerodynamic using a standard ambient aerosol density (1.5 g cm^{-3}, Hinds, 1999). The final matrix had 2905 rows (samples) and 43 columns (bins/variables, Table S2). The uncertainties were calculated according to Vu et al. (2015). The total variable was calculated summing all the bins. PMF was run using: (i) different uncertainty input matrices, different C_3 value (Vu et al., 2015) in order to obtain the highest S/N ratio and the Q_{true} closest to $Q_{theoretical}$; (ii) different extra modeling uncertainty; (iii) different number of factors.

2-h integration time $PM_{0.09\text{-}1.15}$ chemical composition was used as input for PMF. The five size ranges of the chemical composition were modeled first separately, however the PMF output of the $PM_{0.09\text{-}1.15}$ chemical composition was adequately informative. To reduce the importance of TC in the model due to the high TC ratio to PM0.09–1.15 in comparison to elemental ratio to PM0.09–1.15 the TC analytical uncertainty was multiplied by a factor of 4, which gain the best output diagnostics also in other studies (Pokorná et al., 2015; Hovorka et al., 2015) The data matrix was composed of 2-h $PM_{0.09\text{-}1.15}$ mass concentrations calculated as a sum of the strip weights by beta gauge balance, corresponding elemental composition for 24 elements and $PM_{2.5}$ TC. The final matrix had 217 rows (samples) and 26 columns (species/elements). Mg, P, V, Ni, Ga and Rb variables were set as bad; Na, Al, Se and TC and PM as total variable were classified as weak.

Polar plots and daily pattern were obtained using the R Openair Package (Carslaw and Ropinks, 2012).

3. Results and discussion

3.1. Campaign overview

The average PM_{10} concentration during the sampling campaign was 47 ± 29 μg m^{-3}, with peaks up to 286 μg m^{-3}, registered with south-west WD (Fig. S14). $PM_{2.5}$ mass concentration, recalculated from merged SMPS and APS number concentration, was on average 37 ± 20.4 μg m^{-3}. The TC content in $PM_{2.5}$ was on average 16.3 ± 14.2 μg m^{-3}. The gaseous pollutant campaign averages for NO_2, NO, SO_2, and CO were 28.3 μg m^{-3}, 12.1 μg m^{-3}, 4.4 ppb, 0.7 ppm, respectively (Fig. S2). The values of PM_{10}, $PM_{2.5}$ and gaseous pollutants measured during the sampling campaign are consistent with the concentrations for air pollutants routinely measured by the Czech Hydro Meteorological Institute (CHMI, 2017) near the sampling station, for the winter season. Consequently, despite the intensive sampling campaign carried out in this study, results are considered representative of the pollution levels recorded in Ostrava-Radvanice for the whole season.

Nanoparticles (14-30 nm), Aitken mode particles (30-80 nm), accumulation mode particles (80 nm–1 μm) and coarse particles (1-10 μm) concentrations were respectively 3.5 × 10^3, 6.4 × 10^3, 6 × 10^3, and 3.7 particles cm^{-3} (Fig. S2). Winds from the third quadrant of the wind-rose (Fig. S4) were the most frequent (180°-270°deg. south-west direction, 32% of the campaign) and had the highest WS (average: 2.1 m s^{-1}). The northeast wind was the second most frequent (10% of the campaign), with an average WS of 1.6 m s^{-1}. The prevailing south-west and north-east WD points to the nearby metallurgical complex and to the urban settlement with single family houses, respectively. The low WS is favorable to NSD/PM contribution of the local sources and high WS of regional pollution.

For a detailed description of the meteorological conditions and of the UFPs number concentration and size distribution dynamics refer to Leoni et al., 2016.

3.2. Factors resolved with NSD PMF

The model was run approximately 120 times to find the most physically meaningful result and the best diagnostics. Four variables showed high scale residuals in the preliminary runs and they were marked as weak and their uncertainty tripled (18.5 nm, 20.6 nm, 0.47 μm and 5 μm). For 18.5 nm, 20.6 nm, the high number of residuals is likely due to the nature of the nanoparticles characterized by fast changes in NSD. The model was run with different factor number (4–9); the most stable solution was found for a 6-factor solution. Extra modeling uncertainty (8.5%) was included to encompass errors not considered in the uncertainty assessment. All run converged, the scales residuals were normally distributed, no unmapped factors were detected with bootstrap error estimation, no swaps were observed with displacement error analysis, indicating that the solution has no data error and it is well defined (Table S1). Solution having <6 factors returned unresolved sources, a high number of scaled residuals >3, and Q_{true} higher than $Q_{theoretical}$. When more than 6 factors were selected, a spurious factor appeared. This extra-factor does not have a physical meaning: it lacks any distinct diurnal pattern, it is uncorrelated to other auxiliary variables, it exhibits very small contribution to particle number concentration (PNC). In addition, solutions with >6 factors returned Q_{true} values well below the $Q_{theoretical}$.

Factor 1. This factor includes most of the particles in the nucleation range; it exhibits a sharp mode at 26 nm (Fig. 2), with the second largest contribution to PNC (26%). The average concentration of this factor is 4.5 × 10^3 particles cm^{-3}, but it shows peaks up to 3.4 × 10^4 particles cm^{-3}. The contribution to the volumetric

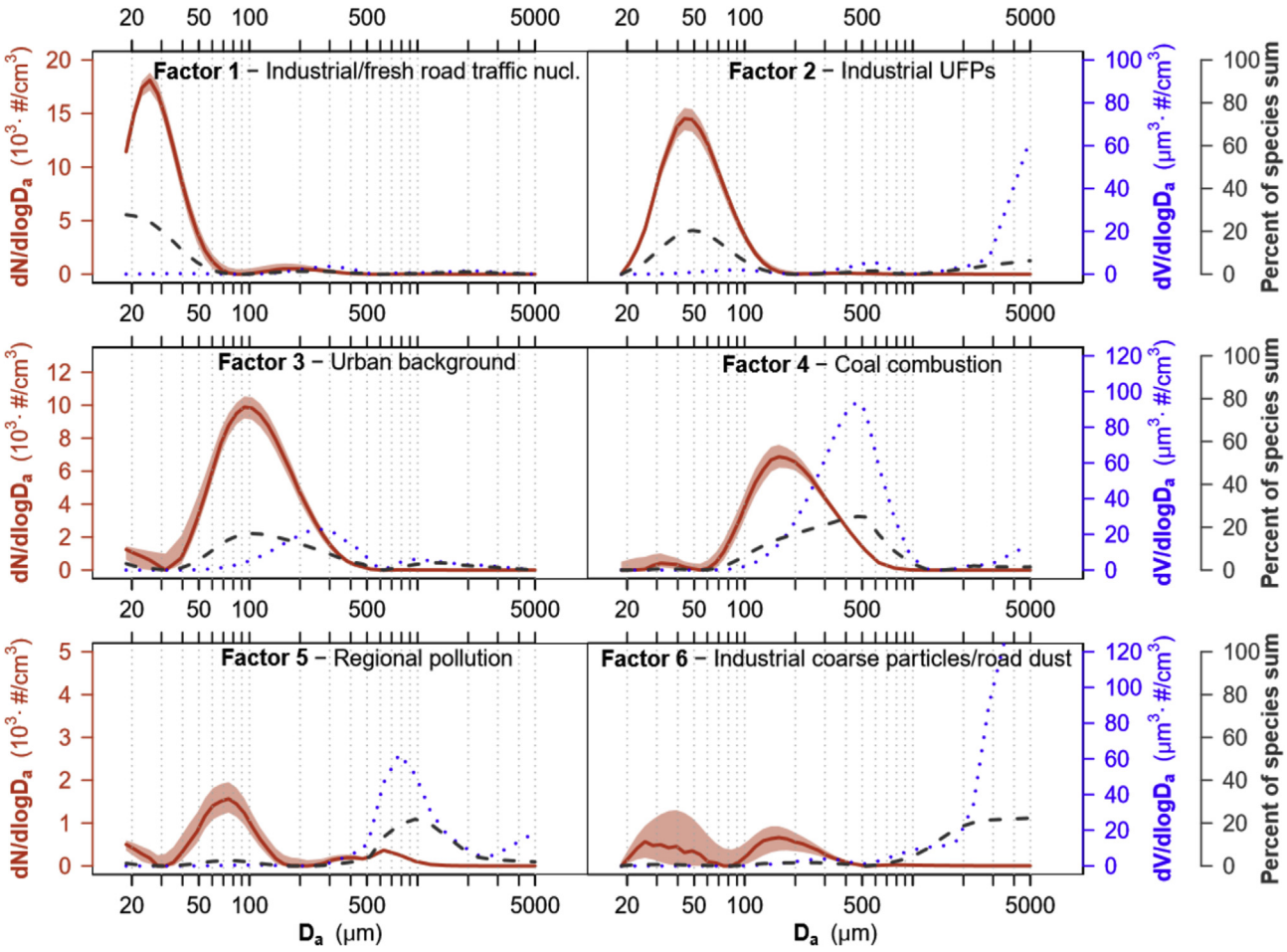

Fig. 2. NSD PMF factors. NSD (red line), volume size distribution (blue dotted line) and explained variation (black dashed line). The volume size distribution was re-calculated from the NSD assuming spherical particles. (For interpretation of the references to colour in this figure legend, the reader is referred to the web version of this article.)

concentration is low (2%). Photochemical nucleation is excluded because we do not observe new particle formation events with clear particle growth (*banana* shape) during the campaign, and we do not observe higher concentration at noon, when the solar radiation has the highest intensity (Leoni et al., 2016). Also, the high pollution level during the campaign is not a favorable condition for nucleation events due to high coagulation rate caused by high number of accumulation mode particles. For winds blowing from south-west, nanoparticles concentration increases with the WS (Fig. 3). The factor shows positive Spearman correlation with WS, NO_2, SO_2 (Fig. 3). The polar plots show the same area of origin for factor 1 and for the gaseous pollutants SO_2 and CO (Fig. S3), on the south west of the sampling station, where the metallurgy complex is located (Fig. 1). However, the daily pattern of factor 1 shows two daily peaks corresponding to rush hours (8 a.m. and 6 p.m.), suggesting road traffic emissions (Fig. 3). Peaks of factor 1 nanoparticles are also observed at the same time with peaks of NO (Fig. S5). These peaks are attributable to fresh road traffic emissions because NO is a pollutant primarily emitted by road traffic. The nanoparticles peaks, simultaneously with NO peaks, are observed on the days 5th, 22nd, 23rd, 24th, 25th and 26th, with a low WS (<1 ms^{-1}). The possible sources of traffic nanoparticles can be the district's main roundabout, located at 130 m north from sampling location, or the street located 60 m in south-west direction. However, a statistically significant difference between weekdays and weekends is not observed (Nonparametric Kruskal Wallis test, p value > 0.05). Industrial emissions and a minor contribution of fresh road traffic emissions can represent the sources of factor 1 nanoparticles. The metallurgy industry has been identified as a source of nanoparticles (Riffault et al., 2015; Leoni et al., 2016). Emissions of stationary combustion sources such as industrial stack plumes can contain high nanoparticles concentrations (Dall'Osto et al., 2008; Marris et al., 2012; Leoni et al., 2016). For example, Marris et al. (2012) observed particles with size 10-30 nm downwind of a large metallurgy facility in northern France.

Other studies reported multi-source factors in the ultrafine size range (Gu et al., 2011; Masiol et al., 2016). Nanoparticles can originate from various sources, and it is sometimes not possible to attribute to this factor only to one source. Even with varying the number of factors in the PMF modeling, this factor appeared in all the solutions, demonstrating its robustness and the lack of artifacts in the PMF solution. The problem in resolving the industrial and the freshly emitted road traffic can be due to the strong emission source represented by industry, close to the receptor. Analogous results are observed other studies having similar circumstances with very large local emissions dominating the PM concentrations (c.f., Owoade et al., 2015).

Factor 2. It is the major contributor to PNC (28%) and a minor contributor to volume concentration (6%), having a prominent mode at 45 nm (Fig. 2). The average concentration of factor 2 is 4.5×10^3 particles cm^{-3} with peaks up to 4.2×10^4 particles cm^{-3}. As for factor 1, the concentration increases with the WS and with

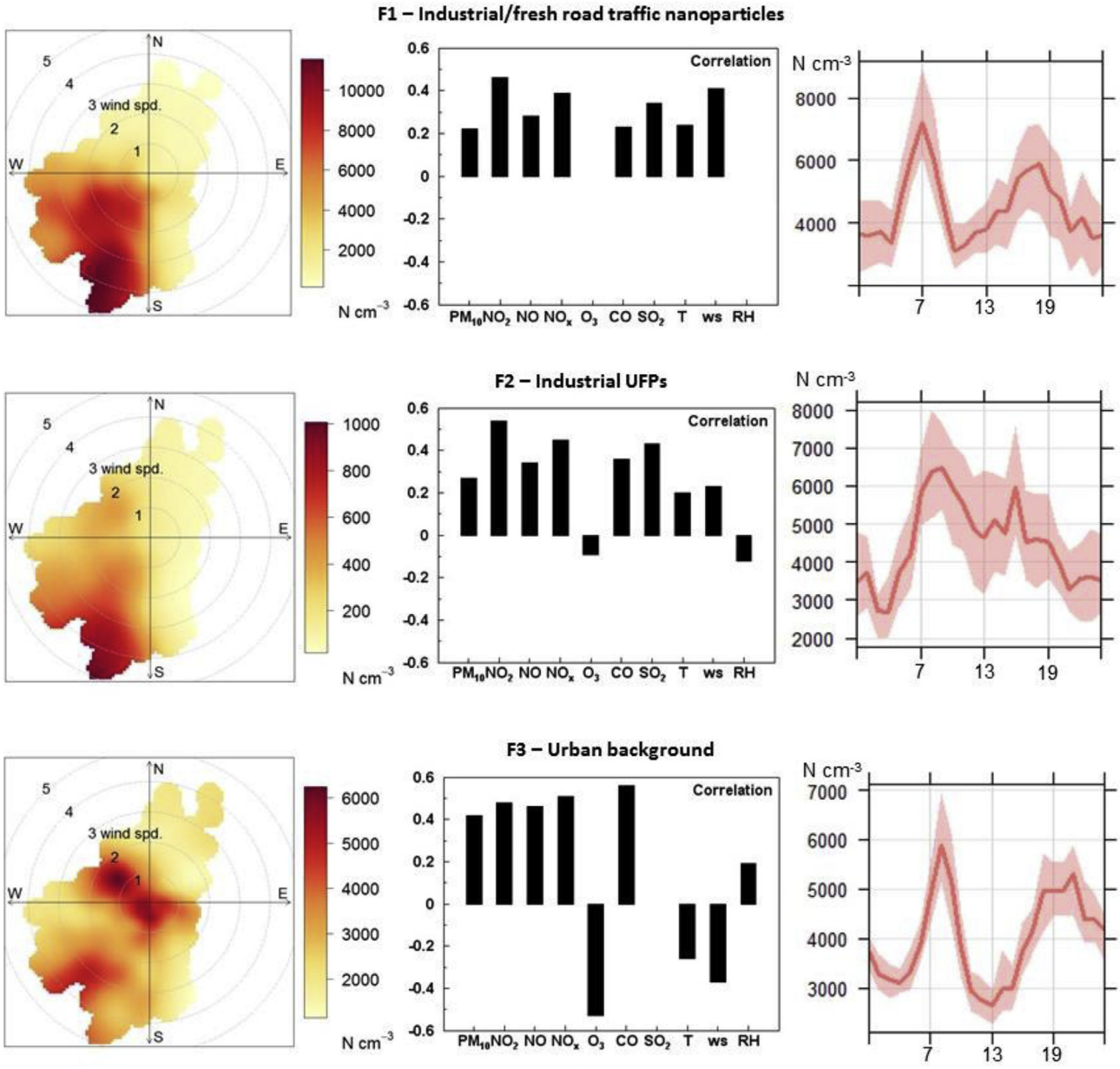

Fig. 3. Left: Polar plot with factors concentrations (15-min vector averaged WS and WD). Middle: histogram of Spearman correlation coefficients for auxiliary variables (only statistical significant coefficients $\rho < 0.05$ are shown). Right: daily pattern of PMF factors, the shaded area represents the 95th% confidence interval.

south western WD (Fig. 3), where the large metallurgy complex is situated (Fig. 1). Additionally, factor 2 polar plot is very similar to the SO_2 and CO polar plots (Fig. S3). The factor shows positive correlation with SO_2, CO, NO_2 (Fig. 3), gaseous pollutants that are emitted by iron and coke production. The factor does not show a clear daily pattern (Fig. 3), and there is no statistically significant difference in the concentration between the weekdays and the weekends (Nonparametric Kruskal Wallis test, p value > 0.05). The auxiliary variables indicate this is the industrial source. Indeed, metallurgy facilities can emit high concentrations of ultrafine particles with this size range (Riffault et al., 2015). In the same location, high concentrations of UFPs were measured with airborne measurement, pointing at steelwork chimney as major source (Leoni et al., 2016). Cheng et al., 2008, measured ultrafine particle size distribution in an iron foundry close to the iron production sector and observed high concentrations of ultrafine particles with a mode at 46 nm. Weitkamp et al., 2005, measured the industrial emissions from a steelwork and observed particles in with 45 nm size, when downwind of the facility.

Factor 3. Includes accumulation mode particles. The size distribution has a predominant mode, with number mode diameter (NMD) at 93 nm and a volume mode diameter (VMD) at 246 nm (Fig. 2). The average concentration was 4×10^3 particles cm^{-3} with peaks up to 2.2×10^4 particles cm^{-3}. This factor is an important contributor to PNC (24%), and a moderate contributor to the volume concentration (14%). This factor represents the urban background composed by particles originating from combustion sources, such as biomass burning and traffic. This factor has a positive correlation with NO_x, CO and PM_{10}, and the daily variability reflects the traffic pattern, with a dominant morning peak at 8 a.m., but also we

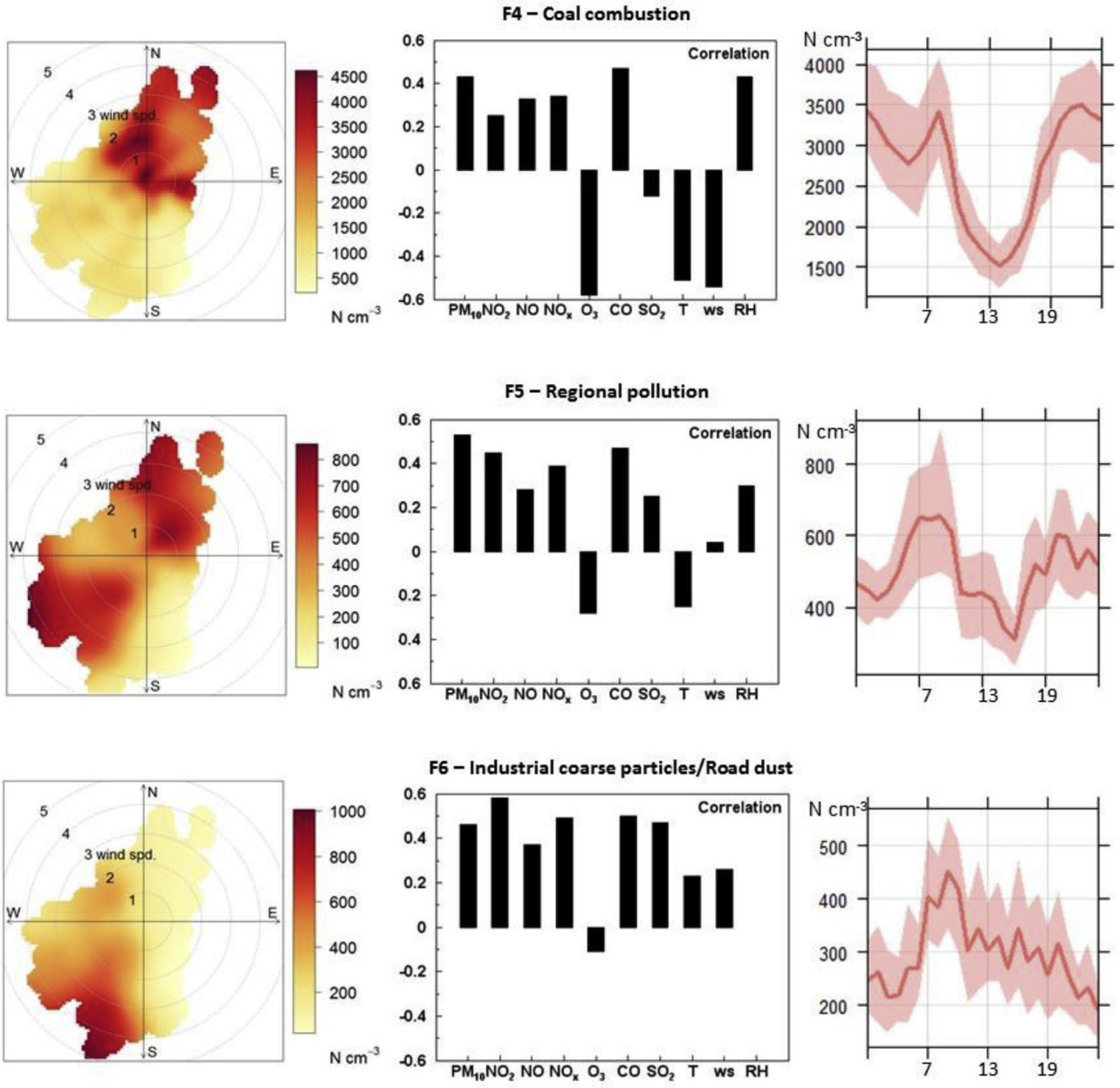

Fig. 3. (*continued*).

observe a broad peak in the evening from 6 p.m. to 10 p.m. (Fig. 3). The same variability is observed in the weekends. The highest concentrations are observed with low WS (<1 m/s), and with north eastern direction, where the major roundabout of the district is situated (Fig. 4). Additionally, lower contribution is observed with south western WD and WS > 2 m/s, where single family houses are located (Fig. 3). Factor 3 correlated well ($r^2 = 0.62$) with 24-h levoglucosan concentrations (Fig. S6). Levoglucosan is a tracer for biomass burning (BB). It is not detectable in smoke from coal burning (Simoneit et al., 1999). Particle emissions from BB are dominated by an accumulation mode peaking at 100-150 nm, and occasionally a nucleation mode (Janhall et al., 2010). A small contribution of nanoparticle can be observed in Fig. 3, with a small mode in the ultrafine size range. Similar factor with NMD at 80 nm and at 22 nm was observed by Dall'Osto et al., 2012 and attributed to urban background. Also, Vu et al., 2016 observed a similar factor with NMD at 93 nm, attributed to a mixture of carbonaceous particles originated by BB, and solid particles originated from traffic emissions. An urban background factor with the same daily pattern as in this study, consistent with both road traffic and with building heating, was observed by Beddows et al. (2015) and by Masiol et al. (2017). A recent study at the same location (Mikuška et al., 2015) found that levoglucosan is the most abundant compound in the $PM_{2.5}$ organic content, and that BB has a large contribution to the organic fraction of the atmospheric aerosol particles collected in Ostrava.

Factor 4. Includes particles in the accumulation size range, with NMD at 160 nm and VMD at 0.5 μm (Fig. 2). This factor has the highest contribution for the volume concentration (42%), and a moderate contribution to the number (14%). The number concentration average was $2.7X10^3$ particles cm^{-3}, with peaks up to 1.3×10^4 particles cm^{-3}. Factor 4 correlates ($r^2 = 0.62$) with R-

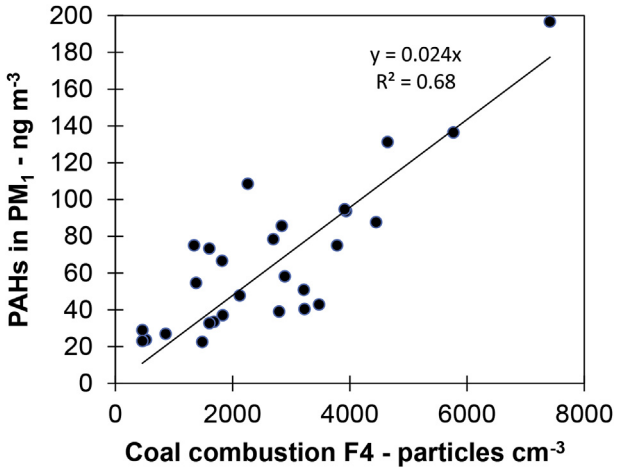

Fig. 4. Linear regression of total PAHs (ng m^{-3}) measured in PM_1 and the factor CC (particles cm^{-3}) resolved with NSD.

17α(H),21β(H)-homohopane, indicating that these particles likely originate from coal combustion (CC) emissions (Fig. S6). The homohopanes are organic compounds present in the smoke of CC but also in the lubricating oils of gasoline and diesel engines. The homohopane index (S/(S + R)) is the ratio between the concentration of R and S isomer of the 17α(H),21β(H)-homohopane and it is used to distinguish CC from traffic emissions and to sort coal according to its maturity. Higher concentrations of R isomer than S isomer, indicates dominant CC emissions, while equal isomer concentration indicates traffic emission being dominant (Křůmal et al., 2013). In a previous study, Mikuška et al., 2015, found that the concentration of R isomer of 17α(H),21β(H)-homohopane were higher than the concentration of S isomer, indicating that hopanes in Ostrava in winter originated predominantly from CC. In this study, the homohopane index ranged between 0.2 and 0.38 indicating emissions of semi-bituminous and bituminous CC (Oros and Simoneit, 2000).

Even if in the area is impacted by coke production emissions, this factor does not seem to be related to the industrial source. In fact, this factor is related to NNE winds (Fig. 3). The time series shows a typical local heating pattern, with a peak in the morning around 8 a.m. and a peak in the evening starting from 7 p.m., with a maximum at 10 p.m. and lasting all night (Fig. 3). This pattern can be also linked to the stagnant atmospheric conditions during winter nights, which trap the emissions in lower altitude. The time series is the mirror image of the air temperature. The positive correlation with NO_x, PM_{10} (Fig. 3) and TC (Fig. S7) indicates combustion sources as well. The highest concentrations of these particles, simultaneously correlated with homohopanes, were registered on the days 12th and 22nd to 25th, with calm winds and low temperature. For example, on February 12 the T did not go over 2 °C. This factor likely depicts local sources, with a contribution from the north-northwest where an urban settlement with single family houses in located.

Factor 5. This factor contributes to 3% of the number and 15% of the volume size distribution. It shows a VMD at 0.8 μm and a small mode with NMD at 75 nm (Fig. 2), an average concentration of 504 particles cm^{-3}. Higher concentrations, up to 3.8 × 10^3 particles cm^{-3}, occur with both south-western and north-eastern WDs, which are the two most frequent WDs, and the concentration increases with WS (Fig. 3). This factor shows a diurnal pattern with a broad peak in the morning, from 7 to 11 a.m., a minimum in the afternoon, and a further increase in the evening from 7 p.m. It does not show correlation with organic compounds, but it has a moderate correlation with PM_{10}, NO_2 and CO, (Fig. 3). The source of this factor is more difficult to attribute. Factor 5 concentration increases with the WS and it rises with both south-western and north-eastern WD. This factor can be attributed to regional pollution sources within Moravia-Silesia region (Fig. S11), but also pollution from the nearby Polish Silesia region cannot be excluded (Pokorná et al., 2015; Mikuška et al., 2015). Even if this factor presents the lower contributor to the number concentration, it makes appreciable contribution to the volume and for this reason was included in the solution. Also, it appeared in all the PMF solutions with 5 or more factors. Its exclusion produced a poor fit of the variables 0.8, 0.9, 1.2 and 1.4 μm, with high scaled residuals and ratio $Q_{true}/Q_{theoretical}$ >1. Similar factor with peak between 0.7 and 3 μm was found by Gu et al. (2011) in Ausburgh, Germany, attributed to long range PM pollution.

Factor 6. It is characterized by super-micrometer mode particles (Fig. 2). This factor makes an appreciable contribution to volume concentration (20%), and the smallest contribution to the number concentration (2%). It shows an average concentration of 296 particles cm^{-3} and peaks up to 3.4 × 10^3 particles cm^{-3} with increasing WS and south-south western direction. Factor 6 does not have a clear daily pattern. The polar plots of factor 1, 2 and 6 are similar (Fig. 3), pointing on industrial source. This factor can be associated with the unloading and stocking of iron ores and coal for the ironmaking processes, and to the preparatory blending of raw materials. Coarse particles with VMD mode at 8 μm are observed when downwind industrial emissions by Mbengue et al., (2014), in Dunkirk (France). Also, Dall'Osto et al., 2008, found in Port Talbot (UK) the vicinity of large steelwork coarse particles with mode centered at 6 μm.

Higher WS can promote soil and road dust re-suspension (Hinds, 1999). Peaks of factor 6 coarse particles appear simultaneously with peaks of the road dust factor in the mass concentration (Fig. S13), for example on February 19, 20, 25, 28. Gu et al., 2011 observed a peak in the NSD between 2 and 8.8 μm associated with natural crustal dust and resuspended road dust. Masiol et al., 2016, observed a peak in the volume concentration at 5 μm attributed to resuspension of crustal dust.

3.3. Factors resolved with chemical composition and association with NDS factors

To estimate the PMF optimal number of sources, 3 to 7 factor solutions were analyzed. The Q values, the resulting source profiles, and the scaled residuals were studied. The optimal factor number was 4 (Figs. S9 and S10).

Factor 1. This factor was associated with high concentrations of S, As, Se, Br, K and TC. According to the chemical profile, the factor represented a mix of secondary inorganic aerosol (SIA), CC, and BB. Due to the lack of BB tracer as soluble-potassium (K^+) or 2-h levoglucosan concentration, the model was not able to resolve the biomass burning factor. The $Q/Q_{expected}$>2 for total-potassium (K) could indicate the missing BB factor. Nevertheless, K should be used with caution as a BB tracer, although it is largely emitted by BB, it also derives from other sources, such as crustal dust, sea-salt, coal usage, waste incinerators and others (Duan et al., 2004; Wang et al., 2007; Caseiro et al., 2009; Mkoma et al., 2013). The time series shows two broad peaks, one in the morning and one in the evening, with a maximum at 10 p.m. reflecting the heating habits (Fig. S8). This factor dominated during the measurement campaign because it accounted for the 52% of $PM_{0.09–1.15}$ mass. The highest concentrations were registered on the 20th, 21st, 22nd and 24th days, when the WS was predominantly low (<2 ms^{-1}). Higher concentration is also observed with higher WS and north/north-east WD

(Fig. S12).

Factor 2. The second factor road dust from re-suspension and abrasion was represented by high contributions of Al, Si, Ca, Ti, Cu and TC (Han et al., 2005; Cheung et al., 2012), and contributed 22% to the $PM_{0.09-1.15}$ mass. Higher concentrations are observed with WSs between 1 and 3 ms^{-1} from the west, where a roundabout of the city district is situated (Fig. S12).

Factor 3. This factor was characterized by Na, Cl, Ca, Zn and TC and it was assigned to the sinter/steel production (Hleis et al., 2013) with a contribution of 16% to the $PM_{0.09-1.15}$ mass. According to the previous studies by Pokorná et al. (2015), 2016 this factor combines two industrial sources. The steel production source of very fine particles ($PM_{0.09-0.26}$) and the sinter production – hot and cold phase source of fine ($PM_{0.15-1.15}$) and coarse particles ($PM_{1.15-10}$), respectively. The high concentration with average WS of 3 m/s and contribution from south-west, points on local industrial source (Fig. S12). In winter with south-west wind episodes, this factor contributes significantly to the PM. This finding is not in agreement with the study by Vossler et al. (2016) due to the choice of the measurement season (10/17–6/12 does not response to the cold season) and consequent factor misinterpretation (factor mixed Cl ascribed to the combustion processes as transportation, biomass burning domestic waste, and/or coke; and road dust and road salt).

Factor 4 was ascribed to raw iron production because its profile shows high concentration of metals especially Mn, Fe and Co (Querol et al., 2007; Zhou et al., 2004; Cohen et al., 2010). The highest concentrations were registered when the average WS was 3 m/s. The polar plot matches the factor 3 polar plot (Fig. S12), pointing to local industrial source. This factor contributed 10% to the $PM_{0.09-1.15}$ mass.

The associations between the factors resolved with chemical composition and with NSD were investigated. Although the two datasets reflect in one case the physical and in the second case the chemical characteristics of the atmospheric particles, several factors show associations. In order to compare the different factors obtained by the separate modeling, the PMF NSD output data were averaged to 2-h time resolution after the modeling. NSD PMF factors industrial coarse particles, industrial UFPs, industrial/fresh traffic emitted nanoparticles have a positive correlation with sinter/steel production and iron production factors (Table 1). The CC factor resolved with NSD has moderate correlation with the SIA/CC/BB factor and moderate inverse correlation with iron and sintering/steel production.

3.4. Association between PAHs and PMF factors

PAHs are formed by the incomplete combustion of fossil fuels and wood and are associated with mobile, domestic and industrial emissions. Domestic emissions are predominantly associated with burning of coal, wood and waste. Metallurgy industry emits PAHs mainly from coke production (Ravindra et al., 2008). PAHs source identification is often challenging because they are produced by several sources and depending on the atmospheric conditions, they can partition between gaseous or particulate phase. In Czech Republic, especially in the urbanized areas of the Moravian-Silesian region and of the Silesia Province in Poland ambient concentrations of PM-bound PAH are the highest in Europe (Rogula-Kozłowska et al., 2013; CHMI, 2017; Mikuška et al., 2015; Topinka et al., 2015; Rogula-Kozłowska, 2015; EEA, 2016). A study conducted in the same location in winter 2012 reported PAHs concentration during a smog and a post-smog episode 1223 ng m^{-3} and 224 ng m^{-3}, respectively (Mikuška et al., 2015). PAHs can be associated with particles with different size ranges (Topinka et al., 2010). Modes in the mass size distribution for PAHs are typically within the ultrafine and accumulation mode (0.1–1 μm) (Keyte et al., 2013). In a previous study performed by Topinka et al. (2015) in the same locality, PAHs were measured in the size segregated PM with 24 h time resolution. PAHs were found in all the PM size fractions, mostly in the upper accumulation mode (0.5–1 μm). Nevertheless, the scanning electron microscopy suggested that the accumulation mode fraction was mostly composed of UFPs aggregates. This finding was confirmed by our previous study: high concentrations of UFPs highly enriched with PAHs were measured when downwind of the large steelworks (Leoni et al., 2016).

In this study, PAH concentrations measured in PM_1 ranged from 23 to 197 ng m^{-3}, with an average of 66 ng m^{-3}. PAHs showed positive correlation with R-homopane ($r^2 = 0.88$) and levoglucosan ($r^2 = 0.67$). Correlation is also found between total PAHs and the CC factor resolved with NSD (Fig. 4), with $r^2 = 0.68$. Higher PAH concentrations are observed with low WS (1-2 m s^{-1}) and north WD (Fig. S12).

In summary, according to the previous and present studies, different sources are contributing to PAH pollution at the receptor site, based on WD: industrial emissions with southwesterly wind, BB and CC with north-northeasterly wind. The size of the particles enriched with PAHs is different: in the case of industrial emissions, PAHs enrich the UFPs; in the case of the combustion emissions, PAHs enrich the accumulation fraction. Higher time resolution analysis can give further insight on the sources of PAHs at this location. Highly resolved PAH analysis and comparison with the WS and direction provide information on the variable impact of industrial/combustion emissions, and consequently can elucidate the major PAHs source.

4. Conclusions

The aim of this study was to identify the major sources of atmospheric particles in an EU air pollution *hot spot* down to nanoparticles using PMF. Here we find that industrial source is the major contributor to the PNC at the receptor. The largest contribution is from UFPs (54%) and a minor contribution is from supermicrometer particles (20% by volume). In the ultrafine size range, a minor source is also fresh traffic emissions. This study was not able to make a clear separation of nanoparticles originated from industry or road traffic. Also, it was not possible to assign a specific

Table 1
Spearman correlation coefficients ρ between PMF factors. Only statistically significant correlation coefficients ($p < 0.05$) are shown. Coefficients with moderate ($0.35 < r < 0.65$) and strong ($p > 65$) correlation are in bold.

	SIA/BB/CC	Iron production	Sinter/steel prod.	RD
Industrial/fresh traffic nanop.	−0.43	**0.65**	**0.35**	0.18
Industrial UFPs	−0.36	**0.4**	**0.37**	0.16
Urban Background		−0.17	0.19	−0.25
Coal Combustion	**0.45**	**−0.51**	**−0.35**	0.03
Regional pollution		0.28		0.10
Industry coarse part./RD	−0.21	**0.51**	**0.34**	0.22

industrial process to the different factors in the ultrafine size range (for example coke production, iron production or sintering) due to the complexity of the industrial emissions, the mixture of stationary and fugitive emissions, the continuous or batch processes, the close proximity of processes in the facility, the vicinity of the facility itself. The major sources of $PM_{0.9\text{-}1.15}$ mass concentration at the receptor during the winter are SIA/CC/BB (52%). The contribution of combustion sources is observed with north-north easterly WD.

Data analysis based on both NSD and chemical composition, elucidated many components in common, as well as other factors which were unique to each method. From this study, we can conclude that the two approaches are complementary: due to the very small mass of the UFPs, it is often not possible to include them in PMF modeling of PM sampled with impaction techniques. Additionally, in this study the two factors in the ultrafine size range were partially below the lowest cutoff of the 8DRUM impactor (90 nm). On the other hand, the source attribution to the NSD factors alone can be challenging due to the lack of chemical information. For the NSD source identification, the auxiliary variables and the meteorology data are important. Nevertheless, multiple sources can emit gaseous pollutants, for example CO, NO, NO_2, can be originated by combustion, vehicular traffic, industry. A more specific tracer of CC is SO_2, which is not produced by traffic emission, but distinguishing between industrial and coal combustion for heating purposes is often difficult. The organic tracers (levoglucosan and homohopanes) played a crucial role in the sources identification in this study, because they allowed apportioning the sources without ambiguity.

Regarding PAHs, the results from this study and from the previous studies were analyzed. Three main sources are contributing to PAH pollution at the receptor: industrial emissions, combustion of biomass and coal. These sources contribute to different particle size and depend on WS and WD. With southwestern WD, industrial sources are dominant, and with north-north eastern WD the combustion sources seem to be dominant. High time resolution PAHs measurements, for example hourly resolved, in Ostrava Radvanice and Bartovice are needed to precisely quantify the PAHs sources.

Acknowledgment

This work was supported by the Czech Science Foundation of the Czech Republic under the project P503/12/G147. The research fellowship of one of the authors (P.P.) at the CARES, Clarkson University was funded by the Fulbright Scholar Program. This research used resources of Beamline 10.3.1 of the Advanced Light Source, which is a DOE Office of Science User Facility under contract no. DE-AC02-05CH11231.

Appendix A. Supplementary data

Supplementary data related to this article can be found at https://doi.org/10.1016/j.envpol.2017.10.097.

References

Ancelet, T., Davy, P.K., Mitschell, T., Trompetter, W.J., Markwitz, A., Weatherburn, D.C., 2012. Source of particulate matter pollution in a small New Zealand city. Environ. Sci. Technol. 46, 4767–4774. https://doi.org/10.5094/APR.2014.066.

Ancelet, T., Davy, P.K., Trompetter, W.J., Markwitz, A., Weatherburn, D.C., 2014. Sources and transport of particulate matter on an hourly time-scale during the winter in a New Zealand urban valley. Urban Clim. 10, 644–655. https://doi.org/10.1016/j.uclim.2014.06.003.

Beddows, D.C.S., Harrison, R.M., Green, D.C., Fuller, G.W., 2015. Receptor modeling of both particle composition and size distribution. Atmos. Chem. Phys. 15, 10107–10125. https://doi.org/10.5194/acp-15-10107-2015.

Birch, M.E., Cary, R.A., 1996. Elemental carbon-based method for occupational monitoring of particulate diesel exhaust: methodology and exposure issues. Analyst 121, 1183–1190. https://doi.org/10.1039/AN9962101183.

Carslaw, D.C., Ropinks, K., 2012. *Openair* – an R package for air quality data analysis. Environ. Model. Soft 27-28, 52–61. https://doi.org/10.1016/j.envsoft.2011.09.008.

Caseiro, A., Bauer, H., Schmidl, C., Pio, C.A., Puxbaum, H., 2009. Wood burning impact on PM_{10} in three Austrian regions. Atmos. Environ. 43, 2186–2195. https://doi.org/10.1016/j.atmosenv.2009.01.012.

Cheng, Y.H., Chao, Y.C., Wu, C.H., Tsai, C.J., Uang, S.N., Shih, T.S., 2008. Measurement of ultrafine particles concentrations and size distribution in an iron foundry. J. Hazard. Mater. 158, 124–130. https://doi.org/10.1016/j.jhazmat.2008.01.036.

Cheung, K., Schafer, M., Schauer, J.J., Sioutas, C., 2012. Historical trends in the mass and chemical species concentrations of coarse particulate matter in the Los Angeles Basin and relation to sources and air quality regulations. J. Air Waste Manag. Assoc. 62, 541–556. https://doi.org/10.1080/10962247.2012.661382.

Cohen, D.D., Crawford, J., Stelcer, E., Bac, V.T., 2010. Characterisation and source apportionment of fine particulate matter at Hanoi 2001 to 2008. Atmos. Environ. 44, 230–328. https://doi.org/10.1016/j.atmosenv.2009.10.037.

Czech Hydro-meteorological Institute (CHMI), 2017. website, annual graphic overview. http://portal.chmi.cz/files/portal/docs/uoco/isko/grafroc/14groc/gr14e/Obsah_GB.html [last accessed: 27.03.2017].

Dall'Osto, M., Booth, M.J., Smith, W., Fisherb, R., Harrison, R.M., 2008. A study of the size distributions and the chemical characterization of airborne particles in the vicinity of a large integrated steelworks. Aerosol Sci. Technol. 42, 981–991. https://doi.org/10.1080/02786820802339587.

Dall'Osto, M., Beddows, D.C.S., Pey, J., Rodriguez, S., Alastuey, A., Harrison, R.M., Querol, X., 2012. Urban aerosol size distributions over the Mediterranean city of Barcelona, NE Spain. Atmos. Chem. Phys. 12, 10693–10707. https://doi.org/10.5194/acp-12-10693-2012.

Duan, M., Zhuang, G., Li, X., Tao, H., Zhuang, Y., 2004. The characteristics of carbonaceous species and their sources in $PM_{2.5}$ in Beijing. Atmos. Environ. 38, 3443–3452. https://doi.org/10.1016/j.atmosenv.2004.02.052.

EEA, European Environment Agency, 2016. EEA Report No 28/2016.

Elsasser, M., Crippa, M., Orasche, J., DeCarlo, P.F., Oster, M., Pitz, M., Cyry, J., Gustafson, T.L., Petterson, J.B.C., Schnelle-Kreis, J., Prevot, A.S.H., Zummermann, R., 2012. Organic molecular markers and signature from wood combustion particles in winter ambient aerosols: aerosol mass spectrometer (AMS) and high time-resolved GC-MS measurements in Augsburg, Germany. Atmos. Chem. Phys. 12, 6113–6128. https://doi.org/10.5194/acp-12-6113-2012.

Gu, J., Pitz, M., Schnelle-Kreis, J., Diemer, J., Reller, A., 2011. Source apportionment of ambient particles: comparison of positive matrix factorization analysis applied to particle size distribution and chemical composition data. Atmos. Environ. 45, 1849–1857. https://doi.org/10.1016/j.atmosenv.2011.01.009.

Han, J.S., Moon, K.J., Ryu, S.Y., Kim, Y.J., Perry, K.D., 2005. Source estimation of anthropogenic aerosols collected by a DRUM sampler during spring 2002 at Gosan, Korea. Atmos. Environ. 39, 3113–3125. https://doi.org/10.1016/j.atmosenv.2005.01.047.

Harrison, R.M., Beddows, D.C.S., Dall'Osto, M., 2011. PMF analysis of wide range particle size spectra collected on a major highway. Environ. Sci. Technol. 45, 5522–5528. https://doi.org/10.1021/es2006622.

Hinds, W.C., 1999. Aerosol Technology, Properties, Behavior, and Measurement of Airborne Particles, second ed. Wiley, U.S.A.

Hleis, D., Fernández-Olmo, I., Ledoux, F., Kfoury, A., Courcot, L., Desmonts, T., Courcot, D., 2013. Chemical profile identification of fugitive and confined particle emissions from integrated iron and steelmaking plant. J. Hazard. Mater. 246–255, 250-251. https://doi.org/10.1016/j.jhazmat.2013.01.080.

Hopke, P.K., 2016. Review of receptor modelling methods for source apportionment. J. Air & Waste Manag. Assoc. 66, 237–259. https://doi.org/10.1080/10962247.2016.1140693.

Hovorka, J., Pokorná, P., Hopke, P.K., Křůmal, K., Mikuška, P., Píšová, M., 2015. Wood combustion, a dominant source of winter aerosol in residential district in proximity to a large automobile factory in Central Europe. Atmos. Environ. 113, 98–107. https://doi.org/10.1016/j.atmosenv.2015.04.068.

Janhall, S., Andreae, M.O., Poschl, U., 2010. Biomass burning aerosol emissions from vegetation fires: particle number and mass emission factors and size distributions. Atmos. Chem. Phys. 10, 1427–1439, 2010. https://doi.org/10.5194/acp-10-1427-2010.

Keyte, I.J., Harrison, R.J., Lammel, G., 2013. Chemical reactivity and long-range transport potential of polycyclic aromatic hydrocarbons – a review. Chem. Soc. Rev. 42, 9333–9391. https://doi.org/10.1039/C3CS60147A.

Křůmal, K., Mikuška, P., Večeřa, Z., 2013. Polycyclic aromatic hydrocarbons and hopanes in PM_1 aerosols in urban areas. Atmos. Environ. 67, 27–37. https://doi.org/10.1016/j.atmosenv.2012.10.033.

Leoni, C., Hovorka, J., Docekalova, V., Cajthaml, T., Marvanova, S., 2016. Source impact determination using airborne and ground measurements of industrial plumes. Environ. Sci. Technol. 50, 9881–9888. https://doi.org/10.1021/acs.est.6b02304.

Marris, H., Deboudt, K., Augustin, P., Flament, P., Blond, F., Fiani, E., Fourmentin, M., Delbarre, H., 2012. Fast changes in chemical composition and size distribution of fine particles during the near-field transport of industrial plumes. Sci. Total Environ. 427-428, 126–138. https://doi.org/10.1016/j.scitotenv.2012.03.068.

Masiol, M., Vu, T.V., Beddows, D.C.S., Harrison, R.M., 2016. Source apportionment of wide range particle size spectra and black carbon collected at the airport of Venice (Italy). Atmos. Environ. 139, 56–74. https://doi.org/10.1016/j.atmosenv.

2016.05.018.
Masiol, M., Hopke, P.K., Felton, H.D., Frank, B.P., Rattigan, O.V., Wurth, M.J., LaDuke, G.H., 2017. Source apportionment of $PM_{2.5}$ chemically speciated mass and particle number concentrations in New York City. Atmos. Environ. 148, 215–229. https://doi.org/10.5094/APR.2013.018.
Mbengue, S., Alleman, L.Y., Flament, P., 2014. Size-distributed metallic elements in submicronic and ultrafine atmospheric particles from urban and industrial areas in northern France. Atmos. Res. 35–47, 135-136. https://doi.org/10.1016/j.atmosres.2013.08.010.
Mikuška, P., Křůmal, K., Večeřa, Z., 2015. Characterization of organic compounds in the $PM_{2.5}$ aerosol in winter in an industrial urban area. Atmos. Environ. 105, 97–108. https://doi.org/10.1016/j.atmosenv.2015.01.028.
Mkoma, S.L., Kawamura, K., Fu, P.Q., 2013. Contributions of biomass/biofuel burning to organic aerosols and particulate matter in Tanzania, East Africa, based on analyses of ionic species, organic and elemental carbon, levoglucosan and mannosan. Atmos. Chem. Phys. 13, 10325–10338. https://doi.org/10.5194/acp-13-10325-2013.
Moreno, T., Kojima, T., Amato, A., Lucarelli, F., de la Rosa, J., Calzolai, G., Nava, S., Chiari, M., Alastuey, A., Querol, X., Gibbons, W., 2013. Daily and hourly chemical impact of springtime transboundary aerosols on Japanese air quality. Atmos. Chem. Phys. 13, 1411–1424, 2013. https://doi.org/10.5194/acp-13-1411-2013.
Oros, D.R., Simoneit, B.R.T., 2000. Identification and emissions rates of molecular tracers in coal smoke particulate matter. Fuel 79, 515–536. https://doi.org/10.1016/S0016-2361(99)00153-2.
Owoade, K.O., Hopke, P.K., Olise, F.S., Oundele, L.T., Fawole, O.G., Olaniyi, B.H., Jegede, O.O., Ayoola, M.A., Bashiru, M.I., 2015. Chemical composition and source identification of particulate matter ($PM_{2.5}$ and $PM_{2.5\text{-}10}$) from a scrap iron and steel smelting industry along the Ife-Ibadan highway, Nigeria. Atmos. Pollut. Res. 6, 107–199. https://doi.org/10.5094/APR.2015.013.
Pancras, J.P., Landis, M.S., Norris, G.A., Vedantham, R., Dvonch, J.T., 2013. Source apportionment of ambient fine particulate matter in Dearborn, Michigan, using hourly resolved PM chemical composition data. Sci. Total Environ. 448, 2–13. https://doi.org/10.1016/j.scitotenv.2012.11.083.
Pokorná, P., Hovorka, J., Hopke, P.K., 2016. Elemental composition and source identification of very fine aerosol particles in a European air pollution hot-spot. Atmos. Pollut. Res. 7, 671–679. https://doi.org/10.106/j.apr.2016.03.001.
Pokorná, P., Hovorka, J., Klán, M., Hopke, P.K., 2015. Source apportionment of size resolved particulate matter at a European air pollution hot spot. Sci. Total Environ. 502, 172–183. https://doi.org/10.1016/j.scitotenv.2014.09.021.
Polissar, A.V., Hopke, P.K., Poirot, R.L., 2001. Atmospheric aerosol over Vermont: chemical composition and sources. Environ. Sci. Technol. 35, 4604–4621. https://doi.org/10.1021/es0105865.
Querol, X., Viana, M., Alastuey, A., Amato, F., Moreno, T., Castillo, S., Pey, J., Rosa, J., Sánchez de la Campa, A., Artínano, B., Salvador, P., García Dos Santos, S., Fernández-Patier, R., Moreno-Grau, S., Negral, L., Minguillón, M.C., Monfort Gil, J.I., Inza, A., Ortega, L.A., Santamaría, J.M., Zabalza, J., 2007. Source origin of trace elements in PM from regional background, urban and industrial sites of Spain. Atmos. Environ. 41, 7219–7231. https://doi.org/10.1016/j.atmosenv.2007.05.022.
Ravindra, K., Sokhi, R., Van Grieken, R., 2008. Atmospheric polycyclic aromatic hydrocarbons: source attribution, emission factors and regulation. Atmos. Environ. 42, 2895–2921. https://doi.org/10.1016/j.atmosenv.2007.12.010.
Riffault, V., Arnds, J., Marris, H., Mbengue, S., Setyan, A., Alleman, L.Y., Deboudt, K., Flament, P., Augustin, P., Delbarre, H., Wenger, J., 2015. Fine and ultrafine particles in the vicinity of industrial activities: a review. Environ. Sci. Technol. 45 (21), 2305–2356. https://doi.org/10.1080/10643389.2015.1025636.
Rogula-Kozłowska, W., 2015. PAH and heavy metals in ambient particulate matter: a review of up-to-date worldwide data. In: Pastuszka, J.S. (Ed.), Synergic Influence of Gaseous, Particulate, and Biological Pollutants on Human Health. Crc Press-Taylor & Francis Group, FL USA, pp. 68–108. https://doi.org/10.1201/b19592-5.
Rogula-Kozłowska, W., Kozielska, B., Klejnowski, K., 2013. Concentration, origin and health hazard from fine particle-bound PAH at three characteristic sites in southern Poland. Bull. Environ. Contam. Toxicol. 91 (3), 349–355. https://doi.org/10.1007/s00128-013-1060-1.
Simoneit, B.R.T., Schauer, J.J., Nolte, C.G., Oros, D.R., Elias, V.O., Fraser, M.P., Rogge, W.F., Cass, G.R., 1999. Levoglucosan, a tracer for cellulose in biomass burning and atmospheric particles. Atmos. Environ. 33, 173–182. https://doi.org/10.1016/S1352-2310(98)00145-9.
Sowlat, M.H., Hasheminassab, S., Sioutas, C., 2016. Source apportionment of ambient particle number concentrations in central Los Angeles using positive matrix factorization (PMF). Atmos. Chem. Phys. 16, 4849–4866. https://doi.org/10.5194/acp-16-4849-2016.
Šrám, R.J., Dostál, M., Libalová, H., Rossner, P., Rossnerová, A., Svecová, V., Topinka, J., Bartonová, A., 2013a. The European hot spot of B[a]P and $PM_{2.5}$ exposure-the Ostrava region, Czech Republic: health research results. ISRN Public Health article ID 416701. https://doi.org/10.1155/2013/416701.
Topinka, J., Hovorka, J., Milcová, A., Schmuczerová, J., Kroužek, J., Rossner Jr., P., Šrám, R.J., 2010. Acellular assay to assess genotoxicity of size segregated aerosols. Part I: DNA adducts. Toxicol. Lett. 198, 304–311.
Topinka, J., Rossner, P., Milcová, A., Schmuczerová, J., Penčíková, K., Rossnerova, A., Ambrož, A., Štolcpartová, J., Bendl, J., Hovorka, J., Machala, M., 2015. Day-to-day variability of toxic events induced by organic compounds bound to size segregated atmospheric aerosol. Environ. Pollut. 202, 135–145. https://doi.org/10.1016/j.envpol.2015.03.024.
Venkatamaraan, C., 1999. Comparison of particle lung doses from the fine and coarse fractions of urban PM_{10} aerosols. Inhal. Toxicol. 11 (2), 151–169. https://doi.org/10.1080/089583799197221.
Vossler, T., Černíkovský, L., Novák, J., Williams, R., 2016. Source apportionment with uncertainty estimates of fine particulate matter in Ostrava, Czech Republic using Positive Matrix Factorization. Atmos. Pollut. Res. 7, 503–5012. https://doi.org/10.1016/j.apr.2015.12.004.
Vu, T., Delgado Saborit, J.M., Harrison, R.M., 2015. Review: particle number size distribution form seven major sources and implications for source apportionment studies. Atmos. Environ. 122, 144–132. https://doi.org/10.1016/j.atmosenv.2015.09.027.
Vu, T.V., Beddows, D.C.S., Delgado-Saborit, J.M., Harrison, R.M., 2016. Source apportionment of the lung dose of ambient submicrometre particulate matter. Aerosol Air Qual. Res. 16 (7), 1548–1557. https://doi.org/10.4209/aaqr.2015.09.0553.
Wang, Q., Shao, M., Liu, Y., William, K., Paul, G., Li, X., Liu, Y., Lu, S., 2007. Impact of biomass burning on urban air quality estimated by organic tracers: guangzhou and Beijing as cases. Atmos. Environ. 41, 8380–8390. https://doi.org/10.1016/j.atmosenv.2007.06.048.
Weitkamp, E.A., Lipsky, E.M., Pancras, P.J., Ondov, J.M., Polidori, A., Turpin, B.J., Robinson, A.L., 2005. Fine particle emission profile for a large coke production facility based on highly time-resolved fence line measurements. Atmos. Environ. 39 (36), 6719–6733. https://doi.org/10.1016/j.atmosenv.2005.06.028.
Zhou, L., Hopke, P.K., Paatero, P., Ondov, J.M., Pancras, J.P., Pekney, N.J., Davidson, C.I., 2004. Advanced factor analysis for multiple time resolution aerosol composition data. Atmos. Environ. 38, 4909–4920. https://doi.org/10.1016/j.atmosenv.2004.05.040.

Supplementary material for:

Source apportionment of aerosol particles at a European air pollution hot spot using particle number size distributions and chemical composition

Cecilia Leoni, Petra Pokorná, Jan Hovorka, Mauro Masiol, Jan Topinka, Yongjing Zhao, Kamil Křůmal, Steven Cliff, Pavel Mikuška, Philip K. Hopke

Number of Figures: 14

Number of Tables: 2

Number of pages: 22

PMF analysis

In aerosol science, receptor models are mathematical approaches used for identifying and quantifying different atmospheric particles sources. Specifically, PMF model identifies and quantifies the contribution to each source to the samples. The identification is based on key species (tracers), combination of species, or size distribution characteristics.

The fundamental principle of PMF is the mass conservation and the goal of PMF is to solve the chemical mass balance equation. The main physical constraint is that the source composition must be non-negative. In fact, a source does not emit a negative quantity of pollution, or it becomes a sink. Also, the sum of the predicted contributions for each source must be less than or equal to the total measured mass for each variable. PMF performs a matrix factorization, which consists of decomposing a matrix of sample data X into two sub-matrices. The two sub-matrices contain the species profile for each factor (G), and the amount of mass/number contributing by each factor to each individual sample (F), plus the unexplained part E (difference between measured and calculated species concentration) (Brown et al., 2015).

$$X = GF + E$$

When using PMF for source apportionment, there are many parameters involved in the determination of the factor matrices, and the change of one of them may lead to a different solution. To find the optimal solution, several runs with different conditions must be made. In the following section, the strategy applied for the PMF analysis is explained, focusing on the evaluation of the diagnostics provided by the model. The interpretation of the PMF results and the choice of the best solution is the most crucial step that must be done by the operator. All the diagnostics must be evaluated and the best solution is a trade-off between the physical meaning of the solution, the diagnostics of the model and the goodness of the fit.

First step: preparation and analysis of the input data. The PMF input data consist of two matrices: concentration and uncertainty. The matrices must have the same dimensions and must not contain missing data or negative/zero values. The data matrices of the mass chemical composition were prepared in compliance with the procedure described in Polissar et al., 1998. For the NSD uncertainty U, this method was used (Vu et al., 2015):

$$\sigma_{i,j} = \begin{cases} \alpha\left(N_{i,j} + \bar{N}_j\right) & N_{i,j} > 0 \\ 2\bar{N}_j & N_{i,j} = 0 \end{cases}$$

$$U = \sigma_{i,j} + C_3(N_{i,j})$$

σ the error for every size bin *i* and measurement *j*. N*i,j* is the particle number concentration for size bin *i* and measurement *j*. α is an arbitrary constant 0.01. The missing data were replaced with the average particle number concentration $\bar{N}$ and the related uncertainties were assumed to be three times $\bar{N}$. C_3 is a constant value ranging between 0.01 and 0.5, which should be chosen according to the distribution of the scaled residuals and the of uncertainty/concentration ratio of 10-20%. The distribution should be between +2 and -2. If the number of scales residuals >3 is high, it can be necessary to increase the uncertainty or to change the number of factors. In this study C_3 was chosen as 0.08. The calculated uncertainty/concentration ratio ranged from a minimum of 10% and a maximum of 17% in average.

A total of 138 missing data (4.7% of the dataset) were excluded from the modeling. 122 data were missing due to data transfer problems and a power outage that occurred on March 4th; 16 data were erased as outliers because of very high pollution peaks.

When the matrices are ready, it is necessary to upload them in the model and a crucial step is to decide if a variable is strong/weak/bad. First, to understand if a variable is strong/weak/bad, a detailed knowledge of the dataset, of the sampling and the analytical techniques is needed. Than the signal to noise ratio (S/R) must be observed. A variable is weak if it has signal and noise in comparable amounts (S/R=1). Similarly, variables having more noise than signal are termed bad variables (Reff et al., 2007). Downweighing the weak variables by a factor 3 is recommended, to protect in the case that the error level of some variables has been underestimated. Regarding bad variables, where hardly a signal is visible from the noise, the recommendation is to omit these variables, or to strongly downweight by a factor 5 or 10 (Paatero and Hopke, 2003). It is important to know whether a variable can be retained in the analysis. For the particle number size distribution, the weak variables that were excluded from previous studies are typically the first and last SMPS size bins, and the last APS bins, due to the high variability and the presence of zeroes. Lastly, it is necessary to observe the time series of very variable, to determine whether temporal patterns are present and if there are unusual events or outliers. Extreme events can be excluded from the

modeling if they perturb the solution, they cause high scale residuals number, they generate spurious factors.

Second step: base model execution. The model must be run with different number of factors and for each run diagnostics must be evaluated. The choice of the factors number is crucial. Too few factors lead to the combination of sources, while too many factors split one source into two non-existing sources. To choose the correct number of factors and to understand if the uncertainty was correctly estimated is necessary to observe the Q value. The $Q_{theoretical}$ gives information about the quality of the fit since the optimal solution should have a Q_{true} not too different from the $Q_{theoretical}$. If the ratio $Q_{true}/Q_{theoretical}$ is around 1, the uncertainty is properly estimated and the number of factors is appropriate. In some cases, the optimal solution does not fully satisfy this requirement, for example when a dataset contains a lot of weak variables. The $Q_{theoretical}$ in this study was calculated according to the EPA PMF 5.0 User Guide. For NSD PMF, $Q_{true}/Q_{theoretical}$ was 0.998. The second diagnostic to analyze are the scaled residuals. If the input data are correct, the plot of scaled residuals values against their frequency should be normally distributed, with the majority between -3 and +3. If some residuals are outside this region, it is possible that there are extreme events or outliers in the data, or the number of factors is not optimal. Distribution with large spread indicates that the uncertainty is too low, while a distribution centered near zero indicates that uncertainty are too high. Third step is to observe the goodness of fit, comparing the predicted species with the original concentrations, using regression and time series. The observed/predicted regression coefficients must be as close as possible to 1 and the time series of modeled variables should fit as best as possible the time series of the original variable (Fig. S1).

Table S1: Summary of PMF diagnostics for NSD and chemical composition modeling.

Diagnostic	**NSD**	**Chemical composition**
N. of observations	2905	120
Missing values	4.7%	10%
Qexpected/theoretical	85028	2327
Qtrue	85216	2641
Qrobust	84866	2640
Species with Q/Qexpected>2	18.5 nm	K
DISP swaps	0	0
BS mapping	100%	92 – 100%

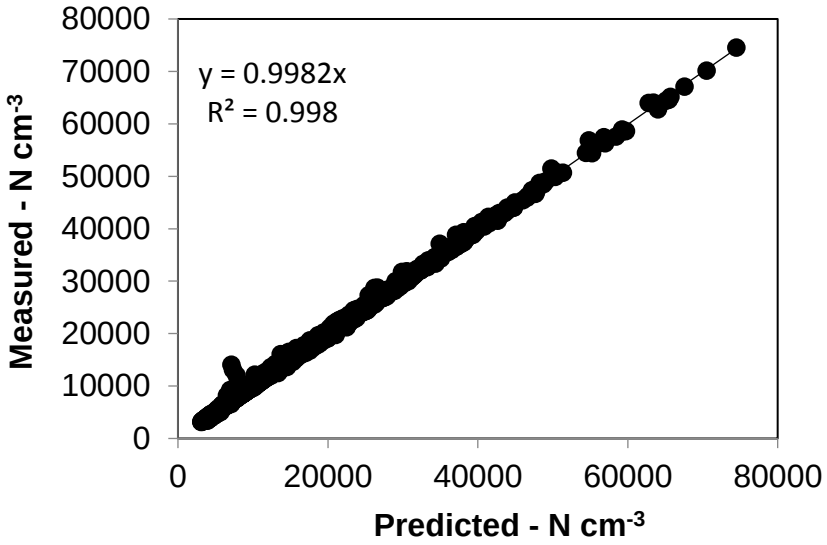

Figure S1. The linear regression between measured/ predicted values.

Lastly, the G-plots must be observed. The G-plots show scatter plots of one factor versus another factor are they are very important to verify the relationship between the factors. The G plots are generated with the assumption that the determined factors are uncorrelated between each other. If the factors are independent one of another, the points should fill the all scatter plot space. The more stable solution will have many samples with zero contribution on both axes. Imagining straight lines passing through the origin of axes including all the points between them, the lines should be as much close to the Cartesian axes. If the points are not aligned with the Cartesian axes, an *edge* can be observed in the plot, which means there might be an overlooked factor or there is rotational ambiguity in the solution.

Third step: error evaluation wit bootstrap (BS) and displacement (DISP). A number of phenomena can contribute to the uncertainty of the solution modeled by PMF: temporal variation of PM sources, measurements errors, sampling variability, errors in the model, for example wrong factor number (Reff et al., 2007). The technique of bootstrapping is used to check the validity of the solution. Bootstrapping consist of randomly selecting n samples to create new datasets and executing the PMF on each new dataset. Multiple PMF solutions are generated using the series of data that are resampled version of the original dataset. Several hundreds of bootstrapped samples can be used, and the summary statistics are calculated by the model. In this study for example, 100

BS runs were performed for both NSD and chemical composition solutions. If the same sources are identified in most of the bootstrapped samples, the solution of the original dataset can be considered stable. Mapping over 80% of the factor indicates that the number of factor can be appropriate (Table S1).

The DISP explores the rotational ambiguity in a PMF solution by assessing the largest range of source profile values without appreciable increase in the Q value. Each fitted element in the factor profile matrix in the base PMF solution is *displaced* from its fitted value far enough so that the Q increases by a predetermined amount called Q_{max}. The variables are *perturbed* within a certain interval, which has a certain extension (the boxplot in the results diagnostics). If the variable is perturbed so much that the factor changes its identity, a swap occurs. If a swap occurs, it means that the solution is not robust enough and another solution might be a better choice.

References

1. Brown S.G., Eberly S., Paatero P., Norris G., A., 2015. Methods for estimating uncertainties in PMF solutions: examples with ambient air and water quality data and guidance reporting PMF results. Science of the Total Environment, 518-519 626-635. . https://doi.org/10.1016/j.scitotenv.2015.01.022
2. Paatero P, Hopke PK., 2003. Discarding or down weighting high-noise variables in factor analytic models. Analytica Chimica Acta 490, 277–89. https://doi.org/10.1016/S0003-2670(02)01643-4
3. Polissar A.V., Hopke, P.K., Paatero, P., Malm, W.C., Sisler, J.F. 1998. Atmospheric aerosol over Alaska-2. Elemental composition and sources. Journal of Geophysical Research, 103, 19045-19057. https://doi.org/10.1029/98JD01212
4. Reff A., Eberly S. I., Bhave, P. V., Receptor modeling of ambient particulate matter data using Positive Matrix Factorisation: Review of existing methods, Air & Waste management Association 57:146-154 2007. http://dx.doi.org/10.1080/10473289.2007.10465319
5. US Environmental Protection Agency PMF 5.0 User Guide – Norris G., Duvall R.,
6. Vu T., Delgado Saborit J. M., Harrison R. M., 2015. Review: particle number size distribution form seven major sources and implications for source apportionment studies, Atmospheric Environment 122, 144-132. https://doi.org/10.1016/j.atmosenv.2015.09.027

Organic molecules analysis method

Sample preparation

Exposed pieces of filters were extracted three times in 20 mL of different organic solvents (total 60 mL) under ultrasonic agitation for 30 minutes; a mixture of dichloromethane and hexane (v/v 1:1) for analysis of 22R-17α(H),21β(H)-homohopane, 22S-17α(H),21β(H)-homohopane and PAHs, and a mixture of dichloromethane and methanol (v/v 1:1) for analysis of levoglucosan were used.

The dried extracts with homohopanes and PAHs were then fractionated by flash chromatography. The column was filled with 5 g of silicagel and 2 g of anhydrous Na_2SO_4. Two fractions were taken after elution with different solvents, hexane and mixture of dichloromethane/hexane (v/v 1:1). The first hexane fraction (30 mL) contained homohopanes and the second dichloromethane/hexane fraction (30 mL) contained PAHs. The fractions were again dried under a stream of nitrogen to 1 mL and then were analyzed by GC-MS.

The dried extracts with levoglucosan were derivatized with the silylation mixture (BSTFA + 1% TMCS and pyridine, 2:1; v/v), for 180 min at 70 °C. After derivatization procedure, the derivatized samples were evaporated to dryness under a stream of nitrogen, redissolved in 1 mL of hexane and analyzed by GC-MS.

GC-MS analysis

All organic compounds were quantified by GC-MS (Agilent, 7890-A, 5975C). The separation was carried out with a capillary column HP5-MS, 1 µm film thickness, 0.32 mm i.d., 30 m length. The sample (1 µL) was injected into a splitless injector (280 °C). The flow rate of carrier gas (helium) was 4 mL min-1. For analysis of homohopanes, the temperature program started at 50 °C for 2 min, a gradient of 10 °C min-1 was used up to 300 °C and held for 20 min. For analysis of PAHs, the temperature program started at 70 °C for 2 min, a gradient of 20 °C min-1 was used up to 150 °C, then a gradient of 5 °C min-1 was used up to 300 °C and held for 24 min. For analysis of levoglucosan, the temperature program started at 120 °C for 2 min, a gradient of 5 °C min-1 was used up to 300 °C and held for 6 min.

The mass spectrometer was operated in an electron ionization (70 eV) with quadrupole as a mass analyzator. First, standards of measured compounds were analyzed in full scan mode and then specific masses m/z were chosen for SIM mode for analysis and quantification of organic compounds in real samples.

Quality assurance and control

Before sampling, all quartz filters were heated at 500 °C for 24 hours to remove organic contaminants. Field blank filters were also analyzed with the exposed samples, however, the concentrations of all organic compounds in the blank filters were under the LODs.

Prior to extraction of organic compounds from filters, recovery standards were added to filters to correct for losses of analytes during sample workup; deuterated PAHs for analysis of PAHs, ααα(20R)-cholestane-D2 for analysis of homohopanes and methyl-β-L-arabinopyranoside for analysis of levoglucosan. Good procedure recoveries ranging from 86 to 106 % were evaluated on PM_1 samples spiked with recovery standards.

The identification of all organic compounds was based on the comparison with retention times and mass spectra of analytical standards. The limits of detection (LODs) were 0.041 ng m^{-3} for 22S-17α(H),21β(H)-homohopane, 0.077 ng m^{-3} for 22R-17α(H),21β(H)-homohopane, 0.004 – 0.022 ng m^{-3} for PAHs and 0.024 ng m^{-3} for levoglucosan.

Elemental composition analysis with DRUM-XRF

For the elemental analysis of the DRUM samples, DRUM-XRF technique has been used. Many studies report measurements of the concentrations of trace elements in the atmosphere with this technique (for example, Perry et al., 2004, VanCuren et al., 2005, 2012, Arwood et al., 2013, and references therein). Principal and accuracy of the technique is described in these references. In summary, DRUM samples were analyzed by synchrotron X-ray fluorescence (S-XRF) using a broad-spectrum soft X-ray beam generated on beam line 10.3.1 at the Advanced Light Source (ALS) in Lawrence Berkeley National Laboratory (LBNL). The ALS S-XRF system is capable of detecting 28 elements from Na to U plus Pb. Since the X-ray beam was 100% polarized, background signal was greatly reduced and the signal-to-noise ratio was dramatically improved. Deconvolutions of the raw X-ray spectra were performed using WinXIL X-ray spectral analysis software that was developed by the International Atomic Energy Agency Laboratories in Seibersdorf, Austria. Elemental concentrations of the DRUM samples were derived by calibrating the response of the system to a comprehensive set of 40 single-element and multi-element NIST-traceable standards (Micromatter, Inc.). A DRUM sample (QA strip) collected in Trinity of California was reanalysed every time when the beam Line 10.3.1 was newly set-up and a new calibration curve was established to verify that the results obtained with the ALS S-XRF system can be repeated.

References

- Atwood S.A., Reid J.S., Kreidenweis S. M., Cliff S., Yongjing Z., Lin N., Tsay S., Chee, Chu Y., Westphal D. L., 2013. Size Resolved Measurements of Springtime Aerosol Particles over the Northern South China Sea for use in Source Identification, Atmospheric Environment, 78, 134-143.
- Perry, K. D., Cliff S. S., and Jimenez-Cruz M. P., 2004. Evidence for hygroscopic mineral dust particles from the Intercontinental Transport and Chemical Transformation Experiment, Journal of Geophysical Research, 109, D23S28. DOI: 10.1029/2004JD004979
- Van Curen R.A., Cahill T., Burkhart J., Barnes D., Zhao Y., Perry K., Cliff S., McConnell J., 2012. Aerosols and their sources at Summit Greenland e first results of continuous size- and time-resolved sampling. Atmospheric Environment 52, 82e97. DOI: 10.1016/j.atmosenv.2011.10.047
- Van Curen, R.A., Cliff S. S., Perry K. D., Jimenez-Cruz M., 2005, Asian continental aerosol persistence above the marine boundary layer over the eastern North Pacific: Continuous aerosol measurements from Intercontinental Transport and Chemical Transformation 2002 (ITCT 2K2), Journal of Geophysical Research, 110, D09S90.

Table S2. Upper/lower and average diameter of the NSD size ranges, used as input variables in the PMF model. In bold is the overlap size range between SMPS and APS.

Variable n.	Size range		PMF input variable
	Lower midpoint diameter	Upper midpoint diameter	Average diameter
1	17.8	19.2	18.5
2	19.9	21.4	20.6
3	22.1	23.8	22.9
4	24.6	26.5	25.5
5	27.5	29.4	28.4
6	30.5	32.8	31.6
7	34.0	36.6	35.3
8	37.9	40.7	39.3
9	42.2	45.4	43.8
10	47.0	50.5	48.8
11	52.3	56.2	54.3
12	58.3	62.7	60.5
13	65.0	69.9	67.4
14	72.5	77.8	75.1
15	80.6	86.6	83.6
16	89.9	96.5	93.2
17	100.0	107.6	103.8
18	111.5	119.8	115.6
19	124.2	133.5	128.8
20	138.3	148.7	143.5
21	154.1	165.7	159.9
22	171.7	184.5	178.0
23	191.3	205.6	198.4
24	213.1	229.0	221.0
25	237.4	255.1	246.2
26	264.4	284.1	274.2
27	294.5	316.6	305.5
28	328.2	352.6	340.3
29	365.5	392.8	379.1
30	407.2	437.6	422.3
31	453.6	487.4	470.4
32	**505.3**	**542.0**	**523.7**

33	583.0	673.0	627.3
34	723.0	835.0	778.3
35	898.0	1037.0	966.7
36	1114.0	1286.0	1199.0
37	1382.0	1596.0	1488.0
38	1715.0	1981.0	1846.3
39	2129.0	2458.0	2291.7
40	2642.0	3051.0	2844.0
41	3278.0	3786.0	3529.0
42	4068.0	10370.0	7219

256

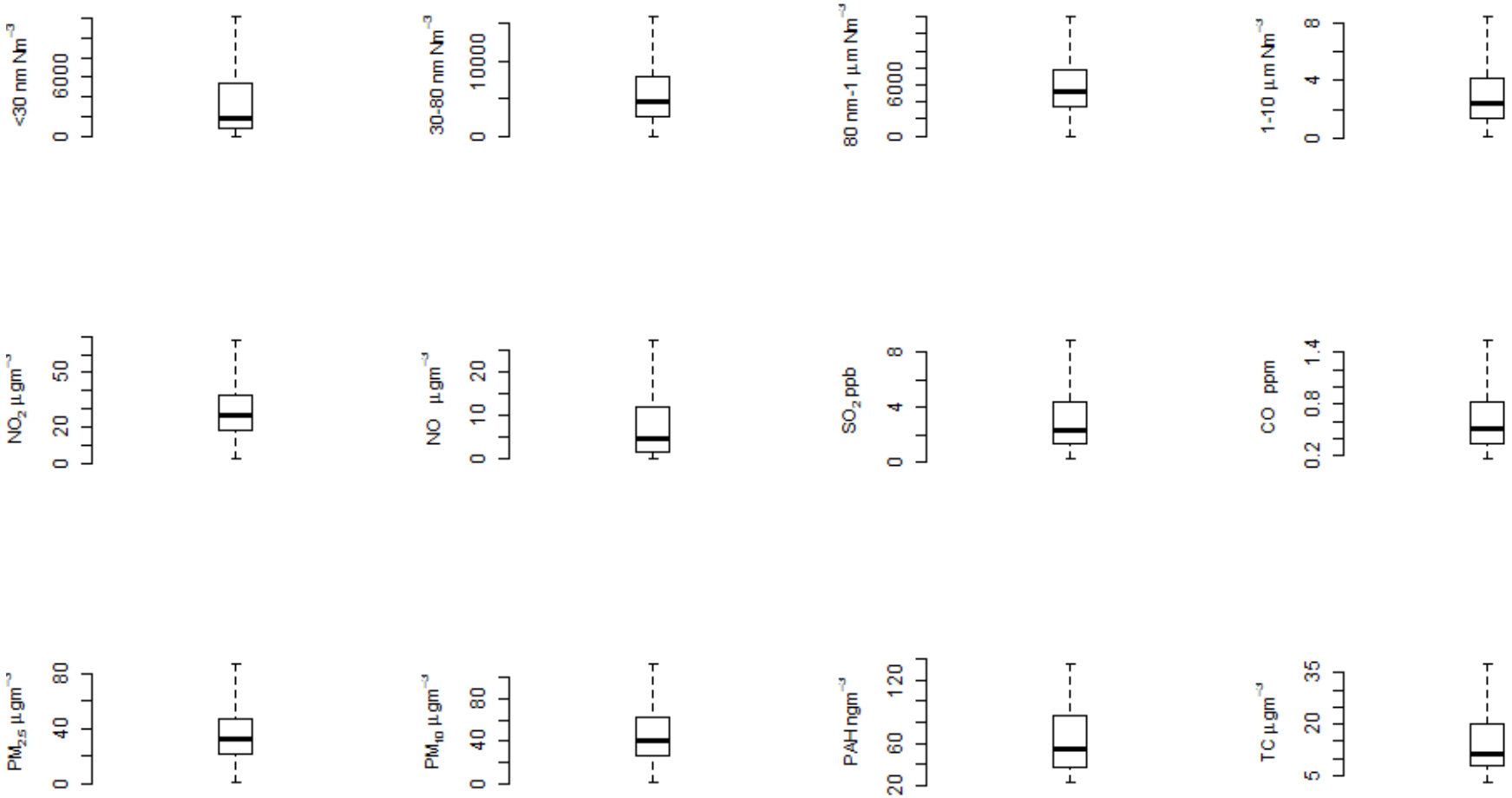

Figure S2. Boxplots of PNCs, gaseous pollutants, $PM_{2.5}$, PM_{10}, PAHs and TC. Middle line represents the median, the box is the inter quartile range, the whiskers indicate 1.5 inter quartile range.

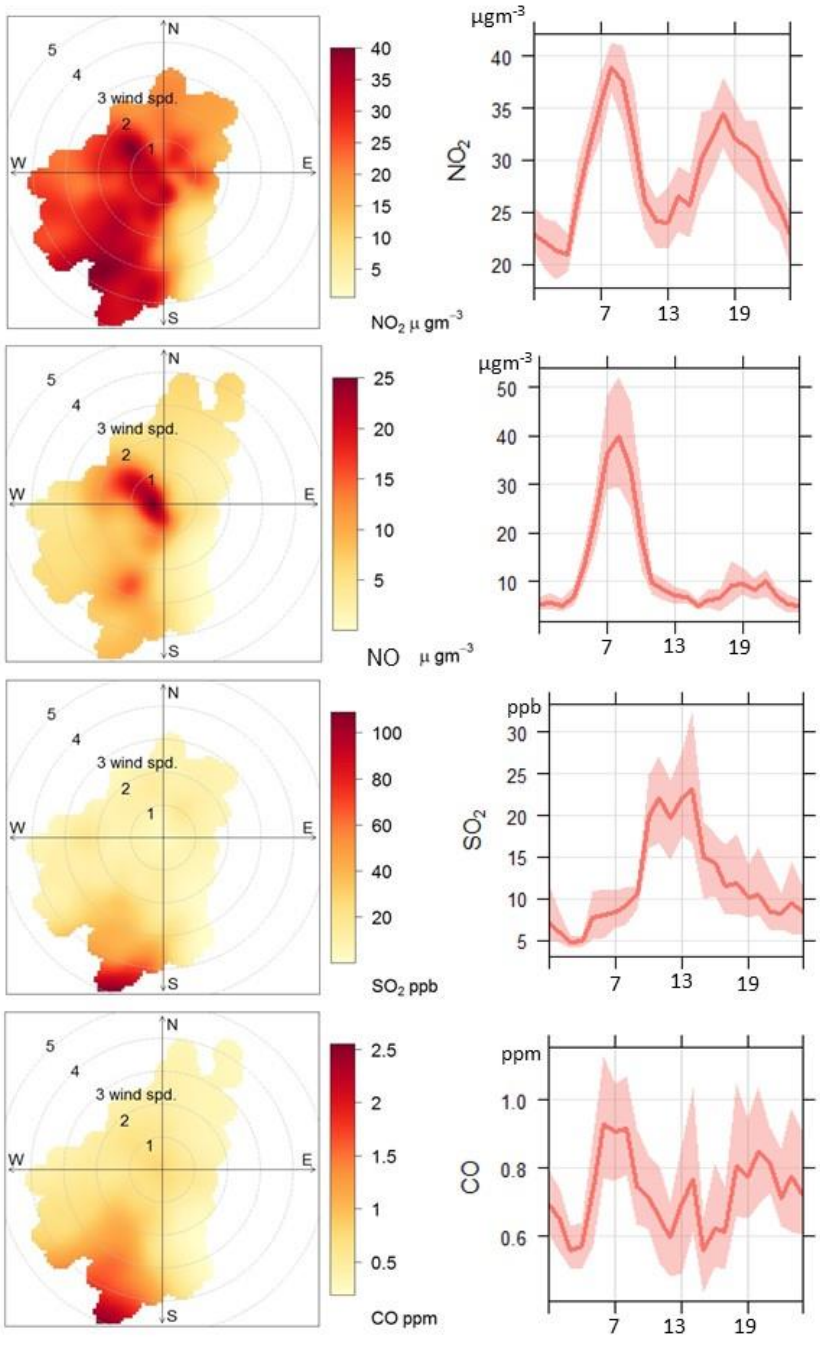

260

261

262

263

264

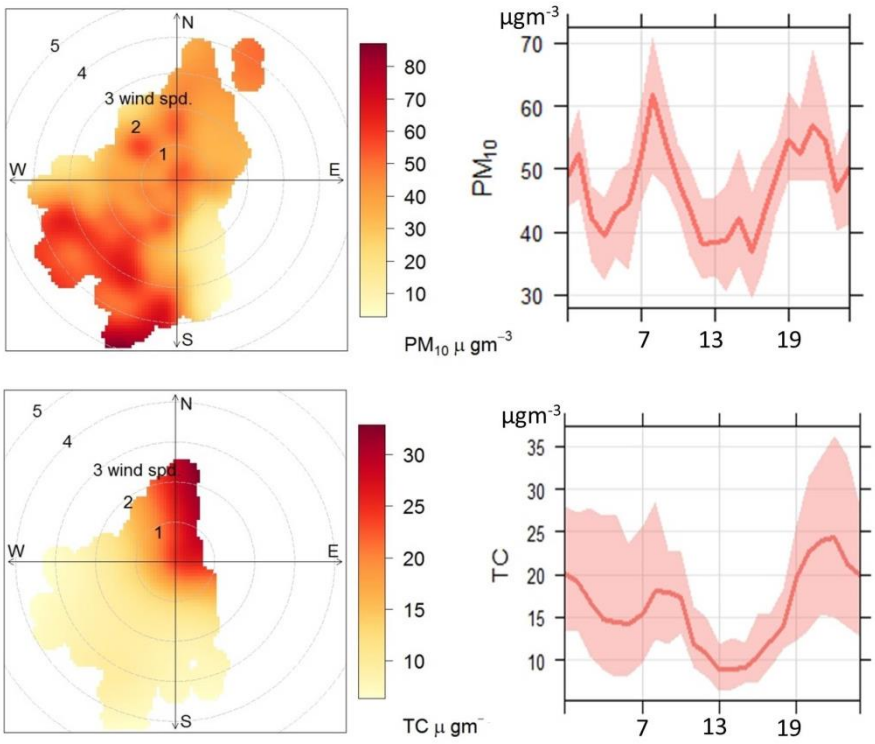

Figure S3. Polar plots and daily patterns of PM_{10}, gaseous pollutants (NO, NO_2, SO_2, CO) and TC, shaded area in the daily pattern plot represents the 95th % confidence interval.

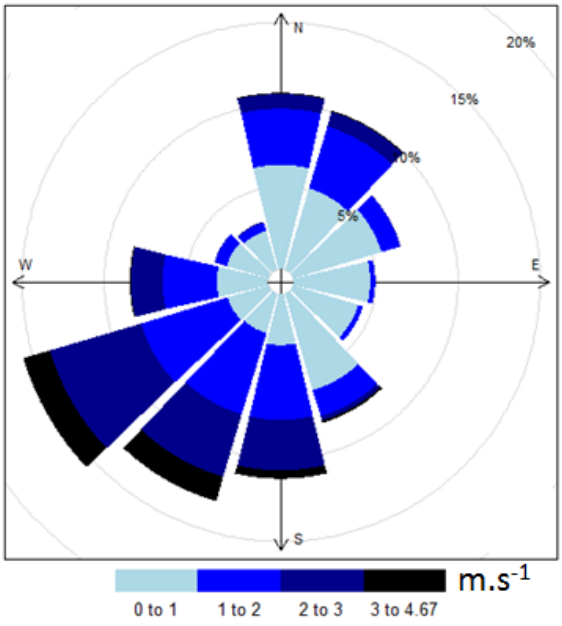

Figure S4. Wind rose for the whole sampling campaign (February 5 to March 7, 2014).

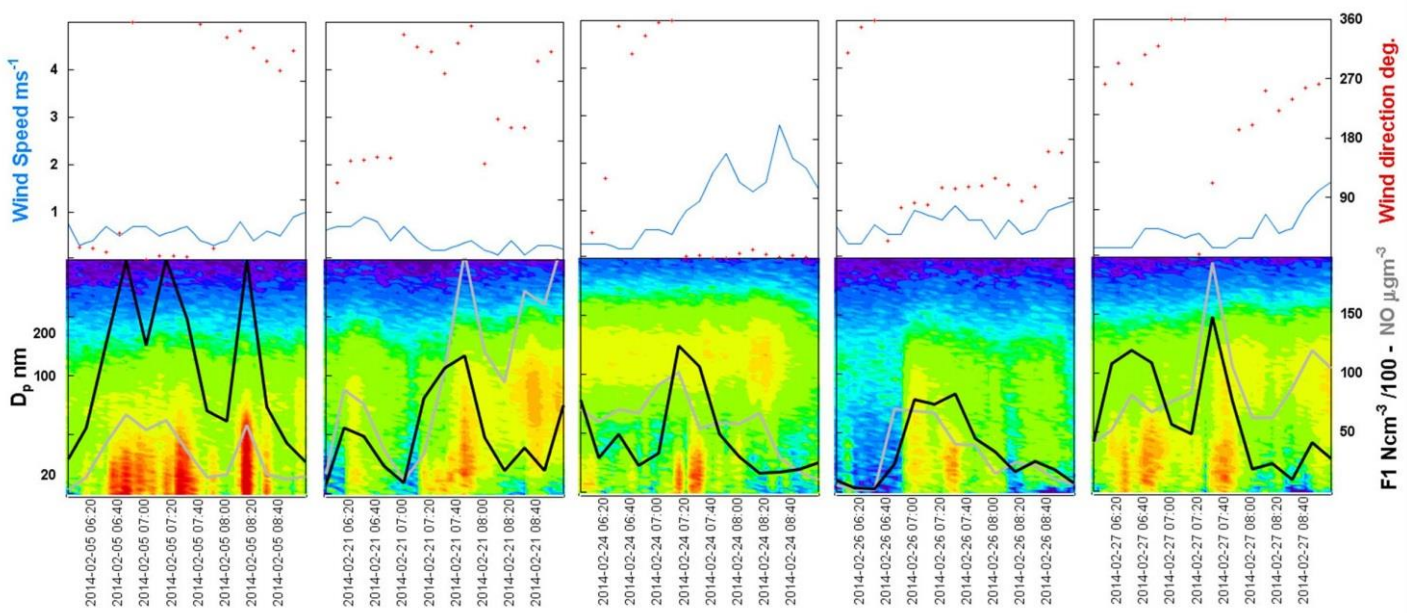

284

285 Figure S5: Time series for wind speed and direction (top) and particle number size distribution
286 (bottom). Black line indicates concentration of industrial/traffic fresh emitted nanoparticles (factor
287 1) and the grey line of NO.

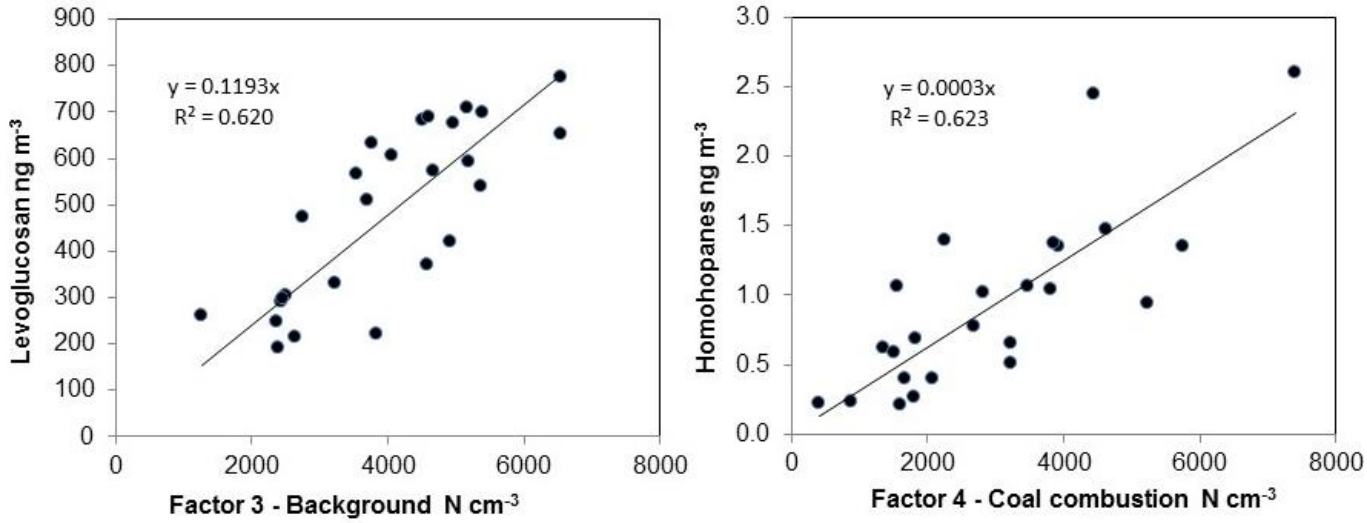

288

289 Figure S6. Left: linear regressions between 24-hours concentration of levoglucosan and Factor 3 -
290 urban background PNC. Right: linear regression of 24-hours averages of R homohopane and
291 Factor 4 - CC PNC.

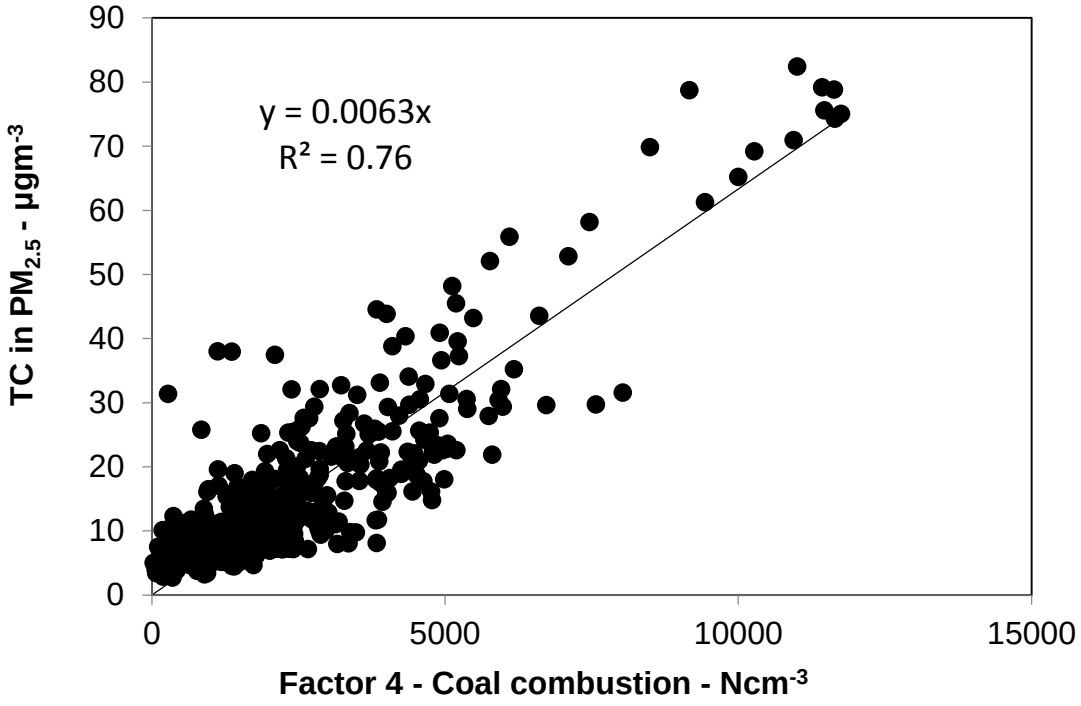

Figure S7. Linear regression between total carbon and NSD factor 4 – coal combustion.

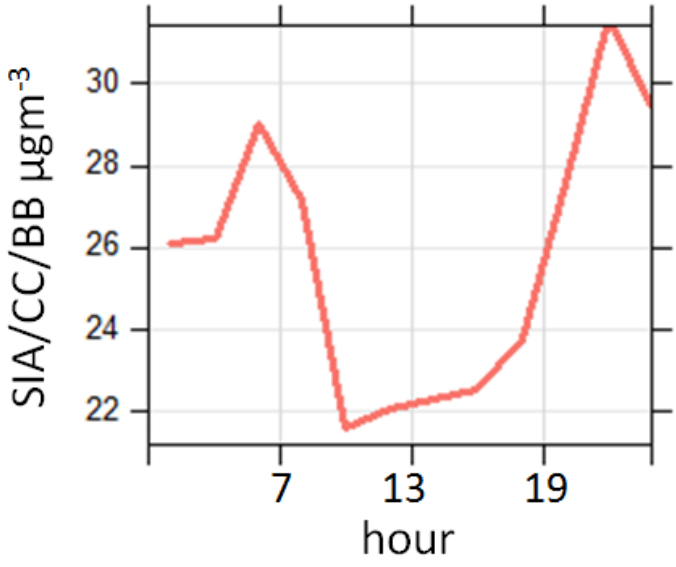

Figure S8. Daily pattern of the factor SIA/CC/BB obtained with chemical composition PMF.

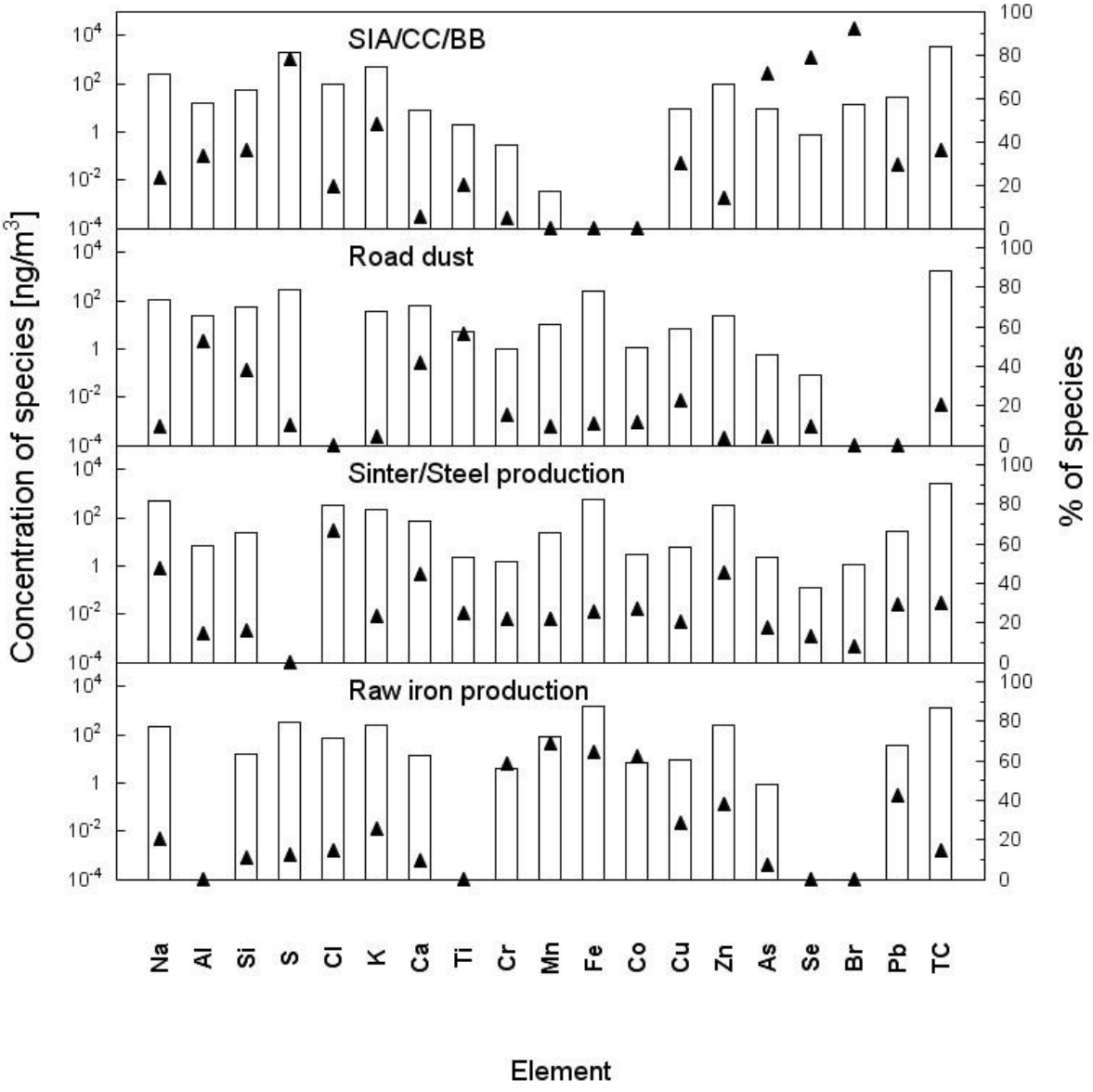

303

304 Figure S9. Factor profiles for the resolved factors of $PM_{0.09\text{-}1.15}$ by PMF.

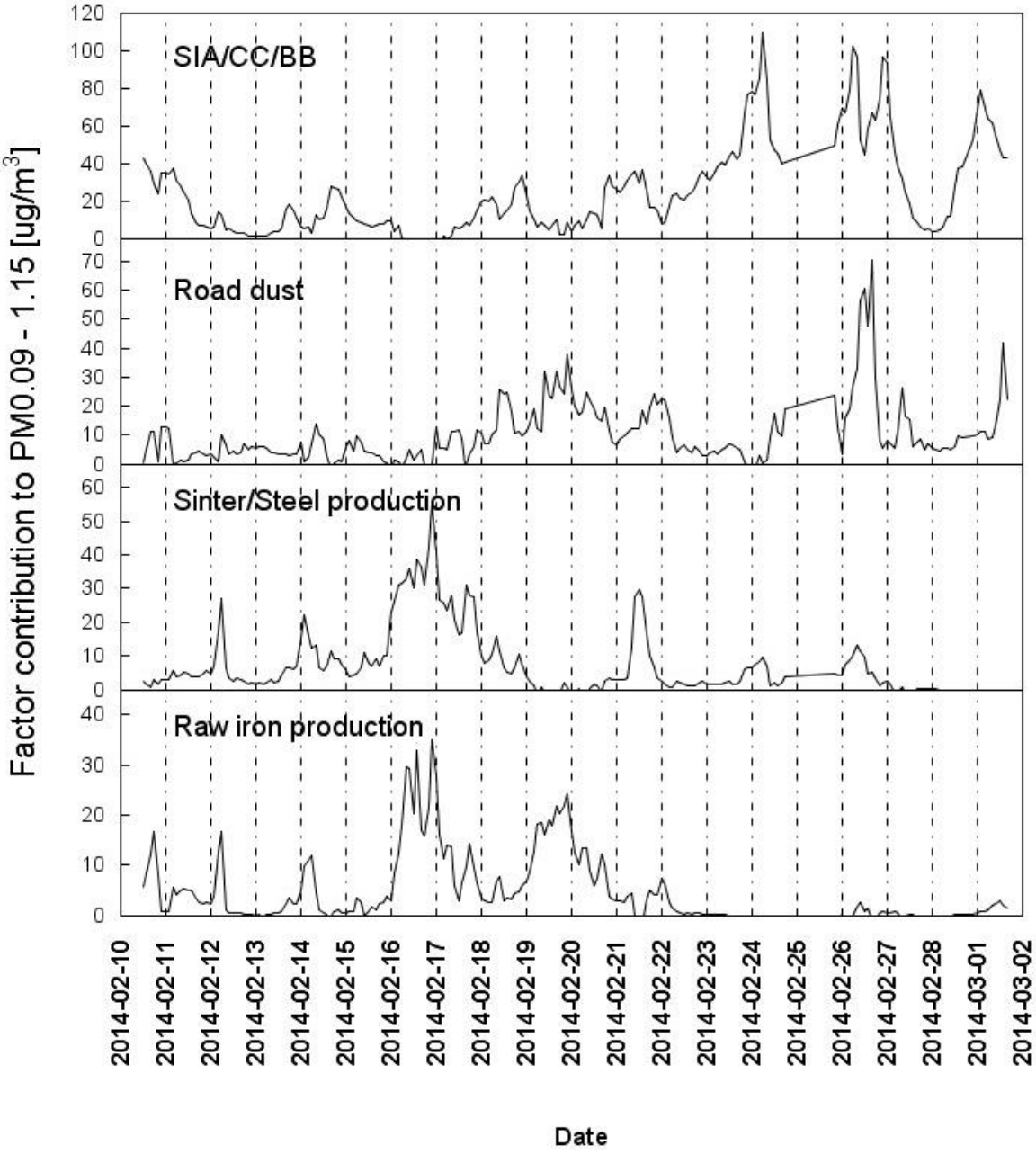

305

306 Figure S10. Temporal variations in the estimated contributions from the four factors resolved by

307 PMF.

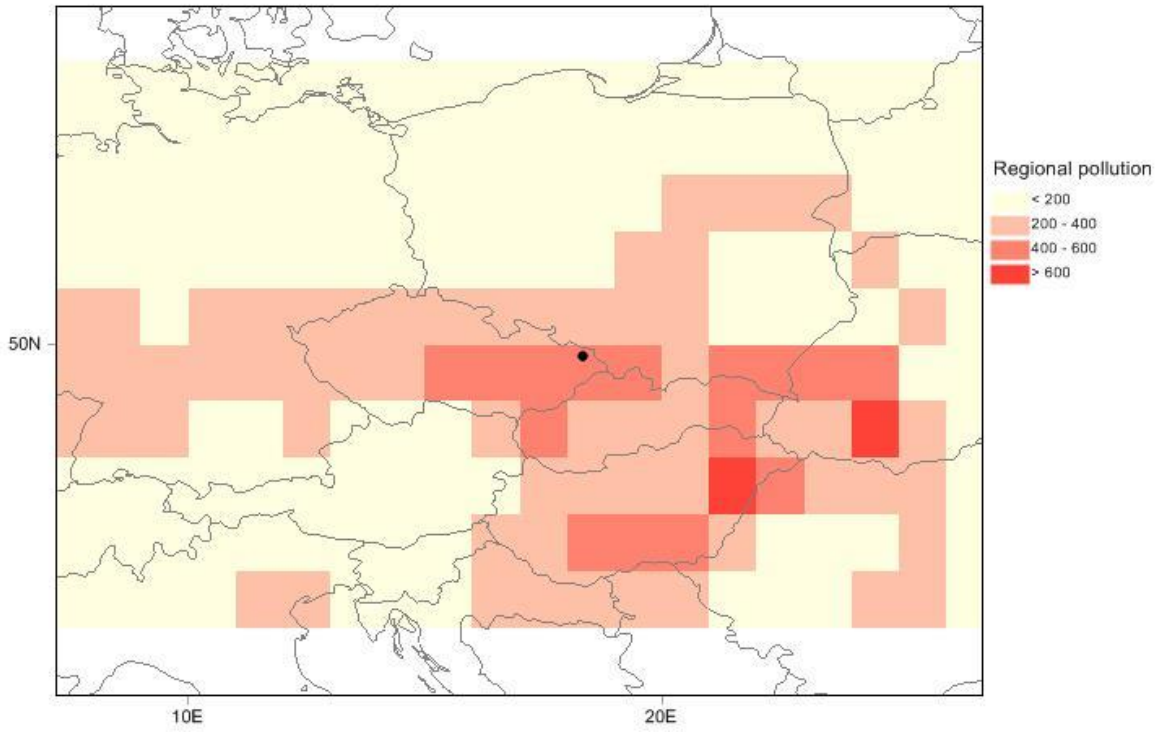

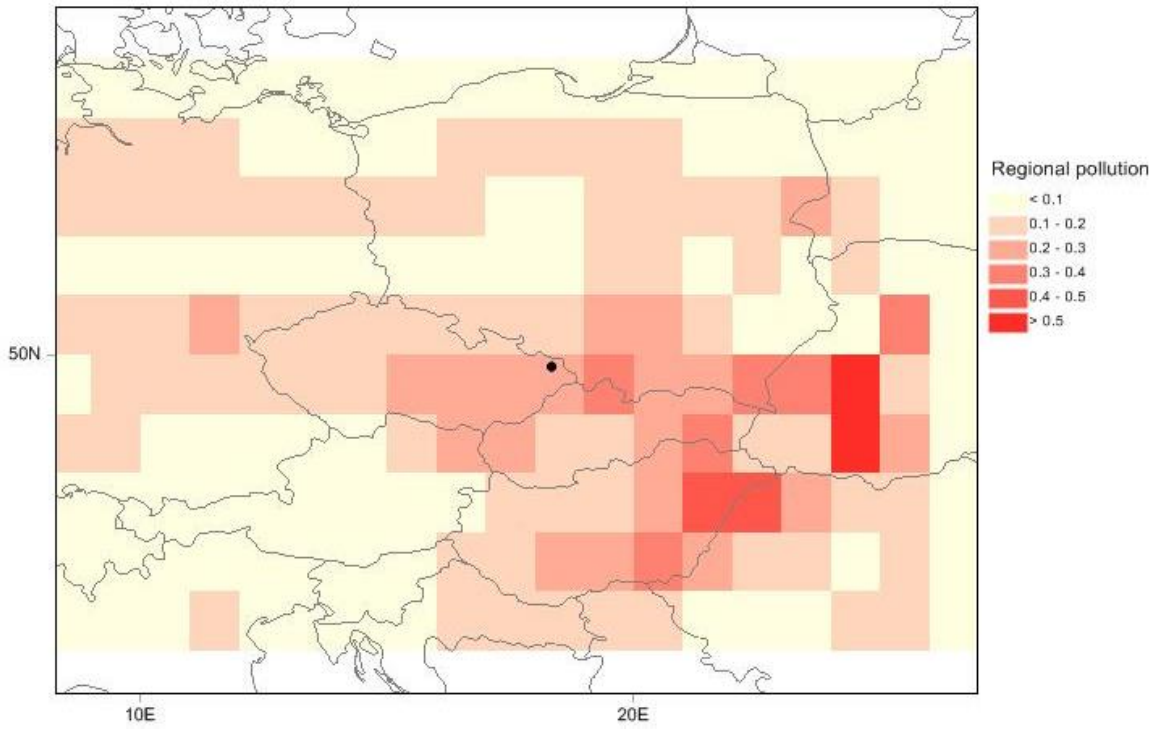

Figure S11. CWT of Factor 5 regional pollution (above) and PSCF (below). The data in the CWT are expressed in Ncm^{-3}. The CWT and the PSCF were calculated using Trajstat (Wang et al., 2009).

PSCF and CWT methods

To apportion the sources of regional origin the Potential Source Contribution Function (PSCF) (Ashbaugh et al., 1985) and concentration weighted trajectory CWT (Hsu et al., 2003; Seibert et al., 1994) methods based on the air mass back-trajectories (AMBT) and receptor model results. AMBT were calculated using the TrajStat (Wang et al., 2009) using meteorological data fields supplied by the ARL NOAA archiving programs input data. In order to characterize the general behavior of air masses in both measurement periods 96 h AMBT were run every 6 h at an endpoint located 500 m AGL. Standard 0.5° latitude/longitude dataset output from the NCEP Global Data Assimilation System model (GDAS). The top of the computational domain was set at 10,000 m AGL.

For the PSCF the pollution criterion was set for upper quartile of the data. The PSCF weighted function was utilized to better reflect the uncertainty in the values for the cells (Polissar et al., 1999). The weighted function was defined as fallows the endpoints were set to 61, 30, 15 with the reduce ratio of 0.72, 0.42 and 0.17. The CWT method was also utilized to distinguish moderate sources from strong ones. The CWT weighted function setting corresponded to the PSCF. The both results were compared.

References

- Ashbaugh, L.L., Malm, W.C. and Sadeh, W.Z., 1985. A residence time probability analysis of sulfur concentrations at Grand Canyon National Park. Atmospheric Environment, 19(8): 1263-1270. DOI: 10.1016/0004-6981(85)90256-2
- Hsu, Y.-K., Holsen, T.M. and Hopke, P.K., 2003. Comparison of hybrid receptor models to locate PCB sources in Chicago. Atmospheric Environment, 37: 545-562. DOI: 10.1016/S1352-2310(02)00886-5
- Polissar, A.V., Hopke, P.K., Paatero, P., Kaufmann, Y.J., Hall, D.K., Bodhaine, B.A., Dutton, E.G. and Harris, J.M., 1999. The aerosol at Barrow, Alaska: long-term trends and source locations. Atmospheric Environment, 33: 2441-2458. DOI: 10.1016/S1352-2310(98)00423-3
- Seibert, P., Kromp-Kolb, H., Baltensperger, U., Jost, D.T., Schwikowski, M., Kasper, A. and Puxbaum, H., 1994. Trajectory analysis of aerosol measurements at high alpine sites. In: B.P. M., B. P., C. T. and S. W. (Editors), Transport and Transformation of Pollutants in the Troposphere. Academic Publishing, Den Haag, pp. 689-693. DOI: 10.1007/978-1-4615-1817-4_65

343

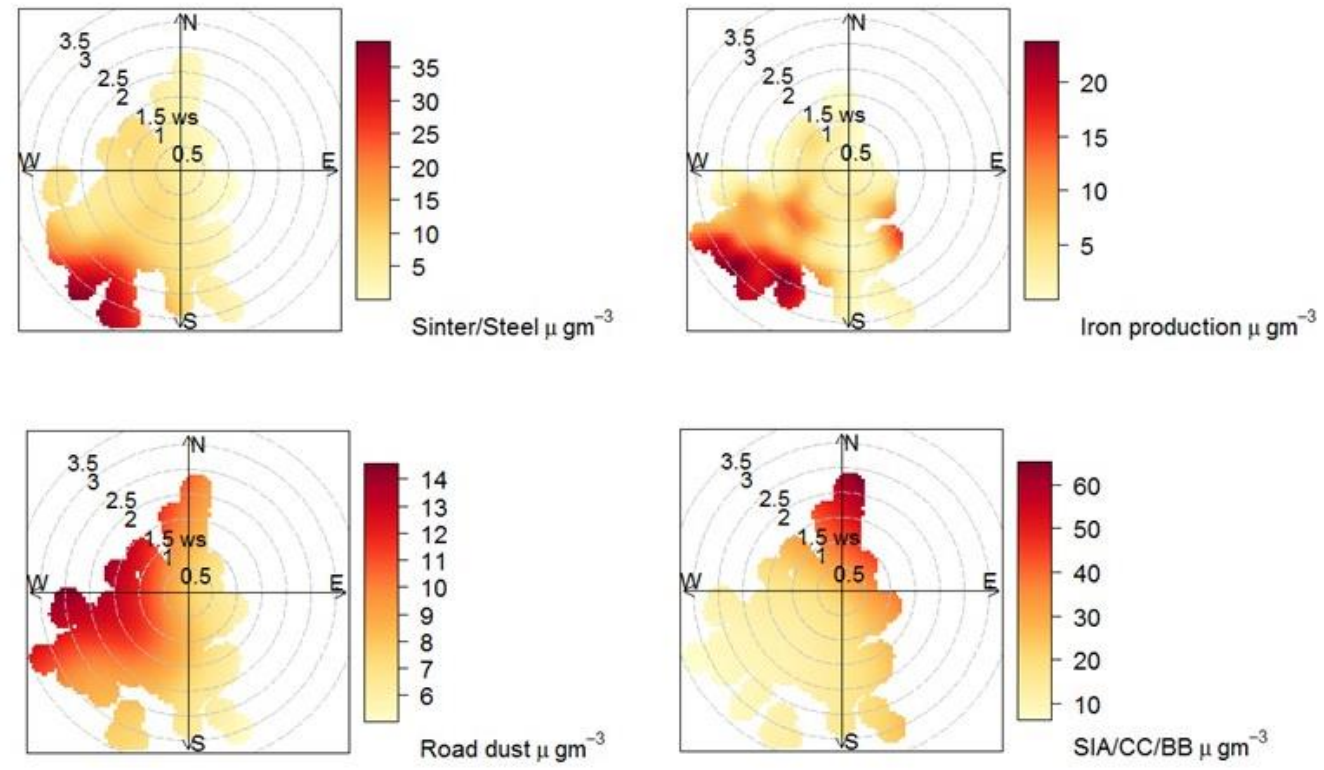

344

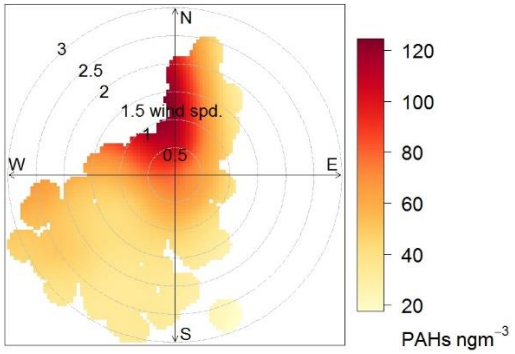

345 Fig. S12. Polar plots for 2-hours chemical composition factors and 24-hours PAHs in PM_1. The
346 24 hours PAHs averages were extended to the 15-minutes vector averages of WS and WD.

347

348

349

350

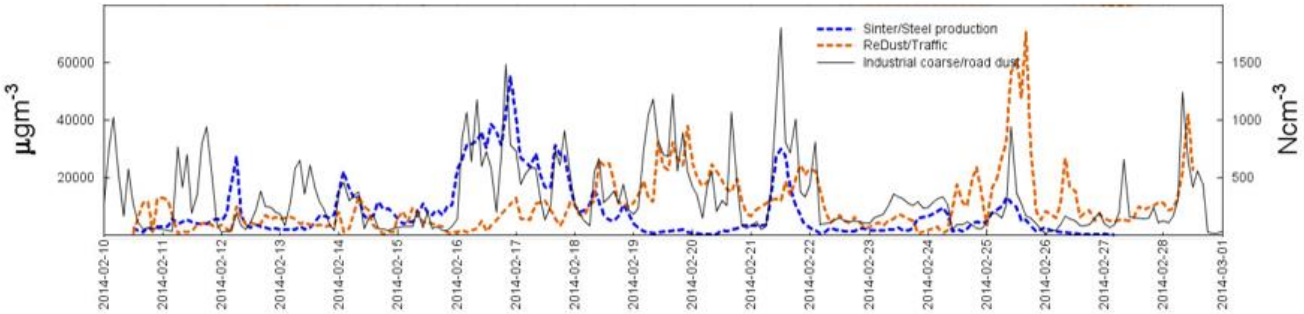

351

352 Fig. S13. Time series of Industrial coarse particles/road dust factor resolved with NSD (solid line)
353 and factors road dust/ Sinter/steel production resolved with chemical composition (dashed lines).

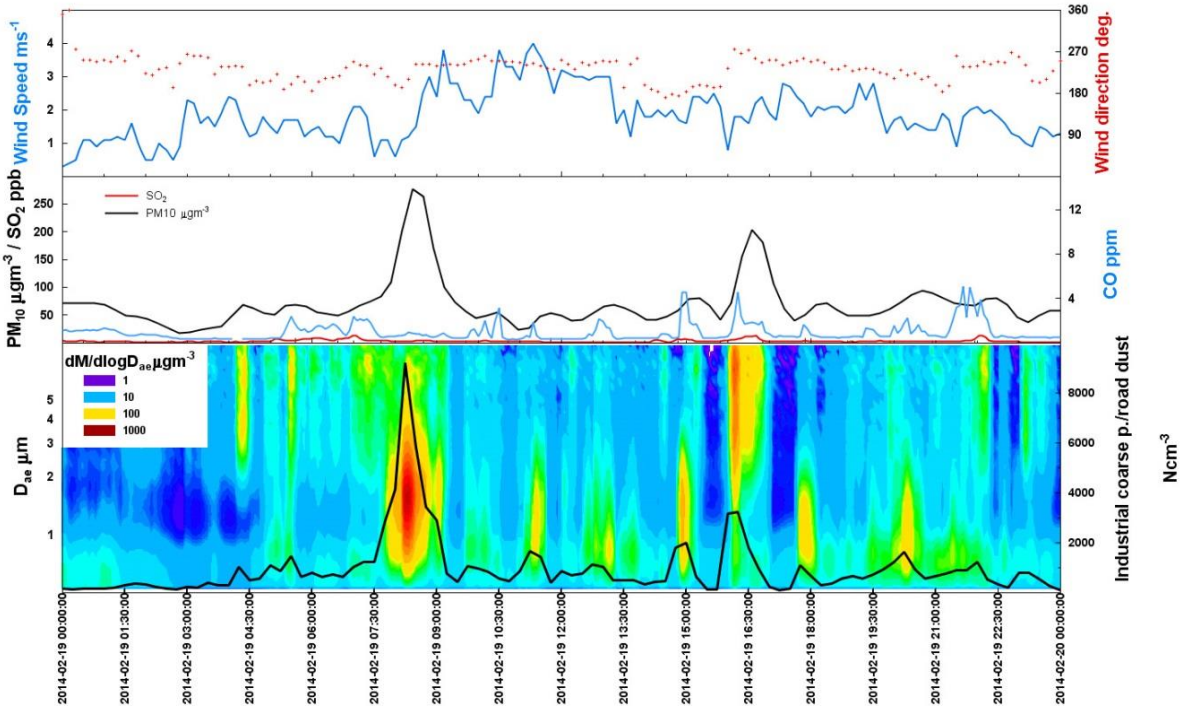

354

355 Figure S14. Pollution episode occurred on the 19.02.2014, approximately from 7:30 to 9 a.m., with
356 PM_{10} concentration up to 286 µg m-3, with a south-western wind direction and wind speed
357 approximately 2 ms^{-1}. From the top to the bottom: wind speed and direction, time series of PM_{10},
358 CO and SO_2, colour plot of APS mass size distribution and time series of factor 6. The pollution
359 event is clearly related to factor 6 coarse industrial particles/road dust.

Manuscript 4:

Kozáková J., Leoni C., Klán M., Hovorka J., Racek M., Ondráček J., Moravec P., Schwarz J.

Chemical characterization of $PM_{1-2.5}$ and its associations with the PM_1, $PM_{2.5-10}$ and meteorology in urban and suburban environments

Chemical characterization of $PM_{1-2.5}$ and its associations with the PM_1, $PM_{2.5-10}$ and meteorology in urban and suburban environments

[*]Jana Kozáková[a, b], Cecilia Leoni[b], Miroslav Klán[b], Jan Hovorka[b], Martin Racek[c], Martin Koštejn[d], Jakub Ondráček[a], Pavel Moravec[a], Jaroslav Schwarz[a]

[a] *Laboratory of Aerosols Chemistry and Physics, Institute of Chemical Process Fundamentals of the CAS, v.v.i., Rozvojová 2, Prague 165 02 Czech Republic*

[b] *Institute for Environmental Studies, Faculty of Science, Charles University, Benátská 2, 12801 Prague 2, Czech Republic*

[c] *Institute of Petrology and Structural Geology, Faculty of Science, Charles University, Albertov 6, Prague128 43, Czech Republic*

[d] *Department of Catalysis and Reaction Engineering, Institute of Chemical Process Fundamentals of the CAS, v.v.i., Rozvojová 2, Prague 165 02 Czech Republic*

Abstract

This study investigated the intermodal fraction of atmospheric aerosols ($PM_{1-2.5}$; particulate matter) representing the transition area between the fine and coarse size ranges. Due to this characteristic, $PM_{1-2.5}$ may contain particles from both modes. The aim of this work was to examine the associations between $PM_{1-2.5}$ and fine (PM_1) and coarse ($PM_{2.5-10}$) fractions using chemical analyses at various sites in the Czech Republic during winter and summer.

Size-resolved PM mass concentrations were determined and meteorological parameters recorded at an urban industrial and a suburban site in Ostrava during winter and at an urban traffic and a suburban site in Prague during summer and winter. The influence of the coarse and fine fraction on $PM_{1-2.5}$ was investigated for all samples with ion analysis (Ca^{2+}-representing $PM_{2.5-10}$ and SO_4^{2-}-representing PM_1) and for selected samples (based on the meteorology) with elemental composition analysis.

$PM_{1-2.5}$ accounted for 3-8% of PM_{10}. In winter, median values of the ratios of Ca^{2+} to SO_4^{2-} in $PM_{1-2.5}$ were lower than one third of the median ratios in $PM_{2.5-10}$ at all site, except at the industrial site with specific sources where the median ratio in $PM_{1-2.5}$ was similar to the ratio in $PM_{2.5-10}$. In summer, the ratios in $PM_{1-2.5}$ were close to those observed in $PM_{2.5-10}$. Relative ratios between S and crustal elements in $PM_{1-2.5}$ were more similar to the ratios in $PM_{2.5-10}$ at every site and in both seasons. The results from chemical analysis were confirmed by positive correlations in the relationships $PM_{1-2.5}$-$PM_{2.5-10}$ in both seasons and $PM_{1-2.5}$-PM_1 in winter, except the industrial site and Prague urban summer campaign characterized by rainy weather.

To conclude, according to performed analyses, $PM_{1-2.5}$ was influenced by the coarse fraction during all campaigns. The influence of both $PM_{2.5-10}$ and PM_1 was evident in winter and during days with rainfall in summer.

Key words: Aerosol Intermodal Fraction; Personal Cascade Impactor Sampler; Enrichment Factor; Elemental Composition; Scanning Electron Microscope

[*]Corresponding author: e-mail kozakova@icpf.cas.cz, tel. 00420 220 390 23

INTRODUCTION

Atmospheric aerosols comprise two fundamental size categories: fine and coarse (Whitby *et al.*, 1972; Lundgren and Burton, 1995). These categories are considered separate classes of pollutants (Wilson and Suh, 1997; US-EPA, 2004) due to their different health effects (Schins *et al.*, 2004; Pope III and Dockery, 2006; Zanobetti and Schwartz, 2009; Stafoggia *et al.*, 2013; WHO, 2013). The national ambient air quality standards (NAAQS), established by the US EPA, define particles with aerodynamic diameters (d_a) less than 2.5 μm ($PM_{2.5}$) and particles with d_a less than 10 μm as PM_{10}, which includes the coarse fraction ($PM_{2.5-10}$). PM_{10} and $PM_{2.5}$ are emitted by a variety of natural and anthropogenic sources. The physical and chemical properties of fine and coarse PM are temporally and spatially highly variable (Anlauf *et al.*, 2006; Herner *et al.*, 2006; Karanasiou *et al.*, 2007; Pérez *et al.*, 2008; Schwarz *et al.*, 2012). Coarse PM, generally formed by mechanical processes, contains earth's crustal metals (e.g., Ca, Fe Si, Al, Ti), sea salt, abrasion products from road traffic, and bioaerosols (Colbeck *et al.*, 2008; Viana *et al.*, 2008). Fine PM is usually formed via combustion or from gas-to-particle conversions and is generally characterized by high contents of carbonaceous material, sulfates, and nitrate and ammonium ions. In addition, minor elements occurring in PM can be excellent tracers for specific sources of aerosols (Colbeck *et al.*, 2008).

A sharp delineation between fine and coarse fractions cannot be clearly defined because that these two fractions overlap in the size range $1<d_a<2.5$ (up to 3) μm. This size range is called the intermodal fraction, or intermediate range, $PM_{1-2.5}$ (Whitby *et al.*, 1972; Whitby, 1978; Lundgren and Burton, 1995; US-EPA, 1996; Wilson and Suh, 1997; Hinds, 1998; Colbeck *et al.*, 2008; Kulkarni *et al.*, 2011). $PM_{1-2.5}$ can constitute a significant part of the respirable fraction measured as NAAQS, on average, 6-22% of PM_{10} and even 11-34% of $PM_{2.5}$ (Lundgren *et al.*, 1996; Geller *et al.*, 2004; Pérez *et al.*, 2008; Kozáková *et al.*, 2017).

Depending on the meteorological conditions, $PM_{1-2.5}$ can consist predominantly of aerosols originating from sources of either the coarse or fine fraction. For example, in arid/semiarid environments, the particles from sources releasing primary coarse particles (coarse PM sources) can occur in the size range below 2.5 μm (Lundgren *et al.*, 1984; Lundgren and Burton, 1995; Claiborn *et al.*, 2000; Husar *et al.*, 2001; Pérez *et al.*, 2008). In environments with high relative humidity (RH), the accumulation mode of fine particles can grow into the intermodal size range (Berner and Lürzer, 1980; Geller *et al.*, 2004; Wang *et al.*, 2012; Tian *et al.*, 2014; Tan *et al.*, 2016).

Several studies have characterised in detail the size resolved PM including the transition area between the accumulation and coarse mode with statistical and chemical analyses (e.g. Gietl and Klemm, 2009; Contini *et al.*, 2014; Tian *et al.*, 2016). Previous studies focused particularly on the intermodal fraction have involved statistical analyses using correlation coefficients (Lundgren *et al.*, 1996; Haller *et al.*, 1999; Claiborn *et al.*, 2000; Vallius *et al.*, 2000; Galindo *et al.*, 2011; Perez *et al.*, 2012), regression analysis (Kozáková *et al.*, 2017), based on the chemical composition of size-resolved aerosol particles (Hughes *et al.*, 2000; Vecchi *et al.*, 2004; Pérez *et al.*, 2008; Perez *et al.*, 2009; Pérez *et al.*, 2010; Pasha and Alharbi, 2015), or on a combination of both statistical and chemical composition methods (Kegler *et al.*, 2001; Geller *et al.*, 2004; Perez *et al.*, 2009). Nevertheless, further investigation of $PM_{1-2.5}$ and its chemical composition is needed for several reasons. The existing studies focus on the chemical composition of $PM_{1-2.5}$ in dry environments (Hughes *et al.*, 2000; Kegler *et al.*, 2001; Geller *et al.*, 2004; Pérez *et al.*, 2008; Perez *et al.*, 2009; Pérez *et al.*, 2010; Pasha and Alharbi, 2015). Only one study was performed in conditions of high RH in a subarctic region, but it did not include a chemical analysis (Vallius *et al.*, 2000). No study in Central Europe with meteorological/climate conditions changing seasonally has been performed. Additionally, the discussion between air quality experts and

legislators as to whether PM_1 should be also considered as the additional air quality standard. The influence of the intermodal fraction on $PM_{2.5}$ has not been well determined or quantified. The contribution of earth's crustal components to $PM_{2.5}$, as well as fine particles growing into PM>1 μm (d_a) during periods of higher RH, can cause inaccuracies in source apportionment and in epidemiological and exposure studies. Therefore, it is necessary to analyze the chemical composition of $PM_{1-2.5}$ in different locations and attempt to describe the conditions under which it is appropriate to consider PM_1 as the independent fraction.

In our project on $PM_{1-2.5}$ characterization, the first part was focused on statistical methods using mass concentrations of PM (Kozáková *et al.*, 2017). Subsequently, in the present study, part of an extensive sample collection was analyzed using chemical methods. The aim of this work was to elucidate the associations between $PM_{1-2.5}$ and fine (PM_1) and coarse ($PM_{2.5-10}$) fractions on the basis of statistical analysis, chemical composition analysis, and meteorological analysis at various urban sites in the Czech Republic during both winter and summer.

METHODS

Sampling sites

Size-resolved PM measurements were performed at two urban and two suburban sites in the Czech Republic, Central Europe, during winter and summer (Supplement: Table S1 and Fig. S1).

Ostrava Radvanice and Bartovice (campaign Radvanice) is a residential district in southeast Ostrava (Fig. S1) composed of family houses and greatly influenced by industrial sources (metallurgy complex), which are approximately 2 kilometers to the southwest (Pokorná *et al.*, 2015; Leoni *et al.*, 2016; Pokorná *et al.*, 2016). The nearest road is 80 m away with a traffic flow of approximately 10,000-15,000 vehicles per day (MoT, 2010; ŘSD, 2010). An air-conditioned

(isothermal, 20°C) monitoring station, containing all instruments, was located in a garden approximately 50 m from the nearest family house.

Ostrava Plesná (campaign Plesná) is a suburban residential area in northwest Ostrava with family houses and low traffic (only residents and approximately 2 regular bus services per hour). The instruments were placed in a garden approximately 20 m from the nearest family house. The cascade impactors were protected against rain and snow, and the spectrometers were placed inside a wooden box.

Prague Benátská (summer campaign Benátská_s, winter campaign Benátská_w) is located in Prague in the city center in the Charles University botanical garden. The nearest intersection has a traffic flow of 15,000-20,000 vehicles per day, and the busiest city road, with a traffic flow of 30,000-50,000 vehicles per day, is located at a distance of 600 m (MoT, 2010). An air-conditioned (winter: 20°C; summer: 20-25°C) rooftop station of the Institute for Environmental Studies with all instruments was located on the fourth floor; for additional details, see Thimmaiah *et al.* (2009).

Prague Suchdol (summer campaign Suchdol_s, winter campaign Suchdol_w) is a suburban background site in northwest Prague with residential houses and the Czech University of Life Sciences campus. The traffic flow along one major two-lane road is 20,000-30,000 vehicles per day (MoT, 2010) with very frequent bus services. The measuring site was located on the research campus of the Institute of Chemical Process Fundamentals, to the north and northeast from the major road at a distance of approximately 250 m. The impactors were placed outside, protected against rain and snow, and the other instruments (online monitoring) were placed inside a building (10 m from the impactor; for more details, see Talbot *et al.* (2016). Information about this sampling site has been provided previously by Smolík *et al.* (2008) and Vodička *et al.* (2013).

140 ***Instrumentation***

141 Twenty-four-hour mass concentrations of size-resolved PM were measured with a US EPA-
142 approved personal cascade impactor sampler (PCIS) at 9 l min^{-1} (Misra *et al.*, 2002). Using a
143 cyclone to cut PM_{10} upstream of the inlet to the impactor, the PCIS separated particles of
144 aerodynamic diameter (d_a) in the following five size stages: A: $10>d_a>2.5$ μm; B: $2.5>d_a>1$ μm;
145 C: $1>d_a>0.5$ μm; D: $0.5>d_a>0.25$ μm; P: $d_a<0.25$ μm. Particles on the stages A through D were
146 collected on 25-mm PTFE filters with porosity 0.5 μm (Pall Corporation, Ann Arbor, Michigan,
147 USA) used as impaction substrates, and particles <0.25 μm (stage P) were collected on 37-mm
148 PTFE backup filters with PMP ring with porosity 2.0 μm (Pall Corporation, Michigan, USA, and
149 SKC Limited, Dorset, United Kingdom).

150 Five (Radvanice, Plesná, Benátská_s/w) or ten (Suchdol_s/w) minutes of integration time of
151 particle number concentration and size distribution were measured with the scanning mobility
152 particle sizer (SMPS model 3936L25 in Radvanice and Benátská, and SMPS model 3936L75 in
153 Plesná and Suchdol, TSI Inc.) and an aerodynamic particle sizer (APS model 3321 at all sites,
154 TSI Inc.) using a PM_{10} sampling head on the top of the sampling tubing. The two aerosol size
155 spectrometers covered the size range from 14 nm to 10 μm.

156 Meteorological data, including wind speed (WS), wind direction (WD), temperature (T) and
157 RH for the Benátská_s campaign, were measured using a Young vane-type monitor (Model
158 05103v, Fondriest Environmental Inc., USA). For the other measuring campaigns (Radvanice,
159 Plesná, Suchdol_s/w, Benátská_w), meteorological data were available from the nearest
160 representative Automated monitoring stations (in the distance of about 477 m from Radvanice
161 site, 4 815 m from Plesná site, 25 m from Suchdol site, and 470 m from Benátská site) managed
162 by the Czech Hydrometeorological Institute.

Gravimetric analysis

The PM concentrations were assessed by gravimetric analysis. Before weighing the PTFE filters were preconditioned for at least 24 hours at 50±5% RH and 20±2°C in weighing room. Every filter was passed over a HaugU-electrode ionizer (PRXU27x18x27 200 radia; Haugh, GmbH&Co. KG, 120 Germany) immediately before weighing with a microbalance (Mettler Toledo MX5; Mettler-121 Toledo, LLC, Ohio, USA) to dissipate any electrostatic charge. Gravimetric analysis of PM samples was fully described in Kozáková *et al.* (2017).

PM concentrations were calculated as follows: PM_1 (fine fraction) as the sum of the aerosol masses on stages C to P (<1 μm), $PM_{2.5}$ as the sum of the aerosol masses on stages B to P (<2.5 μm), PM_{10} as the sum of the aerosol masses of all stages (A-P); $PM_{1-2.5}$ represented by stage B, and $PM_{2.5-10}$ (coarse fraction) represented by stage A.

For every measurement campaign, at least 10% of the field blank filters were used to determine the limit of detection (LOD) of the weighing procedure. Field blanks were exposed to the same conditions as the samples except for the sampling period. The LOD was calculated as three times the standard deviation of the mass changes of all field blanks. The lowest level of the 24-h concentration (concentration lowest level) that could be measured was determined as the ratio of LOD to the nominal volume of the air flowing through the impactor (12.96 m^3). The measured concentrations below the concentration lowest level were replaced by half of this level (5% of the concentrations in the data set).

Chemical analyses

Ion chromatography (IC) was used for the determination of Ca^{2+} and SO_4^{2-} mass concentration in every aerosol size fraction. Ca^{2+} was selected as a marker for $PM_{2.5-10}$ due to its abundant presence in the mineral coarse fraction (Harrison and Van Grieken, 1998; Kertész *et al.*, 2002; Salma *et al.*, 2002; Colbeck *et al.*, 2008; Ondráček *et al.*, 2011; Spindler *et al.*, 2013). SO_4^{2-} was

187 chosen as a marker of PM_1 since it is one of the major constituents of fine particles in outdoor
188 environments (Matta *et al.*, 2002; Perry *et al.*, 2004) in Central Europe (Kertész *et al.*, 2002;
189 Salma *et al.*, 2002; Ondráček *et al.*, 2011; Schwarz *et al.*, 2012; Spindler *et al.*, 2013; Talbot *et*
190 *al.*, 2016). Other ions, such as NO_3^-, Cl^- and others, occur in the fine as well as in the coarse mode
191 in urban and rural environments. For example, distribution of NO_3^- was bimodal in urban and
192 suburban atmospheric aerosols (Colbeck *et al.*, 2008), even in Prague region during winter and
193 summer (Ondráček *et al.*, 2011; Schwarz *et al.*, 2012). Chloride ion was also not considered in
194 our analysis due to its presence in both, fine and coarse mode of Prague atmospheric aerosols
195 found out in our previous study (Schwarz *et al.*, 2012).

196 From every campaign, all samples from Prague campaigns and 18 days from each Ostrava
197 campaign were analyzed using ion chromatography. One-half of each 25-mm filter and a circular
198 slice (13 mm diameter) of each 37-mm backup filter were extracted separately in a solution of 0.3
199 ml methanol and 2.7 ml deionized ultrapure water with conductivity below 0.08 μS m^{-1}
200 (Ultrapure, Watrex Ltd.). After 30 min inside an ultrasonic bath and 1 h of automatic shaking, the
201 solution was filtered using a Millipore syringe filter with porosity 0.22 μm. IC analysis was
202 performed with a Watrex Ltd. instrument with a SHODEX CD-5 conductivity detector, an
203 Alltech universal cation 7 μm 100 x 4.6 mm column and a Transgenomic ICSep AN300 150 x
204 5.5 mm column. A solution of methane sulfonic acid (1.15 mmol l^{-1}) and oxalic acid (2.0 mmol l^{-1})
205 was used as an eluent for the cation column, and a solution of sodium bicarbonate (1.8 mmol l^{-1})
206 and sodium carbonate (1.7 mmol l^{-1}) in water was used for the anion column. Ca^{2+}/SO_4^{2-} ratios
207 were calculated for a comparison of individual PM fractions.

208 A scanning electron microscope (TESCAN Vega, TESCAN ORSAY HOLDING a.s., Czech
209 Republic) equipped with an energy dispersive spectroscope (EDS-detector X-Max 50, Oxford
210 Instruments plc, United Kingdom; SEM+EDX) was used for the elemental semiquantitative

211 microanalysis (C, F, Na, Mg, Al, Si, P, S, Cl, K, Ca, Ti, Cr, Mn, Fe, and Zn) of all days/impactors
212 from Prague campaigns, 17 days for Radvanice, and 12 days for Plesná campaigns. The samples
213 were coated with a thin electroconductive layer of amorphous carbon (c. 15 nm thick). On each
214 filter, seven square areas containing PM sample with an edge length of 200 μm were scanned for
215 200 seconds of live time in order to cover a representative area and minimize the effects of
216 possible heterogeneities. Elements C and F were excluded from subsequent analysis because the
217 C and F are presented in the PTFE filters and the C presented in the coating layer as well as in the
218 samples. Individual elements (without C and F) were expressed as percentages of their sum
219 normalized to 100% (not percentages from the total aerosol mass). The normalization to 100% is
220 necessary in order to avoid the effect of variations in the amount of material covering the surface
221 of the filters. The analyses were conducted with accelerating voltage 15 kV and beam current
222 1.5 nA. The percentages of elements in PM_1 were calculated as a mass of weighted averages of
223 impactor stages C, D, and P. For more details, see the Supplementary material.

224 Ion and elemental analysis of PM_1, $PM_{1\text{-}2.5}$, and $PM_{2.5\text{-}10}$ was performed with the aim of
225 finding associations between the size fractions.

226 The enrichment factor, EF, was calculated to characterize the origin of airborne PM. EF relates
227 the concentration of an element (X) to the concentration of an airborne crustal element
228 normalized to the ratio of these elements in the average continental crust (Saliba *et al.*, 2007):

229 $$EF_x = (X / Si)_{air} / (X / Si)_{crust} \quad (1)$$

230 where *X* indicates the element concentration in the sample of atmospheric aerosol (air) or
231 upper continental crust (crust) and *Si* is the concentration of Si in the sample of atmospheric
232 aerosol (air) or upper continental crust (crust). Si was chosen as a normalizing crustal element
233 (Saliba *et al.*, 2007), and element concentrations in the upper continental crust were given by

234 Wedepohl (1995). An EF value greater than 10 indicates high enrichment due to contributions
235 from non-crustal sources (Torfs and van Grieken, 1997; Chester *et al.*, 1999).

236 ***Data analysis***

237 The mass concentrations of PM_1, $PM_{1\text{-}2.5}$, and $PM_{2.5\text{-}10}$ were calculated from SMPS and APS
238 number concentrations with particle density 1.5 g cm^{-3} (Shen *et al.*, 2002) as described in the
239 Supplementary material. The comparison between SMPS-APS and PCIS measurements was
240 performed for three PM fractions. Despite some imperfections in this comparison given by the
241 different measurement principles of instrumentations and uniform particle density, the SMPS-
242 APS dataset was used for an analysis of PM concentrations versus WD and WS (polar plots) in
243 order to find the potential sources. The PCIS dataset was used for other analyses, i.e. statistical
244 and chemical, because both, the PM mass and chemical species, were analyzed from PCIS filters.

245 The impactor PM mass concentration data were not normally distributed (Shapiro-Wilk test of
246 normality). Therefore, nonparametric Spearman's rank correlation coefficients (r_s) were
247 calculated. The correlation test was calculated to detect statistically significant correlations
248 between two variables (p-value<0.05). The non-parametric Kruskal-Wallis test and the two-
249 sample Wilcoxon test (p-value<0.05) were used to determine statistically significant differences
250 among individual campaigns and between seasons, respectively. The meteorological and
251 statistical analyses were performed with R software and the package Openair (Carslaw and
252 Ropkins, 2012; Carslaw, 2015).

253

254 # RESULTS AND DISCUSSION
255

256 ***Campaign overview***

257 Median values of the monitored meteorological variables (T, RH, and WS) for each campaign
258 are presented in Table S3, and the WS and WD are shown in Figure S3 (Supplement). Seasonal

differences at Prague sites Benátská and Suchdol were evident for T but not as apparent for RH. During summer days at the Suchdol site, RH varied more significantly, resulting in a wide interquartile range (25^{th} and 75^{th} percentiles). Generally, the prevailing WDs were from SW during campaign in Plesná, from SW and NE in Radvanice, and from SW/W during summer and winter campaigns in Benátská. Prevailing WDs for the entire Suchdol campaigns were not possible to determine (Fig. S3).

Median mass concentrations of PM_{10}, $PM_{2.5}$ and the investigated PM fractions $PM_{2.5-10}$, $PM_{1-2.5}$, and PM_1 are displayed in Table 1 for each campaign. The differences in mass concentrations of $PM_{2.5-10}$, $PM_{1-2.5}$, and PM_1 among campaigns were statistically significant (p-values<0.001).

The highest pollution level was observed in Radvanice for all PM fractions. This site is influenced by industrial sources and is an air pollution hotspot (Jančík and Pavlíková, 2013; Pokorná *et al.*, 2015; Leoni *et al.*, 2016; Pokorná *et al.*, 2016). The measuring station was frequently downwind from a large metallurgy complex (during 40% of the sampling period). Other pollution sources included domestic heating; the houses are heated with central heating (53%) and natural gas (34%) as well as coal (10%) and wood (3%; ČSO, 2011; Sram *et al.*, 2013) and road traffic. Additionally, it is not possible to exclude transported pollution from the Polish Silesian province, a heavily industrialized region with metallurgy industry, black coal mining, coke production, and combustion of coal dust, a by-product of coal processing, for heating purposes (Pokorná *et al.*, 2015; Pokorná *et al.*, 2016).

The second highest PM mass concentrations were measured in Plesná, where domestic heating represents the main PM source and the pollution transported from the industrial region can also contribute to increase the pollution level (Swietlicki and Krejci, 1996; Pokorná *et al.*, 2015; Hovorka *et al.*, 2016).

282 At the Suchdol and Benátská sites, PM_{10}, $PM_{2.5}$, and PM_1 mass concentrations were typically
283 three times higher in winter than in summer. In addition to traffic emissions, increased
284 concentrations of PM level are caused by residential heating. Higher (1.9 times and 1.6 times)
285 mass concentrations of $PM_{2.5-10}$ were observed in summer at both sites, probably due to increased
286 resuspension (Vallius *et al.*, 2000) and the presence of bioaerosols, especially pollen and plant
287 debris (Hinds, 1998; Colbeck *et al.*, 2008).

288 In detail, median mass size distributions determined with PCIS varied for every campaign
289 (Supplement Fig. S4). In winter, they were unimodal with the modes around d_a=350 nm. Similar
290 distributions are observed between Prague summer campaigns.

291 A measurement at an urban site in Como (northern Italy) showed similar median mass size
292 distribution with dominant peak in an accumulation mode (around d_a=400 nm) during heating
293 season (Rovelli *et al.*, 2017) as was observed in winter Prague (Benátská and Suchdol) and
294 Plesná campaigns. A study conducted at an industrial site in Port Talbot (South Wales) and in a
295 suburban site in Birmingham during spring (Taiwo *et al.*, 2014) presented that the average mass
296 size distributions were bimodal with dominant peaks in the accumulation mode at both site. In
297 addition, the coarse mode was dominant at the industrial site in Port Talbot compared to the
298 industrial site Radvanice where the coarse mode was only slightly elevated. Similar winter mass
299 size distribution as measured at Radvanice site was observed in Zabrze, an industrial town in
300 southern Poland (Zwozdziak *et al.*, 2017) with the dominant peak in the accumulation range.

301 Mass size distributions were different for summer and winter campaigns in Prague (Figure S4)
302 and at urban site in Como as well (Rovelli *et al.*, 2017).

303 ***Median mass portions of PM fractions***

304 The median masses of PM fractions for different types of localities were presented in our
305 previous work (Kozáková *et al.*, 2017) and included data from campaigns that were also

306 investigated in the present study. Figure 1 presents median masses only for the campaigns of
307 interest. PM_1 was the predominant component of the PM_{10}, while $PM_{1-2.5}$ accounted for 3-8% of
308 PM_{10} and $PM_{2.5-10}$ for 4-15% of PM_{10}. In the Benátská and Suchdol campaigns, the seasonality of
309 PM mass portions was compared. In summer, the mass portions of $PM_{1-2.5}$ (5%, 8%) and $PM_{2.5-10}$
310 (13%, 15%) of PM_{10} were higher than in winter ($PM_{1-2.5}$: 4% and 3%, $PM_{2.5-10}$: 4% and 4%,
311 respectively) probably due to increased contribution of soil dust as evidence by Kegler *et al.*
312 (2001) and Vecchi *et al.* (2004) in summer whilst the high RH reduced the ability of dust
313 resuspension in winter (Vallius *et al.*, 2000). In contrast, the PM_1 contribution was 11-15
314 percentage points higher in winter (93% and 92%) than in summer (82% and 77%).
315 Nevertheless, higher portions of $PM_{1-2.5}$ in PM_{10} were observed in Barcelona (16-22%; 2 years
316 of measurement) by Pérez *et al.* (2008), in Phoenix (8%; 6 months of measurement: May to
317 October) by Lundgren *et al.* (1996), and in Helsinki (18-26%; 6 months of measurement: October
318 to May) by Vallius *et al.* (2000). Barcelona and Phoenix are located in regions that are strongly
319 influenced by desert-blown dust that causes enrichment of the intermodal fraction (Pérez *et al.*,
320 2008). The city of Helsinki, however, is located in a subarctic region, with a generally higher RH,
321 and the reason for the higher coarse fraction (including $PM_{1-2.5}$) may be the application of sand to
322 streets and pavement (Vallius *et al.*, 2000).
323 ***$PM_{1-2.5}$ investigation at various sites***
324 The investigation of the intermodal fraction in terms of its association with the coarse or fine
325 fraction at various sites was performed using different analyses: statistical, chemical, and
326 meteorological. The Spearman correlation coefficients for the relationship of $PM_{1-2.5}$ with $PM_{2.5-10}$, PM_1 and meteorological parameters are displayed in Table 2. The EFs (Fig. 2) and Ca^{2+}/SO_4^{2-}
328 ratios (Fig. 3) were calculated for individual PM fractions. Ca^{2+} and SO_4^{2-} mass concentrations
329 are presented in the Supplement (Table S4). The analysis of the polar plots (Fig. 4) obtained with

online measurements helps to investigate the PM sources according to WS and WD. The sources can have same directionality and be related to either low or high speeds (local versus distant sources).

Radvanice:

In Radvanice, $PM_{1\text{-}2.5}$ is correlated with $PM_{2.5\text{-}10}$ ($r_s = 0.39$; Table 2). This variable corresponds to the WD analysis (Fig. 4), where the highest mass concentrations of $PM_{1\text{-}2.5}$ and $PM_{2.5\text{-}10}$ occurred from the same southwest direction with higher WS (>3 m s^{-1}), and thus, they have the same source location, likely the industrial zone. In contrast, the highest mass concentrations of PM_1 originated from local sources or from sources located to the north and northeast. The Ca^{2+}/SO_4^{2-} ratios in $PM_{1\text{-}2.5}$ were more similar to those in $PM_{2.5\text{-}10}$ than to those in PM_1 (Fig. 3).

Similar percentages of elements were observed between $PM_{2.5\text{-}10}$ and $PM_{1\text{-}2.5}$, and the most abundant elements were Fe, Si, Ca, and Na, whereas Fe, S, and Cl were the most abundant elements in PM_1 (Fig. 5). Fe was the predominant element in all PM fractions, even in PM_1. It is necessary to mention that the Fig. 5 shows the percentages of elements related to their sum (not related to the total aerosol mass). Due to the fact that some main chemical species, for example carbon and nitrate, were omitted from the analyses, this approach has the limitation to determine size distributions of individual species, the mass reconstruction, and source apportionment analysis, such as Positive Matrix Factorization as performed other studies (e.g. Contini *et al.*, 2014; Tian *et al.*, 2016). But for the determination of the similarity between the individual PM fractions, these methods based on ratios of species are sufficient and used to identify possible indicators for relative importance of various sources in the atmosphere (Prospero *et al.*, 2001; Wang *et al.*, 2005; Anlauf *et al.*, 2006; Alharbi *et al.*, 2015; Cesari *et al.*, 2016). Some elements mentioned in the legend (Fig. 5) are invisible in the pie charts due to their too low percentage proportions.

354 The EFs in $PM_{1\text{-}2.5}$ and $PM_{2.5\text{-}10}$ had similar values for elements Cl, K, Mn, Fe (EF lower than
355 for PM_1), and Ca (EF higher than for PM_1; Fig. 2). Previous source apportionment studies
356 conducted in this region have suggested that the main air pollution sources are industry
357 (processing of iron ore and production of raw iron and steel), coal combustion, biomass burning,
358 and traffic emissions (Rogula-Kozłowska *et al.*, 2012; Pokorná *et al.*, 2015; Pokorná *et al.*, 2016).
359 Plesná:
360 In Plesná, $PM_{1\text{-}2.5}$ is correlated with PM_1 (r_s = 0.53), $PM_{2.5\text{-}10}$ (r_s = 0.35) and with RH (r_s =
361 0.49). The highest mass concentrations of all three PM fractions occurred from northeast WD.
362 This result suggested that the Plesná site could be influenced by pollution transported from the
363 Polish region (Swietlicki and Krejci, 1996; Pokorná *et al.*, 2015; Hovorka *et al.*, 2016). In all
364 three fractions, the SO_4^{2-} concentrations were higher than Ca^{2+} concentrations (see Fig. 3), and the
365 variability expressed as the 25^{th} and 75^{th} percentile was low. The percentages of elements were
366 similar for $PM_{2.5\text{-}10}$ and $PM_{1\text{-}2.5}$, with high percentages of Si, Na, and Fe. S was more abundant in
367 $PM_{1\text{-}2.5}$ (9% points more) than in $PM_{2.5\text{-}10}$. S, Cl, and K were the predominant elements in PM_1.
368 The EFs in $PM_{1\text{-}2.5}$ and $PM_{2.5\text{-}10}$ showed similar values for Mg (EF slightly higher than for
369 PM_1), the typical crustal element, as well as Fe, Mn, Cl, and K (EF lower than for PM_1). The
370 origin of Fe and Mn could be from the industrial sources affecting likely the whole region
371 (Pokorná *et al.*, 2015). Cl and K being highly enriched in the fine fraction are probably the result
372 of coal combustion and biomass burning (Swietlicki and Krejci, 1996; Almeida *et al.*, 2005; Han
373 *et al.*, 2005; Rogula-Kozłowska *et al.*, 2012). This conjecture was also confirmed by the high
374 enrichments in S and Zn.
375 SO_4^{2-} or S in atmospheric aerosol is primarily raised as a secondary component from
376 atmospheric oxidation of SO_2 (Colbeck *et al.*, 2008). Sulfur, although it is also part of the

377 minerals (sulfid-S^{2-} and sulfate-SO_4^{2-} minerals), was highly enriched in Plesná due to the
378 atmospheric pollution transport as the secondary component.
379 Suchdol:
380 During the **Suchdol_s (summer)** campaign, the highest concentrations of all three fractions
381 were measured from north WD with WS higher than 1.5 m s^{-1}. $PM_{1\text{-}2.5}$ was highly correlated with
382 $PM_{2.5\text{-}10}$ ($r_s = 0.59$). A negative correlation was observed between $PM_{1\text{-}2.5}$ and RH ($r_s = -0.38$),
383 which confirmed the similarity with the coarse fraction because the decrease in RH enhances the
384 resuspension (Vallius *et al.*, 2000; Hien *et al.*, 2002; Galindo *et al.*, 2011). The Ca^{2+}/SO_4^{2-} ratio in
385 $PM_{1\text{-}2.5}$ was more similar to the ratio in $PM_{2.5\text{-}10}$ than in PM_1, and it was characterized by high
386 variability (Fig. 3), similar to that in $PM_{2.5\text{-}10}$. The elemental percentage distribution of the
387 predominant crustal components (Si, Fe, Na, Ca, and Al) in $PM_{1\text{-}2.5}$ was similar to that in $PM_{2.5\text{-}10}$.
388 In PM_1, S was predominant and elements such as Fe and Si were significant. A closer
389 examination of the upper part of the fine fraction, $PM_{0.5\text{-}1}$ (particles d_a = 0.5-1 μm), showed a
390 significant influence of the crustal elements Si, Na, and Fe, as in the coarse and intermodal
391 fractions (Supplement, Fig. S5), which was also observed by Schwarz *et al.* (2012) for sea salt-
392 related ions (Na^+ and Cl^-) at the Suchdol site. This phenomenon may be an artifact created by a
393 particle bounce-off effect inside the impactors that changes the size distribution (Cheng and Yeh,
394 1976). The PCIS loaded with PTFE collection substrate used in our study was tested by Misra *et*
395 *al.* (2002) and Singh *et al.* (2003). However, their laboratory evaluations of the 1.0 and 2.5 μm
396 (d_a) impactor stages using polydisperse ammonium sulfate aerosols indicated that the 50%
397 collection efficiency cut-off points were very close to the theoretical cut-off points.
398 The EFs in $PM_{1\text{-}2.5}$ and $PM_{2.5\text{-}10}$ revealed similar low values (EF<10) for elements K and Mn
399 and further increased values (EF>10) for P, S, Cl, Cr, and Zn. But EFs for S and Zn in both
400 fractions were significantly lower than in PM_1. The Mn, Cr, and Zn in coarse PM could be related

401 to a traffic emissions source (Veron *et al.*, 1992; Manoli *et al.*, 2002; Samara and Voutsa, 2005;
402 Viana *et al.*, 2008; Chang *et al.*, 2009). Sources of P in non-desert environments are mostly
403 biogenic or from fossil fuel and biomass burning (Mahowald *et al.*, 2008).

404 Different results were found at the **Suchdol site in winter (Suchdol_w)**. The highest
405 concentrations of $PM_{1-2.5}$ were measured with southeast WD and WS of approximately 1 m s^{-1}.
406 PM_1 appeared to originate from local source(s) because the highest concentrations occurred with
407 low WS (less than 1 m s^{-1}), and a strong negative correlation between PM_1 and WS was found
408 (r_s = -0.81). The highest concentrations of $PM_{2.5-10}$ were observed with a northeast WD. $PM_{1-2.5}$
409 was positively correlated with PM_1 and $PM_{2.5-10}$ and negatively correlated with WS (r_s = 0.75,
410 0.59, -0.52, respectively); $PM_{2.5-10}$ was also negatively correlated with WS (r_s = -0.50). In
411 general, strong winds disperse PM_{10}, $PM_{2.5}$, and PM_1 pollution in the atmosphere, and low WSs
412 allow pollution levels to increase (Chaloulakou *et al.*, 2003). A correlation between $PM_{1-2.5}$ and
413 RH (r_s = 0.40) was also apparent. SO_4^{2-} in all three fractions was more abundant than Ca^{2+}, and
414 the variability was very low in comparison with other campaigns (Fig. 3).

415 The elemental distribution showed that S, Si, Na, and Fe were the most abundant elements in
416 $PM_{1-2.5}$. Si, Na, and Fe were the most abundant elements in $PM_{2.5-10}$ in contrast with S, which was
417 the most abundant element in PM_1. The EFs in $PM_{1-2.5}$ and $PM_{2.5-10}$ showed similar values for Cl,
418 K (slightly lower than in PM_1; Fig. 2).

419 In addition, the winter mass concentrations of SO_4^{2-} measured in PM fractions were
420 significantly elevated (p-values = 0.0004-0.001) in comparison with summer (Supplement Table
421 S4). No seasonal differences in Ca^{2+} mass concentrations were found (p-values = 0.3399-0.9667).
422 Benátská:

423 In the **summer campaign (Benátská_s)**, $PM_{1-2.5}$ was strongly correlated with PM_1 (r_s = 0.71)
424 and weakly correlated with $PM_{2.5-10}$ (r_s = 0.45). The weather conditions during the second half of

425 the measuring campaign were rainy and thus more humid. In addition, the median mass
426 concentration of $PM_{1-2.5}$ was higher on rainy days (2.0 μg m^{-3}) than on sunny days (0.6 μg m^{-3}).
427 Furthermore, SO_4^{2-} was more abundant than Ca^{2+} on rainy days (median of Ca^{2+}/SO_4^{2-} for rainy
428 days: 0.57; for sunny days: 1.45).

429 The percentages of elements were similar between $PM_{1-2.5}$ and $PM_{2.5-10}$ for the most abundant
430 crustal elements (Si, Fe, further Ca, Na, and Al). S and Fe with Si and K were predominant in
431 PM_1. As we observed in Suchdol, the coarser part of the fine fraction, $PM_{0.5-1}$, was also highly
432 influenced by the crustal elements because Si, Fe, and Na were predominant (Fig. S5). The
433 highest mass concentrations of all PM fractions occurred with east and southeast WD (WS = 0.5-
434 1 m s^{-1}), i.e., they corresponded to a strong traffic source (busy city road at a distance of 600 m),
435 and this was confirmed by the enrichment in elements such as Cr, Mn, Fe, and Zn (Veron *et al.*,
436 1992; Manoli *et al.*, 2002; Samara and Voutsa, 2005; Viana *et al.*, 2008; Chang *et al.*, 2009) . The
437 EFs in $PM_{1-2.5}$ and $PM_{2.5-10}$ had similarly low values for S, Cl, K, and Mn in comparison with the
438 EFs in PM_1. $PM_{1-2.5}$ and $PM_{2.5-10}$ were more enriched in P than PM_1 due to the greater abundance
439 of bioaerosols, especially pollen and plant debris, in the coarse fraction (Mahowald *et al.*, 2008).

440 During the **Benátská_w** campaign, the $PM_{1-2.5}$ was strongly correlated with $PM_{2.5-10}$ (r_s = 0.79)
441 and weakly correlated with PM_1 (r_s = 0.36). A negative correlation was observed between $PM_{1-2.5}$
442 and WS (r_s = -0.63), and $PM_{2.5-10}$ and PM_1 were negatively correlated with WS (r_s = -0.61, and -
443 0.63). The highest concentrations of $PM_{1-2.5}$ and $PM_{2.5-10}$ were from local traffic (the nearest road
444 and intersection), and the highest concentrations of PM_1 occurred with an east WD (busy city
445 road). This finding was confirmed by the enrichment in the same elements (Cr, Fe, and Zn) as
446 those in summer. The EFs for S and K in $PM_{1-2.5}$ and $PM_{2.5-10}$ achieved similar lower values in
447 comparison with their EFs in PM_1, confirming their origin in sources of the fine fraction.

448 The percentages of elements were very similar between $PM_{1\text{-}2.5}$ and $PM_{2.5\text{-}10}$; Fe, Si, and Na
449 were the most abundant together with substantial amounts of Ca and Al. The predominant
450 element in PM_1 was S, followed by much lower abundant of Na, K, Fe, and Si (Fig. 5). The
451 percentages of elements in $PM_{0.5\text{-}1}$ were very similar to those in PM_1 (Fig. S5), and the influence
452 of the coarse PM sources was not observed as it was in summer. SO_4^{2-} was more abundant than
453 Ca^{2+} in $PM_{1\text{-}2.5}$ in most cases with low variability during the campaign.
454 At the Benátská site, seasonal differences of SO_4^{2-} concentrations in $PM_{1\text{-}2.5}$ and $PM_{2.5\text{-}10}$ were
455 found (p-value = 0.0003 and 0.007, respectively). In contrast, seasonal differences of Ca^{2+} in all
456 three fractions were not statistically significant (p-values from 0.136 to 0.967). As traffic is the
457 source of both the fine and coarse PM and concentration variations occurred in parallel,
458 correlations with both fractions were found.
459 At a traffic site in Barcelona, $PM_{1\text{-}2.5}$ was made up of a mixture originating from fine and
460 coarse PM sources consisting predominantly of mineral dust and secondary inorganic aerosols
461 (SIA: SO_4^{2-}, NO_3^-, and NH_4^+) and lesser parts of carbonaceous matter and sea spray (Pérez *et al.*,
462 2008; Perez *et al.*, 2009; Pérez *et al.*, 2010). More than half of $PM_{1\text{-}2.5}$ mass came from crustal
463 elements such as Al, Si, Ca, and Ti in a Milano urban site (Vecchi *et al.*, 2004). Furthermore,
464 during summer, elevated concentrations of these elements caused an increase of the $PM_{1\text{-}2.5}$ mass
465 portion in contrast with winter (Vecchi *et al.*, 2004). Kegler *et al.* (2001) also reported a strong
466 linear relationship between the soil components of $PM_{2.5}$ and the concentration of $PM_{1\text{-}2.5}$ in an
467 arid area in Phoenix, Arizona.
468 In winter, when the humidity is generally higher than it is in summer, particles of the
469 accumulation mode can grow into PM with d_a>1, even >2.5 μm (Berner and Lürzer, 1980; Geller
470 *et al.*, 2004; Wang *et al.*, 2012; Tian *et al.*, 2014; Tan *et al.*, 2016). This process is most likely
471 due to the hygroscopic properties of inorganic salts such as sulfates and nitrates (Charlson *et al.*,

1978; Tang, 1980; Geller *et al.*, 2004) contributing the predominant portion of atmospheric aerosols, especially in industrial regions, for example see Zhuang *et al.* (1999); Alharbi *et al.* (2015), and significantly elevated mass concentrations of sulfates were observed in our study in winter. Thus, the presence of a source producing primary fine PM can influence not only the intermodal but also the coarse fraction, as was observed in winter at the Plesná, Suchdol, and Benátská sites as well as in summer during rainy days at the Benátská site. Although the Radvanice campaign was performed in winter, this phenomenon was not observed, probably due to the effects of the important industrial source of coarse PM on the intermodal fraction.

CONCLUSIONS

The behavior of the intermodal fraction was variable and differed by measuring site and season. The influence of the fine and coarse fractions of the atmospheric aerosols on $PM_{1\text{-}2.5}$ depended on the meteorological conditions, especially on RH, and on the characteristics of PM sources present at the investigated site.

In summer, the percentages of elements were almost identical for $PM_{1\text{-}2.5}$ and $PM_{2.5\text{-}10}$ and crustal elements were predominant. In addition, the crustal elements highly influenced the part of the fine fraction $1>d_a>0.5$ to a greater extent than they did in the winter season. In winter, $PM_{1\text{-}2.5}$ was composed of elements that were also predominant in $PM_{2.5\text{-}10}$, and a significant influence of the fine fraction (represented by sulfate/sulfur) was also observed.

The investigation of $PM_{1\text{-}2.5}$ at four urban sites in the Czech Republic suggested that $PM_{2.5}$, often considered as the fine fraction, included a significant portion of particles originating from sources of coarse PM, especially in summer but also sometimes in winter. Therefore, PM_1 should be monitored at air quality stations and chemical analysis of both PM_1 and $PM_{2.5}$ is needed to accurately assess the influences of pollution sources to fine and coarse aerosols.

497 Future studies focused on source apportionment and epidemiology/exposure should consider
498 our findings and target the appropriate PM fraction according to the prevailing meteorological
499 conditions and the location where the investigation will be conducted.
500
501 ## ACKNOWLEDGMENTS
502
503 This work was supported by Charles University [project GA UK No 274213] and the Czech
504 Grant Agency [project No P503/12/G147]. We thank American Journal Experts (AJE) for
505 English language editing.
506
507 ## REFERENCES
508
509 Alharbi, B., Shareef, M.M. and Husain, T. (2015). Study of Chemical Characteristics of
510 Particulate Matter Concentrations in Riyadh, Saudi Arabia. *Atmospheric Pollution*
511 *Research* 6: 88-98.
512 Almeida, S.M., Pio, C.A., Freitas, M.C., Reis, M.A. and Trancoso, M.A. (2005). Source
513 Apportionment of Fine and Coarse Particulate Matter in a Sub-Urban Area at the Western
514 European Coast. *Atmospheric Environment* 39: 3127-3138.
515 Anlauf, K., Li, S.-M., Leaitch, R., Brook, J., Hayden, K., Toom-Sauntry, D. and Wiebe, A.
516 (2006). Ionic Composition and Size Characteristics of Particles in the Lower Fraser
517 Valley: Pacific 2001 Field Study. *Atmospheric Environment* 40: 2662-2675.
518 Berner, A. and Lürzer, C. (1980). Mass Size Distributions of Traffic Aerosols at Vienna. *Journal*
519 *of Physical Chemistry* 84: 2079-2083.
520 Carslaw, D.C. (2015). The Openair Manual Open-Source Tools for Analysing Air Pollution Data.
521 *King's College London*: 287-287.

522 Carslaw, D.C. and Ropkins, K. (2012). Openair - an R Package for Air Quality Data Analysis.
523 *Environmental Modelling and Software* 27-28: 52-61.
524 Cesari, D., Donateo, A., Conte, M., Merico, E., Giangreco, A., Giangreco, F. and Contini, D.
525 (2016). An Inter-Comparison of Pm2.5 at Urban and Urban Background Sites: Chemical
526 Characterization and Source Apportionment. *Atmospheric Research* 174-175: 106-119.
527 Claiborn, C.S., Finn, D., Larson, T.V. and Koenig, J.Q. (2000). Windblown Dust Contributes to
528 High Pm2.5 Concentrations. *Journal of the Air & Waste Management Association* 50:
529 1440-1445.
530 Colbeck, I., Turner, J., Laaksonen, A., Lehtinen, K.E.J., Clement, C.F., Lazaridis, M., Grgi´c, I.,
531 Topping, D., MacKenzie, R., Baltensperger, U. and Furger, M. (2008). *Environmental*
532 *Chemistry of Aerosols*, 1st ed. Blackwell Publishing Ltd., Oxford.
533 Contini, D., Cesari, D., Genga, A., Siciliano, M., Ielpo, P., Guascito, M.R. and Conte, M. (2014).
534 Source Apportionment of Size-Segregated Atmospheric Particles Based on the Major
535 Water-Soluble Components in Lecce (Italy). *Science of the Total Environment* 472: 248-
536 261.
537 ČSO (2011). Population and Housing Census 2011.
538 Galindo, N., Varea, M., Gil-Moltó, J., Yubero, E. and Nicolás, J. (2011). The Influence of
539 Meteorology on Particulate Matter Concentrations at an Urban Mediterranean Location.
540 *Water, Air, and Soil Pollution* 215: 365-372.
541 Geller, M.D., Fine, P.M. and Sioutas, C. (2004). The Relationship between Real-Time and Time-
542 Integrated Coarse (2.5–10 Mm), Intermodal (1–2.5 Mm), and Fine (<2.5 Mm) Particulate
543 Matter in the Los Angeles Basin. *Journal of the Air & Waste Management Association*
544 54: 1029-1039.

545 Gietl, J.K. and Klemm, O. (2009). Source Identification of Size-Segregated Aerosol in Munster,
546 Germany, by Factor Analysis. *Aerosol Science and Technology* 43: 828-837.
547 Haller, L., Claiborn, C., Larson, T., Koenig, J., Norris, G. and Edgar, R. (1999). Airborne
548 Particulate Matter Size Distributions in an Arid Urban Area. *J Air Waste Manag Assoc*
549 49: 161-168.
550 Han, J.S., Moon, K.J., Ryu, S.Y., Kim, Y.J. and Perry, K.D. (2005). Source Estimation of
551 Anthropogenic Aerosols Collected by a Drum Sampler During Spring of 2002 at Gosan,
552 Korea. *Atmospheric Environment* 39: 3113-3125.
553 Harrison, R.M. and Van Grieken, R. (1998). *Atmospheric Particles*. John Wiley & Sons, Inc.,
554 Chichester; New York.
555 Herner, J.D., Ying, Q., Aw, J., Gao, O., Chang, D.P.Y. and Kleeman, M.J. (2006). Dominant
556 Mechanisms That Shape the Airborne Particle Size and Composition Distribution in
557 Central California. *Aerosol Science and Technology* 40: 827-844.
558 Hien, P.D., Bac, V.T., Tham, H.C., Nhan, D.D. and Vinh, L.D. (2002). Influence of
559 Meteorological Conditions on Pm2.5 and Pm2.5-10 Concentrations During the Monsoon
560 Season in Hanoi, Vietnam. *Atmospheric Environment* 36: 3473-3484.
561 Hinds, W.C. (1998). *Aerosol Technology-Properties, Behavior, and Measurement of Airborne*
562 *Particles*, 2nd ed. John Wiley & Sons, Inc., New York.
563 Hovorka, J., Leoni, C., Dočekalová, V., Ondráček, J. and Zíková, N. (2016). Aerosol Distribution
564 in the Planetary Boundary Layer Aloft a Residential Area. *IOP Conference Series: Earth*
565 *and Environmental Science* 44: 1-6.
566 Hughes, L.S., Allen, J.O., Bhave, P., Kleeman, M.J., Cass, G.R., Liu, D.Y., Fergenson, D.P.,
567 Morrical, B.D. and Prather, K.A. (2000). Evolution of Atmospheric Particles Along

568 Trajectories Crossing the Los Angeles Basin. *Environmental Science and Technology* 34:
569 3058-3068.
570 Husar, R.B., Tratt, D.M., Schichtel, B.A., Falke, S.R., Li, F., Jaffe, D., Gill, T., Laulainen, N.S.,
571 Lu, F., Reheis, M.C., Chun, Y., Westphal, D., McKendry, I., Kuring, N., Feldman, G.C.,
572 Frouin, R.J., Merrill, J., Dubois, D., Vignola, F., Murayama, T., Nickovic, S., Wilson,
573 W.E., Sassen, K., Sugimoto, N. and Malm, W.C. (2001). Asian Dust Events of April
574 1998. *Journal of Geophysical Research* 106: 18317-18330.
575 Chaloulakou, A., Kassomenos, P., Spyrellis, N., Demokritou, P. and Koutrakis, P. (2003).
576 Measurements of Pm10 and Pm2.5 Particle Concentrations in Athens, Greece.
577 *Atmospheric Environment* 37: 649-660.
578 Chang, S.-h., Wang, K.-s. and Chang, H.-f. (2009). Comparison of Source Identification of
579 Metals in Road-Dust and Soil. *Soil and Sediment Contamination* 18: 669-683.
580 Charlson, R.J., Covert, D.S., Larson, T.V. and Waggoner, A.P. (1978). Chemical Properties of
581 Tropospheric Sulfur Aerosols. *Atmospheric Environment* 12: 39-53.
582 Cheng, Y.-S. and Yeh, H.-C. (1976). Particle Bounce Errors in Cascade Impactors.
583 *Environmental Science & Technology* 13: 1392-1396.
584 Chester, R., Nimmo, M. and Preston, M.R. (1999). The Trace Metal Chemistry of Atmospheric
585 Dry Deposition Samples Collected at Cap Ferrat: A Coastal Site in the Western
586 Mediterranean. *Marine Chemistry* 68: 15-30.
587 Jančík, P. and Pavlíková, I. (2013). Metallurgical Source-Contribution Analysis of Pm10 Annual
588 Average Concentration: A Dispergion Modeling Approach in Moravian-Silesian Region.
589 *Metalurgija* 52: 497-500.

590 Karanasiou, A.A., Sitaras, I.E., Siskos, P.A. and Eleftheriadis, K. (2007). Size Distribution and
591 Sources of Trace Metals and N-Alkanes in the Athens Urban Aerosol During Summer.
592 *Atmospheric Environment* 41: 2368-2381.
593 Kegler, S.R., Wilson, W.E. and Marcus, A.H. (2001). Pm 1 , Intermodal (Pm 2.5-1) Mass, and
594 the Soil Component of Pm 2.5 in Phoenix, Az, 1995-1996. *Aerosol Science and*
595 *Technology* 35: 914-920.
596 Kertész, Z., Balásházy, I., Borbély-Kiss, I., Hofmann, W., Hunyadi, I., Salma, I. and Winkler-
597 Heil, R. (2002). Composition, Size Distribution and Lung Deposition Distribution of
598 Aerosols Collected in the Atmosphere of a Speleotherapeutic Cave Situated Below
599 Budapest, Hungary. *Nuclear Instruments and Methods in Physics Research, Section B:*
600 *Beam Interactions with Materials and Atoms* 189: 221-226.
601 Kozáková, J., Pokorná, P., Černíková, A., Hovorka, J., Braniš, M., Moravec, P. and Schwarz, J.
602 (2017). The Association between Intermodal (Pm1-2.5) and Pm1, Pm2.5, Coarse
603 Fractionand Meteorological Parameters in Various Environments in Central Europe.
604 *Aerosol and Air Quality Research* 17: 1234-1243.
605 Kulkarni, P., Baron, P.A. and Willeke, K. (2011). *Aerosol Measurement: Principles, Techniques,*
606 *and Applications*, 3rd ed. John Wiley & Sons, Inc., New York.
607 Leoni, C., Hovorka, J., Docekalova, V., Cajthaml, T. and Marvanova, S. (2016). Source Impact
608 Determination Using Airborne and Ground Measurements of Industrial Plumes.
609 *Environmental Science & Technology* 50: 9881-9888.
610 Lundgren, D.A. and Burton, R.M. (1995). Effect of Particle Size Distribution on the Cut Point
611 between Fine and Coarse Ambient Mass Fractions. *Inhalation Toxicology* 7: 131-148.

612 Lundgren, D.A., Hausknecht, B.J. and Burton, R.M. (1984). Large Particle Size Distribution in
613 Five U.S. Cities and the Effect on a New Ambient Particulate Matter Standard (Pm10).
614 *Aerosol Science and Technology* 3: 467-473.
615 Lundgren, D.A., Hlaing, D.N., Rich, T.A. and Marple, V.A. (1996). Data from a Trichotomous
616 Sampler. *Aerosol Science and Technology* 25: 353-357.
617 Mahowald, N., Jickells, T.D., Baker, A.R., Artaxo, P., Benitez-Nelson, C.R., Bergametti, G.,
618 Bond, T.C., Chen, Y., Cohen, D.D., Herut, B., Kubilay, N., Losno, R., Luo, C., Maenhaut,
619 W., McGee, K.A., Okin, G.S., Siefert, R.L. and Tsukuda, S. (2008). Global Distribution
620 of Atmospheric Phosphorus Sources, Concentrations and Deposition Rates, and
621 Anthropogenic Impacts. *Global Biogeochemical Cycles* 22: 1-19.
622 Manoli, E., Voutsa, D. and Samara, C. (2002). Chemical Characterization and Source
623 Identification/Apportionment of Fine and Coarse Air Particles in Thessaloniki, Greece.
624 *Atmospheric Environment* 36: 949-961.
625 Matta, E., Facchini, M.C., Decesari, S., Mircea, M., Cavalli, F., Fuzzi, S., Putaud, J.P. and
626 Dell'Acqua, a. (2002). Chemical Mass Balance of Size-Segregated Atmospheric Aerosol
627 in an Urban Area of the Po Valley, Italy. *Atmospheric Chemistry and Physics Discussions*
628 2: 2167-2208.
629 Misra, C., Singh, M., Shen, S., Sioutas, C. and Hall, P.M. (2002). Development and Evaluation of
630 a Personal Cascade Impactor Sampler (Pcis). *Journal of Aerosol Science* 33: 1027-1047.
631 MoT (2010). Tématická Mapa Intenzit Provozu, http://www.jdvm.cz/cz/s525/Rozcestnik/c7341-
632 Tematicka-mapa-intenzit-provozu.
633 Ondráček, J., Schwarz, J., Ždímal, V., Andělová, L., Vodička, P., Bízek, V., Tsai, C.J., Chen,
634 S.C. and Smolík, J. (2011). Contribution of the Road Traffic to Air Pollution in the

635 Prague City (Busy Speedway and Suburban Crossroads). *Atmospheric Environment* 45:
636 5090-5100.
637 Pasha, M.J. and Alharbi, B.H. (2015). Characterization of Size-Fractionated Pm10 and
638 Associated Heavy Metals at Two Semi-Arid Holy Sites During Hajj in Saudi Arabia.
639 *Atmospheric Pollution Research* 6: 162-172.
640 Perez, L., Medina-Ramón, M., Künzli, N., Alastuey, A., Pey, J., Pérez, N., Garcia, R., Tobias, A.,
641 Querol, X. and Sunyer, J. (2009). Size Fractionate Particulate Matter, Xehicle Traffic, and
642 Case-Specific Daily Mortality in Barcelona, Spain. *Environmental Science and*
643 *Technology* 43: 4707-4714.
644 Perez, L., Tobías, A., Querol, X., Pey, J., Alastuey, A., Díaz, J. and Sunyer, J. (2012). Saharan
645 Dust, Particulate Matter and Cause-Specific Mortality: A Case-Crossover Study in
646 Barcelona (Spain). *Environment International* 48: 150-155.
647 Pérez, N., Pey, J., Cusack, M., Reche, C., Querol, X., Alastuey, A. and Viana, M. (2010).
648 Variability of Particle Number, Black Carbon, and Pm10, Pm2.5, and Pm1 Levels and
649 Speciation: Influence of Road Traffic Emissions on Urban Air Quality. *Aerosol Science*
650 *and Technology* 44: 487-499.
651 Pérez, N., Pey, J., Querol, X., Alastuey, A., López, J.M. and Viana, M. (2008). Partitioning of
652 Major and Trace Components in Pm10–Pm2.5–Pm1 at an Urban Site in Southern Europe.
653 *Atmospheric Environment* 42: 1677-1691.
654 Perry, K.D., Cliff, S.S. and Jimenez-Cruz, M.P. (2004). Evidence for Hygroscopic Mineral Dust
655 Particles from the Intercontinental Transport and Chemical Transformation Experiment.
656 *Journal of Geophysical Research D: Atmospheres* 109: 1-9.

657 Pokorná, P., Hovorka, J. and Hopke, P.K. (2016). Elemental Composition and Source
658 Identification of Very Fine Aerosol Particles in a European Air Pollution Hot-Spot.
659 *Atmospheric Pollution Research* 7: 671-679.
660 Pokorná, P., Hovorka, J., Klán, M. and Hopke, P.K. (2015). Source Apportionment of Size
661 Resolved Particulate Matter at a European Air Pollution Hot Spot. *The Science of the total*
662 *environment* 502: 172-183.
663 Pope III, C.A. and Dockery, D.W. (2006). Health Effects of Fine Particulate Air Pollution: Lines
664 That Connect. *Journal of the Air & Waste Management Association* 56: 709-742.
665 Prospero, J.M., Olmez, I. and Ames, M. (2001). Al and Fe in Pm 2.5 and Pm 10 Suspended
666 Particles in South-Central Florida: The Impact of the Long Range Transport of African
667 Mineral Dust. *Water, Air, and Soil Pollution* 125: 291-317.
668 Rogula-Kozłowska, W., Klejnowski, K., Rogula-Kopiec, P., Mathews, B. and Szopa, S. (2012).
669 A Study on the Seasonal Mass Closure of Ambient Fine and Coarse Dusts in Zabrze,
670 Poland. *Bulletin of Environmental Contamination and Toxicology* 88: 722-729.
671 Rovelli, S., Cattaneo, A., Borghi, F., Spinazzè, A., Campagnolo, D., Limbeck, A. and Cavallo,
672 D.M. (2017). Mass Concentration and Size-Distribution of Atmospheric Particulate
673 Matter in an Urban Environment. *Aerosol and Air Quality Research* 17: 1142-1155.
674 ŘSD (2010). Celostátní Sčítání Dopravy 2010, http://scitani2010.rsd.cz/pages/map/default.aspx.
675 Saliba, N.A., Kouyoumdjian, H. and Roumié, M. (2007). Effect of Local and Long-Range
676 Transport Emissions on the Elemental Composition of Pm10-2.5 and Pm2.5 in Beirut.
677 *Atmospheric Environment* 41: 6497-6509.
678 Salma, I., Maenhaut, W. and Záray, G. (2002). Comparative Study of Elemental Mass Size
679 Distributions in Urban Atmospheric Aerosol. *Journal of Aerosol Science* 33: 339-356.

680 Samara, C. and Voutsa, D. (2005). Size Distribution of Airborne Particulate Matter and
681 Associated Heavy Metals in the Roadside Environment. *Chemosphere* 59: 1197-1206.
682 Shen, S., Jaques, P.A., Zhu, Y., Geller, M.D. and Sioutas, C. (2002). Evaluation of the Smps-Aps
683 System as a Continuous Monitor for Measuring Pm2.5, Pm10 and Coarse (Pm2.5-10)
684 Concentrations. *Atmospheric Environment* 36: 3939-3950.
685 Schins, R.P.F., Lightbody, J.H., Borm, P.J.A., Shi, T., Donaldson, K. and Stone, V. (2004).
686 Inflammatory Effects of Coarse and Fine Particulate Matter in Relation to Chemical and
687 Biological Constituents. *Toxicology and Applied Pharmacology* 195: 1-11.
688 Schwarz, J., Štefancová, L., Maenhaut, W., Smolík, J. and Ždímal, V. (2012). Mass and
689 Chemically Speciated Size Distribution of Prague Aerosol Using an Aerosol Dryer-the
690 Influence of Air Mass Origin. *The Science of the total environment* 437: 348-362.
691 Singh, M., Misra, C. and Sioutas, C. (2003). Field Evaluation of a Personal Cascade Impactor
692 Sampler (Pcis). *Atmospheric Environment* 37: 4781-4793.
693 Smolík, J., Dohányosová, P., Schwarz, J., Ždímal, V. and Lazaridis, M. (2008). Characterization
694 of Indoor and Outdoor Aerosols in a Suburban Area of Prague. *Water, Air, and Soil*
695 *Pollution: Focus* 8: 35-47.
696 Spindler, G., Grüner, A., Müller, K., Schlimper, S. and Herrmann, H. (2013). Long-Term Size-
697 Segregated Particle (Pm10, Pm2.5, Pm1) Characterization Study at Melpitz - Influence of
698 Air Mass Inflow, Weather Conditions and Season. *Journal of Atmospheric Chemistry* 70:
699 165-195.
700 Sram, R.J., Dostal, M., Libalova, H., Rossner, P., Rossnerova, A., Svecova, V., Topinka, J. and
701 Bartonova, A. (2013). The European Hot Spot of B[a]P and Pm 2.5 Exposure-the Ostrava
702 Region, Czech Republic: Health Research Results. *ISRN Public Health* 2013: 1-12.

703 Stafoggia, M., Samoli, E., Alessandrini, E., Cadum, E., Ostro, B., Berti, G., Faustini, A.,
704 Jacquemin, B., Linares, C., Pascal, M., Randi, G., Ranzi, A., Stivanello, E. and Forastiere,
705 F. (2013). Short-Term Associations between Fine and Coarse Particulate Matter and
706 Hospitalizations in Southern Europe: Results from the Med-Particles Project.
707 *Environmental Health Perspectives* 121: 1026-1033.
708 Swietlicki, E. and Krejci, R. (1996). Source Characterisation of the Central European
709 Atmospheric Using Multivariate Statistical Methods. *Nuclear Instruments and Methods in*
710 *Physics Research B* 109/110: 519-525.
711 Taiwo, A.M., Beddows, D.C.S., Shi, Z. and Harrison, R.M. (2014). Mass and Number Size
712 Distributions of Particulate Matter Components: Comparison of an Industrial Site and an
713 Urban Background Site. *Science of the Total Environment* 475: 29-38.
714 Talbot, N., Kubelova, L., Makes, O., Cusack, M., Ondracek, J., Vodička, P., Schwarz, J. and
715 Zdimal, V. (2016). Outdoor and Indoor Aerosol Size, Number, Mass and Compositional
716 Dynamics at an Urban Background Site During Warm Season. *Atmospheric Environment*
717 131: 171-184.
718 Tan, J., Duan, J., Zhen, N., He, K. and Hao, J. (2016). Chemical Characteristics and Source of
719 Size-Fractionated Atmospheric Particle in Haze Episode in Beijing. *Atmospheric*
720 *Research* 167: 24-33.
721 Tang, I.N. (1980). Deliquescence Properties and Particle Size Change of Hygroscopic Aerosols.
722 *AGARD Report*: 153-167.
723 Thimmaiah, D., Hovorka, J. and Hopke, P.K. (2009). Source Apportionment of Winter
724 Submicron Prague Aerosols from Combined Particle Number Size Distribution and
725 Gaseous Composition Data. *Aerosol and Air Quality Research* 9: 209-236.

726 Tian, S., Pan, Y., Liu, Z., Wen, T. and Wang, Y. (2014). Size-Resolved Aerosol Chemical
727 Analysis of Extreme Haze Pollution Events During Early 2013 in Urban Beijing, China.
728 *Journal of Hazardous Materials* 279: 452-460.
729 Tian, S.L., Pan, Y.P. and Wang, Y.S. (2016). Size-Resolved Source Apportionment of Particulate
730 Matter in Urban Beijing During Haze and Non-Haze Episodes. *Atmospheric Chemistry*
731 *and Physics* 16: 1-19.
732 Torfs, K. and van Grieken, R. (1997). Chemical Relations between Atmospheric Aerosols,
733 Deposition and Stone Decay Layers on Historic Buildings at the Mediterranean Coast.
734 *Atmospheric Environment* 31: 2179-2192.
735 US-EPA (1996). Review of the National Ambient Air Quality Standards for Particulate Matter:
736 Policy Assessment of Scientific and Technical Information. *EPA-452 \ R-96-013*.
737 US-EPA (2004). Air Quality Criteria for Particulate Matter, Volume 2 of 2. *EPA/600/P-99/002bF*
738 II.
739 Vallius, M.J., Ruuskanen, J., Mirme, A. and Pekkanen, J. (2000). Concentration and Estimated
740 Soot Content of Pm1, Pm2.5 and Pm10 in a Subarctic Urban Atmosphere. *Environmental*
741 *Science and Technology* 34: 1919-1925.
742 Vecchi, R., Marcazzan, G., Valli, G., Ceriani, M. and Antoniazzi, C. (2004). The Role of
743 Atmospheric Dispersion in the Seasonal Variation of Pm1 and Pm2.5 Concentration and
744 Composition in the Urban Area of Milan (Italy). *Atmospheric Environment* 38: 4437-
745 4446.
746 Veron, A., Church, T.M., Patterson, C.C., Erel, Y. and Merrill, J.T. (1992). Continental Origin
747 and Industrial Sources of Trace Metals in the Northwest Atlantic Troposphere. *Journal of*
748 *Atmospheric Chemistry* 14: 339-351.

749 Viana, M., Kuhlbusch, T.A.J., Querol, X., Alastuey, A., Harrison, R.M., Hopke, P.K.,
750 Winiwarter, W., Vallius, M., Szidat, S., Prévôt, A.S.H., Hueglin, C., Bloemen, H.,
751 Wåhlin, P., Vecchi, R., Miranda, A.I., Kasper-Giebl, A., Maenhaut, W. and Hitzenberger,
752 R. (2008). Source Apportionment of Particulate Matter in Europe: A Review of Methods
753 and Results. *Journal of Aerosol Science* 39: 827-849.
754 Vodička, P., Schwarz, J. and Ždímal, V. (2013). Analysis of One Year's Oc/Ec Data at a Prague
755 Suburban Site with 2-Htime Resolution. *Atmospheric Environment* 77: 865-872.
756 Wang, X., Wang, W., Yang, L., Gao, X., Nie, W., Yu, Y., Xu, P., Zhou, Y. and Wang, Z. (2012).
757 The Secondary Formation of Inorganic Aerosols in the Droplet Mode through
758 Heterogeneous Aqueous Reactions under Haze Conditions. *Atmospheric Environment* 63:
759 68-76.
760 Wang, Y., Zhuang, G., Tang, A., Yuan, H., Sun, Y., Chen, S. and Zheng, A. (2005). The Ion
761 Chemistry and the Source of Pm2.5 Aerosol in Beijing. *Atmospheric Environment* 39:
762 3771-3784.
763 Wedepohl, K.H. (1995). Ingerson Lecture: The Composition of the Continental Crust.
764 *Geochimica et Cosmochimica Acta* 59: 1217-1232.
765 Whitby, K.T. (1978). The Physical Characteristics of Sulfur Aerosols. *Atmospheric Environment*
766 12: 135-159.
767 Whitby, K.T., Husar, R.B. and Liu, B.Y.H. (1972). The Aerosol Size Distribution of Los Angeles
768 Smog, pp. 177-204.
769 WHO (2013). Review of Evidence on Health Aspects of Air Pollution – Revihaap Project, pp.
770 309-309.

771 Wilson, W.E. and Suh, H.H. (1997). Fine Particles and Coarse Particles: Concentration
772 Relationships Relevant to Epidemiologic Studies. *Journal of the Air & Waste*
773 *Management Association* 47: 1238-1249.
774 Zanobetti, A. and Schwartz, J. (2009). The Effect of Fine and Coarse Particulate Air Pollution on
775 Mortality: A National Analysis. *Environmental Health Perspectives* 117: 898-903.
776 Zhuang, H., Chan, C.K., Fang, M. and Wexler, A.S. (1999). Size Distributions of Particulate
777 Sulfate, Nitrate, and Ammonium at a Coastal Site in Hong Kong. *Atmospheric*
778 *Environment* 33: 843-853.
779 Zwozdziak, A., Gini, M.I., Samek, L., Rogula-Kozlowska, W., Sowka, I. and Eleftheriadis, K.
780 (2017). Implications of the Aerosol Size Distribution Modal Structure of Trace and Major
781 Elements on Human Exposure, Inhaled Dose and Relevance to the Pm2.5 and Pm10
782 Metrics in a European Pollution Hotspot Urban Area. *Journal of Aerosol Science* 103: 38-
783 52.

784

785

Table Captions

Table 1. Median values of PM fractions from impactor with the 25^{th} and the 75^{th} percentiles.

Table 2. Spearman correlation coefficients between $PM_{1\text{-}2.5}$ and other monitored variables (statistically significant correlations in bold, p-value<0.05).

790 **Table 1.** Median values of PM fractions from impactor with the 25th and the 75th percentiles.

campaign	PM_{10} $\mu g\ m^{-3}$	$PM_{2.5-10}$ $\mu g\ m^{-3}$	$PM_{2.5}$ $\mu g\ m^{-3}$	$PM_{1-2.5}$ $\mu g\ m^{-3}$	PM_{1} $\mu g\ m^{-3}$
Radvanice	48.0	4.1	41.6	3.0	38.5
	(39.3-56.5)	(3.6-5.5)	(32.8-52.4)	(2.2-4.4)	(29.7-49.2)
Plesná	34.2	2.0	30.6	2.8	29.2
	(25.2-48.2)	(1.2-2.7)	(23.4-46.3)	(1.5-3.9)	(19.6-41.7)
Benátská_s	9.4	1.3	8.5	0.6	7.9
	(8.2-12.5)	(1.0-1.7)	(6.9-11.1)	(0.2-1.1)	(6.8-9.8)
Suchdol_s	11.3	1.6	9.6	0.9	8.5
	(8.4-13.5)	(1.2-2.0)	(6.8-12.0)	(0.5-0.9)	(6.3-11.3)
Benátská_w	28.4	0.7	27.7	1.1	24.8
	(10.3-35.3)	(0.1-1.6)	(9.7-34.6)	(0.3-1.7)	(8.9-33.7)
Suchdol_w	27.9	1.0	27.6	1.0	26.2
	(17.8-40.2)	(0.7-1.3)	(16.9-39.2)	(0.5-1.8)	(16.5-35.9)

791

792 **Table 2.** Spearman correlation coefficients between $PM_{1-2.5}$ and other monitored variables
793 (statistically significant correlations in bold, p-value<0.05).

	$PM_{1-2.5}$					
Parameter	Ostrava Radvanice winter	Ostrava Plesná winter	Prague Benátská summer	Prague Suchdol summer	Prague Benátská winter	Prague Suchdol winter
PM_1	-0.03	**0.53**	**0.71**	-0.03	0.36	**0.75**
$PM_{2.5-10}$	**0.39**	**0.35**	0.45	**0.59**	**0.79**	**0.59**
$PM_{2.5}$	0.06	**0.62**	**0.79**	0.02	0.42	**0.79**
RH	0.17	**0.49**	-0.08	-0.38	-0.41	0.40
T	0.08	0.06	0.31	-0.07	-0.19	-0.35
WS	-0.02	-0.10	-0.29	-0.21	**-0.63**	**-0.52**
count of obs.	23	22	15	15	15	15

794

795 **Figure Captions**

796 **Figure 1.** Median mass portions of PM_1, $PM_{1\text{-}2.5}$, and $PM_{2.5\text{-}10}$ in PM_{10}; error bars represent the
797 25^{th} and the 75^{th} percentiles.

798 **Figure 2.** EFs for PM_1, $PM_{1\text{-}2.5}$ and $PM_{2.5\text{-}10}$ with Si as a normalizing crustal element.

799 **Figure 3.** Median of ratio Ca^{2+} to SO_4^{2-} in all three fractions for individual campaigns; error bars
800 represent the 25^{th} and the 75^{th} percentiles.

801 **Figure 4.** Polar plots: $PM_{1\text{-}2.5}$, $PM_{2.5\text{-}10}$, and PM_1 concentrations ($\mu g\ m^{-3}$) by WD and WS.

802 **Figure 5.** Semiquantitative elemental composition of PM fractions for each campaign (expressed
803 as percentages of individual elements normalized to 100.

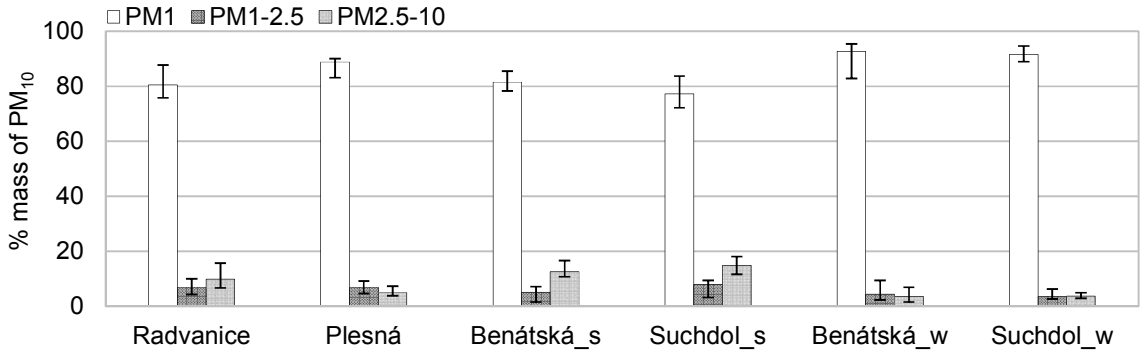

804

805 **Figure 1.** Median mass portions of PM_1, $PM_{1-2.5}$, and $PM_{2.5-10}$ in PM_{10}; error bars represent the
806 25^{th} and the 75^{th} percentiles.

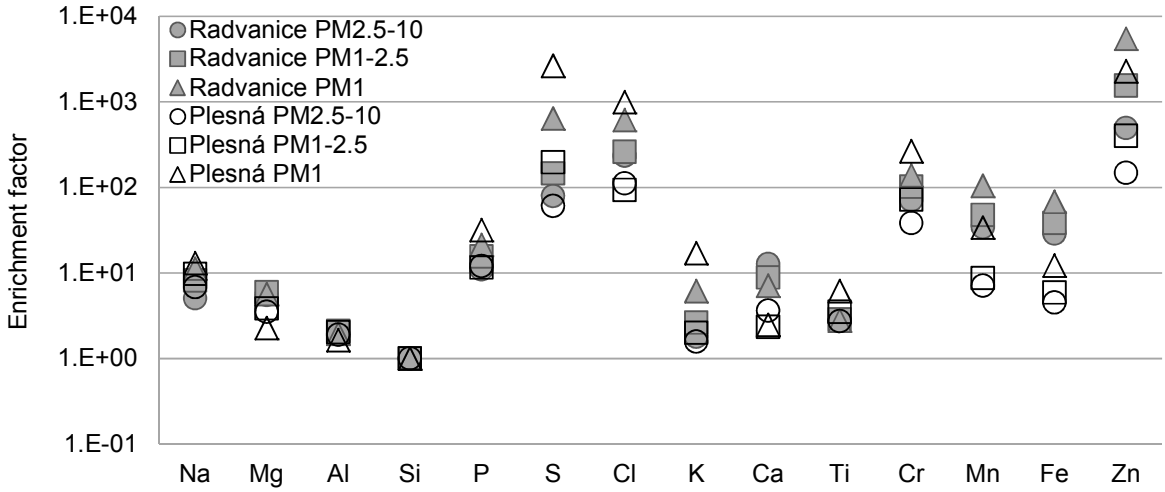

807

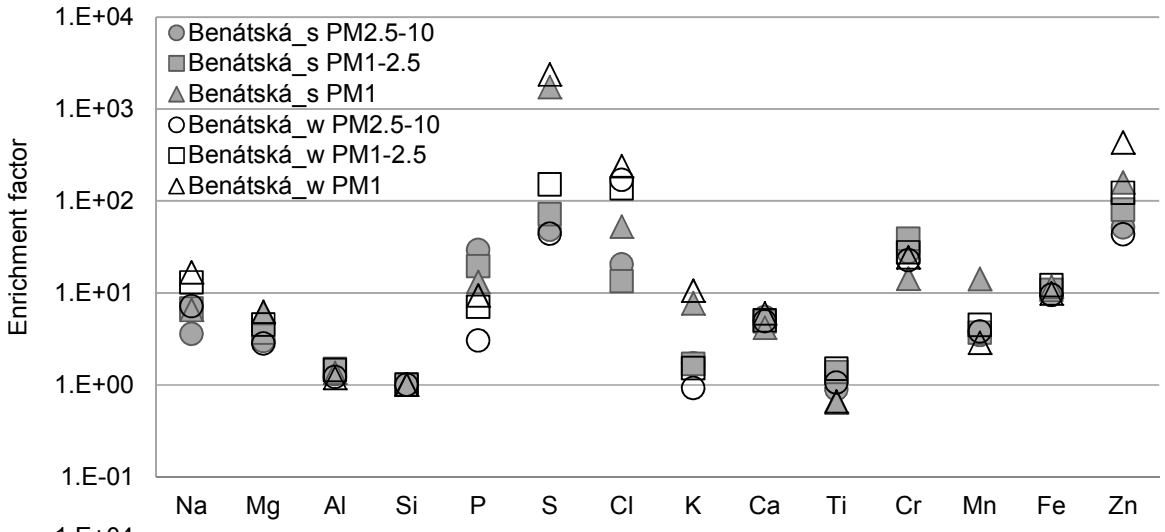

808

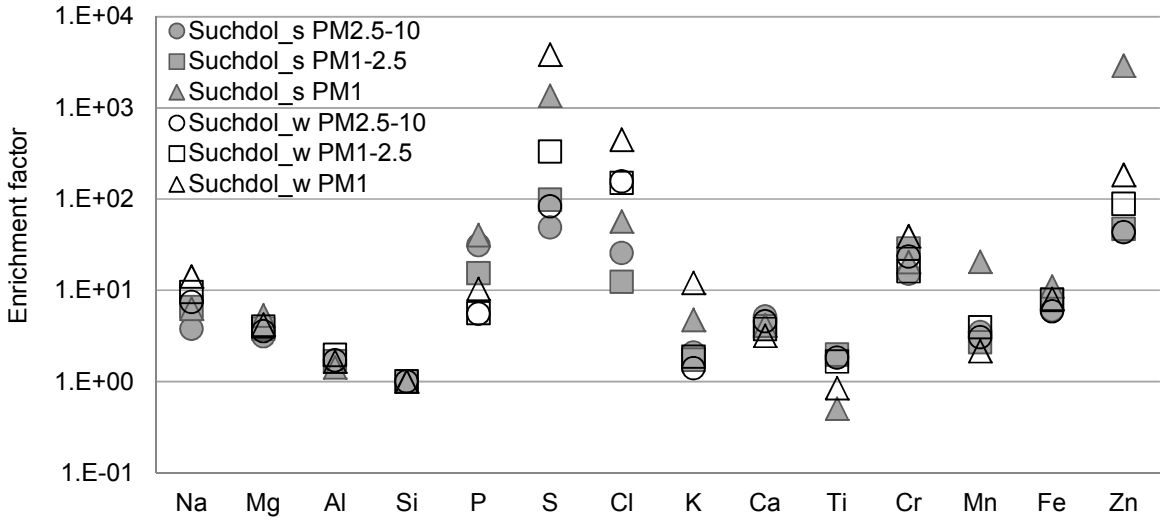

809

810

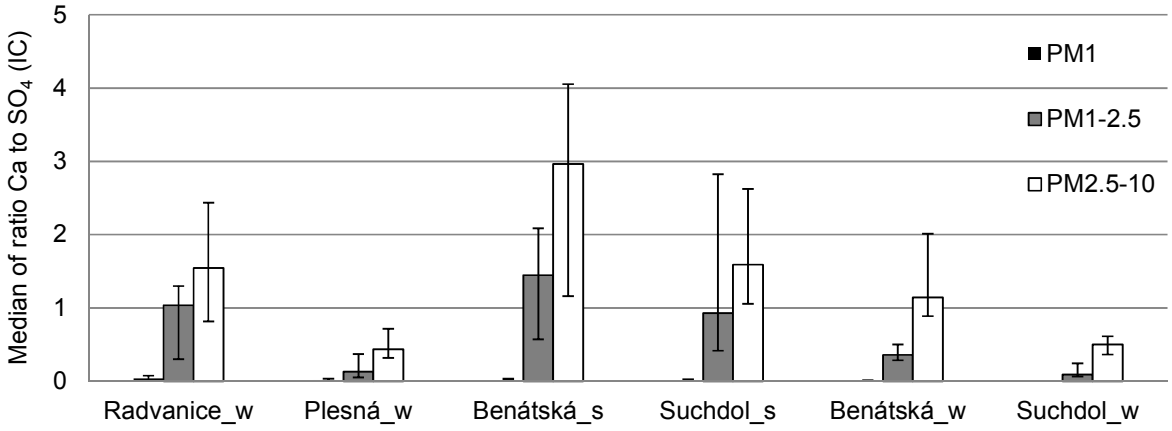

Figure 3. Median of ratio Ca^{2+} to SO_4^{2-} in all three fractions for individual campaigns; error bars represent the 25th and the 75th percentile.

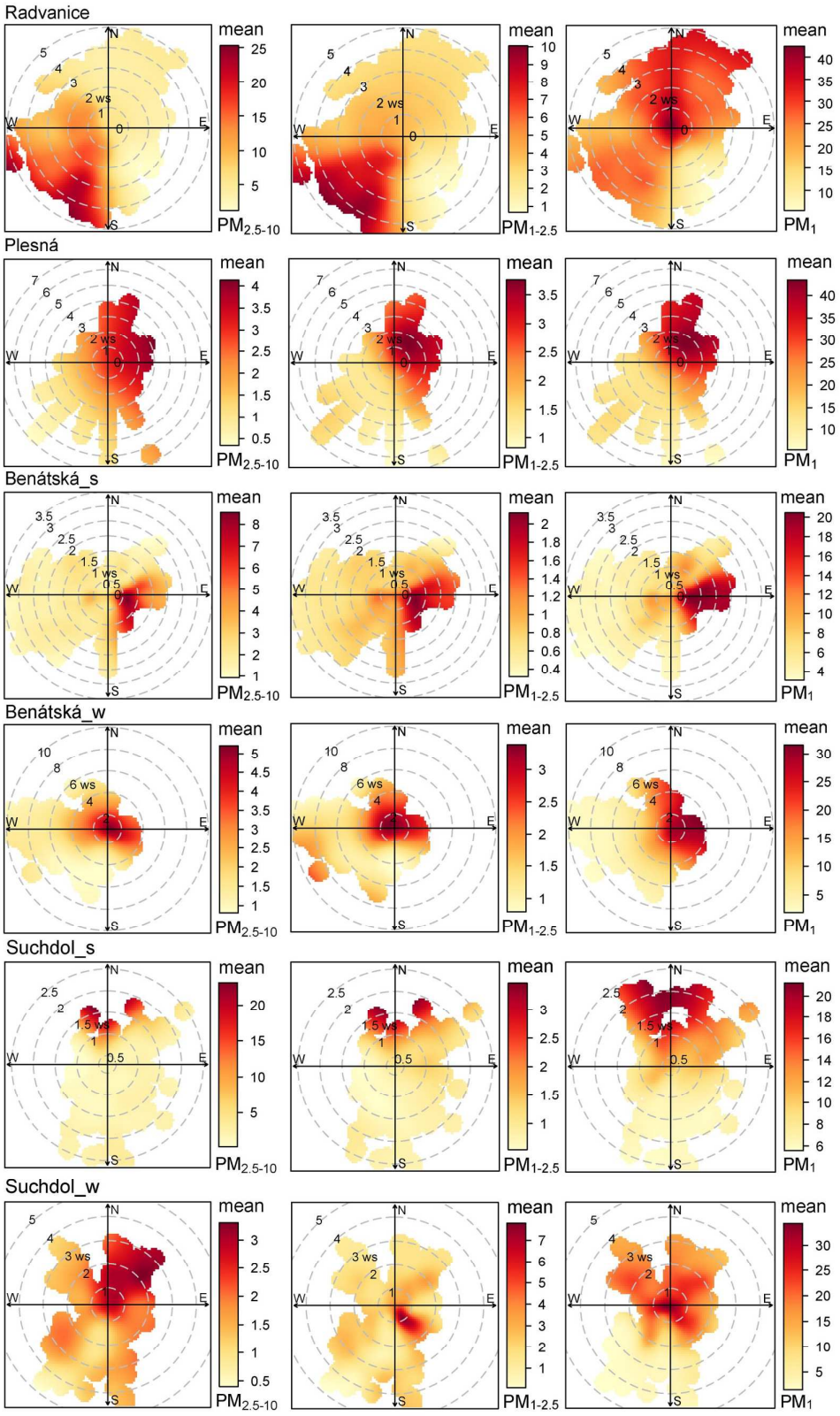

Figure 4. Polar plots: $PM_{1\text{-}2.5}$, $PM_{2.5\text{-}10}$, and PM_1 concentrations (µg m^{-3}) by WD and WS.

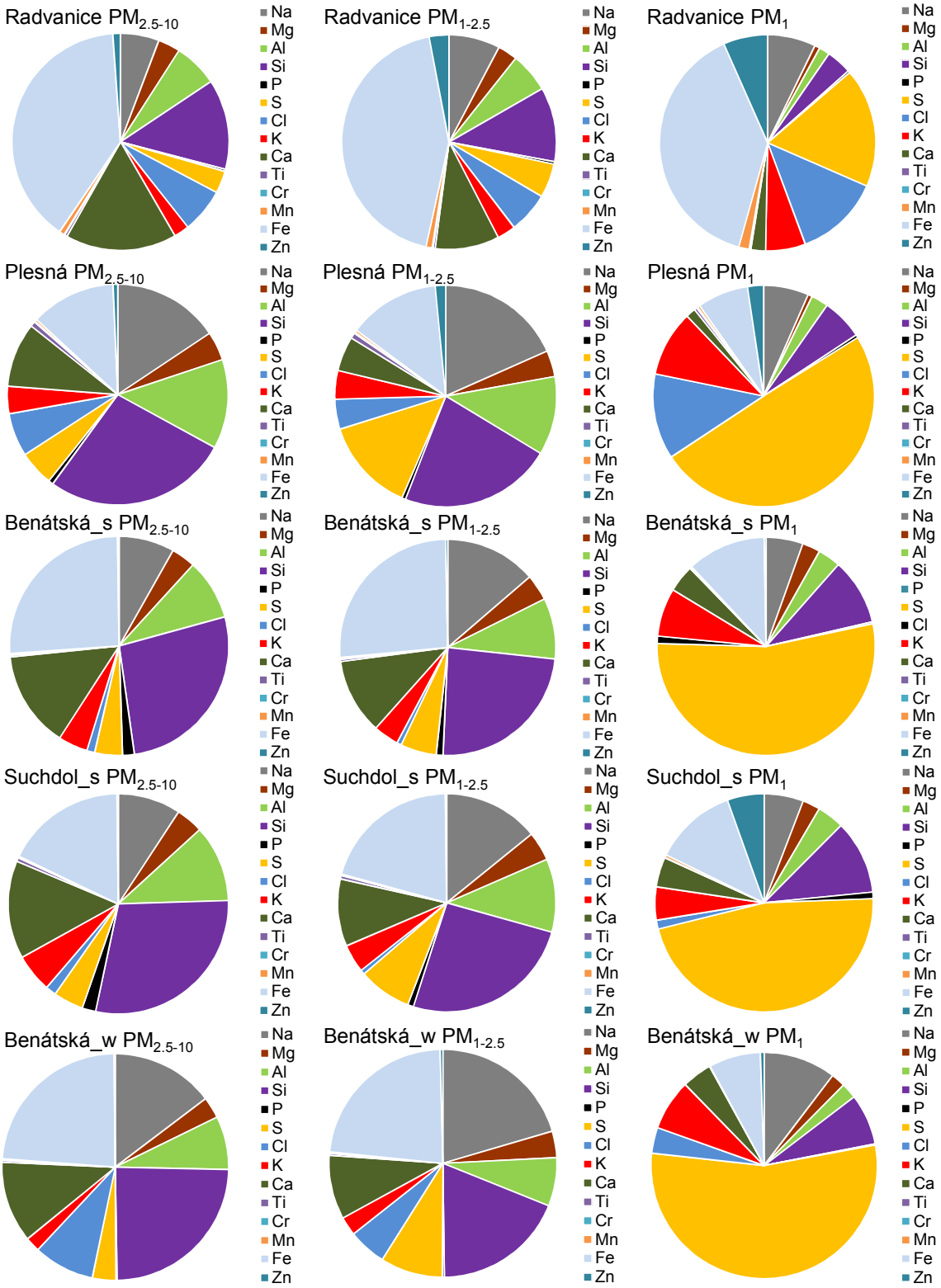
Radvanice PM2.5-10
Radvanice PM1-2.5
Radvanice PM1
Plesná PM2.5-10
Plesná PM1-2.5
Plesná PM1
Benátská_s PM2.5-10
Benátská_s PM1-2.5
Benátská_s PM1
Suchdol_s PM2.5-10
Suchdol_s PM1-2.5
Suchdol_s PM1
Benátská_w PM2.5-10
Benátská_w PM1-2.5
Benátská_w PM1
Na
Mg
Al
Si
P
S
Cl
K
Ca
Ti
Cr
Mn
Fe
Zn

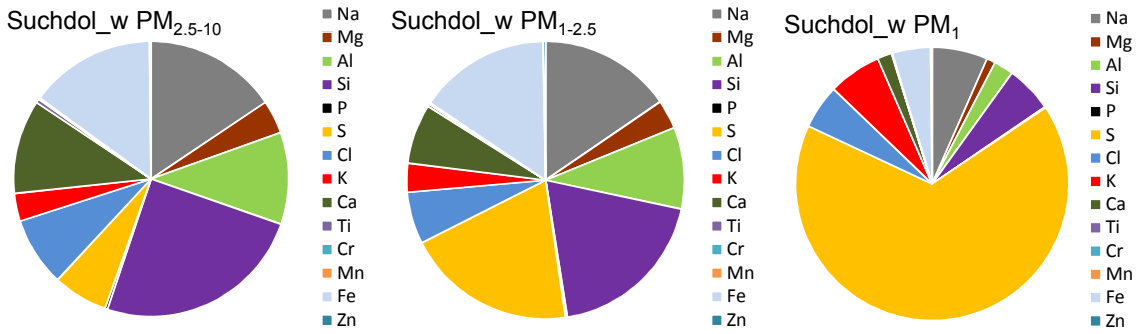

Figure 5. Semiquantitative elemental composition of PM fractions for each campaign (expressed as percentages of individual elements normalized to 100%).

Supplementary material

Chemical characterization of $PM_{1-2.5}$ and its association with PM_1, $PM_{2.5-10}$ and meteorology in urban and suburban environments

Sampling sites

Table S1. Details of measuring sites.

measuring site	type of locality	GPS	measuring periods	place of instruments	sampling height
Ostrava Radvanice and Bartovice	urban industrial	49.811161 N, 18.337922 E	2/11-3/5/2014 (winter)	inside the monitoring station	5 m AGL[a]
Ostrava Plesná	suburban	49.865920 N, 18.132090 E	2/11-3/5/2014 (winter)	outside (impactor), inside of a wooden box (other devices)	2 m AGL[a]
Prague Benátská	urban traffic	50.071318 N, 14.420950 E	8/21-9/4/2014 (summer) 2/17/-3/3/2015 (winter)	inside the monitoring station	15 m AGL[a]
Prague Suchdol	suburban	50.127523 N, 14.385224 E	8/21-9/4/2014 (summer) 2/5-19/2015 (winter)	outside (impactor), inside (other devices)	2 m AGL[a]

[a] AGL = above ground level

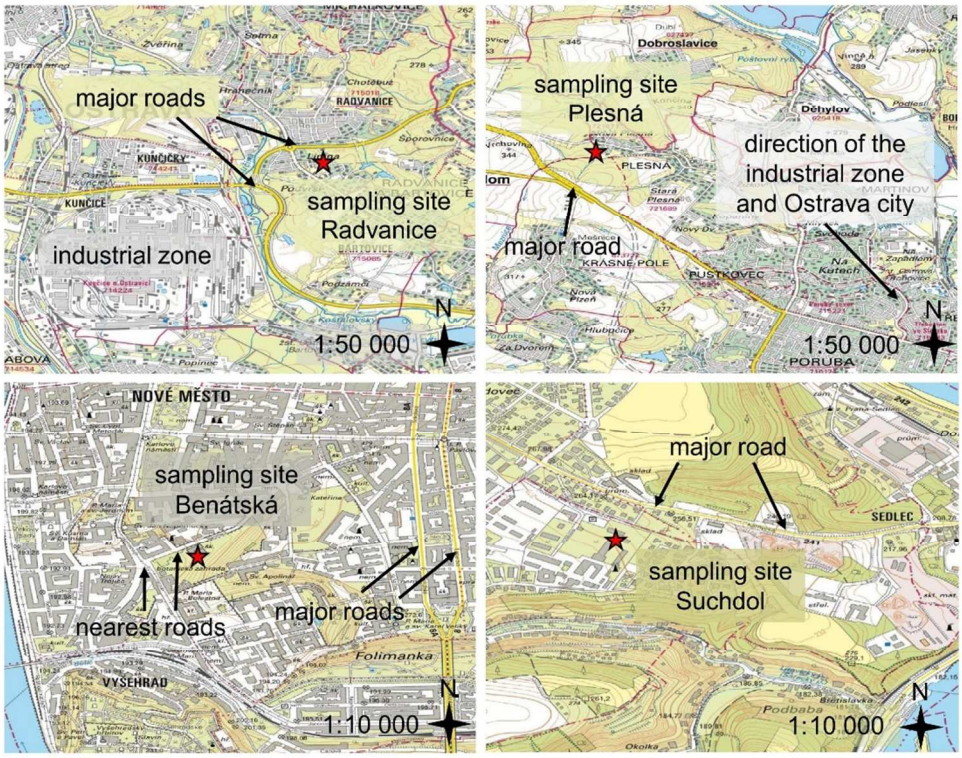

Figure S1. Sampling sites with main pollution sources (maps provided by State Administration of Land Surveying and Cadaster).

SEM+EDX analysis

Similar approach as we employed in our study was already used by several authors (Broussolle *et al.*, 2015; Jiang *et al.*, 2015; Peřestý *et al.*, 2017) in order to get reliable estimates of whole rock chemical composition by EDX analysis of representative area of rock sample in form of thin-section. While these authors analyzed polished samples, in our case the surface of the samples is uneven, which may have some effect on the quality of the analysis. In order to estimate if and how much this can influence ratios of analyzed elements, the method was tested on powders of samples with known composition (rock pulps analyzed by inductively coupled plasma mass spectrometry (ICP MS) at Bureau Veritas Laboratories, Vancouver, Canada). The results have shown that there is a good agreement in the ratios of the main elements obtained by the EDX analysis of the rock pulp spread on a horizontal surface with the data coming from precise ICP MS analyses of the rocks. Therefore, this approach can be used at least as a semiquantitative method allowing the comparison of relative concentrations of elements (Fig. S2).

A XRF matrix correction procedure (Pouchou and Pichoir, 1984) was applied to mitigate an effect of absorption of electron radiation and X-ray in the sample. However, for elemental heterogeneous stratification in the sample, e.g. heavier elements predominantly occurring in the surface layer in contrast with lower layers, the applied correction is ineffective and results can be influenced by absorption effect. It can happen when a significant air pollution source(s) occurred at a certain time just before the end of the sampling period (in our case 24-h period). On the other hand, the correction procedure is effective for samples with the homogenous stratification (examined material is randomly mixed).

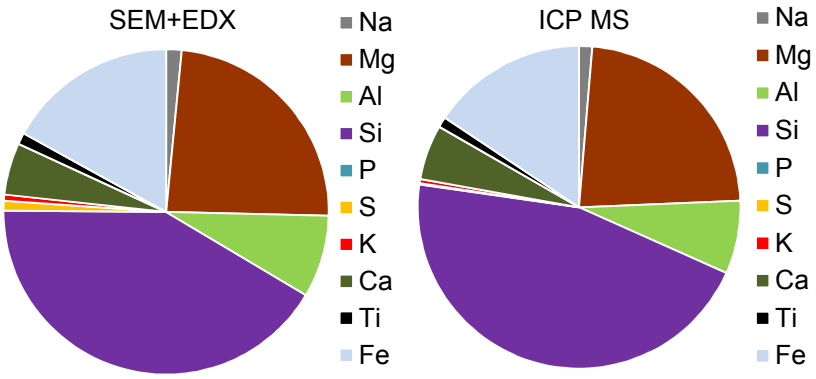

Figure S2. Comparison of the powder sample (rock pulps) analyzed by SEM+EDX and ICP MS.

SMPS and APS data processing

All the datasets were carefully observed and the outliers originated by instruments malfunctioning were removed (Table S2). The data were directly exported with Aerosol Instrument Manager Software (TSI Inc.) as mass concentration (dM). Stokes correction was applied to APS data. For the SMPS data multiple charges correction and diffusion correction were applied.

Table S2. Missing data.

Missing data	Plesná	Radvanice	Benátská_w	Benátská_s	Suchdol_w	Suchdol_s
SMPS	3.2%	1.2%	5.2%	0%	0%	0%
APS	3.8%	1.2%	11.6%	0.1%	0%	0%

The size distribution for SMPS and APS was combined without considering merging approaches. This choice is allowed by the compatibility between SMPS and APS measurements in the overlapping region. Data from SMPS and APS size distribution were selected according to these three fractions:

- PM_1 (APS size range 0.542 – 0.965 µm + SMPS size range 14-532 nm)
- $PM_{1\text{-}2.5}$ (APS size range 1.037-2.458 µm)
- $PM_{2.5\text{-}10}$ (APS size range 2.642-10.37 µm)

To calculate the total PM_1 mass concentration, semi-continuous APS + SMPS mass concentration was obtained summing the fractions 0.542-0.965 µm and <0.532 µm. The SMPS mobility diameter (d_{eq}) was converted in aerodynamic (d_a) according to Hinds (1998), with an assumption that particles are spherical and particle density is 1.5 g cm^{-3} (Shen *et al.*, 2002): $d_a = d_{eq}\sqrt{\rho_p}$. Mass concentrations for SMPS and APS data were computed by averaging the 5-minutes (Radvanice, Plesná, Benátská sites) and 10-minutes (Suchdol site) concentrations over the sampling duration of the gravimetric method (from 9 AM to 9 AM the next day, according to the PCIS sampling protocol).

Campaign overview

Table S3. Median values and the 25th and the 75th percentiles of meteorological parameters.

campaign	T, °C	RH, %	**WS, m s^{-1}**
Radvanice	4.9 (1.8-7.2)	79.0 (66.0-89.0)	1.0 (0.5-1.8)
Plesná	4.6 (2.2-6.8)	74.5 (62.0-86.0)	1.6 (0.9-2.4)
Benátská_s	14.5 (12.3-17.2)	78.5 (63.7-85.8)	0.5 (0.2-0.9)
Suchdol_s	15.6 (13.3-18.4)	84.1 (66.8-93.1)	0.9 (0.6-1.4)
Benátská_w	2.8 (0.9-5.3)	76.0 (61.0-84.0)	2.0 (1.2-3.4)
Suchdol_w	0.7 (-0.9-2.6)	80.0 (74.2-84.1)	1.3 (0.9-2.1)

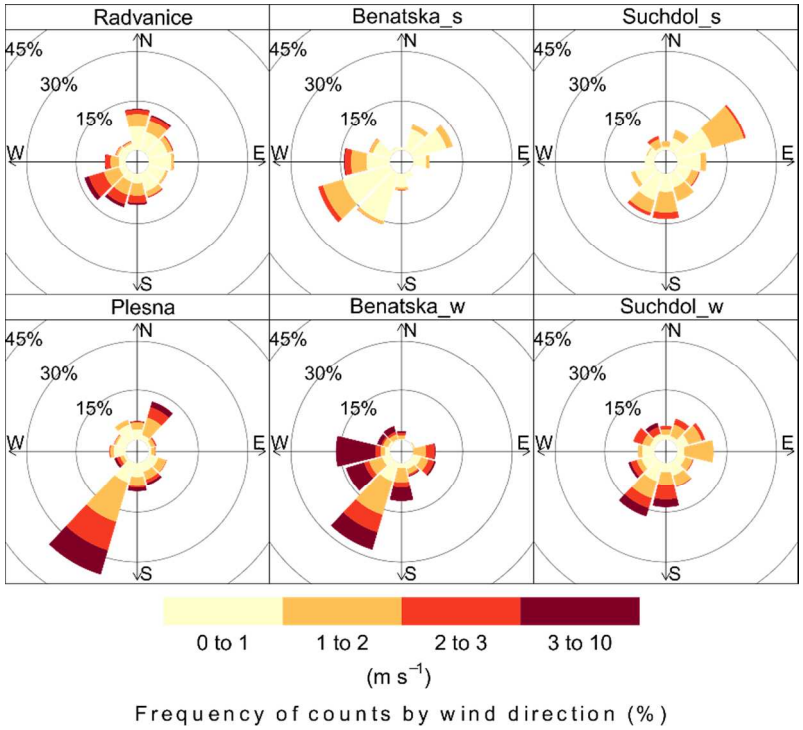

Figure S3. WS according to WD during individual campaigns.

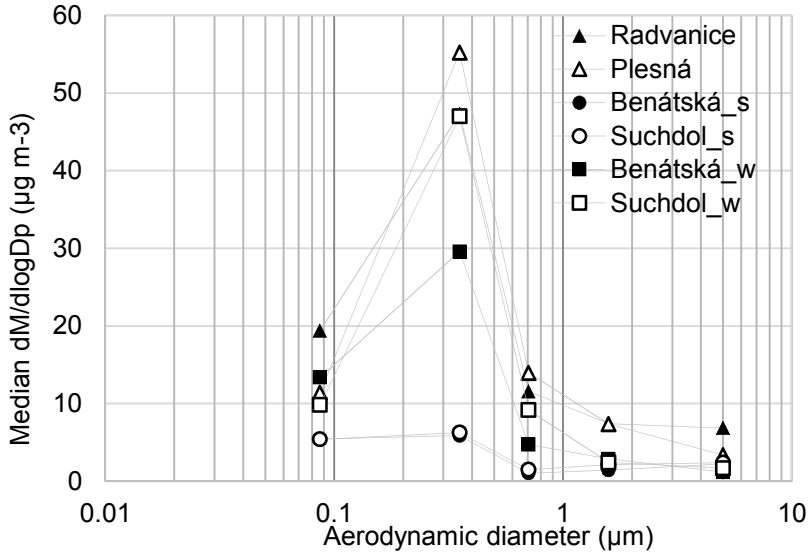

Figure S4. Median mass size distribution measured by PCIS (the lower limit of 0.03 µm used for back-up filter to construct the mass size distribution).

$PM_{1\text{-}2.5}$ investigation at various sites

Table S4. Median mass concentrations of Ca^{2+} and SO_4^{2-} in size fractions $PM_{2.5\text{-}10}$, $PM_{1\text{-}2.5}$, and PM_1.

	Ca^{2+} (ng m^{-3})			SO_4^{2-} (ng m^{-3})		
	$PM_{2.5\text{-}10}$	$PM_{1\text{-}2.5}$	PM_1	$PM_{2.5\text{-}10}$	$PM_{1\text{-}2.5}$	PM_1
Radvanice	1 544.4	52.7	60.2	114.1	73.9	1 904.6
Plesná	20.5	9.2	22.9	54.1	103.9	1 796.4
Benátská_s	29.9	12.7	17. 9	11.9	15.7	644.2
Suchdol_s	32.2	15.4	7.4	29.0	17.9	725.1
Benátská_w	38.1	25.6	13.2	37.1	84.5	1 975.4
Suchdol_w	19.5	12.2	13.8	50.0	94.4	3 672.3

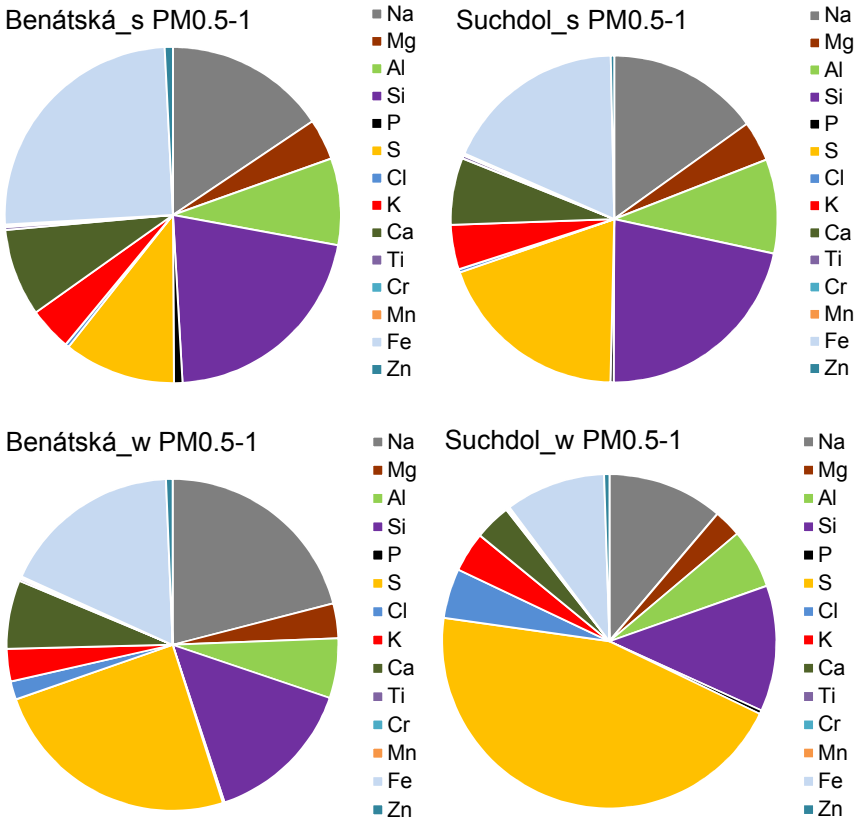

Figure S5. Seasonal comparison in semiquantitative elemental composition of $PM_{0.5\text{-}1}$.

References

Broussolle, A., Štípská, P., Lehmann, J., Schulmann, K., Hacker, B.R., Holder, R., Kylander-Clark, A.R.C., Hanžl, P., Racek, M., Hasalová, P., Lexa, O., Hrdličková, K. and Buriánek, D. (2015). P-T-T-D Record of Crustal-Scale Horizontal Flow and Magma-Assisted Doming in the Sw Mongolian Altai. *Journal of Metamorphic Geology* 33: 359-383.

Hinds, W.C. (1998). *Aerosol Technology-Properties, Behavior, and Measurement of Airborne Particles*, 2nd ed. John Wiley & Sons, Inc., New York.

Jiang, Y.D., Štípská, P., Sun, M., Schulmann, K., Zhang, J., Wu, Q.H., Long, X.P., Yuan, C., Racek, M., Zhao, G.C. and Xiao, W.J. (2015). Juxtaposition of Barrovian and Migmatite Domains in the Chinese Altai: A Result of Crustal Thickening Followed by Doming of Partially Molten Lower Crust. *Journal of Metamorphic Geology* 33: 45-70.

Peřestý, V., Lexa, O., Holder, R., Jeřábek, P., Racek, M., Štípská, P., Schulmann, K. and Hacker, B.R. (2017). Metamorphic Inheritance of Rheic Passive Margin Evolution and Its Early Variscan Overprint in the Teplá-Barrandian Unit, Bohemian Massif. *Journal of Metamorphic Geology*: 327-355.

Pouchou, J.L. and Pichoir, F. (1984). A new model for quantitative analysis. Application to the analysis of homogeneous samples. *La recherche aérospatiale* 5: 47-65.

Shen, S., Jaques, P.A., Zhu, Y., Geller, M.D. and Sioutas, C. (2002). Evaluation of the Smps-Aps System as a Continuous Monitor for Measuring PM2.5, PM10 and Coarse (PM2.5-10) Concentrations. *Atmospheric Environment* 36: 3939-3950.